Design and development of prognostic and health management system for fly-by-wire primary flight control electrohydraulic servoactuators

Candidate:
Andrea Mornacchi

Thesis advisor:
Prof. G. Jacazio

COMMISSIONE GIUDICATRICE

Il dott. **Andrea MORNACCHI** ha discusso in data ha discusso in data 29 aprile 2016 presso il Dipartimento di Ingegneria Meccanica e Aerospaziale del Politecnico di Torino la tesi di Dottorato avente il seguente titolo:

Design and development of prognostic and health management system for fly-by-wire primary fly control electrohydraulic servoactuators

Le ricerche oggetto della tesi sono eccellente livello.

Le metodologie appaiono molto buone.

I risultati sono interessanti ed analizzati con elevato senso critico.

Nel colloquio il candidato dimostra ottima conoscenza delle problematiche trattate.

La Commissione unanime giudica estremamente positivo il lavoro svolto

e propone che al dott. **Andrea MORNACCHI** venga conferito il titolo di
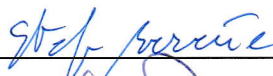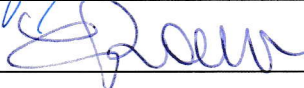
Dottore di Ricerca

Data, 29 aprile 2016

Prof. Carlo Ferraresi (Presidente)   _____

Prof. Stefano Beretta (Componente)   _____

Prof. Enrico Ravina (Segretario)   _____

Prediction is very difficult,
especially if it's about the future.

Nils Bohr

Abstract

Electro-Hydraulic Servo Actuators (EHSA) is the principal technology used for primary flight control in new aircrafts and legacy platforms. The development of Prognostic and Health Management technologies and their application to EHSA systems is of great interest in both the aerospace industry and the air fleet operators.

This Ph.D. thesis is the results of research activity focused on the development of a PHM system for servovalve of fly-by-wire primary flight EHSA. One of the key features of the research is the implementation of a PHM system without the addition of new sensors, taking advantage of sensing and information already available. This choice allows extending the PHM capability to the EHSAs of legacy platforms and not only to new aircrafts. The enabling technologies borrow from the area of Bayesian estimation theory and specifically particle filtering and the information acquired from EHSA during pre-flight check is processed by appropriate algorithms in order to obtain relevant features, detect the degradation and estimate the Remaining Useful Life (RUL). The results are evaluated through appropriate metrics in order to assess the performance and effectiveness of the implemented PHM system.

The major objective of this contribution is to develop an innovative fault diagnosis and failure prognosis framework for critical aircraft components that integrates effectively mathematically rigorous and validated signal processing, feature extraction, diagnostic and prognostic algorithms with novel uncertainty representation and management tools in a platform that is computationally efficient and ready to be transitioned on-board an aircraft.

Keywords:
Prognostics and Health Management (PHM), Condition Based Maintenance (CBM), fly-by-wire primary flight control, ElectroHydraulic ServoValve (EHSV)

Contents

List of Figures

List of Tables

1

Introduction to PHM

Prognostics and health management (PHM) and condition-based maintenance (CBM) have emerged over recent years as significant technologies that are making an impact on both military and commercial maintenance practices. These technologies represent a true paradigm shift in the way complex dynamic systems, in all different fields, are designed, monitored and maintained. The idea is to transform maintenance from a passive to an active action, so know in advance when it is required, and also transform indications provided from faults and degradations in useful information to develop new products more durable and required less maintenance.

The area of automatic diagnostic, intelligent maintenance and prognostic is vital for today complex systems; the aerospace, automotive, military and all the others industries are concerned about critical components reliability and availability. The goals are both to minimize maintenance costs and to maximize systems useful life. As equipment becomes more complex, intelligent maintenance schemes must replace the old reactive and scheduled ones to ensure that equipment continues to function and maximize the up time of the systems.

The increase in diagnostic capability naturally has evolved into something more: the desire of prognosis. The exiting data before used to diagnose failed components, are now employ to detect and monitoring the onset of the failure, thus catching failures before they actually hinder the ability of the systems to perform they function.

This chapter begins a brief introduction to the history of airplanes maintenance. After it introduces the concepts of automatic diagnostics and prognostics, making a tour of the main techniques used. Subsequently the status of the art as regards the field PHM for hydraulic primary flight control actuators are shown.

1.1   Historical perspective

Maintenance programs keep aircraft in safe, working order, ensure passenger comfort, preserve the airline valuable physical assets, and ensure maximum utilization of the aircraft (ATA 2001). Correct maintenance can assist in ensuring that the designed-in reliability performance is achieved, avoid failures, and reduce the cost (Barabady 2007). Actually maintenance accounts for the second greater percentage of cost (after fuel), in approximately 10-15% of operating expenses (ATA 2001). Therefore optimal maintenance strategy is vital for the financial success of airline; this should not only reduce the maintenance costs, but increase the possible flight hours ,so as to contribute to the increase in operating profits.

In the past decades the relevance of maintenance programs as a key role to gain cost effectiveness has evolved during years along with the complexity of components that caused an increased awareness on the necessity to develop an effective solution for technical failure management.

In the early days of civil aviation, components were mostly simple, which made easy to maintain. The common maintenance strategy was corrective maintenance, in other words correction after breakdown.

One of the first research project on maintenance was started by United Airlines 1965, in order to provide a generally applicable systematic review of the aircraft design. The handbook *"Maintenance Evaluation and Program Development"*, also referred to as *"MSG-1"* (ATA 1968), was developed in 1968 for the 747 by the Air Transport Association (ATA) Maintenance Steering Group (MSG), a group of airframe manufacturers, airlines, U.S. Federal Aviation Administration (FAA) representatives, and suppliers. *MSG-1* used decision logic to develop scheduled maintenance. The *MSG-1* proposed an approach focused on a single component in a system and analyzed which part of that component might fail. Then, the kind of maintenance action required to prevent the failure was determined and classify in: Hard Time (HT), On-Condition (OC) and Condition Monitoring (CM).

Few year later ATA released *"Airline/Manufacturer Maintenance Program Planning Document (MSG-2)"*, a small upgrade of the previous document. The same approach proposed in *MSG-1* has been preserved but the

integrity of components in sub-systems was considered before those of the overall system.

The most important advantage of *MSG-1* and *MSG-2*, respect to the pass, was the application of OC maintenance. With introduction of the OC, for the first time in aeronautics, postpone the required maintenance until the next earliest opportunity, as long as the appropriate physical standard and prescribed limitations were met, was possible; the condition of the systems are evaluated by periodically tests. This approach guarantees several advantages:

- **Down time reduction:** maintenance schedules could be modify in order to minimize the obstacles to the operations.

- **Maintenance costs decrease:**

- **Safety increase:** a warning during the tests leave time to stop the system before a safety-critical situation.

The efforts of Nowlan and Heap(1978), senior executive engineers at United Airline, gave birth to *"Reliability-Centered Maintenance (RCM)"*. The documents propose three new policies used for manage the failure mode that could cause failure of any physical systems in a given operating context. The three policies are: preventive maintenance, predictive maintenance and redesign, a first flavor of PHM begins to be smelled.

The basis of the RCM methodology is a structured decision diagram that used the Failure Mode & Effects Analysis (FMEA) methodology to identify functional failures, and failure modes. FMEA classifies the severity of each failure effect according to severity classification criteria established by each program; hence, the quality of the RCM analysis strongly depends on the quality of the FMEA execution.

Large benefits can be obtained by implementing RCM, include higher safety and operating performance, better understanding of the failure modes, and reduction of operation and maintenance costs. respect to earlier methodologies the RCM was based on function preservation instead of failure prevention, and use a failure consequences approach.

System continued to become more complex ed integrated. A single fault could case fault indications for many systems, and in many case for the laborers were very difficult to understand which indication identified the source of failure and which was merely an effect. To solve this issues, the standard for aircraft on-board maintenance system (OMS)*ARINC 624* was developed in the early 1990s. It can be considered the most integrated maintenance systems, that can consolidate the fault indication from multiple systems and

provide additional functionality to support condition based maintenance. Implementing this architecture a minimal ground-support equipment is needed to test airplane systems because most of this capability is just included in the maintenance system implemented on-board.

Today, with increasing complexity of the systems, the rising of maintenance costs and the market for commercial flights ever more globalized and saturated, the only path for evolve the maintenance and reduce service values, seems to be the PHM. Prognostics and health management is an evolution of the CBM, in witch failure detection is automatically made during airplane normal operations, without costs correlate to human and down-time and the RUL estimation clear the street for new connected logistic systems.

1.2   Prognostics and health management

A simple definition of the Prognostics and Health Management could be: an engineering discipline focused on autonomous degradation detection and predicting the time at which a system or a component will no longer perform its intended function. But as often happens, the reality is much more complex than a definition, see teh PHM as a simple system to identify and estimate the degradation RUL is reductive, Prognostics and Health Management is a new way to approach the design, the development, the logistic and also the maintenance. It is characterized by the merging and strong coupling of interdisciplinary disciplines from engineering sciences to communications and from maintenance and logistic to management.

PHM systems are conceived to meet multiple objective by providing useful information to a number of potential subjects: the maintainers, the logistics managers, the process managers or fleet managers and the system designers. Specifically, PHM assist the maintainers to determinate the optimum time to perform maintenance and consequently logistics managers are supported in warehouse management and purchasing of spare parts. It provide the process managers or fleet manager with confident bounds on the availability of critical assets to meet production schedules or mission requirements. Finally, the implementation and the results obtained from a PHM system may help the designer in improving the operational capability of legacy systems or in guiding the design of new systems more fault tolerant.

The strength of the prognostic are the information produced by the observed systems during the normal operations; have large quantities of data, collected in all possible operating conditions from birth to death of a system, offers a huge decision-making power and can offer a detailed knowledge of the real capacity of the component. And if these data are merged with those

from similar systems, imagine an airplane fleet, information that can be extracted are almost endless. Determine how the environmental and operating conditions affect the life of a component or as degradation of a system affects those close finally becomes possible, simplify analyzing with the right statistical techniques the data generated by PHM architecture: the systems could be transformed in the most realistic all life long test benches.
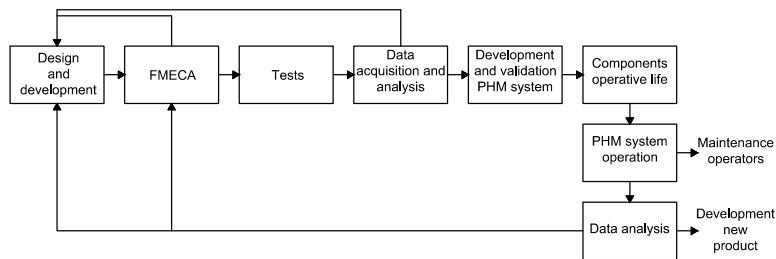
Figure 1.1: An integrate PHM approach

Good representation of an integrated approach to prognostics and health management is offered from figure 1.1, as one can see the stages from design to the end of life of a product are no longer placed in a linear timeline, but rather in an ideal infinite loop, where the maintenance and end of life are sources of information to further improve what has been done or next products. Often also nowadays, the development phase of a product end with its commissioning, the tests are carried out by companies using test benches and prototypes, on which however all the different operating conditions are impossible to be simulated both for reasons of time and feasibility. The data obtained from the maintainers are often incomplete and only related to the fault and not on the evolution of the fail. Contrariwise the PHM proposes an exhaustive and automatic data collection during the stages of degradation, enabling to understand how the problem was born and grew up to be a failure.
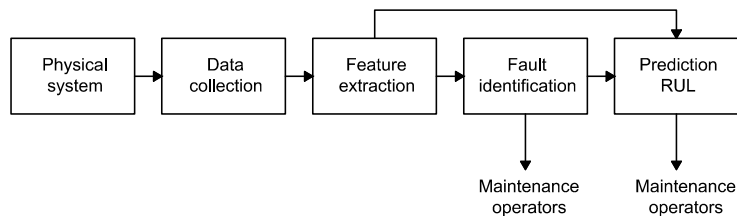
Figure 1.2: PHM cycle

The PhD project presented in the following chapters are focused only on a small area of the whole galaxy of prognostics and health management architecture, the automatic diagnostic and the prediction of the remaining useful life, the part that are more close with the maintenance. This branch of the PHM can be decomposed into four successive phases, as shown in the figure 1.2:

- Data collection

- Feature extraction

- Fault identification

- Prediction RUL

The first phase is to purchase directly from the system the signals from different sources, such signals must then be processed in order to obtain the features. The features are the indexes, or parameters, whose value is closely related to the state of the system. A good feature shall provide a correlation possibly unitary with the value of the degradation and needs to be little affected by noise and environmental conditions (Guyon et al. 2006); a reflected choice of features is essential to be able to identify degradation early and accurately. Identified the degradation, the next step is the estimation of the remaining useful life, this can be carried out using different techniques depending on the system and on the type of information available; the ultimate goal is of course the accuracy of prediction (A. Saxena et al. 2008).

Of the four stages that compose the PHM treated by the thesis, the first is the only one which must be carried on-board the aircraft, the other three can be performed on computers inside the plane devoted to PHM or on external computing server, the data acquired by the system can be downloaded for analysis at set intervals or using modern cloud computing technology in real time. This flexibility is very important, because at first it allows to not modify excessively the legacy aircraft, to reduce the costs adding a basic CPUs on-board, to treat acquisitions, and condense all the computing power in one, or more, server places on the ground. But the real benefit of on-ground analysis is the possibility to fusion set of data provided from the same family of aircrafts; the data can be made to converge into a single data base, thus forming a broad base of information useful to understand how systems evolve and to optimize the algorithms of diagnostic and prognostic.

1.3   Automatic diagnostic

Automatic fault diagnosis has been the subject of numerous investigation over the past decades; researcher in such different engineering disciplines, but also in medicine and finance, have been developing methodologies to detect failure or anomaly condition and to decide on the potential impact of a failing of failed components on the health of the system. The diversity of application domains is matched by the plurality of enabling technologies that have surfaced over the years in attempts to diagnose such damaging events and to meet certain performance specification. Research ad developing have increased more recently owing to the need of maintain legacy equipment, to improve their reliability. The thesis will focus here on few historical reference that provided a significant evolution to fault diagnosis techniques.

U.S. Navy initiated an integrated diagnostic support system, which includes adaptive diagnostic functions, feedback analysis and faults precursors identification (Rosenberg 1989). An integrated system that processes sensor data from shipboard machinery, asses machine condition and provided early fault detection was developed, implemented and successfully tested on a U.S. Navy ship by a research team (Hadden et al. 1999a and Hadden et al. 1999b). The proposed open system architecture suggests seven levels of activity to integrate data acquisition, data manipulation, condition monitoring, health assessment, prognostics in order to provide decision support, the seven layer is the presentation of the results to end users. In parallel, International Standard Organization (ISO) has attempted to capture the conceptual framework for processing models aimed to providing the basic PHM modules from data acquisition and analysis to health and prognostics assessment; figure 1.3 depicts the ISO 13374-1 processing model. Several major companies have produced promising results focusing on specific application domain, but without widespread acceptance as technology standard. Fault detection and identification can be considered a mature field with the advent of the data-driven and model-based technologies, which capitalize the computational power of the new generation computers (Konrad and R. Isermann 1996 and Mylaraswamy and Venkatasubramanian 1997). Excellent examples of design methodology can be found in paper by Willsky (1976) and Rolf Isermann (1984).

Modern diagnostic tools required a massive set of data collected from multiple and diverse sensor suites. Acquired data are topically transformed in features,or condition indicators, which are used as input to diagnostic routines. Automatic diagnostic systems normally presents the following main modules:
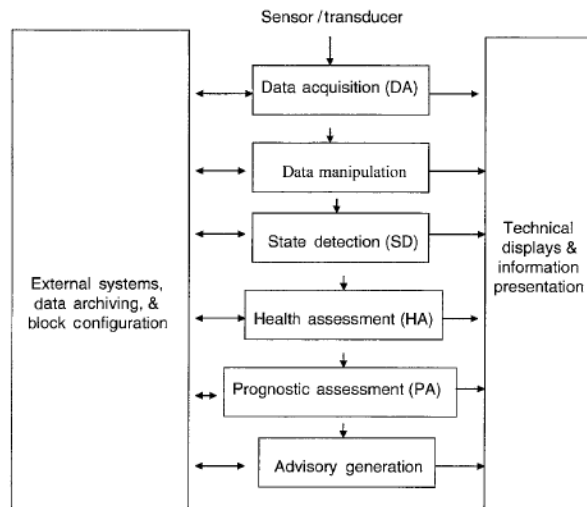
Figure 1.3: ISO 13374-1 processing model

- **Sensor suite:** to collect and process data of critical process variables and parameters

- **Operating modes identification routine:** that determines the current operational status of the systems

- **Failure extraction:** that extracts from the set of data the condition indicators to be used by diagnostic module

- **End user interface:** which must be as clear and simple as possible, to provide, without possible misunderstanding, the system that origins the fail and the type of degradation.

In the remainder of the section the main techniques used to diagnose the state of a system are presented, highlighting the advantages and disadvantages of each approach.

1.3.1 Requirements and performance metrics

Automatic diagnostic system designers must adhere to requirements imposed by the system user and conforming to overall system objectives; although it may be possible to define a generic set of requirements associated with diagnostic routines. In general the fault diagnostic requirements include:

- **Number of failure mode monitoring:** system shall monitoring no less than a percentage of the failure identified through RCM or FMECA analysis. The percentage is required from the end user

- **Number of failure identified:** system shall detect no less than a required percentage of the total monitored failures that occur to the component

- **False alarm rate:** the number of false alarms provided by the system must be a lower than a user-defined percentage, called also false positive

- **Time delay:** time span between the initiation and the detection of a fault event

- **False negative:** percentage of the missed fault condition. Missed detection may lead to a catastrophic catastrophic failure results.

Specific numerical requirement must be prescribed by the end users. It should be pointed out that there are no accepted standards for requirements, the community is currently debating these issues. Fault-diagnostic algorithms must have the ability to detect system performance, degradation level and failures based on physical property change through detectable phenomena. Furthermore, such algorithm must have the ability to identify the specific subsystem within the system being monitored that is falling, as well as the specific failure mechanism that has occurred. Since the ultimate objective of a PHM system is the prediction of the RUL, it is essential that faults be detected and isolate as early as possible.

Reduction false positives and false negatives, is a major objective of diagnostic system, several strategies are available to facilitate this important task:

- Data validation

- Optimal feature selection/extraction

- Optimal choice of fault detection algorithm

- Fusing features and evidence

The combination of these different techniques improves the results of the degradation identification algorithms; another important strategy is to validate and to optimize the algorithm in a continuous loop, using information provided from the system and the algorithm itself during the normal operations.

1.3.2 Alarm bounds approach

The use of bands of tolerance is one of the first approaches implemented to perform an automatic identification of the degradation. The idea, showing in figure 1.4, is to create the specific boundaries on measured sensor signals that indicate when an anomaly situation may be occurring. If the signal passes outside these bounds, an alarm is signaled. Note that the signal itself has confidence boundaries, due to the uncertainty of measurement, that must be take in to account in the detection of the degradation.
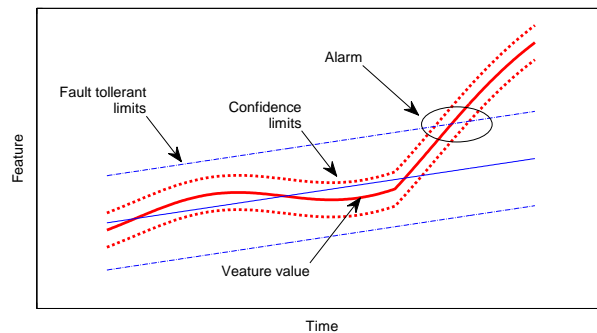
Figure 1.4: Alarm bounds

The alarm bounds can be determined using two basic methods. The first involves computing of the bounds directly on the current measured signals. An example is the Bollinger bands (Bollinger 2001), imported from the economy field,computed as the moving average plus/minus the moving variance. When the signal variation exceed the Bollinger bands, it has been observed that the significant trend changes may be imminent. The advantage of computing the bounds from the actual measures is that no pretraining or historical data are required.

However, in some situation historical data are available, therefore the useful information contained in them can be used to generate bounds; the advantage of this second case, is to be able to optimize the bands using known data.

In general, whatever is the choice to implement them, alarm bounds approach has the advantage to be easy to implemented, and the disadvantage of being strongly dependent on the amplitude of the bands. Narrow bands allow early identification of degradation, but are very sensitive to operating conditions then carry a high number of false alarms; in contrast bands too large are very robust, but favor false negatives.

1.3.3   Data-based approach

The data-based approach includes all the techniques whose implementation is based on historical data series. The series of historical data are analyzed using different technique to identify how the features vary between the nominal and degraded condition, the feature/degradation correlation and the feature/operative condition correlation.

The information obtained from data can be implemented in different algorithms, the most common are: alarm bounds, as seen above, statistical clustering and classification algorithms, and fuzzy logic. The data series are could even be used with machine learning algorithms, such ad neural network. In this case the data are used to make training cycles, in order to train the algorithms to recognize the degradations.

Clustering and classification   Statistical clustering and classification techniques are used to identify the mathematical laws that enabling the division of features, between the different operating conditions, depending on their value. The classification may occur in two or more dimensions, clearly much high is the number of dimensions, greater is the complexity of data interpretation.

In order to implement a system robust enough the choice of legacy data is very important, only component that are significantly correlated with the fault must be used, bootstrapping techniques could be use to determinate the confidence correlation levels.

Fuzzy logic classification   Fuzzy logic can be used to classify the status of the system. The definition of the fuzzy set of rules is obtained starting from the historical data; but the shape and the number of the ruler can be changed according to prior engineering knowledge. Example of the application of these techniques are proposed by T. I. Liu, Singonahalli, and Iyer 1996 and Mechefske 1998.

In some studies the fuzzy logic is implemented with neural networks, the combination of two techniques is called fuzzy artificial neural network (Sinha and Pandey 2002). The results of the neural network becomes the input of the fuzzy subsystem. The advantage is the possibility to correct the results of the neural network with the laws of fuzzy logic that are more easily modify and optimized.

Neural network classification   Several techniques for Neural Network (NN) classification are available in literature (Haykin 2011, Lippmann 1987 and F. W. Lewis, Jagannathan, and Yesildirak 1998). Neural network are

highly useful cor classification and clustering owing to their formal mathematical structure, their intuitive as being based on biologic nervous systems for data processing, and their learning features. NNs are classified according to the number of layers of neuron with which are implemented (in figure 1.5 a triple layers are shown). At each neuron in the layers (represented by circle), one can implement a non linear activation function, which is responsible for the powerful processing power of NN.
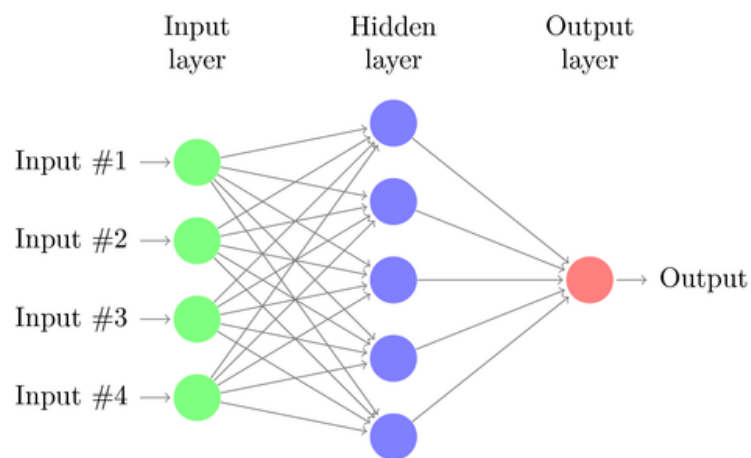
Figure 1.5: Neural network example

The number of layers defines the type of classification that the network can do, as shown in figure 1.6. A one-layer NN can only divided data using linear equation, two-layers NN can partition data in to convex regions. To solve more general sort of classification problems a three-layer NN is needed.

The accuracy of the identification algorithms based on historical data series, independently of the type of algorithms used, depends strongly on the quality of the data series. Using huge databases, collected by the same systems with different serial number and in a large number operating conditions, it is a solution that allows to have the best accuracy degradation identification. However, if the data sets are not sufficiently large, the quality of the results will suffer greatly, because the statistics, at the basis of this approach, can not identify the real correlations between the different variables, also analyzes performed on the data does not highlight how operative conditions affect the behavior of the system.
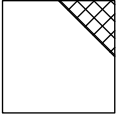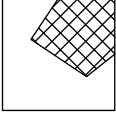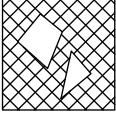
Structure	Types of decision regions	Most general region shapes
1-layer NN	Hyperplane	
2-layers NN	Convex regions	
3-layers NN	Arbitrary complexity depending on nr. of neurons	

Figure 1.6: Neural network decision regions

1.3.4 Data-driven approach

The availability of historical data series is often limited or absent, this forces the designer to develop algorithms that operate only with the data acquired by the system of prognostic during its operation. Data-driven approach could be considered as a kind of data-based approach, in which the databases are generated during the operations.

The data-driven approach requires a sufficient database, both in normal and fault condition, to train the algorithm. The generation of the database in normal conditions can become a limitation of this approach, because it means that until the generation of the data set, the PHM system is not functioning. In the case of systems with a quick dynamics, or in which a high frequency acquisition could made, the solution normally adopted is to accept that for a short period the PHM system does not protect the component. On other systems it is made of trial periods, in which the component is also monitored in another way, or the generation of the data set is seed up providing an initial set of data acquired from other components or from a test bench.

The same techniques presented in data-based approach could be implemented also for data-drive, but taking into account that the processes of learning and tuning of the algorithms will have to be made during the first phase of life of the system. Two other techniques, however, are specifically designed for a data-driven approach: expert system rulebase, Probability Density Function (PDF) comparison.

Expert system rulebase   It is a technique adopted only in the simplest cases, the idea is to translate the human approach in a set of rules implemented in the algorithm. Therefore the identification of the fault is made by following the same approach that would make the maintenance operator.

This approach, although not functional for complex systems, is often used because it is very easy to implement, and is easily understood by the end user. Normally, the expert indications are translate in a *IF* and *Logical connective* (*AND*, *OR*, *NOT*, etc.). Table 1.1 shown an example of expert rule implementation, proposed by G. Vachtsevanos et al. (2006).

Table 1.1: Expert rule detection

Condition	Fault Mode
IF(shaft vibration second mode is large) AND (motor vibration RMS vale is large)	THEN(Fault is gear tooth wear)
IF(third harmonic of shaft speed is present) AND (kurtosis of load vibration is large)	THEN(Fault is worn other ball bearing)

The conditions (left-column of table 1.1) can be physical parameters, sensor data and moments, frequency content information, etc. The problem of these conditions is to define a clear characterization of the terms used, as the term *large*. Such information may be obtained by a combination of physical modeling, expert opinion, and historical legacy fault data.

Probability density function comparison   The probability distribution of the values of the features changes depending on system status, comparing the PDF of the data obtained from a capture window made under normal conditions, and that obtained instead degraded condition is therefore possible to recognize the presence of a fail. The idea is generate a PDF distribution in normal condition, called *baseline*, during the initial of the operative life of the component. Subsequently, the *baseline* is compared with the probability distribution function that is obtained within a moving acquisition window, called *actual*.

If the system remains in good condition the two PDF will be superimposed or little moved, instead in the presence of a degradation of the *actual* begins to move away from *baseline*. When the two curves will be completely separate degradation can be identified with confidence of 100%.

The centerpiece of this methodology is the possibility to easy translate customer specifications into acceptable margins the detection routine:

- **False alarm rate:** defined as the probability of a false alarm. It is translate in type I error coefficient.

- **Confidence:** coincides with 100-Type II error and it expresses the level of confidence with which a degradation is detected.

Type I error coefficient represents the part of *baseline* PDF which is eliminated by the algorithm, the algorithm considers only the part of the PDF whose area subtended is 100-type I error. In this way time from start of the degradation to its identification is reduced, but the possibility of false alarms increases. Type II error represents the maximum overlap between the two curves for which degradation is identified. Being that the two PDF curves are not completely separated, the confidence of the degradation is then equal to 100-Type II error.

The figure 1.7 shows the instant in which the presence of the degradation is identified, two PDF curves are superimposed only by an amount equal to the type II error, net of type I error.
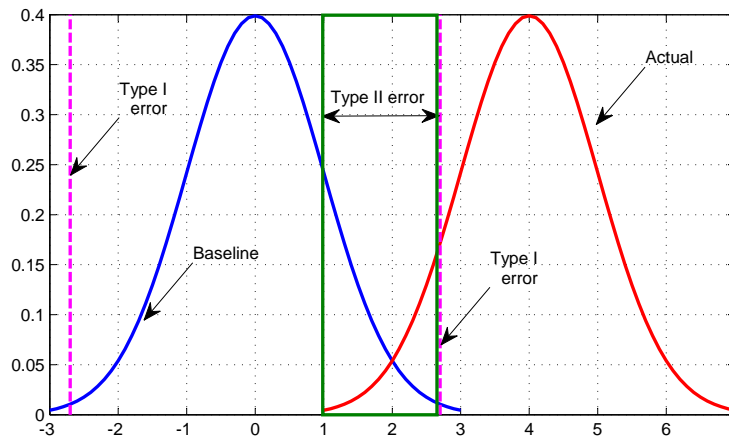
Figure 1.7: Detection using PDF comparison

1.3.5   Model-based approach

Model-based approach takes advantage of the actual system and model outputs to generate a "discrepancy" or residual (innovation), as it is known, between the two outputs that is indicative of a potential fault condition.

Model-based techniques rely on an accurate dynamic model of the system and are capable of detecting unanticipated faults.

This approach can be pursued in two distinct ways: using dynamic system models or physical-based models. In both cases the main problems are the accuracy of the model and take into account all the external conditions that may affect the behavior of the modeled system. Using a model inaccurate, the source of the discrepancy between model and real system output is not certain: it may be due to a degradation or to a model error or to an external disturbance. For this reason adaptive models are often used, they are system able to auto tuning the parameter during the early stages of life.

Another problem of the model-based approach is the high computing power required, generally the models are not able to work on on-board electronic units, therefore a system for the transmission of the acquisitions from the vehicle to the processing server must be provided. With the increase in computing power of the processors, and the reduction of costs, some real-time models are beginning to be implemented on-board, but generally they have a lower accuracy than those that run on dedicated server.

Ordinary Differential Equations model   Modeling in terms of Ordinary Differential Equations (ODEs) provides a powerful method for extracting physical models of processes and can be performed in terms of Lagrangian or Hamiltonian dynamics, approximation methods applied to partial differential equations, distributed models, and other techniques. ODEs can be further expressed in the state-variable form, which opens the door for exploiting a host of modern techniques for signal and system processing based on firmly established numerical computational techniques. An example is provided from Skormin, Apone, and Dunphy (1994), that use ODE model for identify the degradation in a electrohydrostatic flight actuator.

Kalman filter   Another mathematical tool which is widely used within the mathematical model is the Kalman Filter (F. L. Lewis 1986). It is a dynamic systems tool for estimating unknown states by combining current measurements with the most recent state estimate. It provides estimates of quantities of interest that may in themselves not be directly measurable. In the case of linear systems and Gaussian noise, these estimates are optimal in the sense of minimizing an estimation-error covariance. Knowledge of noise processes is used to minimize this estimation error covariance via the optimal determination of the so-called Kalman gain. The Kalman filter also provides confidence bounds for the estimates in terms of the error covariance matrix. It is also commonly used in prognostic applications. Worthy examples of the

Kalman filter application are An and Sepehri 2003 and Oliva, Weihrauch, and Bertram 2011.

Particle filter   Particle filtering is an emerging and powerful methodology for sequential signal processing with a wide range of applications in science and engineering (Arulampalam et al. 2002). Founded on the concept of sequential importance sampling (SIS) and the use of Bayesian theory, particle filtering is very suitable in the case where the system is nonlinear or in the presence of non-Gaussian process/observation noises. Furthermore, particle filtering allows information from multiple measurement sources to be fused in a principled manner, which is an attribute of decisive significance for fault detection/diagnosis purposes.

The underlying principle of the methodology is the approximation of the conditional state probability distribution using a swarm of points called particles and a set of weights associated with them representing the discrete probability masses. Particles can be generated and recursively updated easily (Arulampalam et al. 2002) given a nonlinear process model, a measurement model, a set of available measurements, and an initial PDF estimation for the state. Among the researcher that have allowed the evolution of the particle filter as a well-structured tool for diagnosis and prognosis, Vachtsevanos George and Orchard Marco deserve a special mention for the number and the quality of the proposed work, M. E. Orchard and G. J. Vachtsevanos 2009, M. E. Orchard and G. J. Vachtsevanos 2007 and Brown et al. 2009.

physical-based model   The physical models, mathematical models are implemented using the physical equations that describe each phenomenon; unlike the tools presented previously in which the models are obtained by fitting experimental data, in this case the models are formed by writing set of physical equations, thus they are very connected to structure of the system. This approach allows to obtain models with very high accuracy, but despite this, they do not get a great application because of their complexity and of the long time required to implement them. In addition a PHM system based on physical model has a very specific structure, modeled on the components considered, apply the same PHM system to a new component is practically impossible.

To date, the physical model-based approach find primarily application in structural integrity application, specifically in fatigue crack propagation and in corrosion propagation. This is due to the fact that the literature provides numerous studies on the two phenomena, also accurate and validated physical models of propagation of fatigue cracks and corrosion can easily be found in

the technical literature.

1.4   Prediction of residual useful life

Prognosis is the ability to predict accurately and precisely the remaining useful life of a failing component or subsystem. Prediction of Residual Useful Life (RUL) is one of the more challenging aspects of the PHM, it also has the potential to be the most beneficial in therm of reduced operational costs, life-cycle total costs and improve safety. Long-term prediction of the fault evolution to the point that may result in a failure requires means to represent and manage the inherent uncertainty. Uncertainty representation implies the ability to model various forms of uncertainty stemming from a variety of sources, whereas uncertainty management concerns itself with the methodologies and tools needed to continuously "shrink" the uncertainty bounds as more data become available. Moreover, accurate and precise prognosis demands good probabilistic models of the fault growth and statistically sufficient samples of failure data to assist in training, validating, and fine-tuning prognostic algorithms.

Foretelling the future in a wide area of disciplines from business to weather forecasting, among many others, has attracted the interest of researchers over the past decades, with results that vary from disappointing to promising. In the engineering disciplines, fault prognosis has been approached via a variety of techniques ranging from Bayesian estimation and other probabilistic methods to artificial intelligence tools and methodologies based on notions from the computational intelligence arena. Specific enabling technologies include multistep adaptive Kalman filtering (F. L. Lewis 1986), autoregressive moving-average models (F. L. Lewis 1992), stochastic autoregressive integrated-moving-average models (Jardim-Goncalves et al. 1996), and parameter estimation methods. Other methodologies, such as neural networks, fuzzy systems, and neuro-fuzzy systems (Studer and Masulli 1996), have found ample utility as prognostic tools.

The choice of strategy to be used to estimate the RUL she depends on many factors, including the information available, the costs that can be supported, and the range of systems that the designer want to cover. Figure 1.8 (G. Vachtsevanos et al. 2006) summarizes the range of possible prognosis approaches as a function of the applicability to various systems and their relative implementation cost. Prognosis technologies typically use measured features, as well as data-driven or physics-based models, to predict the condition of the system at some future time. Inherently probabilistic or uncertain in nature, prognosis can be applied to failure modes governed by material
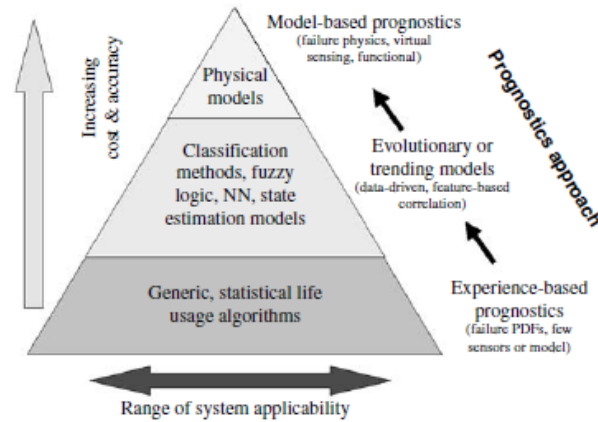
Figure 1.8: Prognosis technical approaches

condition or by functional loss. Prognosis algorithms can be generic in design but specific in terms of application. Depending on the criticality of the subsystem being monitored, various levels of data, models, and historical information will be needed to develop and implement the desired prognostic approach.

1.4.1   Requirements and performance metrics

There is no general agreement as to an appropriate and acceptable set of metrics that can be employed effectively to assess the technical performance of prognostic systems. A prognostic algorithm should provide two basic results: the predicted time of failure and the confidence interval, therefore quantitative measures of the prediction performance should take both results into account.

Two performance measures are historically considered to dominate the prognosis task: accuracy and precision:accuracy measures the closeness of the predicted value to the real value, and precision implies how close the predictions are clustered together. A comprehensive review on metrics for prognostics was proposed by A. Saxena et al. (2008), which are not oly analyzed the metrics used in various fields, from economics to engineering, but also innovative ones have been proposed.

Subsequently the metrics used for this Ph.D. project will be presented, but first make a brief introduction to the nomenclature used in PHM could be useful. Figure 1.9 shows an example of RUL estimation, the blue line called r_* is the real RUL while the red line, indicated as r', is the estimated RUL; i is the index for time instant t_i. Graph displays three important time

instants: t_P is time at which the first prediction is made by the prognostic system, t_{EOL} is the time index of actual End Of Life and t_{EOP} is the earliest time index when prediction has crossed the failure threshold. As show in the graph t_{EOL} and t_{EOP} generally do not coincide, otherwise the accuracy of the prediction would be maximum.
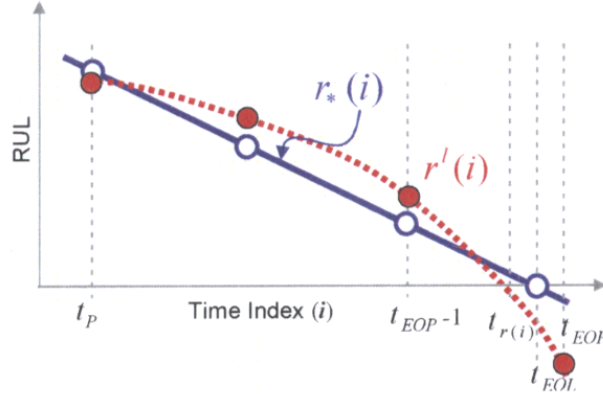
Figure 1.9: Prognosis result example

In the presented Ph.D. research project five different metrics are use for to assess the quality of the forecast, three evaluate the overall accuracy, one for the precision and the last one the prognostic horizon, below all the metrics are detailed.

Relative accuracy (RA) Defined as the relative accuracy between actual and estimate end of life time instant, perfect score is obtained for RA = 1. It is calculated using the equation 1.1, where t_λ is defined as $t_\lambda = t_P + \lambda(t_{EOL} - t_P)$, λ is in the rage 0 to 1.

$$RA(t_\lambda) = 1 - \frac{r_*(t_\lambda) - r'(t_\lambda)}{r_*(t_\lambda)} \tag{1.1}$$

Cumulative Relative Accuracy (CRA) The cumulative relative accuracy is the normalized sum of the relative prediction accuracies at specific time instances. It provides a more complete idea respect the relative accuracy, since no only evaluate in a specific time instant but offers a overall valuation of the algorithm.

$$RA(t_\lambda) = \frac{1}{t_{EOL} - tP - 1} \sum k = 1^2 RA(k) \tag{1.2}$$

α-λ **performance** Allows to verify that the prediction to a generic time instant λ has an accuracy better than α, where α is a percentage indication

of the desired accuracy. The results of equation 1.3 are two bounds that represent the minimum accuracy required, if the prediction is inside of the bounds the accuracy is achieved. t_λ is defined as $t_\lambda = t_P + \lambda(t_{EOL} - t_P)$, λ is in the rage 0 to 1

$$(1 - \alpha)r_*(t_\lambda) \leq r'(t_\lambda) \leq (1 + \alpha)r_*(t_\lambda) \qquad (1.3)$$

Precision Precision is a measure of the narrowness of an interval in which the remaining life falls, the precision associated with a prediction algorithm is high if the predicted values are clustered together around the actual value and it is low if the predicted values are scattered over the output range. Defining the prediction error $E_{EOL} = t_{EOL} - t_{EOP}$, the mean error and the variance of the prediction error are obtained as follow, where N is the number of samples.

$$\bar{E} = 1/N \sum k = 1^N E_k$$
$$\sigma^2 = 1/N \sum k = 1^N (E_k - \bar{E}) \qquad (1.4)$$

The precision at a specific prediction time t_i is given by the formula 1.5, where R_i is the confidence interval of the prediction at a specific time interval i, σ_i is the variance at a specific time interval i, R_0 and σ_0 are are normalizing factors depending on specific applications.

$$P(t_i) = \left(1/N \sum k = 1^N e^{R_i/R_0}\right) e^{\sigma_i^2/\sigma_0} \qquad (1.5)$$

Prognostic horizon $(H(i))$ Defined as the difference between the current time index i and the end of prediction (EOP) utilizing data accumulated up to the index i, provided the prediction meets desired specification. Wider prognostic horizon ensures more time between the prediction and the need for maintenance, thus facilitating logistics operations and the schedule of maintenance.

1.4.2 Model-based approach

Model-based approaches include the algorithms that using dynamic model in order to predict the RUL. These can include physics-based models, autoregressive moving-average (ARMA) techniques, Kalman/particle filtering, and physical-based models. Model-based methods provide a technically comprehensive approach that has been used traditionally to understand component failure mode progression. By combining mathematical models and stochastic, the model can be used to evaluate the distribution of remaining useful

component life as a function of uncertainties in component strength/stress properties, loading, external conditions for a particular fault. Statistical representations of historical operational profiles serve as the basis for calculating future damage accumulation.

Model-based approaches to prognosis differ from data-driven or probability-based approaches in that they can make RUL estimates in the absence of any measurable events, but when related diagnostic information is present, the model often can be calibrated based on data acquired from the observed system. Therefore, a combination of data-driven and model-based approaches provides full prognostic ability over the entire life of the component.

To perform a prognosis with a model, an operational profile prediction must be developed using the steady-state and transient loads, temperature or other online measurements. With this capability, probabilistic critical-component models then can be the RUL estimation by creating statistical simulations of future operating profiles from the statistics of past operational profiles or expected future operating profiles. The nonlinear nature associated with many damage mechanisms depends on both the inherent characteristics of the profiles and the operational mix types. Significant component damage resulting from the large variability in the operating environment and severity of the missions directly affects the system component lifetimes. Therefore a careful and precise definition of the external condition and operative load is absolutely necessary.

The model-based approach is mainly used in those fields in which accurate and validate fail to failure model could be easy found in the literature, as fatigue crack. Also the use of models is limited by the computing power of the processor used, therefore this approach is preferred when the prediction can be evaluated off-line using specific server or computer. In the case of prognostic completely on board other systems, such as those data-driven they are generally preferred.

Physical-based model Dynamic models of fault progression are derived by using principles of physics, these models are in fact much appreciated by the scientific community because they maintain a strong connection with the physical structure of the component. The main limits to their diffusion are two: the elevate computation resources required and the absence of fail to failure model in literature. The primary application field is the fatigue models, because crack propagation models are well defined and validate.

Autoregressive method The autoregressive family is a set of mathematics tools very useful when is difficult or impossible to derive dynamic models

based on all the physical processes involved. In such cases, it is possible to assume a certain form for the dynamic model and then use observed inputs and outputs of the system to determine the model parameters needed so that the model indeed serves as an accurate surrogate for the system. This engineering and mathematics field is known as model identification, input-output data provided from the real system are use by means of special algorithms in order to estimate and validate the parameters of the mathematical model. The literature provides several examples of techniques to optimize the extraction of the coefficients as Ljung 1987 and Makridakis, Wheelwright, and Hyndman 2008.

Particle filter   Bayesian estimation techniques are finding application domains in machinery fault diagnosis and prognosis of the remaining useful life of a failing component/subsystem; the name was coined in 1996 by Del Moral 1996 in reference to mean field interacting particle methods used in fluid mechanics since the beginning of the 1960s, but an important development for its use in the RUL estimation was performed at Georgia Institute of Technology M. Orchard, Wu, and G. Vachtsevanos 2005. The approach proposed by M. Orchard, Wu, and G. Vachtsevanos employs a state dynamic model and a measurement model to predict the posterior probability density function of the state, that is, to predict the time evolution of features. It avoids the linearity and Gaussian noise assumption of Kalman filtering and provides a robust framework for long-term prognosis while accounting effectively for uncertainties. Correction terms are estimated in a learning paradigm to improve the accuracy and precision of the algorithm for long-term prediction.

Prediction of the evolution of a fault indicator entails large uncertainty. Accurate and precise prognosis of the time to failure of a failing component/subsystem must consider critical-state variables as random variables with associated probability distribution vectors. Once the probability distribution of the failure is estimated, other important prognosis attributes, such as external and operative conditions, must be computed. Recursive Bayesian estimation techniques that combine both the information from fail to failure models and online data obtained from sensors monitoring key fault parameters are a possible solution.

1.4.3   Probability-based approach

Probabilistic methods for prognosis are very effective in situations in which historical data from previous are they are available in an amount sufficient to be able to perform statistical analyzes, and when determining a complete dynamic model in terms of differential being considered may be unnecessary

or impractical. These methods require less detailed information than model-based techniques because the information needed for prognosis resides in various probability density functions; advantages are that the required PDFs can be found from observed statistical data and that the PDFs are sufficient to predict the quantities of interest in prognosis. Predicting failure based on model-approach is further complicated by the fact that one must take into account manufacturing variability, mission history variations, and life degradation that are probabilistic information and effect, so implement such effects in a probability-based approach is more immediate.

The provability-based approach also generally give confidence limits about the results, which are important in giving a feeling for the accuracy and precision of the predictions. The family of statistical algorithms most used in the probabilistic-based approach is the Bayesian probability theory, A complete viewpoint on probabilistic techniques in prognosis as related to predicting the remaining useful life (RUL) is given by Engel et al. 2000.

1.4.4   Data-driven approach

In many cases use large set of historical data to implement probability-based algorithms or to identified the parameters or an autoregressive model is impossible, for example in case of design and development of new components or in case of PHM system for legacy components of which historical databases are not presents. In such situations, one may use nonlinear network approximators that can be tuned using well-established formal algorithms to provide desired outputs directly in terms of the data. Nonlinear networks include the neural network and fuzzy-logic systems, which are based on the linguistic and reasoning abilities of humans. These are similar in that they provide structured nonlinear function mappings with very desirable properties between the available data and the desired outputs.

In prediction, artificial neural networks (ANNs), fuzzy systems, and other computational intelligence methods have provided an alternative tool for both forecasting researchers and practitioners (Sharda 1994). Werbos(1988) reported that ANNs trained with the backpropagation algorithm outperform traditional statistical methods such as regression and Box-Jenkins approaches. Unlike the traditional model-based methods, ANNs are data-driven and self-adaptive, and they make very few assumptions about the models for problems under study. ANNs learn from examples and attempt to capture the subtle functional relationship among the data. Thus ANNs are well suited for practical problems, where it is easier to have data than knowledge governing the underlying system being studied. The main problem of ANNs is that their decisions are not always evident. Nevertheless,

they provide a feasible tool for practical prediction problems.

Unfortunately, standard statistical methods for confidence estimation are not directly applicable to neural networks, but in the last years same research correlated to this problem were published. Chryssolouris, Lee, and Ramsey (1996) used an assumption of normally distributed error associated with a neural network to compute a confidence interval. Nonlinear regression to estimate prediction intervals by using weight decay to fit the network is proposed by Ungar, De Veaux, and Rosengarten 1996. Other methodologies are proposed by Hwang and Ding 1997 and by Carney, Cunningham, and Bhagwan 1999.

1.5 PHM for flight control actuators

The aerospace industry is likely the field with the most vibrant research and development activity in systems prognostics today, the reasons are the difficult and cost of systems health inspections, in addition the consequence of a premature failure can be catastrophic. The transition to PHM architectures is the natural continuation of the evolution trend seen in the area of airplane maintenance; which has always progress towards the maintenance based on condition in order to reduce costs and to increase the safety. As the prognostic systems make their way into the commercial aerospace sector, they are expected to help with maintenance scheduling, optimal operating mode determination, and asset purchasing decisions. Prognostic algorithms are beginning to be applied to monitoring condition of aircraft structures, avionics, wiring, power supplies, and propulsion systems. Prognostic functionality is being incorporated into the health management system of the latest military aircraft (e.g. Joint Strike Fighter Ferrel 1999, and Hess 2001) and civilian aircrafts, in order to reduce the overall lifecycle cost and improve flight readiness.

Hydraulic flight control systems are an aerospace engineering area where PHM has found so far very limited interest, although they are one of the critical aircraft systems. Moreover primary flight control actuators for fly-by-wire commercial airplanes service and for aircrafts under development are almost invariably electrohydraulic servoactuators; the only exception are some Electro-Hydrostatic Actuators (EHAs) used as a backup to conventional EHSAs in the flight control systems of Airbus A380, A350 and Gulfstream G650. Even if ElectroMechanical flight control Actuators (EMAs) are considered by the engineers and large companies the future solution for the drives of flight controls, the sensitivity to certain single point of failures, that can lead to mechanical jams, results in a reluctance to adopt EMAs for

flight safety critical applications; EMAs for primary flight controls have so far been limited to UAVs (Jacazio 2008).

Byington and colleagues are one of the few research groups interested in the development of prognostics and health management system for electrohydraulic flight control actuators. In Byington, Watson, and Edwards 2004 the authors examined the possibility of developing a PHM system for the electrohydraulic servovalve of *F/A-18* stabilizer. The data-drive approach developed uses neural network error-tracking techniques, along with automated fuzzy logic classifiers; the estimation of the RUL is made using Kalman filter state predictors. The algorithms of identification degradations were validated using a set of EHSVs with known levels of degradation that were obtained from the Naval Air Depot in North Island (USA), while the prediction phase has not been validated.
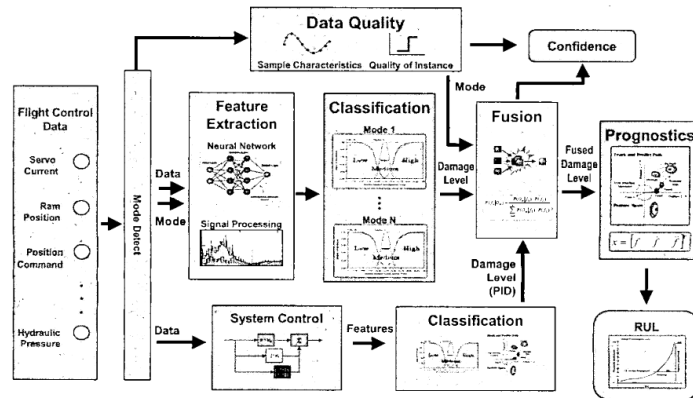
Figure 1.10: PHM system proposed by Byington et al

The paper provided important insights for the research project presented in this thesis, but two technical solutions adopted make impossible to use the same methodology for legacy commercial airplanes. First, the algorithm for degradations identification takes advantage from the differential pressure sensor placed on the actuator, the information provided from this transducer are very useful for estimate the external force acting on the actuator. But the differential pressure sensor is not normally present in commercial airplanes EHSAs, therefore in the present thesis it was not considered. The second limitation of the proposed strategy is its complexity, as shown in the figure 1.10, the strategy implemented presents different subsystems interconnected, these different tools allow to refine the feature extraction process, and thus improve the overall performance PHM system. However, the combination of all these different tools greatly increases the capacity of calculation, and reduces the flexibility of implementation, such a complex system can hardly

be installed in a real-time on-bord platform.

The work presented by De Oliveira Bizarria and Yoneyama (2009) is model-based approach to prognostics and health monitoring for an electrohydraulic flight control actuator. The aim of the research is to develop a model-based methodology to detect, diagnose and prognosticate a fault in an electrohydraulic primary flight control actuator that precedes an imminent failure. The authors proposed a good selection of features, even if some of these, for example the frequency response, are difficult to extract from EHSAs in operative conditions. The work, however, does not take into account different operating conditions in which the component can operate, thus the algorithms are not robust to changing of environmental conditions and external loads.

Two interesting paper about the identification of optimal strategies for the identification of faults in the hydraulic valves have been proposed by Ribeiro et al. 2015 and Ramos Filho and De Negri 2013. First work presents a method to select parameters used to identify the degradation level of an aeronautic pressure regulator and shutoff valve; the second proposes a mathematical model for online fault detection on single solenoid servo-proportional valves. In both searches, important studies for the identification of the best features were conducted, each index of health was evaluated for different pressures, oil temperatures and other operative conditions. Unfortunately, both the research study the behavior of the valve isolated from the rest of the system, thus the influence of the other components is not taken into account in the features selection, this means that the research work are little significance.

Borello et al. 2009 have presented a PHM model-based approach for electrohydraulic servovalves, the proposed solution is robust and functional for the fails identification part, while it is lacking in the RUL estimation. The PHM functions are performed during the pre-flight check because, with the airplane on ground, the loads acting on the wing surface are very small and actually negligible. The RUL are estimated using a linear interpolating function, this solution has the advantage of being little time consuming, but does not offer a sufficient accuracy level, also no confidence estimation algorithm is implemented.

An interesting research, even if not strictly connected with the prognostics and health management, was developed by Angadi et al. (2009a, 2009b); the goal of this work is characterize solenoid valve failures using accelerated tests and finite element models. The papers allow to understand what are the main causes of failure of the electric part of solenoid valves, and how these affect the overall behavior of the component. The indications have proved very useful in the selection and modeling of the degradation of a servovalve.

In the last years several research and development of PHM systems for

electromechanical flight control actuators were presented due to growing interest in Unmanned Aerial Vehicle (UAV). Although the type of actuation is different these works can provide important ideas for the development of a PHM system for EHSAs, that because the operational conditions and various problems are common for both EHSAs and EMAs.

One of the most complete research regarding the EMAs diagnostic was developed by NASA Ames Research Center (Narasimhan et al. 2010), the presented approach uses analytical models for the electrical, mechanical and thermal properties in conjunction with a classifier based on features derived from vibration data. The tested EMA has been involved in two flight experiments on *C-17* aircraft and on *UH-60* helicopters. The collected data, in nominal and fail conditions are used for tested the PHM systems, the results are considered very encouraging. An interesting preliminary work of the same group shows all the steps that led to the definition of degradation deserving to be identified (Balaban et al. 2009).

Remarkable is the research work presented by Brown et al. (2009), in which is explored the possibility of using the particle filter not only for the RLU estimation but also for the failures identification in EMAs. The results presented show that the particle filter, combined with update model parameters algorithm, is robust enough to work in different operating conditions, always providing the good level of accuracy and high confidence.

For completeness and abundance of details also the work of Gillen, Bernstein, and Wilson (2005) has been introduced in this paper review. Authors derive a method for estimate the lifetime of o-rings, the methodology was validated with empirical tests conducted in the laboratory. The paper provides a variety of information about the causes of degradation and about the parameters that affect the life of polymer seals, these indications provide a useful support in the development of degradation models and in the implementation of PHM algorithms.

2

Reference servoactuator

The choice of the reference ElectroHydraulic Servo Actuator (EHSA) has been dictated by the desire to design and develop a Prognostic and Health Management (PHM) system for the largest number of legacy aircraft. Nowadays civil aircraft that have known the greatest commercial success are the *Airbus A320 family* and the *Boeing 737 series* (Airbus S.A.S. 2013 and Boeing Company 2015); both are short to medium-range twinjet narrow-body airliner, used by airlines company mainly for continental flights. In the ranking of commercial successes a good level is achieved by *Boeing 777 series* (Boeing Company 2015), a family of medium to long-range wide-body twin-engine jet airliners.

The limited autonomy and the use in continental routes, implies that these types of aircraft carry a number of take-offs and landing much greater compared to long-range aircraft, for the same flight hours. The large number of units and the exhausting flight conditions to which these aircraft are subjected, make the *Airbus A320 family*, the *Boeing 737 series* and *Boeing 777 series* the ideal objectives for a PHM system. Another point in favor of this type of aircraft is the use of digital fly-by-wire flight control systems, which allow, unlike the mechanical or hydromechanical structure, the acquisition of various signals during their operation, without the necessity to add new sensors.

Between the different flight controls, this research project focuses the attention on the primary control, inasmuch are the most most safety-critical surfaces because guarantee the stability of the aircraft; in particular, the flaperon has been chosen as the reference surface.

29

2.1   Flight control system overview

Airplanes, as every rigid body free to move in a fluid without any constraint, are characterized by 6 degrees of freedom: 3 translation and 3 rotation. Defined a Cartesian coordinate system with the origin coincident with the center of mass of the airplane as shown in figure 2.1, and the three principal axes oriented as:

- **Longitudinal axis:** passes through the plane from nose to tail, positive in the normal direction of flight

- **Vertical axis:** perpendicular to the wings with its origin at the center of gravity and directed towards the bottom of the aircraft

- **Lateral axis:** parallel to the wings

the three translations along the three axes could be called with the same name of the axes, the rotation around the longitudinal axis takes the name of roll, the one around the lateral axis is call pitch and the last yaw. The variation of the 6 degrees of freedom is controlled by the pilot acting on the thrust generated by the engine and on the flight control surfaces.
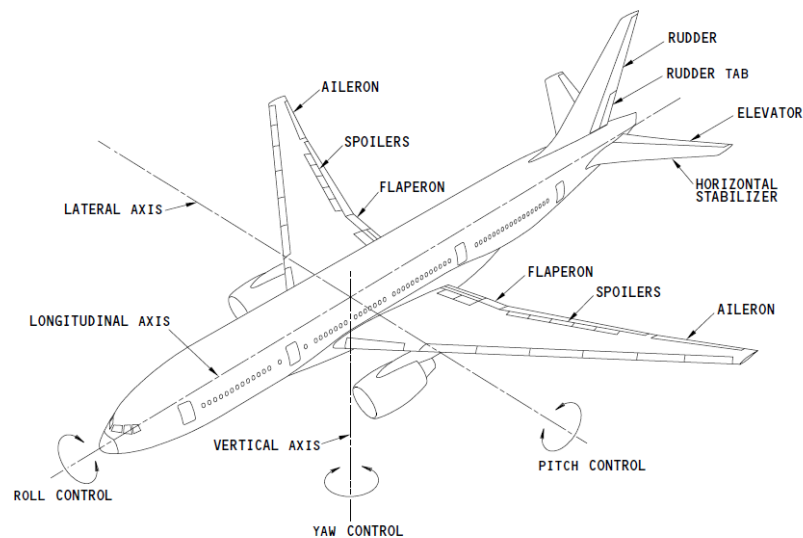
Figure 2.1: Position of the three principal axes

A modern airplane have two types of flight control surfaces: the primary flight control systems and the high lift control systems. The primary flight

controls are used to control aircraft movement the three principal axes, and are essential for maintaining the trim of the aircraft, therefore can be considered safety-critical components. Secondary flight controls, or high lift control systems, are used to optimize the aerodynamic configuration. Operation of the high lift control systems increases the wing lift so the airplane can take off and land at lower speed and higher weight. They are operated intermittently so they are less flight critical.

Flight control actuation systems have evolved through three generations since the general adoption, for commercial aircraft, of full digital fly-by-wire flight controls. Mechanical or manually operated flight control systems were used in early aircraft and are currently used in small aircraft where the aerodynamic forces are not excessive. A manual flight control system uses a collection of mechanical parts such as pushrods, tension cables, pulleys, counterweights, and sometimes chains to transmit the forces applied to the cockpit controls directly to the control surfaces. Increases in the control surface area required by large aircraft, or higher loads caused by high air speed, lead to a large increase in the forces needed to move them, consequently complicated mechanical gearing arrangements were developed to extract maximum mechanical advantage in order to reduce the forces required from the pilots (Taylor 1996).

When the complexity and weight of mechanical flight control systems increase considerably with the size and performance of the aircrafts, the hydraulically powered control surfaces help to overcome these limitations. With hydraulic flight control systems, the aircraft's size and performance are limited by economics rather than a pilot's muscular strength. At first, only-partially boosted systems were used in which the pilot could still feel some of the aerodynamic loads on the control surfaces (Taylor 1996).

A hydro-mechanical flight control system has two parts: the mechanical circuit, which links the cockpit controls with the hydraulic circuits. Like the mechanical flight control system, it consists of rods, cables, pulleys, and sometimes chains. The hydraulic circuit, which has hydraulic pumps, reservoirs, filters, pipes, valves and actuators. The actuators are powered by the hydraulic pressure generated by the pumps in the hydraulic circuit. The actuators convert hydraulic pressure into control surface movements. The pilot's movement of a control causes the mechanical circuit to open the matching valve in the hydraulic circuit. The hydraulic circuit powers the actuators which then move the control surfaces. As the actuator moves, the valve is closed by a mechanical feedback linkage - one that stops movement of the control surface at the desired position.

The last evolution of flight controls is fly-by-wire (FBW) system, that replaces mechanical circuit of hydro-mechanical controls with an electronic

interface. The movements of cockpit are converted to electronic signals transmitted by wires (see figure 2.2), and flight control computers determine how to move the actuators of each control surface to provide the expected response. The flight computer processes, in addition to the cockpit position, even the information provided from motion sensors, airstream sensors and fuel sensors in order to maintain the stability of the airplane (Pratt 2000).
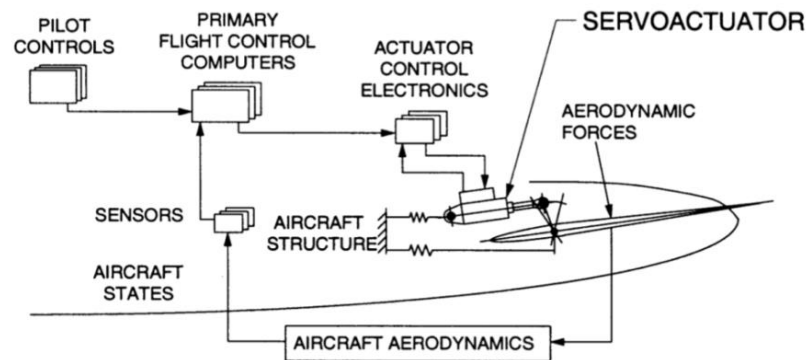
Figure 2.2: The fly-by wire EHSA and its interactions

2.1.1   Primary flight control systems

The primary flight controls are the surface used to control the airplane around the thee axes: longitudinal, vertical and lateral. In the FBW system the command position of each surface is generated from the flight control computer as result of pilot command and information from motion sensors, airstream sensors and fuel sensors. The primary flight control ensure the maneuverability and stability of the aircraft, hence they are considered safety critical systems. In order to ensure a redundancy, in case of failure of one of the EHSAs, these are duplicated and / or tripled depending on the important of the surface.

The figure 2.3 shows the layout of the primary controls of *Boeing 777*, the aircraft has three independent hydraulic circuits, which are used to supply the different EHSAs that act on the various surfaces. As seen in the scheme, each surface is controlled by two EHSAs in parallel, except the rudder that is controlled by three EHSAs, this allows you to control the aircraft even when an actuator or a hydraulic system fails (SAE International Group 2012).

Normally, in the absence of a fault only one of the two EHSAs is active, while the other actuator sees its chambers connected through a by-pass, this configuration has two advantages, the first is to avoid the creation of fighting
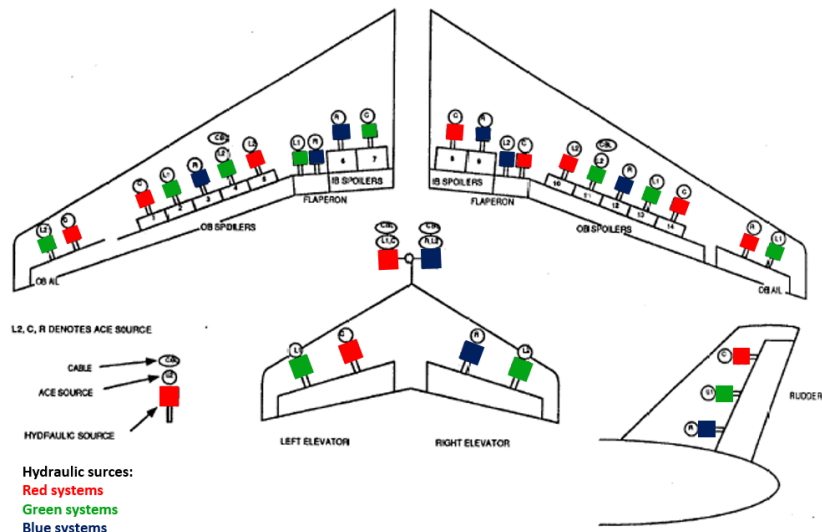
Figure 2.3: Layout of the primary controls of *Boeing 777*

force, and also, second advantage, the by-pass actuator acts like a damper thus reducing the oscillations of the wing surface. In case of failure the active actuator , the one the by-pass is connected to the respective hydraulic system, while the broken one is placed in by-pass.

The *Boeing 777* primary flight control EHSAs are: rudder, left and right ailerons, left and right elevators, left and right flaperons, horizontal stabilizers and spoilers. The rotation around the roll axis is obtained by controlling the ailerons and flaperons, sometimes the effect of spoiler is combined with ailerons and flaperons in order to obtain more rapid turns. During a turn around roll, the aileron and flaperon on one wing move in an opposite direction from the aileron and flaperon on the other wing. The spoilers move only on the down wing and do not move on the up wing. The pitch variation controlled by the horizontal stabilizer and the elevator, the first are used for long slow changes while the second for rapid variations. The rudder controls the yaw displacement.

2.1.2 High lift control systems

In addition to the primary flight controls for roll, pitch, and yaw, there are often secondary controls are available to give the pilot finer control over flight or to ease the workload. The most commonly available secondary surface are flaps, slats and air brakes. Normally the secondary controls are not controlled in continuous, but progressing at discrete positions according

to flight condition.

Flaps are devices used to alter the lift characteristics of a wing and are mounted on the trailing edges of the wings of a fixed-wing aircraft to reduce the speed at which the aircraft can be safely flown and to increase the angle of descent for landing. They do this by lowering the stall speed and increasing the drag. Flaps shorten takeoff and landing distances. The flaps work symmetrically on the two wings, and are controlled through discrete positions, depending on the speed of the aircraft and the angle of descent. Flaperons can be used in order to increase the effects of the flaps.

The slat work like the flap, are on the leading edge of the wings and when deployed, allow the wing to operate at a higher angle of attack. A higher coefficient of lift is produced as a result of angle of attack and speed, so by deploying slats an aircraft can fly at slower speeds, or take off and land in shorter distances. They are usually used while landing or performing maneuvers which take the aircraft close to the stall, but are usually retracted in normal flight to minimize drag.

In aeronautics, air brakes or speedbrakes are a type of flight control surfaces used on an aircraft to increase drag or increase the angle of approach during landing. Air brakes differ from spoilers in that air brakes are designed to increase drag while making little change to lift, whereas spoilers reduce the lift-to-drag ratio and require a higher angle of attack to maintain lift.

2.2   *Boeing 777* flaperon EHSAs

The *Boeing 777* flaperon (figure 2.4) flight control systems is a fully integrated fly-by-wire flight control unit that control the flaperon surface in response to electronic signals from the flight control computer. Each flaperon surface, one for wing, is controlled by two different EHSAs supply by two separated hydraulic systems, in normal configuration one is active and the other one is in by-pass.

Figure 2.4: *Boeing 777* flaperon

The position loop for a single EHSA is close by two controller placed in parallel, in normal operation each controller provide the half of the servovalve command current, in the case one of the two fails, the remaining controller is capable overcome the lack providing all the necessary current.

The servoactuators are positioned between the flaps and aileron, the EHSAs are located in the cavity wing, refer to figure 2.5 the head end bearing assembly connects the EHSA to the structural part, and it gives to the actuator the possibility to rotate respect the wing. The actuator rod is connects to the control surface by means a leverage that allows the transformation of the motion from rectilinear to rotary (Boeing Company 2010).
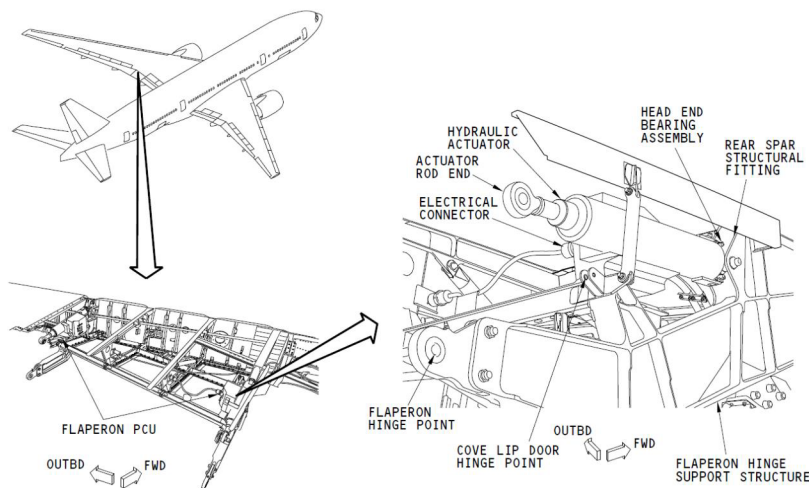
Figure 2.5: Flaperon scheme

The EHSA consists of an balanced actuator, a servovalve and the manifold part, this last has the function of distributing the hydraulic fluid, and commutes the operation mode between the active and by-pass.

2.2.1 Hydraulic manifold

The EHSA is connected to the supply and return pipes of the hydraulic system with two specific ports, when powered the manifold the servosystem is not yet fully active, since, in normal conditions, the by-pass valve connects the two actuator chamber between them and to the return line,please refer to scheme 2.6. In order to connect the actuator to the servovalve is necessary that the solenoid of the mode valve is powered, this generates the pressure signal that switches the by-pass valve.
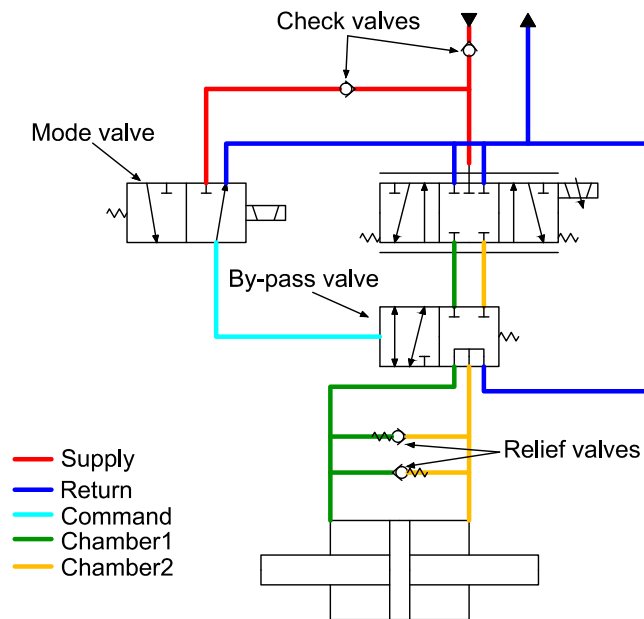
Figure 2.6: Flaperon manifold scheme

The mode valve as well as ensuring the absence of unwanted movement, allows to decide the status of the command:

- **Active mode:** mode valve solenoid is energized. The pilot ports of by-pass valve is connected to the supply port, then sercoactuator is powered. The controller commands the EHSV to a specific position that translates electrical input to a fluid flow rate to the actuator, either to the retract or extend cylinder side; when the desired position is reached, the EHSV shuts off.

- **Damping mode:** mode valve Solenoid Valve is de-energized. Without pilot by-pass valve stay in the normal position pressure, the actuator chambers are plce in by-pass. In this condition the cylinder is isolated, and its movement is imposed on the other EHSAs.

The damping mode can be active: under normal conditions when the other EHSA is placed into active, or under fault conditions to isolate the fail servoactuator. In case of fault in the bypass valve, the relief valves avoid the jamming of the surface, ensuring the flow passage between the two chambers.

2.2.2 ElectroHydraulic Servovalve

The control valve use in the flaperon EHSAs is a two stage servovalve, four ports and 3 positions (4/3), flapper nozzles type as the one displayed in figure 2.7. The valve consists of two stages: the first is a hydraulic amplifier and includes the engine torque, and the system nozzles and flapper. The second is composed of the spool that acts as a hydraulic distributor. Mechanical feedback between stages is provided by a spring that connects spool and flapper (Moog 2009). A filter provides contamination protection to the first stage.
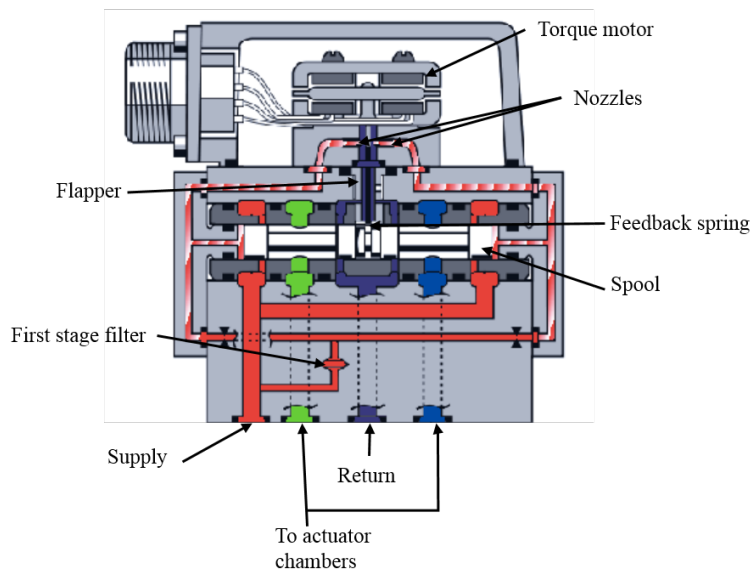
Figure 2.7: EHSV scheme

When the controllers apply electrical current to the torque motor, coils creates magnetic forces, which are translated into a torque acting on the armature. Armature and flapper assembly rotates around the armature support, therefore flapper closes off one nozzle and diverts flow to that end of spool. The variation of the flow due to an imbalance between the pressures at the ends of the drawer, this induces a displacement of the spool respect the equilibrium position. Depending on the direction of spool displacement, a cylinder chamber is connected to power, the other to the return.

Torque, in proportion to spool displacement, is applied to the flapper and to the spool by the feedback spring. This torque is opposed to the one generated vy the motor and a condition of torque equilibrium exists when the magnitude of the to torques are equal. In this condition, the spool displacement, and therefore the flow rates, are proportional to input current.

3

Servovalve degradations

The development of a prognostic system requires, in addition to a good competence of the physical system characteristics, a knowledge of the degradations that can develop in the system under study. The implement a PHM algorithms capable of identifying all possible causes of failure is an investment of money and time that can hardly get a return, for this reason is very important, especially in a first initial phase define what are the fails for which develop prognostic algorithms are convenient. Degradations should be classified according to their severity and their probability of happening, those that are most safety-critical and those that happen more often must be absolutely considered, and then they will have to be studied in detail in order to understand the origin and growth mechanisms.

In literature there are no accurate studies about the degradations that affect a EHSV, or EHSA in general, and even manufacturers of valves not been shown well predisposed to disclose such information. This Ph.D. thesis project has therefore been advanced base on engineering intuition, on feedback from users, as *Lufthansa Technik AG*, and on few information whispered by major manufacturers oh EHSV. A first validation of the chosen path was provided by a research project developed by *Embraer* presented in the 2015 meeting of *PHM Society* (Ribeiro et al. 2015).

Even once identified the main degradation, develop a robust system of PHM has proved particularly difficult because no consolidated models for such failures exist which can be taken as a basis for predicting their fault

progression. Therefore models of development and growth of degradation have been hypothesized, although these fault growth models are not yet fully validated, their physical based approach ensures that the fault growth pattern is described correctly allowing for a virtual testing of the efficacy of health monitoring algorithms.

In the next pages of this chapter are presented the considered degradations of EHSVs and their effect on the servocatuators behavior, besides some considerations about their origin and propagation are proposed.

3.1   Selected degradations

The servo valves are complex components, composed by a elevated number of parts and whit very small geometrical tolerances, therefore present a higher number of failure cases. Generally three types of failure can be identified: mechanical, linked to backlash or yield strength of the spring; hydraulic, as leakage, and electromagnetic, related torque motor. However, not every failure is possible, or convenient, to implement a system of prognostic.

Failures that involving an immediate break of servovalve, for example the jamming of the spool, do not get benefit of using PHM techniques. This is due to their rapid evolution, which does not provide enough time to analyze the features and estimate the useful life. For this damage type the solution is not to predict the fault, but to implement diagnostic techniques able to identify failure as soon as possible, and hardware and/or software systems that allow to isolate the failed component.

There are, also, degradations types that can be controlled with PHM systems, but to date there is no economic advantage. For example, consider the oil leakages to the outside of the EHSV body, certainly these could be detected using specific algorithms, but their slow growth involves that the oil leak can be identified during one of the scheduled inspections, before it becomes a problem. In the hypothetical case where the leakage grows in a manner so abrupt as to leave no time to take action, prognostic algorithms would not have power for what has been said previously.

Among all the possible fails, discard those that translate immediately into a fault and those improbable, as the breaking of the seal that isolates the torque motor, eight degradations have been identified (figure 3.1):

- Reduction of the torque motor magnetomotive force

- Contamination of nozzles

- Contamination of first stage filter

- Variation of the stiffness of the feedback spring

- Increase of the backlash between spool and feedback spring

- Variation of the friction force between spool and sleeve

- Increase of the radial gap
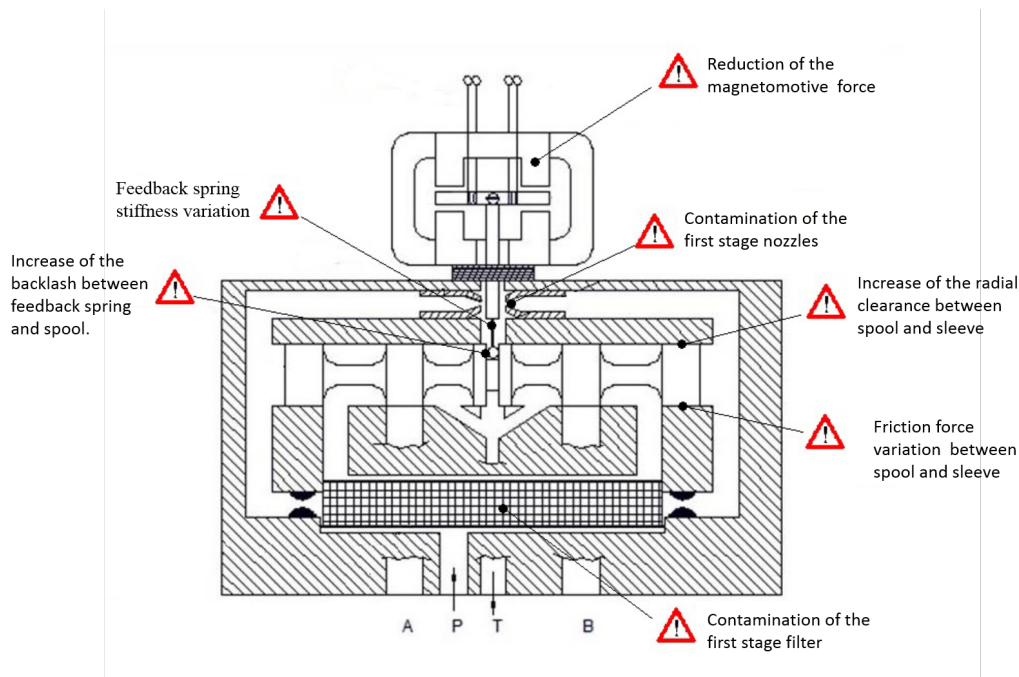
Figure 3.1: Selected degradations

The prognostic algorithm implemented in the continuation of work is concerned with identifying the eight degrdadazioni listed and to estimate the remaining useful life of the servovalve. The following sections described in detail all eight the fails.

3.2 Reduction magnetomotive force

The reduction of the magnetomotive force is related to a degradation of the torque motor, normally due to a degeneration of the permanent magnets, but sometimes caused by a short circuit between adjacent coils.

The origin of the degeneration of the magnets could to be found in the metallurgical characteristics of the magnetic components which show in time

irreversible aging process (Eckert, Muller, et al. 1993) Parameters such as the operating temperature (Eckert, Hinz, et al. 1987), excessive currents and the contact with oil accelerate the aging of the magnets, thus reducing their useful life. The main cause of short circuits are the high temperatures and excessive drive currents.

The effect of a reduction of the magnetomotive force is a decrease in the torque generated by the motor at the same current, this translates into a smaller displacement of the flapper, and then a lower displacement of the spool. Thus at the same current lower flows directed to the two actuator chambers are generated. If the current generated by the two controllers is not yet saturated and the degradation is small, the reduction of the force will be compensated by the controllers increasing the command currents, otherwise the dynamic of the controller will be less than that in nominal conditions.

3.3   Contamination of nozzles and filter

The contamination of the filter or nozzles of the first stage is caused by the presence of debris in the hydraulic fluid, which may be small pieces of seal, metal filings or products due to the sintering of the oil. A hydraulic system has a large number of filters in order to keep the fluid clean from any contaminated, furthermore the servovalve has a special filter on the first stage with high levels of filtering, to stop even the smaller debris that could clog the nozzles.

In normal conditions, the debris in the fluid will not create problems to the EHSV. But due to a collapse of a filter that a number of pollutants may flow in the plant going to contaminate the filter of the first stage, and if sufficiently small even the nozzles. Collapse of first stage filter causes instead the passage of debris of all sizes directly to the nozzles.

The occlusion of the filter of the first stage causes a greater pressure drop to the fluid that supplies the nozzles, and therefore reduces the delta pressure at the ends of the spool. This means less force available to move the drawer, but the pressure force is much bigger than the other acting, thus the drawer will however reach the required position, but in a longer time. The dynamics of the EHSA will be slightly delayed, as said before the controllers can try to compensate for the degradation by increasing the control current.

The partial obstruction, or total, of one of the nozzles (figure 3.2) causes a an increase in pressure in the corresponding chamber located in the extreme of the spool. This causes an unwanted movement of the shutter, which is, as long as possible, compensated by the controllers. If the clogging can
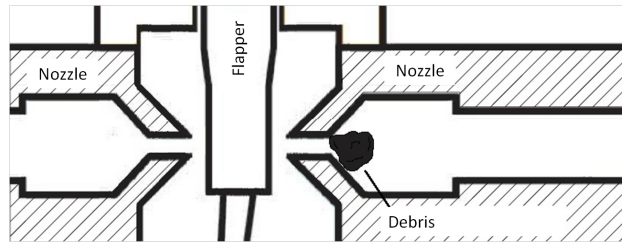
Figure 3.2: Nozzle clogging

be considered a sort of bias, because the controller will provide a non-zero current to keep the spool in zero position, in other words the torque motor will have to move the flapper to obstruct the nozzle opposite to that contaminated to compensate the increase of pressure. If the obstruction is total the spool could move only in one direction, and so the EHSA is inoperable.

3.4   Yield feedback spring

Stiffness variation of internal feedback spring (figure 3.3) is generally caused by yield in strength due to excessive loads or to normal aging of the component. As known from the theory of materials a continuous elastic deformation leads in e metallic component to aging for fatigue, and through the variation of the internal structure, to a change of their physical features. The yield results to be one of the consequences of fatigue phenomenon, and decrease the elastic resistance of the constituent material
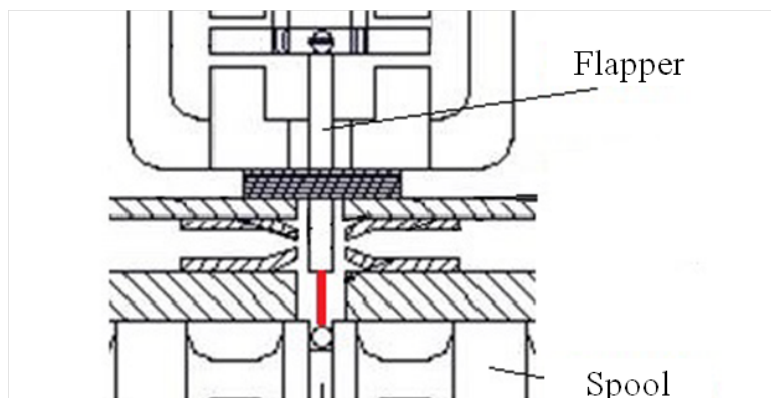
Figure 3.3: Yield feedback spring

The feedback spring is indispensable for the internal mechanical feedback, the correct regulation of the servovalve is therefore strictly dependent on the

characteristics of this component. A yield spring decreases the mechanical force feedback between the spool and flapper, thus the dynamic equilibrium of the two components change. Although odd, the reduction of the stiffness of the feedback spring improves the dynamic performance of the spool, and consequently those of actuator. This particular behavior is due to the fact that a yield offers a lower resistance to the displacement of the spool then the nominal one.

The increase in dynamic performance, however, is balanced by the emergence of hysteresis and instability phenomena, which initially only affected the drawer, but as the yield strength increases their propagate even to the cylinder.

3.5   Feedback spring backlash

Increase of the backlash at the mechanical interface between the internal feedback spring and spool (figure 3.4) is the result of a wear due to the relative movement between these two parts.
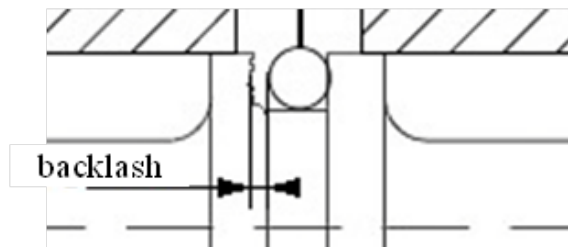
Figure 3.4: Feedback spring backlash

The backlash brings spring and spool to have not a simultaneous movement, as a single rigid body, but on the contrary the drawer in the presence of a motion reversal has a first phase of displacement in which it is not in contact with the spring. During this period the forces acting on the spool are lower than the normal ones, so the dynamics of the shutter, as seen for the yield of the spring, has an improvement. Retrieving the game, the drawer collides against the spring developing oscillator phenomena.

If the oscillator phenomena are small, will affect only the spool, otherwise phenomena of instability and hysteresis can also be observed in the cylinder.

3.6 Friction force variation

Variation of the friction force between spool and sleeve is due to a silting effect associated either to debris contamination caused by hydraulic fluid unfiltered (figure 3.5), or to the decay of the hydraulic fluid additives which tend to polymerize when the fluid is subjected to large shear stresses, such as for example the passage through the radial clearance.
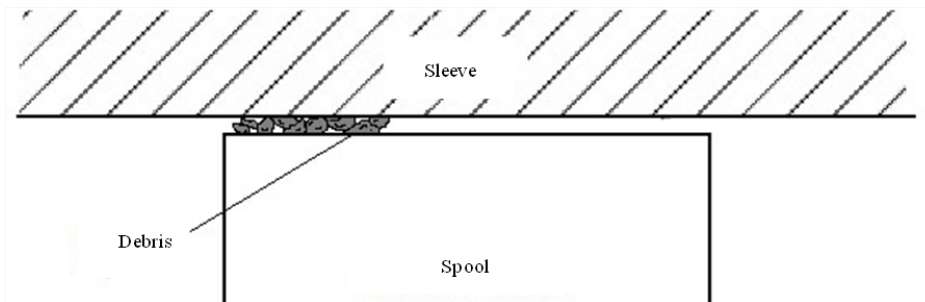
Figure 3.5: Friction force variation

The increase of the friction force has little influence on the behavior of the servovalve, since the pressure force that is generated at the ends of the spool is about two orders of magnitude greater than the force of the nominal friction. As is understandable, little increases in the Coulomb friction force are then readily compensated by the pressure force. Despite its little influence, try to identify this degradation is important, because a variation of the friction force can be one of the precursors of the spool jamming.

The identification of the variation of the friction force is one of the most complicated to cuase of its low influence on the behavior of the EHSAs, the implemented algorithms must be very sensitive to the variation of the features, but equally robust to external influences, so as not to give false alarms. Find the right balance between sensitivity and accuracy is the real challenge that must be addressed in the development of diagnostic and fails identification algorithms.

3.7 Radial gap increase

Increase of the radial clearance between spool and sleeve (figure 3.6) and change of the shape of the corners dues to wear between these two moving parts or to the presence of particular resistant debris. Like many other degradations of the servo valve also this is closely linked to the impurities

present in the hydraulic fluid; but unlike the first stage, the second does not have a special filter, hence is more exposed to contaminants.
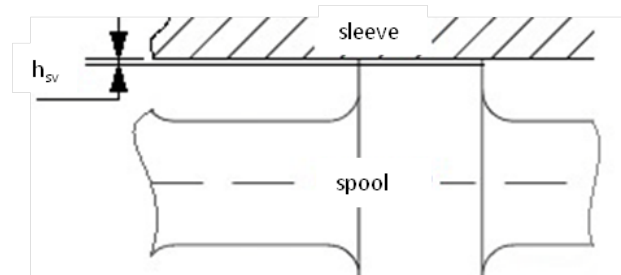
Figure 3.6: Radial gap increase

An increase in clearance induces an increase in the servovalve internal leakages: if the variation of the radial clearance is symmetrical over the entire drawer, this will reduce the dynamic performance of the actuator equal in both directions. The reduction of the dynamic performance is due to an increase in the leakage flux; the flow direct to each actuator chamber can be considered the difference between the flow from supply, and the flow to return. Taking the example of a chamber placed in contact with the power supply, the increase of the radial clearance due to an increase of leakage flux through the return port therefore, for the same pressure drop the flow directed to the chamber is lower than that in nominal conditions.

If the variation of the radial clearance is not symmetrical, the same effect presented before occurs but only for one of the two chambers. In this situation it may also arise an imbalance between zero electric and hydraulic zero, in other words for a zero current a flow in one of the two chambers is not null. This condition is generally compensated by the controllers, which generate a non-zero current to find a spool that compensate the variation in flux and maintain the actuator stationary.

4

Mathematical model

Implement a PHM system required a depth knowledge of the influence of the single degradation on the electro-hydraulic servo actuator take as benchmark. These information, ideally, should be obtained through series of historical data collected during the usual operations of the aircrafts or using test benches and endurance tests; however both methods require economic and time investments that are not compatible with a PhD project. Due to these considerations, the choice of studying the influence of degradation using a high fidelity mathematical model was considered the only practicable.

Using a mathematical model has significant advantages, first of all possibility of apply a single degradation at a time in order to highlight its real influence, net of all other; this is practically impossible in the real systems, where even if a degradation is predominant , the components are affected by minors wears that cannot be isolated or prevented. Furthermore a mathematical model has the advantage of being easy to modified, allowing to test the system in different operating and environmental conditions difficult to replicate on a test bench.

The mathematical model used to perform the necessary tests has to be particularly accurate, in order to provide the results truthful in all operation condition, both nominal and degraded. A physical-based model has been chosen to obtain the necessary precision. Furthermore this type of models facilitates the simulation of the different degradations, since to simulate degradation is simply required the change of one or more parameters of the physic equations that describing the behaviour of the components.

This aspect creates a link between the real degradation and the implemented degradation, which, although it is represented by mathematical equations, maintains its physical nature.

With the goal to obtaining a model as accurate as possible, all the main nonlinearities that characterize the EHSAs have been introduced and the principal sources of noise have been added, with the possibility of modifying the amplitude and frequency. To complete the model, the specific subsystem to simulate the environmental conditions and the load acting on the wing surface have been implemented.

In the following paragraphs, for each component, the physical equations used to describe it in the mathematical model are reported, are clarified their origin and the assumptions made to arrive at the set of equations. In addition, the subsystems that allow you to set the environmental conditions and inject noise are presented.

4.1   Model structure

The high fidelity mathematical model is implemented in Matlab and Matlab Simulink; it could be divided in three layers,following the scheme of figure 4.1, the top one is an mfile, called "MainFile" and holds the instructions for controlled and managed the model. From this file is possible determine the type of simulation, pre (post) flight test or entire flight, and the list of commands. The high layer contains also the code needed to introduce the different degradations in the model, for each fail amplitude and starting time could be setting. Acting on the *"Mainfile"* the user can set the operating conditions, such as the average supply and return pressures, the oil temperature at the simulation start and the presence of noise on the control current of the servovalve and on the feedback signal generated from the LVDT. The last facilities of the top layer are concerned to the environmental condition: presence of external load, average velocity of the wind on the ground, probability of gusts and the turbulence intensity, use in the Dryden wind turbulence model (MIL-HDBK-1797 1997, MIL-F-8785C 1991), could be setting.

The second layer of the model includes the three m-files that contain the geometric data, the material information and the oil characteristics. The first one called *"EHSAData"* contains the dimension of the EHSA components, the data of the different coefficients, the values of equivalent stiffness and damping and the parameters of the control law. The second m-file, *"EHSASeal"*, starting from the material and geometric data of the seals calculates the co-efficients of Columbian friction of the actuator with the equations presented in section 4.2.1. The last file *"EHSAOil"*, is a set of equations that express
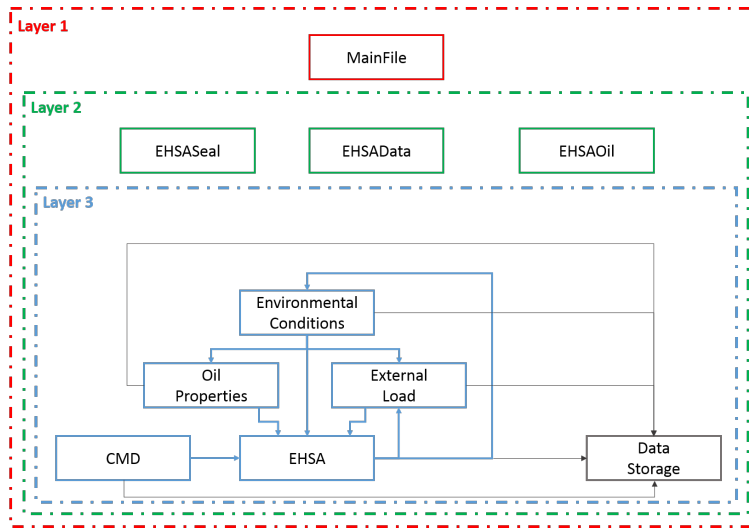
Figure 4.1: Mathematical model layers

the oil parameter as function of temperature and in minimum part of supply pressure(see section 4.8). This m-file run a single time for pre (post) flight simulation, because the oil temperature is assumed constant during the test, otherwise the oil parameters are update every five second of simulation.

The last layer is implemented in Matlab Simulink and it is composed by six subsystem interconnected to each other. The most important is the *"EHSA"*, which includes the mathematical model of the servo actuator and of the fight surface. The principal input of *"EHSA"* is the command position generated from the *"CMD"* subroutine. Other three accessory inputs come from the *"Oil"*, *"Environmental"* and *"External Load"*, The *"EHSA"* outputs are connected to all the other subsystem, except *"CMD"*. The output from all subsystem are connected to *"Data Storage"* in order to save the values on the hard-disk, for the future analysis. The inputs/outputs will be explain in detail in the next paragraphs.

The *"EHSA"* mathematical model is structured in different subsystems, each one coincides with a physical component of the servosystem; moreover, the inputs and outputs of each subsystem are identical to the real ones (4.2). This choice allows to have a very flexible tool, inasmuch the model can be used for different EHSAs simply changing the data files *"EHSAData"* and/or the necessary subsystems. In addition changes to the *"Mainfile"* allows exchanging the different simulation conditions such as environmental conditions travel time.
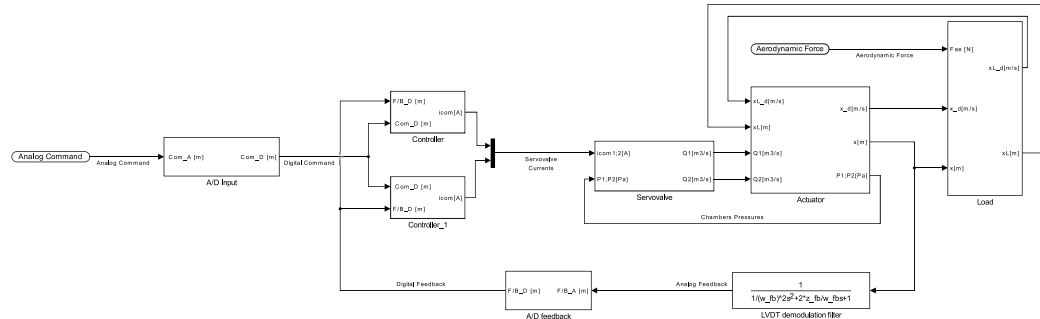
Figure 4.2: EHSA model scheme

4.2   Actuator

The hydraulic cylinder has been modeled as lumped system with two degrees of freedom, the first is the position of the rod (x_R, $\dot{x}_R$ and $\ddot{x}_R$); the second corresponds to the deformation of the interface between the aircraft structure and actuator (x_C, $\dot{x}_C$ and $\ddot{x}_C$); the damper (C_{ext1}) has the task of stabilizes the mathematical model. From the diagram 4.3 the three main inputs of the model can be identified: the two control flow rates provided from the servovalve (Q_1 and Q_2) the external load called F_{ext}. The principal output of the model is the absolute position of the rod respect the fixed structure x defined as the difference between the position of the sleeve x_C and the relative rod position x_R.
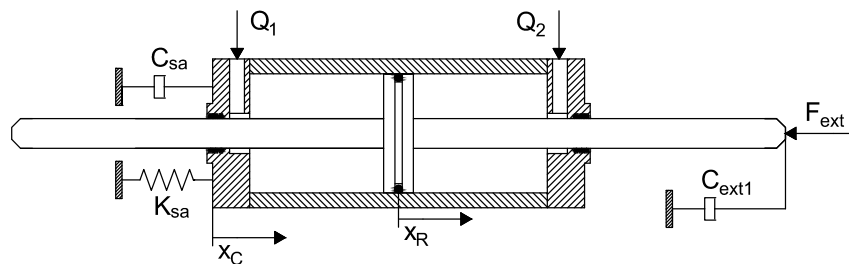
Figure 4.3: Actuator lumped model

As declared previously, the flow rates Q_1 and Q_2 are the inputs to the model of the actuator, these are used to calculate the pressure in the actuator chambers applying the continuity equation to the chamber volumes.

$$\frac{\partial M_1}{\partial t} = V_1 \frac{\partial \rho}{\partial t} + \rho \frac{\partial V_1}{\partial t} \qquad \text{Chamber 1} \qquad (4.1)$$

$$\frac{\partial M_2}{\partial t} = V_2 \frac{\partial \rho}{\partial t} + \rho \frac{\partial V_2}{\partial t} \qquad \text{Chamber 2}$$

Where M is the mass of the oil in the chamber, V is the volume of the chamber, ρ is the oil density.

Applying the definition of the Bulk modulus (β) to the the equations 4.1, the following new expressions can be obtained:

$$\frac{\partial M_1}{\partial t} = \frac{V_1 \rho}{\beta} \frac{\partial P_1}{\partial t} + \rho \frac{\partial V_1}{\partial t} \qquad \text{Chamber 1} \qquad (4.2)$$

$$\frac{\partial M_2}{\partial t} = \frac{V_2 \rho}{\beta} \frac{\partial P_2}{\partial t} + \rho \frac{\partial V_2}{\partial t} \qquad \text{Chamber 2}$$

The volume of the two chambers is not constant, but it is function of the piston position (x_R). The dependence between position and volume can be expressed assuming an initial volume (V_0), which coincides with the volume of the chambers with actuator positioned at half stoke, and expressing the volume of the chambers in function of the area (A) and of piston position as $V_1 = V_0 + x_R A$ and $V_2 = V_0 - x_R A$. The equations 4.2 become:

$$\frac{1}{\rho} \frac{\partial M_1}{\partial t} = \frac{V_0 + x_R A}{\beta} \frac{\partial P_1}{\partial t} + \dot{x}_R A \qquad \text{Chamber 1} \qquad (4.3)$$

$$\frac{1}{\rho} \frac{\partial M_2}{\partial t} = \frac{V_0 - x_R A}{\beta} \frac{\partial P_2}{\partial t} - \dot{x}_R A \qquad \text{Chamber 2}$$

In order to express the equations 4.3 as a function of volumetric flow rates, and not mass flow rates, the relationship $Q = \frac{1}{\rho} \frac{\partial M}{\partial t}$ was apply.

$$\frac{\partial P_1}{\partial t} = \beta \frac{Q_1 - \dot{x}_R A}{V_0 + x_R A} \qquad \text{Chamber 1} \qquad (4.4)$$

$$\frac{\partial P_2}{\partial t} = \beta \frac{Q_2 - \dot{x}_R A}{V_0 + x_R A} \qquad \text{Chamber 2}$$

The equations 4.4 allow us to express the pressure in each chamber as a function of volumetric flow rate. With the aims of increasing the accuracy of the model and simulate the seals fails, the contribution of the leakages is taken into account by adding their amounts with proper sign to the control flow rates.

$$\frac{\partial P_1}{\partial t} = \beta \frac{Q_1 - Q_{le1} - Q_{li} - \dot{x}_R A}{V_0 + x_R A} \qquad \text{Chamber 1} \qquad (4.5)$$

$$\frac{\partial P_2}{\partial t} = \beta \frac{Q_2 - Q_{le2} + Q_{li} - \dot{x}_R A}{V_0 + x_R A} \qquad \text{Chamber 2}$$

The terms Q_{le1} and Q_{le2} are the external leakages respectively from chamber 1 and chamber 2, while Q_{li} is the internal leakage, positive from chamber 1 to chamber 2.

The values of the three leakages are calculated within the mathematical model with the equations 4.6, which express the leakages as a function of the difference of pressure between the two sides of the seal.

$$Q_{le1} = k_{le1,1} P_1 + k_{le1,2} \sqrt{|P_1|} \qquad \text{External chamber 1} \qquad (4.6)$$

$$Q_{le2} = k_{le2,1} P_1 + k_{le2,2} \sqrt{|P_2|} \qquad \text{External chamber 2}$$

$$Q_{li} = k_{li,1} P_1 + k_{li,2} \sqrt{|P_1 - P_2|} \qquad \text{Internal}$$

The outputs of the equations 4.5 are the derivatives of the pressures over time, with a simple integration, saturated at supply and return pressure, is possible to obtain the actual pressures in the two chambers. This information is used in the dynamic equations, presented below, in order to obtain the position of the two degrees of freedom of the model.

The dynamic equation of the rod is derived from the free body diagram, where m_r is the mass of the rod, F_{ext} is the external force, F_{fric} is the Coulomb friction between rod and sleeve and γ is the viscous friction coefficient. Below the dynamic equation of the rod in static condition is shown.

$$m_R \ddot{x}_R = (P_1 - P_2)A - F_{ext} - \gamma x - F_{fric} - C_{ext1} \dot{x}_R \qquad (4.7)$$
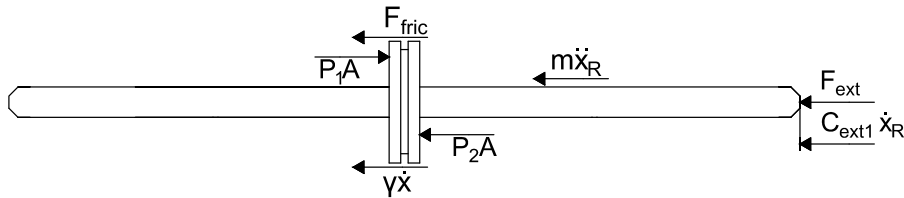
Figure 4.4: Rod free body diagram

The position of the rod is obtained by double integration of the acceleration, position is saturated by a specific code implemented in the model, which is discussed in detail in section 4.2.2.

The strength of the Coulomb friction as mentioned previously is a function of the seals and of the chambers pressures, its implementation is illustrated in the section 4.2.1.

Exactly as for the piston it is possible to obtain the dynamic equation of the cylinder starting from the free body diagram (figure); where K_{sa} and C_{sa} are, respectively, the equivalent stiffness and damping of the connection point between cylinder and the aircraft structure. the dynamic equation of the cylinder is reported below.

$$m_C \ddot{x}_C = (-P_1 + P_2)A + \gamma \dot{x} + F_{fric} - K_{sa} x_C - C_{sa} \dot{x}_C \qquad (4.8)$$
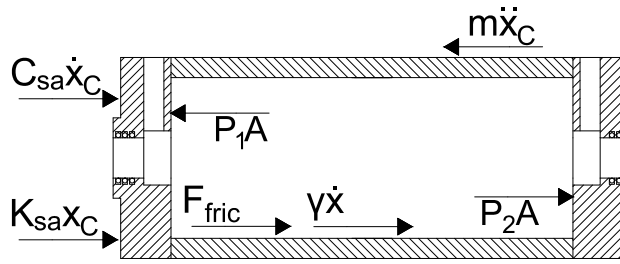
Figure 4.5: Sleeve free body diagram

The position of the ball joint, respect to a point integral to rigid structure, is defined as the difference between the rod and the sleeve position.

4.2.1 Coulomb friction

Obtain a good model of Coulomb friction has always been considered a hard task, first because quantifying, in a realistic manner, the value of the friction force is complex and requires considerable expertise, second because the discontinuity between static and dynamic conditions is often due to the emergence of numerical instabilities. Nowadays the scientific literature presents an high number of studies on friction models, which generally provides very accuracy results, but at the same time are greedy of computational resources. The implementation of one of these models within the mathematical model of the servoactuator would have resulted in an unacceptable increase of the times of computation, without ensuring a corresponding increase of accuracy.

In this work the identification of Coulomb friction model has been divided into two parts, the first was responsible for determining the value of dynamic

friction, while in the second a stable and robust mathematical model has been implemented.

The computation of dynamic friction was performed following the directions proposed by Martini (1984). The author presents in the book the results of a series of tests conducted to determine the value of the dynamic Coulomb friction in different operating conditions and different seals. The experimental results show that the friction force generated by each seal may be represented as the sum of two components, F_H and F_C and which are both functions of the characteristics of seals, but only the first is a function of the pressure difference between the sides of the seals. The two experimental equations are shown below.

$$F_{fric_{dynamic}} = F_H + FC \tag{4.9}$$
$$F_H = 7.82 \cdot 10^{-2} \pi Dm_{se} W_{se} \Delta P^{0.61}$$
$$F_C = 0.175 \pi Dd_{se}(-0.884 + 0.0206 Hs_{se} - 0.0001 Hs_{se}^2 Tw_{se})$$

Where Dm_{se} is the seal mean diameter in mm, W_{se} is the seal cross-section express in mm, Dd_{se} is the sliding seal diameter in mm, Hs_{se} is the shore hardness and Tw_{se} is the squeeze of the seal in %. The numerical coefficients differ from those present by Martini due to the conversion from Imperial Units to International System of Units.
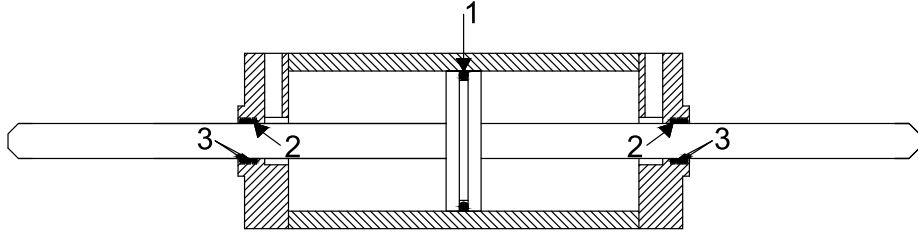
Figure 4.6: Actuator seals

The actuator considered in the work has seven seals, three for each rod and one on piston, see scheme 4.6. The frictional force generated by the seal 1 is the sum of the components F_H and F_C, and it is function of the chamber differential pressure. The friction forces of seals 2 are also function of each component and ΔP is the pressure in the chambers. The seals 3 do not have a component of friction force function of the pressure difference, since the pressures in both sides is identical and equal to the atmospheric.

The code implemented calculates the value of the overall friction force updating the component F_H for the seals 1 and 2 as a function of the actual chambers pressures. The result is added to the component F_C, which is constant in time, since it depends only from the geometry and the material of the seals.

The transition between static Coulomb friction to the dynamic one is source of numerical instabilities, because the friction value instantly changes from a static to a motion condition. In order to mitigate this transition, some precautions that improve the stability have been introduced in the code.

First speed signal, $\dot{x}$ passes through a dead-band, with amplitude equal to $\pm 0.1 mm/s$, in order to eliminate all the micro oscillations and machine errors. The characteristic discontinuous at $v = 0$, which creates considerable computational problems, has been proven that is a nonphysical simplification in the sense that the mechanical contact with distributed mass and compliance cannot exhibit an instantaneous change in force (Brian and De Wit 1995). There are numerous models of friction without discontinuity. The translational friction code implements one of the simplest versions of continuous friction models.

The implemented solution simulates the transition between static and dynamic by an exponential function, in which the exponent is equal to $\dot{x}$ multiply by negative coefficient (k_{fric}) which it allows to set the slope of the exponential. The friction force is then defined as follow.

$$F_{fric} = (1 + 0.5e^{-k_{fric}\dot{x}})F_{fric_{dynamic}} \qquad (4.10)$$

The last term of the equation 4.10 comes directly from the set of equations 4.9,therefore the friction force is a function of both speed and pressures.

The final problem addressed in the definition of the mathematical model is the determination of the sign of the friction force for speed equal to zero. The implemented model poses the sign of the friction force opposite to the speed sign in dynamic conditions, while under static conditions, the sign of the friction force is the opposite of the sign of the summation of the forces of pressure with the external force. In this way the sign of the force of friction is always defined and in conditions of incipient motion is opposite to the active forces.

Graph 4.7 shows the friction force for different values of velocity and chamber 2 pressure. The chamber 1 pressure is set constant and equal to the supply pressure.
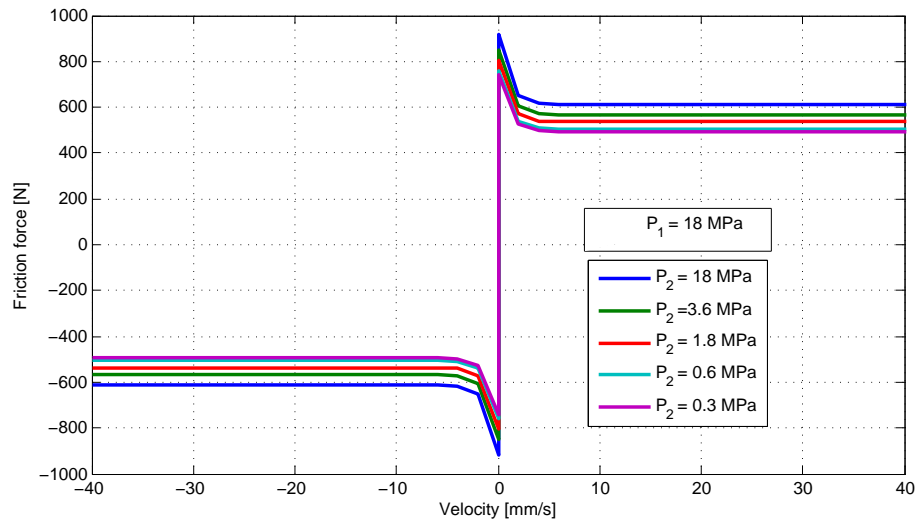
Figure 4.7: Coulomb friction

4.2.2 Actuator stoke limits

In the EHSA mathematical model logic stoke limits have been implemented, these were preferred to a physical model of limits as they have a more stable behavior and they eliminate the possibility that instability mathematical propagate in the solution. To prevent that the output of the position integrator exceeding specifiable levels, Limit output option has been selected; when the output reaches the limits, the integral action is turned off to prevent integral wind up. Simulink also indicates the status of the integrator using a specific signal that has one of three values:

- 1 indicates that the upper limit is being applied.

- 0 indicates that the integral is not limited

- −1 indicates that the lower limit is being applied.
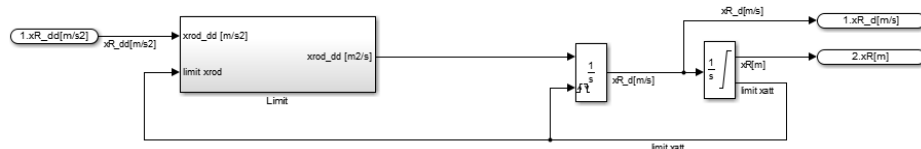
Figure 4.8: Stroke limits - saturation signal

The status signal of the position integrator, as shown in the scheme 4.8, is used for the reset the speed integrator and inside of the *"Limit"* block. Within this subsystem a logic function has been implemented in order to set zero the value of the acceleration when it is not in agreement with the state of the limits, see scheme 4.9. When the reset signal is equal to zero the logic function does not active; when the piston is in the upper stroke end: if the acceleration is positive it will be set to zero otherwise there will be no variations. The subsystem function identically, but with reversed signs, in the case of the piston to the lower stroke end.
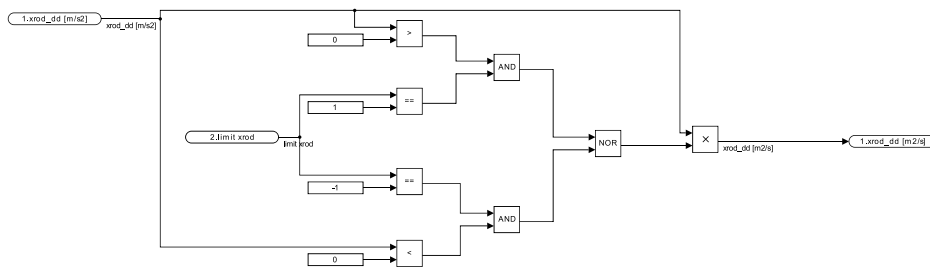
Figure 4.9: Stroke limits - subsystem

4.3   Servovalve

The servovalve (EHSV) is a complex component, it have a first part, that acts as a hydraulic amplifier, in which the dynamics of the components is the most important aspect; while in the second part, which has the task of hydraulic distributor, the flow equations have a dominant feature. The mathematical model, as represented in the scheme 4.10 , has been implemented following this division: the first subsystem connects the currents (i_{com}) in input with the position of the spool ($x_{s_{sv}}$) in output following the kinematic chain; the second one, known the position of the spool, calculates the flows rates to the two actuator chambers (Q_1 and Q_2).

Following the natural energy conversion from electrical to hydraulic, the first element implemented is the torque motor. The torque generation has been described using the equations proposed by Urata, who has done interesting studies on servovalves and proposed a first set of equations that providing an accurate description of the torque motor in Urata 2007a. Subsequently the equations have been refined by introducing the influence on unequal air-gap (Urata 2007b) and the effect of the stiffness of the elastic components (Urata and Suzuki 2011). For torque motors using permanent
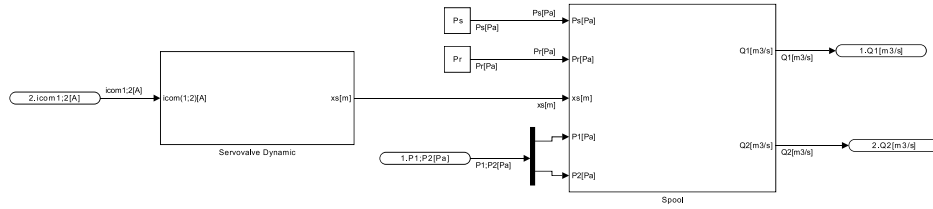
Figure 4.10: Model EHSV scheme

magnets another famous theory has been developed by Merritt (1967). Unfortunately, however, the theory gives totally erroneous results because it ignores the magnetic reluctance of permanent magnets and accompanying leakage flux. The theory of Urata corrected the Merritt results starting from experimental observations.

The magnetic circuit of the torque motor can be represented using the equivalent circuit of figure 4.11 , where the sources of magnetomotive force are is the of permanent magnet (V_P) and servovalve currents (i_{com}) time the number of coil turn (n), indicated in the scheme as ni. $\Re_1$, $\Re_2$, $\Re_3$ and $\Re_4$ are the reluctance of air-gaps, $\Re_P$ is the reluctance of permanent magnet and $\Re_l$ is reluctance of leakage path. The magnetic reluctance of yokes is neglected because it is much less than that of permanent magnets and air-gaps. The The Φ therms are the fluxes through the different fields. The flux leakage ratio r expresses the efficiency of the permanent magnets; $r = 1$ means no leakage flux, $r = 0$ means no effect of the permanent magnets. This ratio depends on the ratio of the magnetic reluctance of the permanent magnets and the air-gaps.
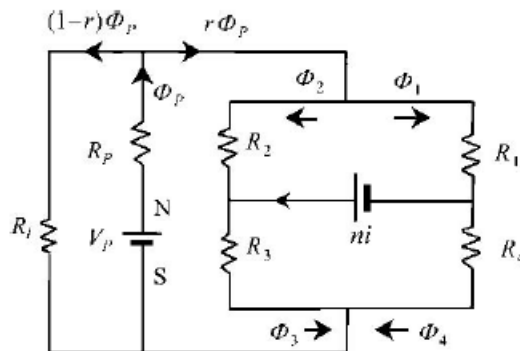
Figure 4.11: Torque motor equivalent circuit

The torque generated by the motor is the sum of the resultant moments in each air-gap, these under the assumption of constant flux density in the gap can be express with the following equation, where N is the number of air-gap.

$$M_N = \frac{B_N H_N}{2} \frac{L_A A_g}{2} = \frac{B_N^2}{4\mu_0} L_A A_g \qquad (4.11)$$

Where B is the magnetic flux density, H is the magnetic field, L_A is distance between poles at both ends of a yoke, A_g is the cross-sectional area of an air gap and μ_a is permeability of air.

The torque working on the armature is obtain, always under the assumption of constant flux density in the gap, as the sum of equation 4.11 apply to each gap.

$$T = \frac{L_A A_g}{4\mu_a}(B_1^2 + B_2^2 + B_3^2 + B_4^2) = \frac{L_A}{4\mu_a A_g}(\Phi_1^2 + \Phi_2^2 + \Phi_3^2 + \Phi_4^2) \qquad (4.12)$$

Hence, the next task is to find the flux that passes through the four gaps. Applying the theorem of Ampere to the magnetic circuit of figure the following set of three equations.

$$\begin{cases} \Phi_1 \Re_1 + \Phi_4 \Re_4 + \Phi_P \Re_P = V_P & \text{(a)} \\ \Phi_2 \Re_2 - \Phi_1 \Re_1 = -ni & \text{(b)} \\ \Phi_4 \Re_4 + \Phi_3 \Re_3 = ni & \text{(c)} \end{cases} \qquad (4.13)$$

Applying the Gauss rule are two equations are obtained

$$r\Phi_P - \Phi_1 - \Phi_2 = 0 \qquad (4.14)$$

$$\Phi_1 + \Phi_2 - \Phi_3 - \Phi_4 = 0 \qquad (4.15)$$

Combining equation 4.13b and equation 4.14 the Φ_P is explicit as a function of Φ_1.

$$\Phi_P = \left(1 + \frac{\Re_1}{\Re_2}\right)\frac{\Phi_1}{r} - \frac{1}{\Re_2}\frac{ni}{r} \qquad (4.16)$$

The flux Φ_4 can be made explicit as a function of the Φ_1 solving the equation 4.13b, equation 4.13c and equation 4.15.

$$\Phi_4 = \frac{\left(1 + \dfrac{\Re_1}{\Re_2}\right)\Phi_1 - \left(\dfrac{1}{\Re_2} + \dfrac{1}{\Re_3}\right)ni}{1 + \dfrac{\Re_4}{\Re_3}} \qquad (4.17)$$

Substituting the equation 4.16 and the equation 4.17 in the equation 4.13a the magnetic flux in the air gap one is obtained.

$$\Phi_1 = \frac{V_p + \left[\dfrac{\Re_4\left(\dfrac{1}{\Re_2} + \dfrac{1}{\Re_3}\right)}{1 + \dfrac{\Re_4}{\Re_3}} + \dfrac{\Re_p}{r\Re_2}\right]ni}{\Re_1 + \dfrac{\Re_P}{r}\left(1 + \dfrac{\Re_1}{\Re_2}\right) + \dfrac{\Re_4\left(1 + \dfrac{\Re_1}{\Re_2}\right)}{1 + \dfrac{\Re_4}{\Re_3}}} \tag{4.18}$$

In order to simplify the notation, the equivalent resistance $\Re_A$ and $\Re_B$ are introduced and defined as following.

$$\Re_A = \frac{\Re_4\left(\dfrac{1}{\Re_2} + \dfrac{1}{\Re_3}\right)}{1 + \dfrac{\Re_4}{\Re_3}} + \frac{\Re_p}{r\Re_2}$$

$$\Re_B = \Re_1 + \frac{\Re_P}{r}\left(1 + \frac{\Re_1}{\Re_2}\right) + \frac{\Re_4\left(1 + \dfrac{\Re_1}{\Re_2}\right)}{1 + \dfrac{\Re_4}{\Re_3}}$$

$$\Phi_1 = \frac{V_P}{\Re_B} + \frac{\Re_A}{\Re_B}ni \tag{4.19}$$

The Φ_2 is obtained putting equation 4.19 in equation 4.13b.

$$\Phi_2 = \frac{\Re_1}{\Re_2\Re_B}V_P + \left(\frac{\Re_A\Re_1}{\Re_B\Re_2} - \frac{1}{\Re_2}\right)ni \tag{4.20}$$

Inserting Φ_1 in equation 4.17, Φ_4 is defined.

$$\Phi_4 = \frac{1 + \dfrac{\Re_1}{\Re_2}}{1 + \dfrac{\Re_4}{\Re_3}}\frac{V_P}{\Re_B} \frac{\left(1 + \dfrac{R_1}{R_2}\right)\dfrac{R_A}{R_B} - \dfrac{1}{\Re_2} - \dfrac{1}{\Re_3}}{1 + \dfrac{\Re_4}{\Re_3}}ni \tag{4.21}$$

Finally the magnetic flux Φ_3 can be obtained.

$$\Phi_3 = \left[\frac{\Re_2\Re_B - \Re_1\Re_2 - \Re_1 - \Re_2}{\Re_2\Re_3\Re_B} \right] V_p +$$

$$+ \left[\frac{\Re_4\Re_P}{\Re_1\Re_2\Re_3} + \frac{1}{\Re_3} - \frac{\Re_A}{\Re_3\Re_B} \frac{\Re_1\Re_2 + \Re_1\Re_P + \Re_2\Re_P}{\Re_2\Re_4} \right] ni \quad (4.22)$$

The reluctances of air-gaps can be expressed in function of the geometrical parameters of the toque motor and armature position, these in optimal conditions are identical for all the gap, but during the assembly or throughout the operative life of the component is possible the formation of misalignments that vary the value reluctances. To be considered in the model this possibility three parameters has been introduced (figure 4.12):

- **H**: air-gap imbalance due to armature height error

- **W**: right and left imbalance of air-gap thickness

- **G**: air-gap imbalance due to incline of armature relative to pole positions
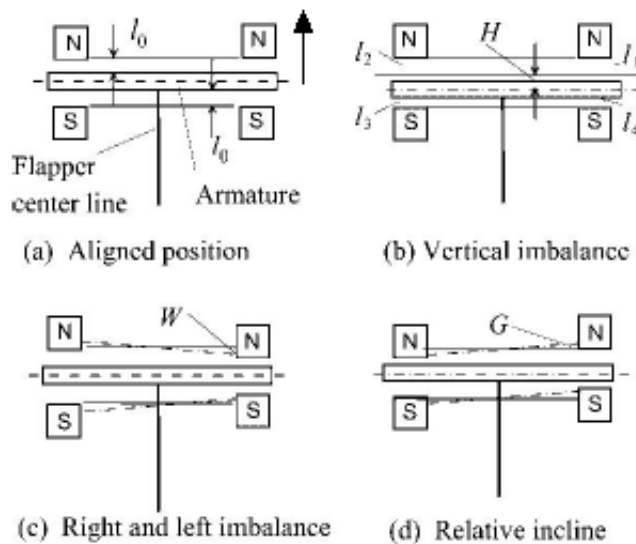
Figure 4.12: Distribution of air-gaps

Referring to the diagram of the figure 4.12, and calling X_A the displacement of the armature from the neutral position, the thickness (l) of the

four gap is defined as follows, l_0 is the nominal thickness. Dividing by l_0 dimensionless parameters have been obtained, the same nomenclature was maintained, passing from upper case to lower case letters.

$$
\begin{aligned}
l_1 &= l_0 + H - W + G - X_A = l_0(1 + h - w + g - x_a) \\
l_2 &= l_0 + H + W - G + X_A = l_0(1 + h + w - g + x_a) \\
l_3 &= l_0 - H + W + G - X_A = l_0(1 - h + w + g - x_a) \\
l_4 &= l_0 - H - W - G + X_A = l_0(1 - h - w - g + x_a)
\end{aligned}
\tag{4.23}
$$

The reluctances of the air-gaps are calculated, under the hypothesis of magnetic flux uniformly distributed, with the equations shown below; where A_g is the cross-sectional area of an air gap and μ_a is permeability of air.

$$
\begin{aligned}
\Re_1 &= \frac{l_0}{\mu_a A_g}(1 + h - w + g - x_a) \\
\Re_2 &= \frac{l_0}{\mu_a A_g}(1 + h + w - g + x_a) \\
\Re_3 &= \frac{l_0}{\mu_a A_g}(1 - h + w + g - x_a) \\
\Re_4 &= \frac{l_0}{\mu_a A_g}(1 - h - w - g + x_a)
\end{aligned}
\tag{4.24}
$$

The parameter of permanent magnets: magnetomotive force and magnetic reluctance are defined as following, where k_l is defined as the factor by demagnetizing of permanent magnet, μ_P is permeability of permanent magnet, B_r is residual flux density of permanent magnet, A_P and l_P are cross-sectional area of an air-gap and length of permanent magnet, respectively.

$$
\Re_P = \frac{k_l l_P}{\mu_P A_P}
\tag{4.25}
$$

$$
V_p = \frac{l_P B_r}{\mu_P}
\tag{4.26}
$$

Substituting in equations of the magnetic fluxes (equations 4.19, 4.20, 4.21 and 4.22) the expressions of reluctances of the air-gaps (4.24) and the characteristics of the permanent magnets (equation 4.25 and 4.26) and dividing all by the air-gap cross section (A_g) four fluxes density are obtained.

$$B_1 = B_0 \frac{(k+1)[(1-h)(1+h+w+x_a-g)}{(k+1)(1-h^2)-w^2-(x_a-g)^2+2hw(z_a-g)}+$$
$$+ \frac{\frac{ni}{V_P}((k+1)(1-h)+(x_a-g)(1+w)-hw-w^2)]}{(k+1)(1-h^2)-w^2-(x_a-g)^2+2hw(z_a-g)} \quad (4.27)$$

$$B_2 = B_0 \frac{(k+1)[(1-h)(1+h-w-x_a+g)}{(k+1)(1-h^2)-w^2-(x_a-g)^2+2hw(z_a-g)}+$$
$$- \frac{\frac{ni}{V_P}((k+1)(1-h)-(x_a-g)(1-w)+hw-w^2)]}{(k+1)(1-h^2)-w^2-(x_a-g)^2+2hw(z_a-g)} \quad (4.28)$$

$$B_3 = B_0 \frac{(k+1)[(1+h)(1-h-w+x_a-g)}{(k+1)(1-h^2)-w^2-(x_a-g)^2+2hw(z_a-g)}+$$
$$+ \frac{\frac{ni}{V_P}((k+1)(1+h)+(x_a-g)(1-w)-hw-w^2)]}{(k+1)(1-h^2)-w^2-(x_a-g)^2+2hw(z_a-g)} \quad (4.29)$$

$$B_4 = B_0 \frac{(k+1)[(1+h)(1-h+w-x_a+g)}{(k+1)(1-h^2)-w^2-(x_a-g)^2+2hw(z_a-g)}+$$
$$- \frac{\frac{ni}{V_P}((k+1)(1+h)-(x_a-g)(1+w)+hw-w^2)]}{(k+1)(1-h^2)-w^2-(x_a-g)^2+2hw(z_a-g)} \quad (4.30)$$

The terms B_0 and k are defined as the normalizing value of flux density and a constant term that depends on the characteristics of the magnets and air, and are obtained as follow.

$$B_0 = \frac{\mu_P V_P}{2(k+1)l_0} \quad (4.31)$$

$$V_p = \frac{k_l \mu_a A_g l_p}{r \mu_P A_P l_0} \quad (4.32)$$

Since, the dimensionless parameters h, w, and g are born for taking in to account the unintended small inaccuracies of machining and assembling, they are small quantities that rarely exceed 0.1. Therefore, terms involving the powers and products of these quantities can be neglected. The equations 4.27, 4.28, 4.29 and 4.30 can be writing in the simplified form that follows.

$$B_1 = B_0\{(1+w) + (1-h)[(x_a - g) + (k+1)\frac{ni}{V_P}]\} \qquad (4.33)$$

$$B_2 = B_0\{(1-w) - (1-h)[(x_a - g) + (k+1)\frac{ni}{V_P}]\} \qquad (4.34)$$

$$B_3 = B_0\{(1-w) + (1+h)[(x_a - g) + (k+1)\frac{ni}{V_P}]\} \qquad (4.35)$$

$$B_3 = B_0\{(1+w) - (1+h)[(x_a - g) + (k+1)\frac{ni}{V_P}]\} \qquad (4.36)$$

Looking at the equations above, appears immediately that the flux densities B_I $(I = 1, 2, 3, 4)$ are composed by two parts; the first part does not change with the input current, while the second part represents the change due to the input current. A detailed analysis of the influence of geometric parameters introduced shows as:

- the relative vertical imbalance, h, does not appear in the quiescent value, it only influences the current coefficient

- the relative imbalance of left and right,w, does not influence the current coefficients

- the relative incline of armature, g, works as an offset of x_a

At the end combining equations 4.33, 4.34, 4.35 and 4.36 in the equation 4.12 the torque is obtained, this depends from the building materials, from the geometric and construction characteristics and from the position of the armature. The term B_0 is collected and fluxes density dimensionless obtained are indicated as b_I $(I = 1, 2, 3, 4)$.

$$T = \frac{L_A A_g B_0}{4\mu_a}(b_1^2 + b_2^2 + b_3^2 + b_4^2) \qquad (4.37)$$

The torque produced by the motor induces a displacement of the armature and consequently a variation of the flapper position (x_f), which is rigidly connected to armature therefore, the two displacements are dependent by a coefficient $(x_f = k_{af}x_a)$. In order to evaluate the flapper position the mathematical model solves the dynamic equation obtained from the free body diagram presented in figure 4.13. The acting torque (T) is contrasted by the inertial effect$(I_f\ddot{x}_f)$, and by the damping $(b_f\dot{x}_f)$ and elastic $(K_f x_f)$ moments related to the physical properties. In addition, the flapper is connected to the spool by a spring which has the function of centering the two components,
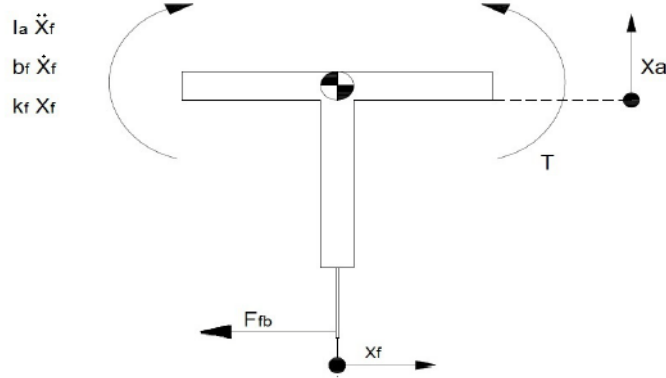
Figure 4.13: Flapper free body diagram

the force generated by the spring acting in the opposite direction respect the displacement ($F_{fb} = x_f + x_s$).

Taking into account all this component and the positive direction concordant with the displacements, the dynamic equilibrium can be written as follow.

$$I_a \ddot{x}_f = T - b_f \dot{x}_f - K_f x_f - F_{fb} \tag{4.38}$$

The displacement of the flapper causes a variation of the discharge coefficients of the two nozzles, therefore a change of the pressures in the chambers (P_{sv_1} and P_{sv_2}) place to extremity of the spool is created. The hydraulic amplifier has been implemented in the model with a linear function dependent on the position of the flapper and the speed of the spool.

$$P_{sv_1} = G_P \left(x_f - \frac{A_{spool} \dot{x}_s}{G_Q} \right) \tag{4.39}$$

$$P_{sv_2} = G_P \left(-x_f + \frac{A_{spool} \dot{x}_s}{G_Q} \right)$$

Where G_P and G_Q are the pressure gain and the flow gain, respectively. $\dot{x}_s$ is the velocity of the spool and A_{spool} is the spool active area. The second term inside the brackets allows to consider the change in volume of the two chambers.

The pressure differential which is formed across of the spool ($\Delta P_{spool} = P_{sv_1} - P_{sv_2}$) involves an imbalance of the forces which in induces a displacement of the shutter. The magnitude of the shift is determined by solving

the dynamic equation that is obtained from the free body diagram shown in figure 4.14.
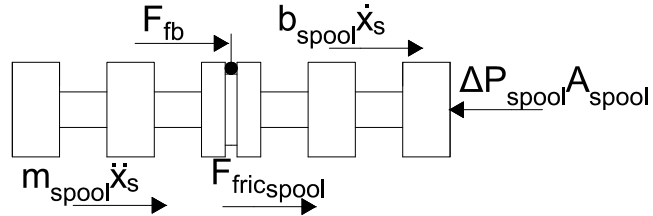
Figure 4.14: Spool free body diagram

$$m_{spool}\ddot{x}_s = \Delta P_{spool} A_{spool} - b_{spool}\dot{x}_s - F_{fric_{spool}} - F_{fb} \qquad (4.40)$$

Where m_{spool} is the mass of the spool, b_s is a damping coefficient and $F_{fric_{spool}}$ is the Coulomb friction force implemented in the model as well as the actuator friction force (section 4.2.1); since there are no seals, the dynamic friction force is a constant value and does not follow the laws proposed by Martini 1984.

With the determination of the position of the spool the first subsystem, in which is divided the servovalve, is concluded. The second subsystem is responsible for computed the control flows generated by the servovalve and direct to the cylinder chambers. The problem of determining the flow rates has been solved by applying the similarity electricity, in particular the Wheatstone bridge (Merritt 1967) shown in figure.
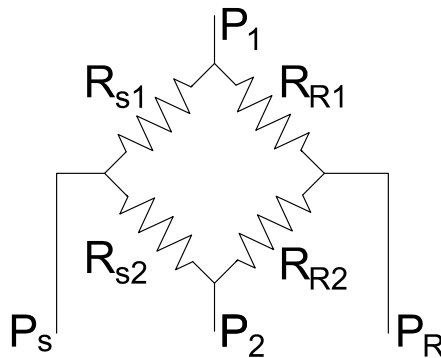
Figure 4.15: Equivalent Wheatstone bridge

The adopted model considers each flow (Q_1 and Q_2) as the difference of two components: a flow from the supply (Q_{1s} and Q_{2s}) and the second one direct to return (Q_{1r} and Q_{2r}). The amount of each component depends on the value of the fluidic resistance and the pressure drop among the resistance.

$$Q_1 = Q_{1s} - Q_{1r} \tag{4.41}$$
$$Q_2 = Q_{2s} - Q_{2r}$$

Each of the four resistances can be divided into two components: a laminar term (R_C) and a turbulence one (R_A). The laminar term represents the lost when the fluid pass through the thin radial gap between sleeve and spool. In this condition the flow rate is so small that **Re** is sufficiently low as to enable the flow laminar. The turbulence term represents the discharge resistance, in the section is characterized by a higher **Re**. The following paragraph describes how the resistance of the supply port connected with the actuator chamber 1 is calculated and the equations that determine the flow rate which passes from the same port. The same considerations and equations can be applied to the other three ports, just changing the signs of various variable. Depending on the position of the spool and the length of the overlap (ov_{1s}) three cases can be defined:

- $\mathbf{x_s} < \mathbf{ov_{1s}}$: R_C and R_A are present, see figure 4.16

- $\mathbf{x_s} = \mathbf{ov_{1s}}$: only R_A is present, see figure 4.17

- $\mathbf{x_s} > \mathbf{ov_{1s}}$: only R_A is present, see figure 4.18
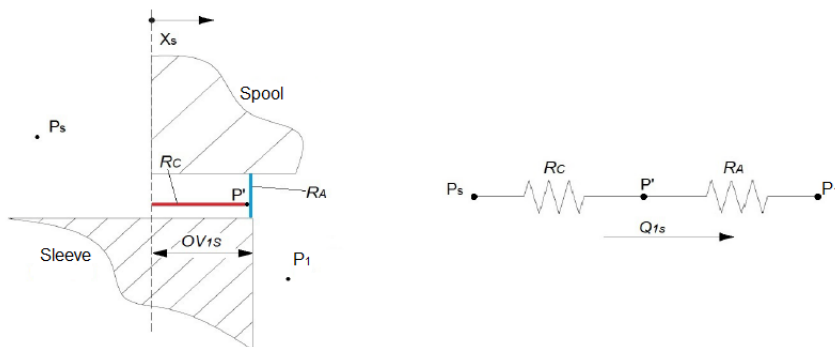
Figure 4.16: Resistances in case of $xs < ov_{1s}$

When the position of the spool is smaller than the overlap (figure 4.16), the flow that moves from supply to actuator chamber first pass through the

radial clearance, at this time the flow is laminar and its pressure drops can be obtained with the resistance R_C. When the flow meets the edge of the sleeve its motion becomes turbulent and the resistance R_A must be used. Using the electrical similitude R_C and R_A are two resistances placed in series, between them an artificial pressure callP' can be assumed.
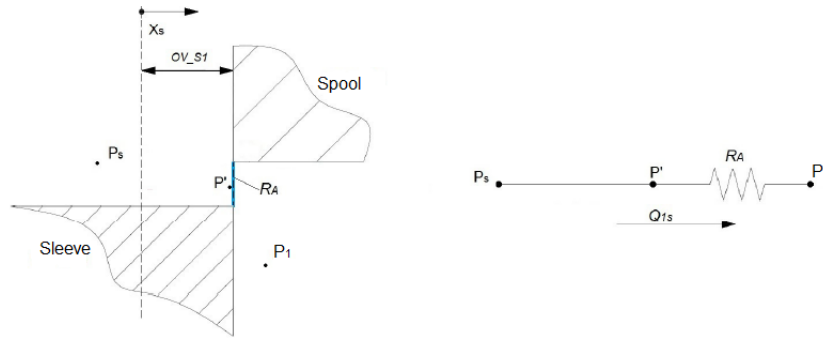
Figure 4.17: Resistances in case of $xs = ov_{1s}$

In case of spool position equal to overlap, the laminar resistance R_C is lost and R_A is the only remaining. The pressures P_S and P' are in fact the same. (Figure 4.17)
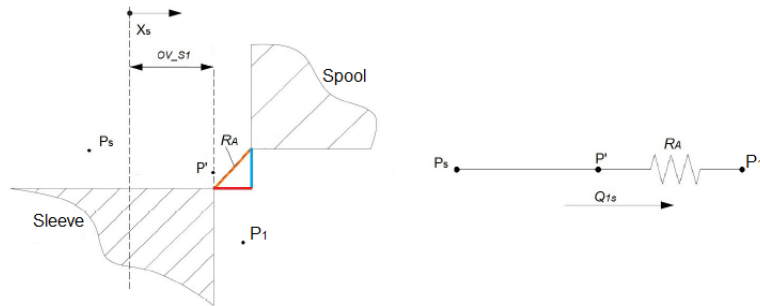
Figure 4.18: Resistances in case of $xs > ov_{1s}$

When x_s surpasses the overlap (figure 4.18), as in the previous case, the resistance R_A is the only one present, but now cross-section is that perpendicular to the oil path from sleeve edge to spool edge. In order to evaluate cross-section, Pythagoras' theorem was applied to the projections of the area on longitudinal and diametrical axes (see figure 4.19): the first, $Ax = w_{sv}(x_s - ov_{s1})$ is variable and depends on spool displacement thus being, the second, $A_{LK} = w_{sv}h_{sv}$ is fixed. In the formulas w_{sv} is the width of the port and h_{sv} is the radial clearance.
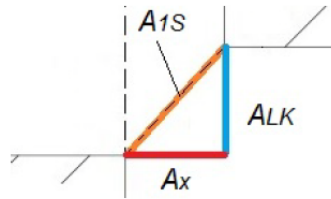
Figure 4.19: cross-section area in case of $xs > ov_{1s}$

From what has been said previously, obviously the two resistances are functions of the position of the spool and of geometric characteristics of the servovalve. The R_C equations (4.42) is linear dependent from x_s and presents an inverse cubic dependence on the radial gap. the R_A (equation 4.43) dependence on the inverse square of the section, which in turn depends on the inverse square of clearance gap. In the graph 4.20 and graph 4.21 are reported the qualitative trends the two resistances according to the spool displacement.

$$R_C = \frac{12\mu_{oil}(x_s - ov_{s1})}{2.5w_{sv}h_{sv}^3} \tag{4.42}$$

$$R_A = \frac{\rho_{oil}Q_{1s}^2}{2Cd^2A_{1s}^2} \tag{4.43}$$

Where μ_{oil} andρ_{oil} are viscosity and density of the hydraulic fluid, A_{1s} is the cross-section area and Cd is the discharge coefficient,for more details on how it is calculated please refer to subsection 4.3.1.
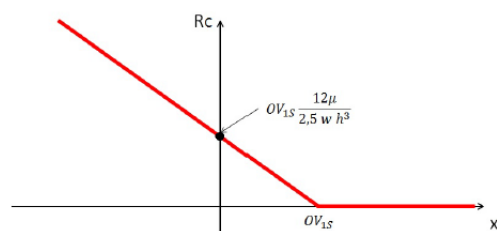
Figure 4.20: Laminar resistance versus spool position

Known the value the two resistances and by applying the similarity electrical presented in the figure, a system of two equations that connects flows and pressures can be writing.
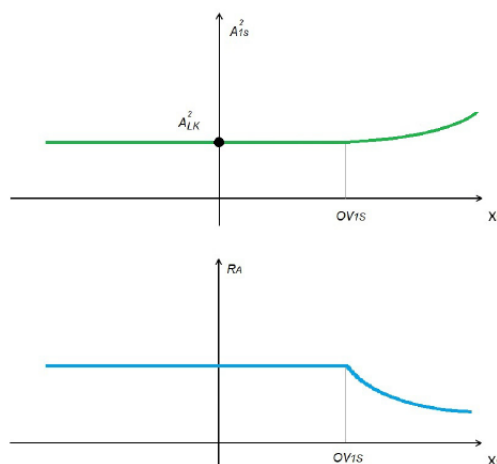
Figure 4.21: Top to bottom: turbulent flow section and resistance versus spool position

$$\begin{cases} P_S - P' = R_C Q_{s1} \\ P' - P_1 = R_A Q_{s1}^2 \end{cases} \tag{4.44}$$

Solving the system of equations 4.44 the equation that defines the flow transiting by the supply port connected to chamber 1 is obtained.

$$Q_{s1} = \frac{-R_C + \sqrt{R_C^2 + 4R_A|(\Delta P)|}}{2R_A} sgn(\Delta P) \tag{4.45}$$

By solving the equations for the three remaining streams, the return from chamber 1 and chamber 2 supply and return, the two control flows rate direct to the actuator are obtained.

4.3.1   Discharge coefficient

The discharge coefficient plays a crucial role in determination of the turbulence resistance R_A and consequently of the flow that passes through a port. In the case study presented, set a constant coefficient does not allow obtain sufficiently accurate results because the field of motion of the fluid changes considerably. Has therefore been decided to include in the model a script that is responsible to updating for each time instant the discharge coefficient according to the flow rate. In the following of paragraph only the case related to the supply port of chamber 1 is presented, in order to reduce the discussion, but the same methodology are applied for all ports.

The discharge coefficient is a function of a first approximation of the Reynolds number and of the geometrical characteristics of the port; therefore the following equation one can get a first good approximation.

$$Cd = 0.22\sqrt{log(1 + \mathbf{Re})}\frac{1 + 0.2h_{sv}}{x_s + h_{sv}} \tag{4.46}$$

The Reynolds number is computed by the equation below and saturated to 5000.

$$\mathbf{Re} = \frac{2\rho_{oil}Q_{1s}}{\mu_{oil}\left(w_{sv} + \sqrt{(x_s - ov_{s1})^2 + h_{sv}^2}\right)} \tag{4.47}$$

The indication given by the equation 4.46 is refined further multiplying the result by a factor (c_{cd}) depending on the ratio between the radius of the edges and the equivalent diameter of the port passage. The factor is defined by the equation presented below, where r_{edge} is the radius of the spool edge.

$$c_{cd} = r_{edge}\frac{w_{sv}\sqrt{(x_s - ov_{s1})^2 + h_{sv}^2}}{2w_{sv}\sqrt{(x_s - ov_{s1})^2 + h_{sv}^2}} \tag{4.48}$$

The coefficient c_{cd} is used to consider the ratio of variation of the oil passage shape. For great value of c_{cd} the shape variation is smoothed therefore, the flow adheres more easily to the border, minimizing the formation of swirls. Less swirls means a larger vena contracta and therefore a greater outflow of fluid.

4.4   Surface

The aileron surface has been modeled as lumped system with a single of freedom (x_L, $\dot{x}_L$, $\ddot{x}_L$), it is connected to the actuator by a stiffness K_L and a damper C_L arranged in parallel. As shown in the figure 4.22 an other damper (C_{ext2}) has been included in the model, situated between the surface and a rigid structure, has the task of simulating the losses due to friction and also stabilizes the mathematical model.

The total force generated by the spring K_L and the damper C_L, called F_{ext} (equation 4.49), represents the force exchanged between the surface and the piston rod . The same force had been previously used in the equation 4.8.

$$F_{ext} = K_L(x - x_L) + C_L(\dot{x} - \dot{x}_L) \tag{4.49}$$
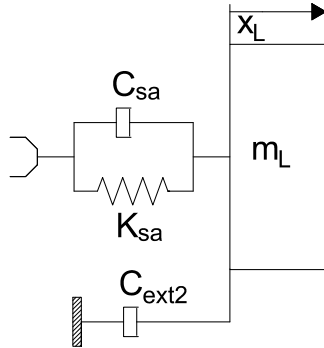
Figure 4.22: Surface lumped model

Starting from the free body diagram of the figure 4.23, the equation of equilibrium of the surface was obtained (4.50).
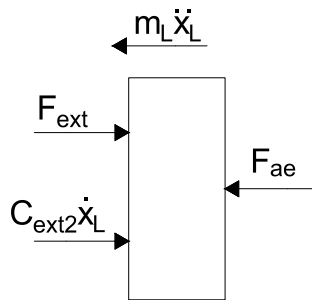
Figure 4.23: Surface free body diagram

$$m_L\ddot{x}_L = +F_{ext} - C_{ext2}\dot{x}_L - F_{ae} \qquad (4.50)$$

Where m_L is the equivalent load mass and F_{ae} is the aerodynamic force presented in the section 4.7. The position of the surface is obtained by a double integrator of the $\ddot{x}_L$.

4.5   Controller

The reference EHSA has two identical controllers placed in parallel, in order to ensure redundancy in case of failure of one of the two; each controller supplies a different winding,also placed in parallel, of the torque motor. In

nominal conditions each controller provides a serovovalve current equal to half of that required; in case of breakdown, the working controller shall provide the totality of the necessary current in order to ensure the correct behavior of the servocommand.

The control law implemented is a PI, proportional and integrative, in which the two contributions are summed together to obtain the control current of the servovalve, see scheme (4.24). The integrative branch has two non-linearity:

- **Dead zone:** placed before the integrator, it has two functions: the first is to deactivate the integral branch when the steady state error is small enough, thus eliminating the limit cycle. The second function is to filter the error oscillations due to machine and solver accuracy.

- **Saturation:** positioned after the integrator, it shall define the contribution of the integral.
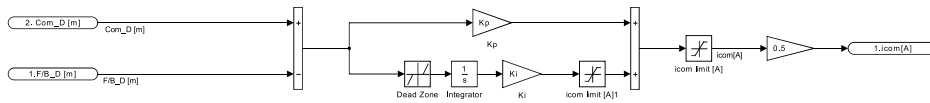
Figure 4.24: Scheme of controller

Downstream of the controller is placed a further saturation block which limits the current to the maximum value accepted by the servovalve; After the current is divided by two only when both controller are active.

The servovalve current was corrupted,as proposed by Borello et al. 2009, by adding a disturbance current i_{noise} defined as the sum of three terms:

$$i_{noise} = i_{noise1} + i_{noise2} + i_{noise3} \qquad (4.51)$$

In the equation the three terms represent a different sources of noise:

- i_{noise1}: is a constant bias and set equal to 2% of the relate current

- i_{noise2}: s a short term variation of the servovalve offset and was assumed to occur as a step, reach a maximum of $\pm 3\%$ of the rated current, last up to 2 s and be repeated with a time interval up to 10 s according to a random pattern.

- i_{noise3}: is a long term variation of the offset, which is mainly related to fluid temperature changes. It was assumed to take place as a ramp variation, have a maximum of $\pm 5\%$ of the rated current, last up to a minute and occur in a random way.

For the generation of the random pattern refer to appendix A.

4.6   Position transducer

The position control loop is closed by linear variable differential transformer transducer (LVDT), its model is a transfer function of the second order, which allows to simulate the delay and attenuation introduced by the sensor.

The signal generated by the LVDT is transform by a 14-bit analog to digital converter with a sample frequency equal to 350 Hz. During conversion the signal is corrupted by a noise with random amplitude comprised in the range ± 4 time the least significant bit.

4.7   Aerodynamic force

The aerodynamic force acting on the surface can be considered the main source of disturbance of the servoactuator, in the definition and implementation of the mathematical model a particular attention has been paid to write this part.

The force, whose scheme is presented in the figure 4.25, is caused by speed the air flow that runs over the wing surface, which it has been modeling as the sum of the following components:

- **Atmospheric wind:** it is represented by a Gaussian distributed random signal, with mean value set by the user as a function of the operating conditions simulated. It can be concordant or discordant with the speed of the plane

- **Atmospheric gust:** the intensity of which is include in random way between one and two times the wind speed, duration is determined by a random number generator. Gust occurs in a random pattern and it can be concordant or discordant with the speed of the plane

- **Aircraft speed:** is the velocity of the airplane respect the ground

- **Turbolence:** has been they were modeled using the model of Dryden by passing band- limited white noise through appropriate forming

filters. According to MIL-HDBK-1797 1997 and MIL-F-8785C 1991 turbulence is a stochastic process defined by velocity spectra. For an aircraft flying at a speed V through a frozen turbulence field with a spatial frequency of Ω radians per meter, the circular frequency ω is calculated by multiplying V by Ω The frozen turbulence field assumption is valid for the cases of mean-wind velocity and the root-mean-square turbulence velocity is small relative to the aircraft ground speed
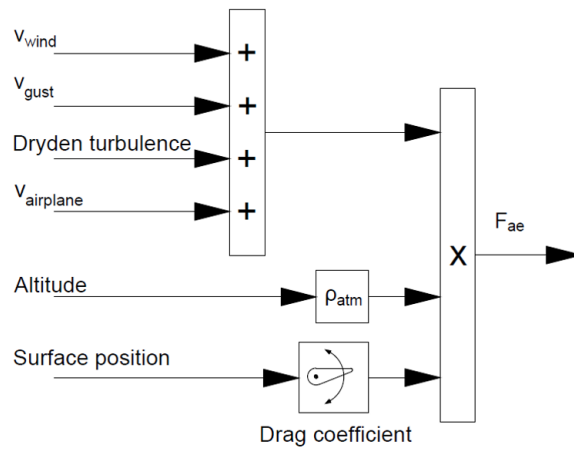
Figure 4.25: Aerodynamic force model

The sum of the four components of the velocity, call $v_{wind_{tot}}$, is then multiplied by the density of the air, function of altitude, and by the position of the surface in order to take account of the variation of the drag coefficient function of surface angle (equation 4.52).

$$F_{ae} = (1 + k_{ae1}|x_L|)\rho_{air}k_{ae2}v_{wind_{tot}}^2 \tag{4.52}$$

Where k_{ae1} and k_{ae2} are numeric coefficients, ρ_{air} is the density of the air at the actual altitude and x_L is the surface position.

4.8 Oil Properties

The hydraulic fluid used in the actuator of reference is the Skydrol 500, a fluid specially designed for an aerospace use, able to work in a wide temperature range. Although its use is guaranteed by the manufacturer from -54 °C to 100 °C (Skydrol Overview 2014), its properties vary significantly as a function

of operating temperature and minor way from supply pressure. Appears, therefore, clear that a model that would allow the studies related to the influence of degradation must absolutely take into account the changes in these parameters. The mathematical model implemented presents a code that allows to upgrade the density, viscosity and Bulk modulus as a function of the instantaneous temperature an pressure.

The density of the fluid varies linearly with temperature and it is not affected by the pressure, it is describe by the equation 4.53 where ρ_0 is the density at 0 °C, *ad* is coefficient and T_{oil} is the oil temperature, the trend of the density is presented in the graph

$$\rho = \rho_0 - ad * T_{oil} \tag{4.53}$$
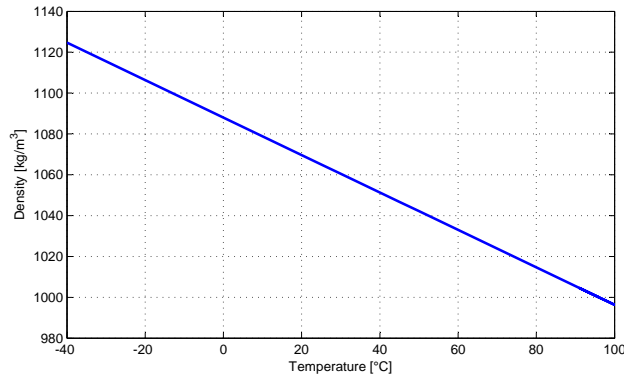
Figure 4.26: Fluid density function of temperature

Absolute viscosity (μ) is dependent from the density of the fluid and the kinematic viscosity (ν) as shown from formula 4.54, the latter is correlated to the temperature only by the equation 4.55, in which *av*, *bv* enc *cv* are numerical coefficients. The diagram 4.27 shows the absolute viscosity trend function of temperature.

$$\mu = \frac{\rho\nu}{1000^2} \tag{4.54}$$

$$\nu = cv + 10^{10^{av-bv*T_{oil}}} \tag{4.55}$$

The Bulk modulus is the parameter most difficult to assess, since it depends directly on the temperature and indirectly from the supply pressure. The dependence from the pressure is due to the non-dissolved fraction of air which is in fluid as bubbles, the air has the same pressure of the fluid that
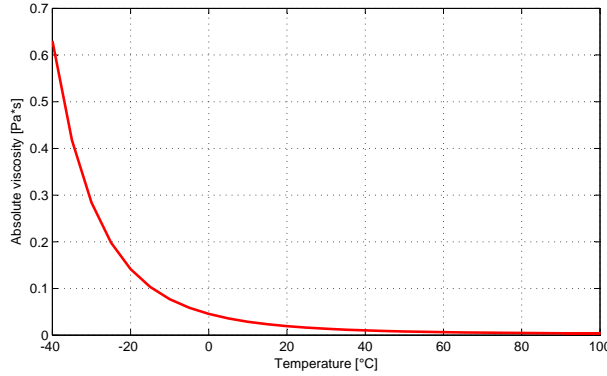
Figure 4.27: Absolute viscosity function of temperature

surrounds it. It seems obvious that an increase in the volume of non-dissolved air does reduce the bulk form, due air has a greater compressibility.

The implemented code first calculates the Bulk modulus assuming no air undissolved by the equation 4.56, where β_0, ab and bb are coefficients.

$$\beta_r = (\beta_0 - ab * (T_{oil} + 54) + bb(T_{oil})^2) \cdot 10^6 \qquad (4.56)$$

The β_r must be adjusted to take account of the volume of free air, the quantity of non-dissolved air at different temperatures is an information difficult to obtain, in order to made an estimation the hypothesis that the quantity in mass of air present in the hydraulic system (free air plus dissolved air) is constant was made; under this assumption it is possible by knowing the percentage of dissolved and not dissolved air at zero degrees Celsius extrapolate the free air at all temperatures. The volumetric fraction of free air at zero degrees Celsius is generally considered a with a good approximation equal to $fr_0 = 0.015$. The volumetric fraction of dissolved air within the fluid at 0 °C (L_0) is determined by the equations of Beerbower 4.57 and Ostwald 4.58, proposals from Hansen 2007, Battino, Rettich, and Tominaga 1983 and Fredlund 1976.

$$lnL_0 = (af(d1 - d2)^2 - bf)(1 - \frac{273}{237 + T_0}) - cfd1 - df(ef - d2)^2 + ff \qquad (4.57)$$

$$L_0 = e^{lnL_0} \qquad (4.58)$$

Where af, bf, cf, df, ef and ff are numerical coefficients, $d1$ is defined as $d1 = kd_1 * nl + kd_2$ where kd_1 and kd_2 depend on the nature of the mixture,

nl is the fluid refractive index and *d2* depends on the type of mixture and is provided by experimental tables.

The same equations proposed above may be used to calculate the volumetric fraction of dissolved air at any temperature (L) by replacing T_0 with the desired temperature. Under the assumptions made previously is therefore possible to obtain the volume of free air applying the equation 4.59, where ρ_{a0} is the density of air at 18 MPa and temperature equal at 0 °C and ρ_a is the density of air in the new pressure and temperature condition.

$$fr = (fr_0 + L_0)\frac{ro_{a0}}{ro_0}\frac{ro}{ro_a} - L \tag{4.59}$$

The Bulk modulus can be then corrected in function of the fraction of free air with the equation 4.60, where P_{oil} is the oil pressure. The diagram 4.28 shows the form of bulk at different temperatures for a pressure of 18 MPa.

$$\beta = \frac{1}{\dfrac{1}{\beta_r} + \dfrac{fr}{P_{oil}}} \tag{4.60}$$
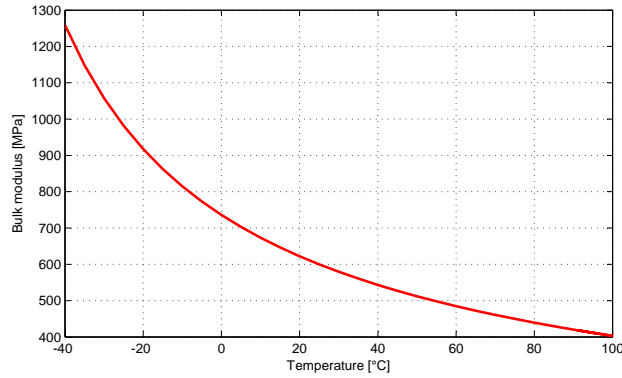
Figure 4.28: Bulk modulus for different temperature

5
Mathematical model validation

The validation of the model, with data obtained from experimental tests, is always a key step to be confident about the goodness of the results produced by the simulation. In the project present in this PhD thesis validation is even more important, because the results produced by the mathematical model are the basis for the development of PHM system; hence an error in the equations implemented or model result inaccurate and untrue, could affect the algorithms implemented, making the prognostic results completely wrong.

The validation was carried out in collaboration with *Lufthansa Technik AG*, which has made available, at Hamburg headquarters, its laboratories and test benches, the fly-by-wire primary flight control actuators and its staff and engineers. The validation process was divided into two different steps: first the response of the open loop model was compared with the experimental data, in the end the model closed loop was evaluated.

Lufthansa Technik AG has provided a *Boeing 777* flaperon coming from a aircraft in its fleet, it is reviewed and is equivalent to a new actuator; therefore, degradations are not present. The validation of servosystem has been facilitated by the layer structure used to implement the model (refer to section 4.1): the three layers, the one containing the mathematical model, has not undergone any change inasmuch the structure of the two servo actuators is identical. In order to correct the parameters of the model *EHSAData* and *EHSASeal*, placed in the second layer, are the only ones that had variations. The data file was modified by replacing, for each parameter, the old values with with those which best fit the experimental results; same change was made in the file *EHSASeal*.

The mathematical model has been validated only with the actuator in nominal conditions, because the equipment available at did not allow to test the servoactuator in the presence of degradations. The cooperation with *Lufthansa Technik AG* is still continuing, and one of the next targets is develop new test benches specifically designed to test actuators with different kind of degradation. More detailed information about the validation procedures can be obtained from the master thesis debated by Ferri (2014), born from the collaboration between *Politecnico di Torino* and *Lufthansa Technik AG*.

5.1   Test Bench

Tests on *Boeing 777* flaperon have been performed according the experiment set up in figure 5.1. The hydraulic test bench provides hydraulic supply and return to ElectroHydraulic Servovalve (EHSV), which receives command current from the real time measurements system. By means of a test console and related software running on PC the user can decide between the two test configurations: open loop and close loop. Selecting the first configuration, the real-time platform provides directly the analogic control current to the servovalve, the position of the rod and that of the spool have acquired and stored for future analysis.
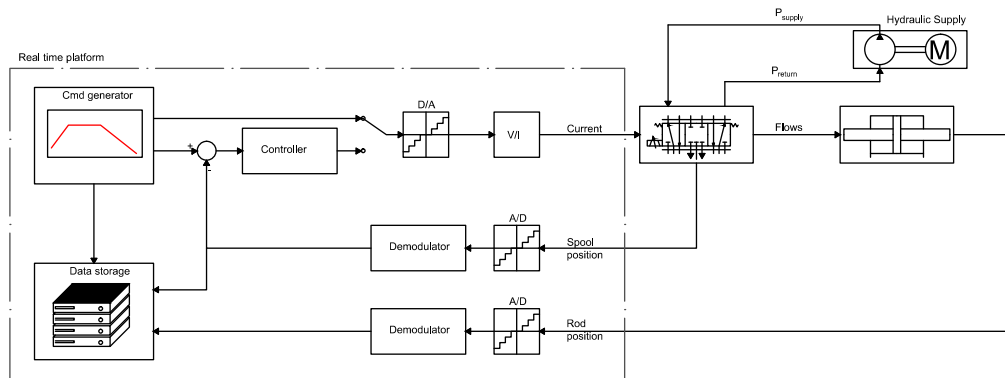
Figure 5.1: Test bench scheme

In the case of closed-loop, real-time platform also performs the function of the controller, comparing the command with the position feedback and then closing the position loop. The compensated error is converted in an analogic signal and converted in current through a V/I converter integrated

in the test console. The spool position LVDT signal, is collected but not used in the control loop.

All tests are performed in the test bench shown in figure 5.2 ; the Unit Under Test (UUT) is installed using the appropriate supports and hydraulic supply and electric supply are controlled directly by the real time measurement system. The tests rig is designed for housing several *Boeing 777* EHSAs through removable modules. The flaperon EHSA bottom part is linked by an orifices plate to a vertical support that act as an hinge suppressing rigid transnational degrees of freedom. The rod ends with a ball-joint that is fixed to the test fixture through linearly guided plate so that the only allowed movement is the piston and cylinder relative translation. Furthermore, the change of position of the plate and with it the position of the main ram, are measured with an incremental sensor installed on the plate.
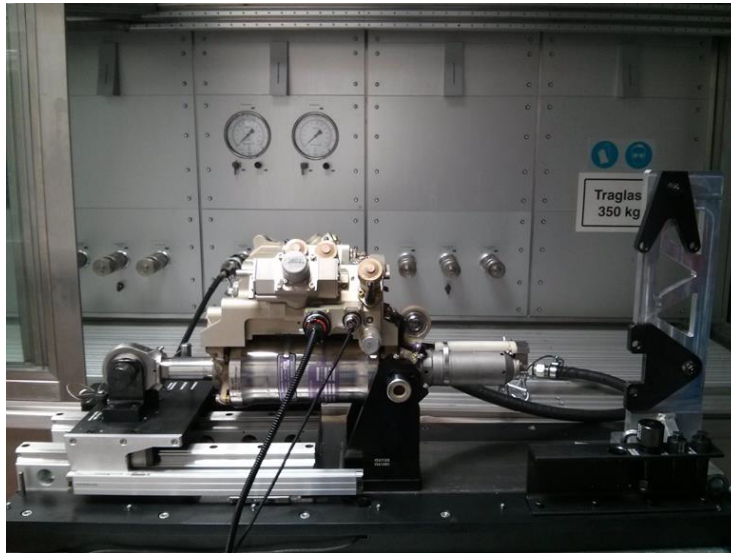
Figure 5.2: Test bench and UUT

The hydraulic power is provided to the UUT by a hydraulic unit and manifold (figure 5.3) through two pressure ports, that providing supply pressure controlled from 0 bar to 350 bar and flow controlled from 0 l/min to 80 l/min at 350 bar, one port has accumulator for pressure oscillation compensation. A conditioning circuit allows acting on Skydroll temperature from ambient temperature till 45 °C.
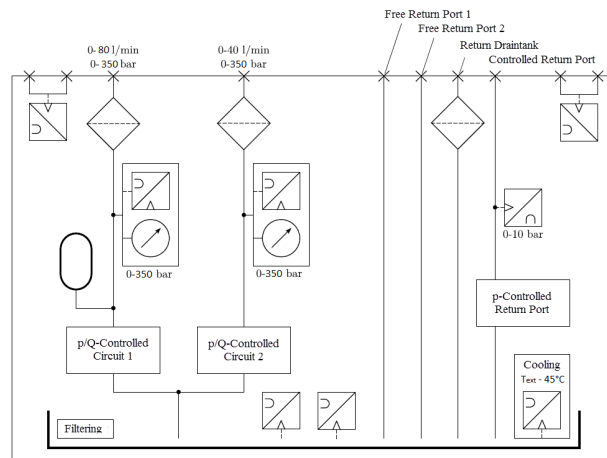
Figure 5.3: Hydraulic unit scheme

5.2   Open loop tests

Tests carried out in open loop are fundamental to understand if the model of the servo valve is sufficiently accurate, since the EHSV is controlled directly by means of a current generated by the the real-time platform: current thus generated is not affected by the position error and the controller. In open loop tests, of the three acquired signals from the test bench, the position of the servovalve spool is the most important, since a great similarity between the model of the experimental data shows that the dynamic model of the servovalve, torque motor, hydraulic amplifier and spool dynamic, is implemented correctly.

All tests were conducted by imposing a step change in EHSV current, below the results of three of the various tests that have been carried out in open loop are shown,these results have been chosen because they are truly representative of the EHSV behavior: the first test presents a small variation of the current equal to ± 5 % of maximum current (figure 5.4a), the second is related to a current step equal to ± 20 % of maximum current (figure 5.4b) and the last test was carried out by imposing a large step change in current equal to ± 80 % of maximum current (figure 5.4c). In all three tests the position of the EHSV spool simulated and that obtained from the experimental tests are superimposed, synonymous of a good dynamic model of the servovalve, while the position of the actuator shows some errors in the order of tenths of a millimeter, these inaccuracies are obviously more evident in the first case because the total displacement is smaller.
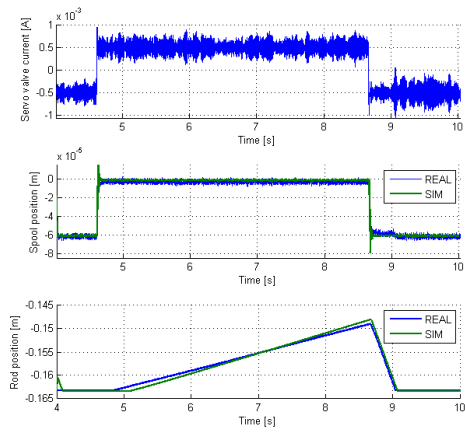
(a) Current step ±5 %
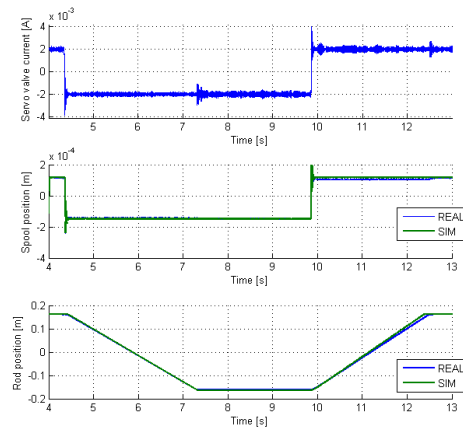
(b) Current step ±20 %
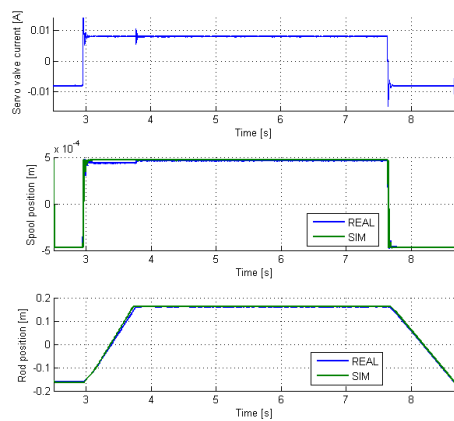
(c) Current step ±80 %

Figure 5.4: Open loop validation results

5.3   Close loop tests

The evidence in closed loop, presenting the feedback loop, are a good starting point to validate the hydraulic model of the EHSV and the actuator. By comparing the position of the actuator experimental with that simulated it is possible to calibrate the radial clearance and the overlap of the spool, while the geometric data of the actuator are considered almost exactly since supplied by the manufacturer with their geometric tolerances. Even the parameters of the controller were not calibrated given that provided by the manufacturer.
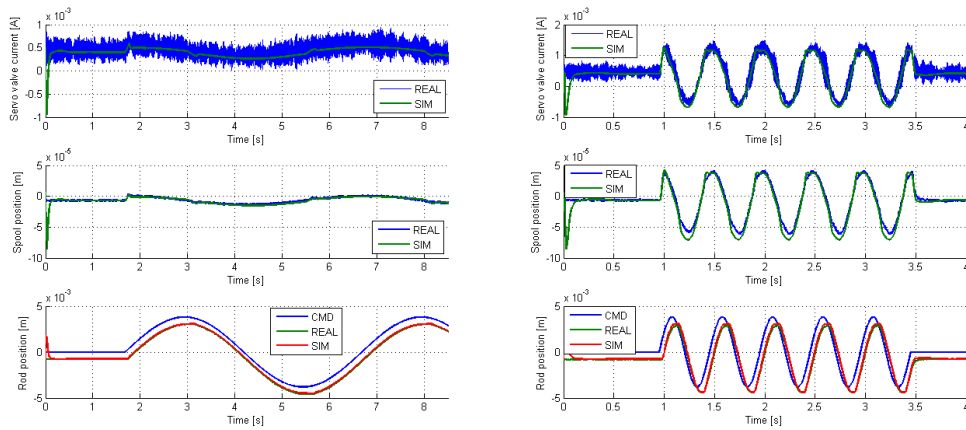
(a) Sinusoidal cmd, amp 4 mm freq. 0.2 H   (b) Sinusoidal cmd, amp 4 mm freq. 2 Hz
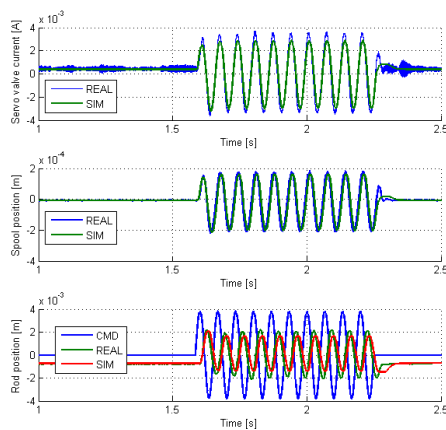
(c) Sinusoidal cmd, amp 4 mm freq. 15 Hz

Figure 5.5: Close loop validation results

The tests were conducted by generating different types of position commands, sinusoidal, ramp and step, in which have been made vary the amplitude and frequency. From all the tests made results of three tests sinusoidal, all made with amplitude equal to 4 mm and variable frequency are proposed. The first was conducted with a frequency of 0.2 Hz (figure 5.5a), the second with a frequency of 2 Hz (figure 5.5b), and the third with a frequency of 15 Hz (figure 5.5c), which is already widely beyond the normal range of EHSA operation.

All three tests have provided exceptional results in term of EHSV current and EHSV spool position, the experimental results and numerical are superimposed. While as regards the position of the actuator, at lower frequencies the model has a good accuracy. In the latter case instead the model response is slightly delayed and attenuated compared to the experimental data but, as stated previously, 15 Hz is not one of the typical operating frequencies of the hydraulic servocontrols, which normally work under the 10 Hz.

5.4   Validation results

The validation carried out in collaboration with *Lufthansa Technik AG* has shown how the mathematical model is sufficiently accurate to be used for the development of a prognostic system. In all tests conducted, both in open loop and in close loop, the EHSV current and position of the spool generate from the mathematical model are superimposed to the signals acquired from the test bench. Some minor differences are observed between the position of the actuator simulated and that acquired experimentally, but these discrepancies appear in the presence of commands with high frequencies, which are normally not used for fly-by-wire primary flight control actuators.

The validation of the mathematical model only in nominal condition, and not in degraded situations introduces obviously some uncertainties linked to the effects of the faults. But the present thesis wants to demonstrate the feasibility of a PHM system able to identify degradations which affect the servovalve; the algorithms that have been developed during the work does not have the claim to be immediately implemented in a boarded EHSA, but will subsequently be verified on the basis of real data and optimized for different servoactuators. So during the validation phase, verify that the equations, the parameters and the structure of the model were accurate and able to provide a good representation of the model was more important than study the effects of each degradation.

6

PHM strategy

Finding the correct strategy to be followed in the development of a system of prognostic and health management is a crucial step because from that derived all the subsequent developments: the identification of optimal features, the selection of the type fault of approach using for the degradation identification and for the estimation of the remaining useful life. The strategy to be adopted is not unambiguous and well defined, there may be various methodologies each with different advantages and disadvantages; as always, the task of every good engineer is to identify the strategy that maximizes the benefits and minimizes the negative points.

In the case study object of this thesis, the main limitations are imposed by the desire to develop a prognostics and health management system suitable for the greatest possible number of legacy airplanes, this choice implies two important limitations: the first is that no new transducer can be added to the existent systems. The second is that no structural variations and / or safety-critical components modification can be made. Therefore one of the key features of the research is the implementation of a PHM system taking advantage of sensing and information already available.

The choose of the PHM strategy to implemented was also conditioned by necessary computing power required to the algorithms, not knowing if these algorithms will be implemented in aircraft systems or dedicated servers, development algorithms that required few computational resource was considered the optimal solution; this position allows to the end user to adopt the configuration more convenient for him.

This chapter explains how the prognostics and health management strategy to be implemented was chosen, at the beginning the information available

on legacy EHSAs are present; then the features extraction process is shown, motivating reasons that led to this choice and highlighting the limitations of the system adopted. The last part is relative to the hypothesized operational scenario.

6.1   Available information

The primary flight control actuators installed on legacy aircraft were not designed for the implementation of prognostic and health management systems, therefore sensors installed are the minimum necessary to carry out their primary function: control the position of a wing surface; to these are added sensors for monitoring and diagnostics. However, these sensors do not always provide useful indications for prognostics, because have been studied to identify the break and not the degradations.

The typical structure of a EHSA for legacy aircraft, see figure 6.1, has only linear position transducers, normally LVDT, used for close the position loop. Traditionally more than one LVDTs are installed on the same actuator in order to ensure a safety redundancy. The position sent to the controller is obtained by merging the information from the different transducers by means of special algorithms, which are able to detect and to isolate potential broken transducers.

The LVDT transducers are analog, so the signals generated by them are converted to digital before being made available to the controller. The quality of the analog to digital converter depends on the plane, for the EHSA described in this thesis the sampling frequency is equal to 350 Hz and the resolution is 14 bit.
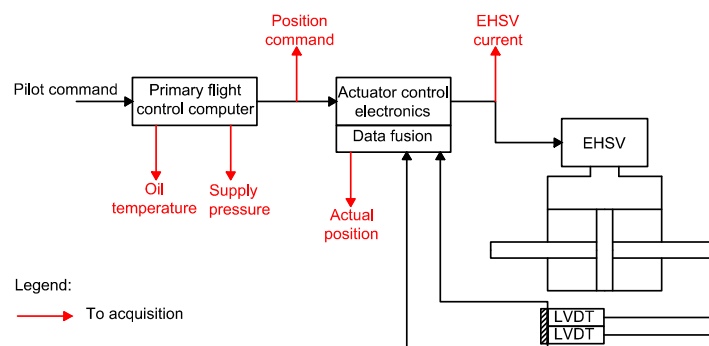
Figure 6.1: Available information in legacy EHSAs

Again with reference to the diagram of the figure 6.1, the other two infor-

mation that can be obtained from a legacy EHSA are the position command and the servovalve current, the first is processed by the primary flight control computer, while the second is provided by the actuator control electronics and it is coincident with the compensated error, both are digital signals.

The primary flight control computer also acquires numerous data coming from sensors located on the aircraft, such as the speed, information about the trim and the status of the different systems and subsystems. Among all this information has been decided to use in prognostic and health management algorithm the supply pressure and the oil temperature, both data are acquired from sensors located downstream of the hydraulic pump. Since these information are acquired only for monitoring, the frequency of acquisition is not high, such as in the case of position transducers, also their slow dynamics allows us to consider constant during each procedure.

In summary, the PHM system implemented must taking advantage for the degradations identification from five data, three principals and two secondary. The first set is composed by position command, servovalve current and rod position, all three are captured at 350 Hz with a resolution of 14 bit. In the secondary set of data there are supply pressure and oil temperature, acquired by the PHM system only at the begin of each test and supposed constant for the entire duration of the test.

6.2 Adopted strategy

The development of a prognostic and health management system for electro-hydraulic primary flight control actuators has encountered two major critical issues: the first related to the non a-priori knowledge of the commands that will be imposed to EHSA during the flight, the second is the load acting on the wing surface. Both problems are not easy to solve, especially if the PHM system must be suitable for legacy platforms.

The aerodynamic load acting on the surface could be easily acquired by placing a load cell between the actuator and the wing, but being EHSAs critical components for the fight safety this change would never be accepted. Another solution for estimate the load acting on the surface by a differential pressure transducer placed between the chambers of the actuator. This kind of transducer is installed on different modern EHSAs, especially on the actuators acting on the rudder and those that provide for an electrohydrostatic backup. In legacy platforms, however, the differential pressure transducer is not common, for so the possibility of use it in the PHM system was discarded.

A-priori knowledge of the stimuli provided to EHSA during the flight instead is definitely impossible to obtain, since they are functions of the fol-

lowed route, the environmental conditions and of any unforeseen occurred during the flight, for example holding maneuvers. One approach to solving this problem is to adopt a PHM strategy based on model-approach. Developing a complex mathematical model of airplane and EHSA, given in input the command generated by the primary flight control computer, the simulation of the EHSA behavior could be possible. Since the response of the actuator is affected by the temperature of the oil, by the supply pressure and by external loads, the model must include subroutines to estimate these quantities starting from the known information. Models of this complexity are usually implemented for flight simulators or for iron-bird, but the computing power required makes them not suitable to an on-bord implementation; also the required accuracy to identify degradations imposes an excellent knowledge of all aircraft, and its aerodynamics.

An interesting solution, proposed by Borello et al. (2009), is to exploit the pre/post-flight time to carry out the prognostic analysis and integrate this new procedure with the pre/post-flight checks. This solution has two significant advantages:

- **Command:** being the plane to the ground, stationary, the actuator can be stimulated with any type of command, therefore a command that maximizes the effect of degradation on the extracted features can be implemented. This possibility offers enormous prospects, since the choice of the features is no longer obligated from the operative behavior of the EHSA, but a recursive selection, in which the features are evaluated and eventually the command are modified in order to obtain new features, can be performed.

- **External load:** with the aircraft on the ground, the aerodynamic force of the depends only on atmospheric wind; therefore, it is small and only marginally affects the response servo actuator. The knowledge, by transducers, or the estimation, using models, of wing load is no longer required, since the external force can be assumed irrelevant.

The absence of external loads is at the same time also one of the main limitations of the adopted solution. Since there are no relevant aerodynamic forces, the actuator operates with a very small difference pressure between the two chambers, compared to the maximum possible; therefore eventual degradations of the actuator can not be detected because the system is able to compensate them by operating at a greater differential pressure. Of course, this reasoning is valid only for initial state degradations, but identifying fails while they are still at their early stage is the goal of the prognostic and health management systems.

As mentioned above can also be understood as an advantage, insensitivity of the actuator to deterioration during ground tests, allows to separate the degradations which affect the servovalve from those that affect the cylinder. Therefore a variation of the features extracted during pre/post-flight is certainly due to a degradation occurred at servovalve. In a further development, not the subject of this thesis, a strategy to identify the degradations of the actuator must definitely be implemented, in order to complete the PHM system.

6.2.1   Implemented command

The command to be given at EHSAs during the pre/post-flight procedure must meet two principal requirements: the most important of all is to allow the extraction of the biggest number of information about the state of the electrohydraulic servovalve. In addition the stimulus should be short enough to be easily integrated into the regular procedures, without slowing down the normal operating cycle of an aircraft; unlikely airlines would agree to further slow an already delicate phase of the flight, where every additional delay results in loss of money.

The definition of the command type has been led by the desire to emulate with a single stimulus all possible conditions of motion that an EHSA may encounter during its operational life. The command is designed as a sequence of various stimuli, each one able to maximize the effect of degradation on different features, referring to the figure 6.2, the four stimuli placed in sequence are:
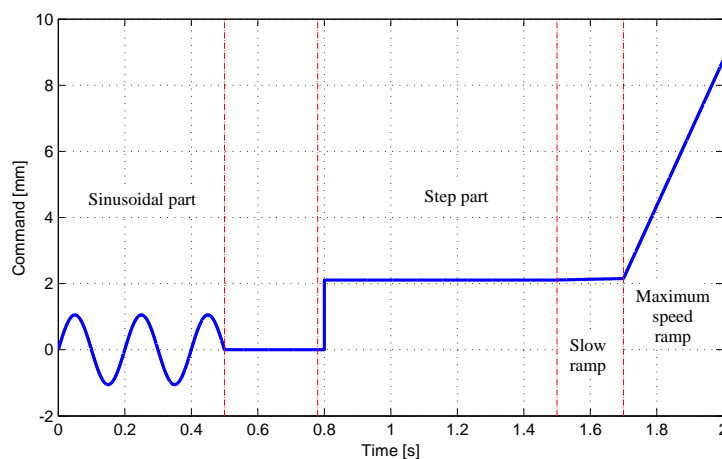
Figure 6.2: First version of the command

- **Sinusoidal:** amplitude 5% of the half actuator stroke and frequency equal to 5 Hz

- **Step:** amplitude equal to 10 % of half stroke

- **Small ratio ramp:** ramp command with a 0.22 mm/s ratio and 0.2 s of duration

- **Big ratio ramp:** the ratio of the command is equal to the maximum speed of the actuator, 22 mm/s, duration equal to 0.3 s

The duration of the command, two seconds, allows an easy integration of the same into the normal pre/post-flight procedures.

The analysis of the actual position of EHSA due to the stimulus, showed that the response of the servoactuator to the small ratio ramp was too influenced by external conditions and by electric disturbances, therefore no useful information about the status of the servovalve could be extracted. This stimulus is,thus, been deleted from the overall control, reducing its length to 1.8 s. The new command, shown in the figure 6.3, is therefore composed of only by three parts:

- **Sinusoidal:** amplitude 5% of the half actuator stroke and frequency equal to 5 Hz

- **Step:** amplitude equal to 10 % of half stroke

- **Big ratio ramp:** the ratio of the command is equal to the maximum speed of the actuator, 22 mm/s, duration equal to 0.3 s
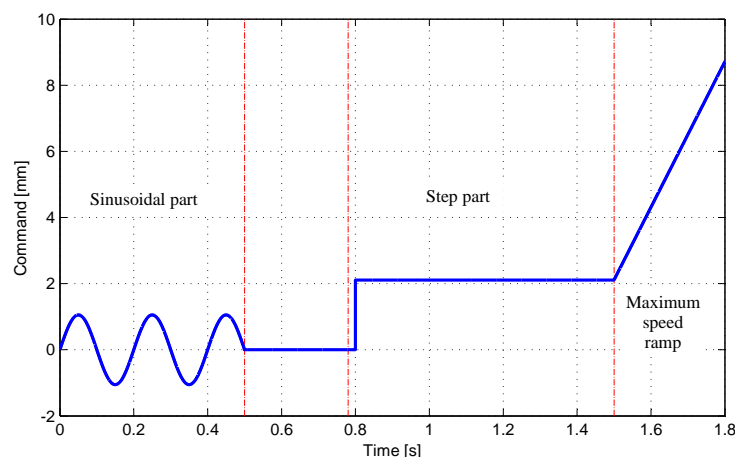
Figure 6.3: Definitive version of the command

The different stimuli are connected by constant command parts, which ensure that the actuator reaches the position demanded also with the servovalve degraded conditions. Moreover the overall response, position and current, is strongly influenced by the temperature of the oil, therefore these constants section also have the function of allowing the achievement of the position request at the lowest temperatures, in the figures 6.4 the response of the EHSA for three different temperatures (20 °C, -40 °C and 100 °C) is shown.
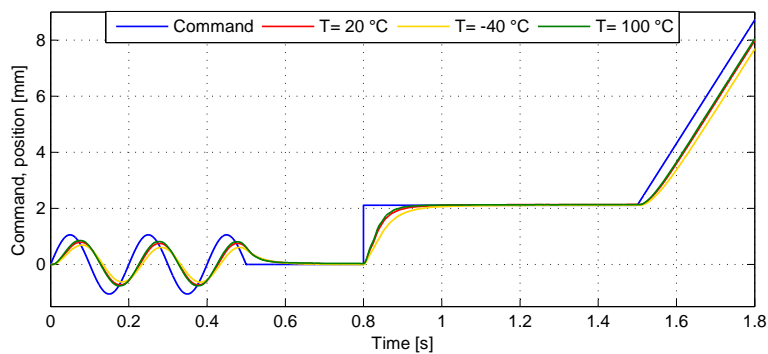
(a) Position
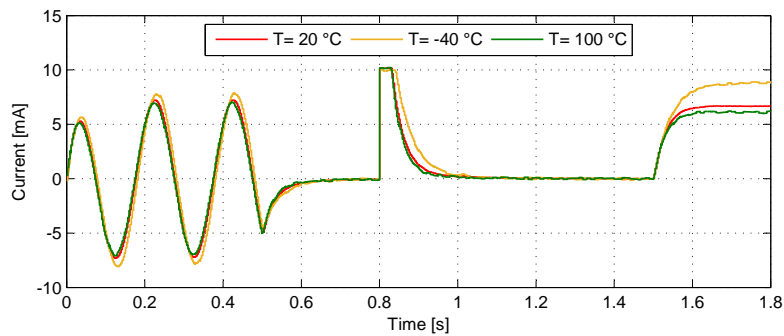
(b) EHSV current

Figure 6.4: Influence of temperature on EHSA behavior

Subdividing the overall response, and analyzing the behavior of the EHSA to the three stimuli individually, nine different features have been identified, four from the position data and five from the current. The features extracted are reported in the table 6.1, divided into type command and data used to extract them. A more detailed discussion of the features is proposed in chapter 7.

Table 6.1: Features identified

Type command	Features position	Features current
Sinusoidal	Gain	Current max
	Phase	Current min
		Current mean
Step	Rise time	Time decrease
Ramp	Steady state error	Current max ramp

The nine features identified are all related to the physics of the system, this decision was made to facilitate the understanding of what is happening to the servovalve and to the servoactuator. Furthermore, the position features coincide with the technical requirements that are used in the process of design and development, so analyzing the trend of the position features is easy to identify when the EHSA is no longer able to meet the minimal technical required.

6.3   PHM algorithm

The structure of the algorithm of prognostic and health management has been designed with the goal of maximizing the information extracted from the data available and obtain a PHM system as flexible as possible. The approaches to be followed have been identified between the methodologies that have found most successful in the field of prognostic and health management; which were presented in chapters 1.3 and 1.4.

Available information, or better that are not available, are the biggest constraint on the choice of approach to be implemented; the absence of the database of signals acquired during the operative life of EHSAs does not allow to adopt data-base approaches for automatic diagnostic and probability-based approach for the prediction of the renaming useful life. In the same way, no presence of validated degradation mathematical models in the literature and the absence of studies and researches on the evolution of the degradations, involve that the model-based approaches are hardly adoptable and especially difficult to validate.

These considerations led the research to lean towards a data-driven approach, this method has a interesting advantage of requiring very little prior knowledge, because it is based on data acquired during operation of the PHM system. Moreover, the techniques that are based on data-driven can be easily completed with self-learning algorithms, allowing the development very

specific algorithms, able to make a tuning of parameters once entered service.

The algorithm implemented, the structure of which is schematically shown in the figure 6.5, have three consecutive levels: the first is concerned to acquire the signals from EHSAs and from the flight computer and extract the features, the second is the automatic faults detection and the last concerns the renaming useful life estimation. An optional fourth layer, is responsible for classifying the degradation that afflicts the servovalve, this operation is not normally considered necessary, since the servovalve is considered a single component by aircraft maintainers, and then is replaced without entering into the detail of the type of fault occurred.
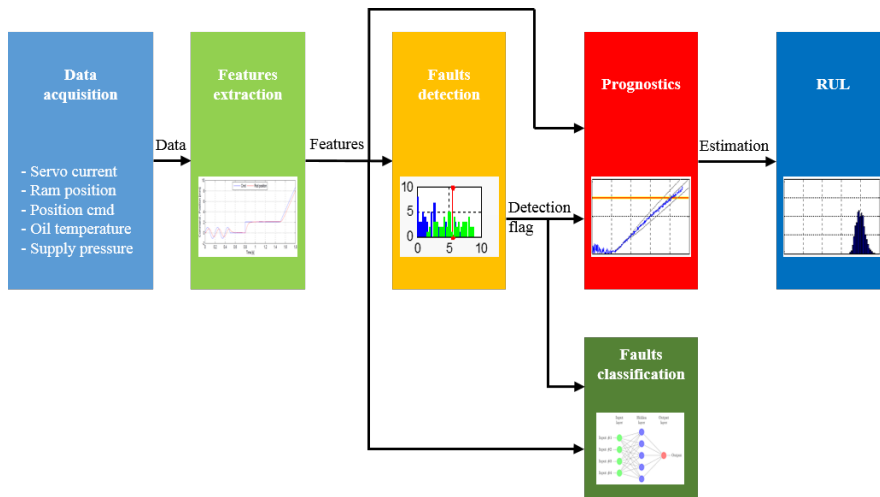
Figure 6.5: PHM algorithm scheme

The first layer, composed by the *"Data acquisition"* and *"Features extraction"* subroutines, is activated every test carried out in pre/post-flight, its task is to extract the features that will be used by subsequent subroutines. With the system in nominal conditions the features are sent to the second layer, which coincides with *"Faults detection"*. This subsystem is activated after each pre/post-flight tests, until a degradation is identified, following the detection of a degradation the algorithm generate an output, called *"Detection flag"* which indicate the presence of a fault, this flag disables the *"Faults detection"* routine and enables the *"Prognostics"* and the *"Faults classification"* routines.

The *"Faults detection"* is concerned with the examination of the features in order to identify the possible degradations, in the course of the doctoral thesis three different methods of degradation detection were tested: the first based on alarm bounds, while the other two exploit the probability den-

sity function comparison, a kind of data-driven approach. The first method obtains the probability density function by means of a moving acquisition window, the other estimate the distribution of the samples using the particle filter. The three fault identification methods are presented in chapter 8.

The first estimate of the remaining useful life is done later identification through the particle filter, then the estimate is updated, always using the same algorithm, at fixed time interval. The update of the estimate of the renaming useful life is carried out using the features, extract from the data acquired, during the operation of the aircraft; this approach allows to obtain very accurate estimates of the RUL without requiring any prior knowledge, or any mathematical model.

6.4   Operative scenario

The behavior of the primary flight control actuators is strongly influenced by operating scenario in which they are working, this also clearly affects the performance of the system of prognostic and health management because the extracted features are strictly correlated to the EHSAs response. Being unable base the development of the PHM system on real data, the results of the mathematical model were used both to develop and to validate the algorithm; in order to obtain simulations more realistic as possible, a probable operating scenario has been assumed.

The operating scenario has been hypothesized to be the most plausible as possible, but at the same time operational differences have been maximized in order to verify the actual robustness of PHM algorithms implemented. The servoactuator considered in this thesis belongs to a short to medium-range commercial aircraft, thus a number of flights within the European network have been defined. The choice of airports has been done trying to maximize the differences of temperature and wind speed during the same period of the year; moreover the different duration of the flights implies that the period of time that elapses between one test and the next are not constant.

The airports identified are three in Italy: Milan Malpensa, Turin Caselle e Rome Fiumicino, plus the airports of Lisbon Portela and Moscow Domodedovo. The aircraft considered will run continuously between the five airports always following the same flight planning: Turin - Rome, Rome - Milan, Milan - Moscow, Moscow - Milan, Milan - Lisbon, Lisbon - Turin and again from the beginning. A map of the flights, with the respective durations is shown in figure 6.6.

The aircraft is assumed in flight for a total of seven / nine hours daily, the day after the plane takes off from the last airport where it landed; this allows
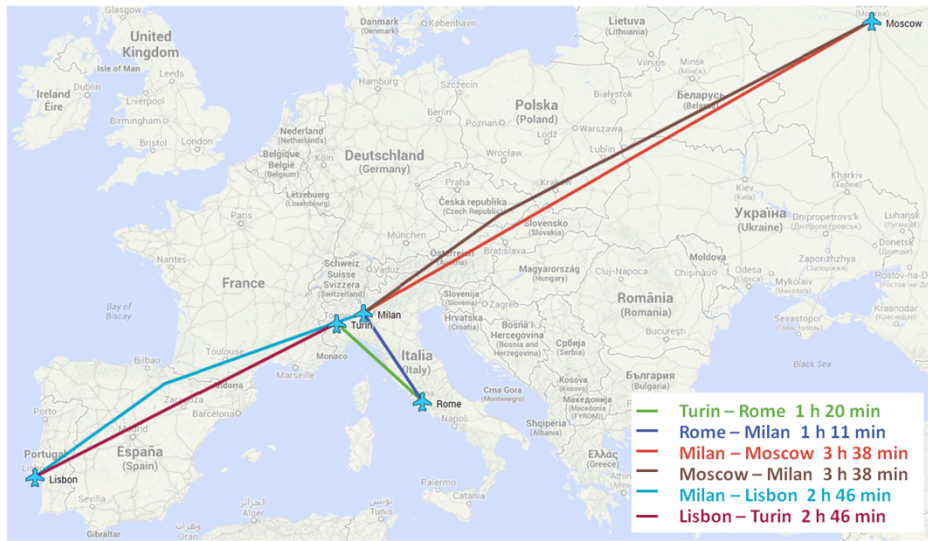
Figure 6.6: Operative scenario

you to have a time axis of flights and to place the operations of the plane in the days of the year. Having a precise time reference allowed to use for environmental temperature and wind speed realistic data extrapolated from the meteorological database of the year 2012 (Underground 2012). Figures 6.7 and 6.8 show the trends of temperature and wind over the year in the considered airports.
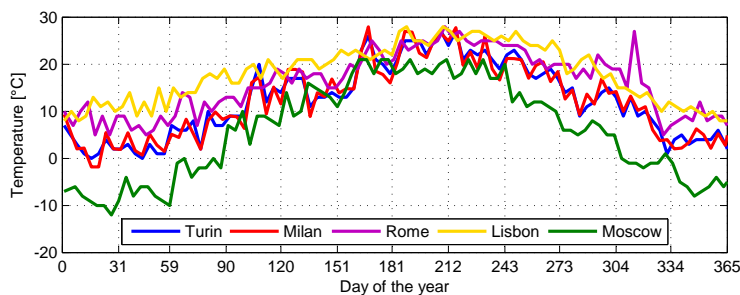
Figure 6.7: Environmental temperature

The oil temperature, the most influence parameter on the EHSA behavior, has been suppose function of the external temperature. In pre-flight situation this assumption is close to the reality, since when the pre-flight checks are carried out the hydraulic systems were started recently. The relationship between oil temperature and external temperature has been hypothesized as show equation 6.1; where T_{oil} is the oil temperature, T_{ext} is the environmental
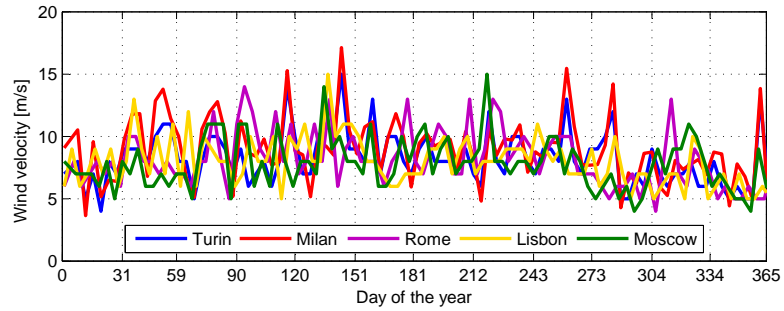
Figure 6.8: Wind velocity

temperature and K_{TT} is a coefficient randomly generated in the range $[1.2 - 1.5]$.

$$T_{oil} = 25 + K_{TT}T_{ext} \qquad (6.1)$$

In order to speed up the simulations a database contenting the oil temperature for all days and all airports has been implemented, the algorithm automatically chooses the correct value for each simulation; the figure 6.9 shows the oil temperature in the different airports.
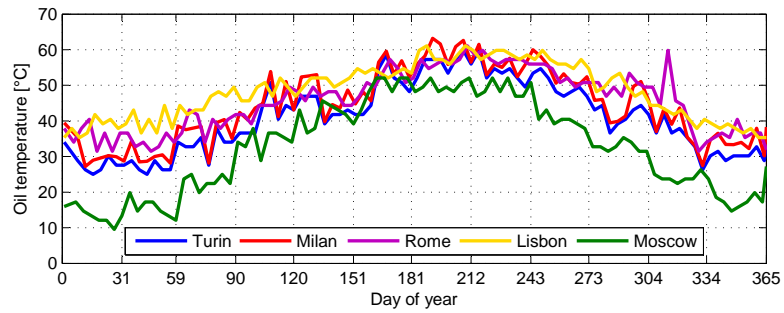
Figure 6.9: Temperature of the oil

7

Features extraction

The features are quantitative or qualitative measures that distill pre-processed data into relevant information for tasks such as failure identification and classification. A feature or condition indicator is the output of an algorithm that processes raw set data and extracts useful information in a compact form in the frequency, time, wavelet, or other domain on the basis of the physics of failure mechanisms experienced by the process, heuristics and experience. If multiple features are extracted, then a fusion scheme may be applied to combine them.

The features must be closely related to deterioration, in order to allow easy identification of them; also they need to be as sensitive as possible to degradations in order to allow an early identification, thereby increasing the time for the estimation of the renaming useful life and for the necessary maintenance interventions. At the same time the features must be robust to the variation of operating and environmental conditions in order to avoid false alarms and increase the accuracy level of the PHM algorithm.

The features never, or almost never, have an ideal behavior, develop algorithms that clean the condition indicator from the influence of disturbances and of operating conditions could be necessary. Often in order to maximize the correlation between degradation and features data fusion techniques are applied, these techniques can be based on previous experiences or self-learning approaches. These techniques have the advantage of facilitating the identification of degradation, but in many cases the features obtained lose their physical meaning, Therefore becomes more difficult to understand which part or component has degraded.

This chapter presented the whole process of selection of features starting with their choice. Subsequently the influence of environmental conditions and of the constructive tolerances is evaluated, in order to define if specific features optimization algorithms are needed, at the end the features are evaluated using specific metrics.

7.1   Extracted features

The identification of the degradation, in the present research project, can be made using only the data acquired during the pre/post-flight tests, he reasons that led to this choice have been explained in detail in the chapter 6.1. During the phase of pre/post-flight, the EHSA is stimulated by imposing a specific command, shown in the figure 7.1, obtained by combining three different stimuli; from the analysis of the response in position (fig. 7.1a) and current (fig. 7.1b), nine features have been identified, that are given in the table 7.1.
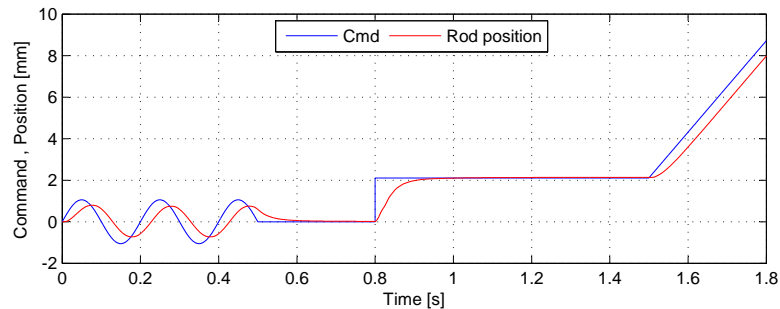
(a) Command and position
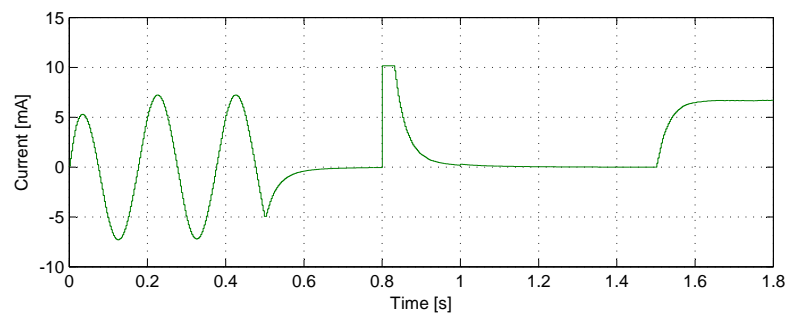
(b) EHSV current

Figure 7.1: PHM command and EHSA behavior

Table 7.1: Features extracted

Type command	Features position	Features current
Sinusoidal	Gain	Current max
	Phase	Current min
		Current mean
Step	Rise time	Time decrease
Ramp	Steady state error	Current max ramp

All features extracted have a net physical meaning, are also closely related with the demands of the technical specifications; this makes very easy to determine when the actuator will no longer be able to operate properly, and consequently the estimation of the remaining useful life. In the following of this section how each feature is extracted from the data acquired during the test carried out in pre/post-flight are described.

7.1.1   Position features

The analysis of the actual position and the position command allow to extract four features: the gain and the phase by the sinusoidal command part, the rise time from the step and the steady state error from the ramp.

Gain and phase   Selected part of the position response relative to the sinusoidal command, see figure 7.2, magnitude and phase of the output as a function of frequency, in comparison to the input can be obtained; in this case the command frequency is constant and equal to 5 Hz, but the same approach can be used for all frequencies.
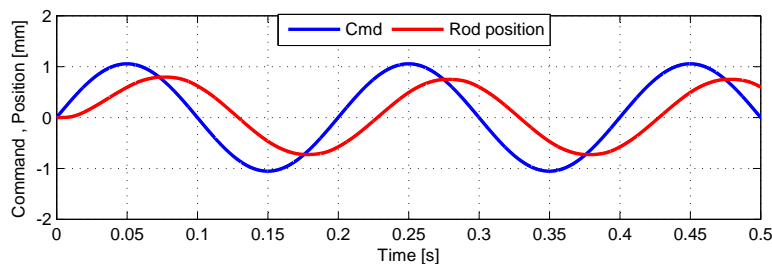
Figure 7.2: Command and position sinusoidal part

The gain and phase are obtained by considering the actual position and the command as two vectors rotating around the origin of the real and imag-

inary reference system, for each instant of time the real and imaginary parts are evaluated with the equations 7.1.

$$Re_{cmd} = \frac{2}{t(end)} \int_t x_{cmd} \sin(\omega_{cmd}t \, dt$$

$$Im_{cmd} = \frac{2}{t(end)} \int_t x_{cmd} \cos(\omega_{cmd}t \, dt$$

$$Re_{act} = \frac{2}{t(end)} \int_t x_{act} \sin(\omega_{cmd}t \, dt \tag{7.1}$$

$$Im_{act} = \frac{2}{t(end)} \int_t x_{act} \cos(\omega_{cmd}t \, dt$$

$$\tag{7.2}$$

Where the subscript *cmd* and *act* refer to the command and the actual position, respectively. The *Re* is the real part of the vector, *Im* the imaginary part, x is the position vector and ω_{cmd} is the frequency of the sinusoidal command expressed in rad/s. t the vector of the sampling time and $t(end)$ is the time of the last sampling.

The gain in decibel is evaluated using the equation 7.3, while the phase is obtained by the formula 7.4 in degree, *angle* is the phase angle function implemented in *Matlab* (MathWorks Inc 2013).

$$Gain = 20 \log_{10}\left(\frac{|Re_{cmd} + iIm_{cmd}|}{|Re_{act} + iIm_{act}|}\right) \tag{7.3}$$

$$Phase = angle\left(\frac{|Re_{cmd} + iIm_{cmd}|}{|Re_{act} + iIm_{act}|}\right)\frac{180}{\pi} \tag{7.4}$$

Rise time   Rise time is the time taken by a signal to change from a specified low value to a specified high value (FED-STD-1037C 1997). These values may be expressed as percentages (Levine 1996) respect to a given reference value, in this case the step command; these percentages are commonly the 90% of the output step height.

Referring to the figure is possible to understand how the rise time of the EHSA is evaluated; in order to eliminate from the calculation of the rise time the effects due to eventual offset between command and actual position at time zero (fig. 7.3), the level to be reached is corrected in function of that offset; therefore the response time can be defined as follows, where t_{rise} is the rise time and OF is the offset.

$$RiseTime = t_{rise} \Rightarrow x_{act}(t_{rise}) = 0.9x_{cmd} + OF \tag{7.5}$$
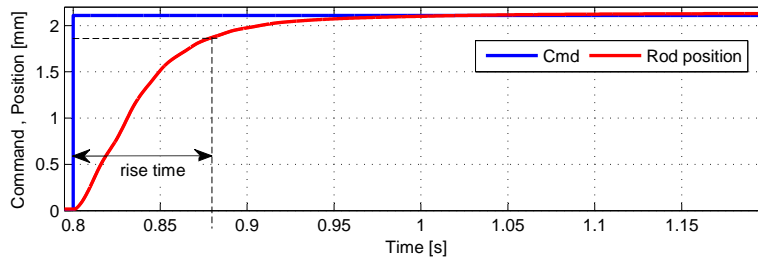
Figure 7.3: Command and position step part

Steady state error   Steady-state error is defined as the difference between the input (command) and the output of a system in the limit as time goes to infinity. The steady-state error will depend on the type of input (step, ramp, etc.) as well as the system type. In the present case the steady state error is defined as the mean of the difference between the command and the response, when this has a linear behavior.

In computing the average of the error the initial phase of the response of EHSA has been removed, in order to consider only the stationary part and not the transient, referring to the figure 7.4.
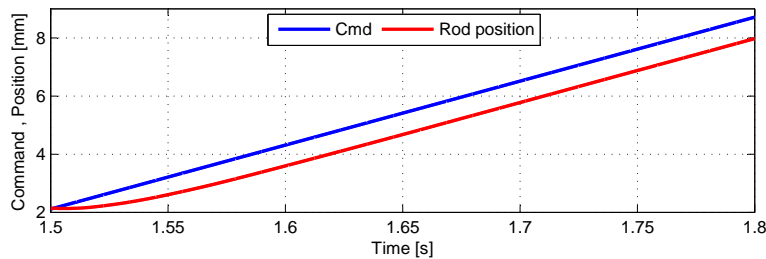
Figure 7.4: Command and position ramp part

7.1.2   Current features

The current servo acquired during the pre/post-flight tests,exactly as for the position, it is divided into three segments. From the various segments are extracted a total of five features: current minimum, maximum and average from the sinusoidal part, time decrease from the step segment and current max from the ramp. The current features are not closely related with the technical specifications as it occurs for those from position, but also they have a physical meaning.

Minimum, maximum and average current   The current servovalve, extracted during the sinusoidal command, has also a sinusoidal trend, see figure 7.5.
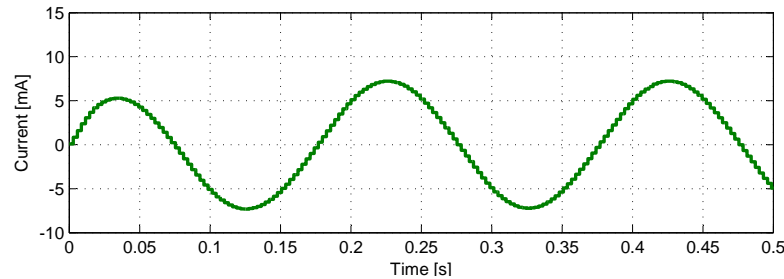
Figure 7.5: Current sinusoidal part

Therefore, from the acquired data the average value of the sine wave, the maximum and minimum values could be extract. Under optimal conditions, the average current is close to zero, while the value of the maximum and the minimum peaks are approximately identical.

Time decrease   The time decrease can be considered the opposite of rise time, therefore it can be defined as the time taken by a signal to change from a specified high value to a specified low value.

When an EHSA is stimulated with a step command, the current of the servovalve saturated to the maximum value. Subsequently, with the decrease of the error between the required position and actual position, the current decreases until it reaches zero. The time is defined as the time required for the current to return to a value equal to 10% of the saturation value, see figure 7.6.
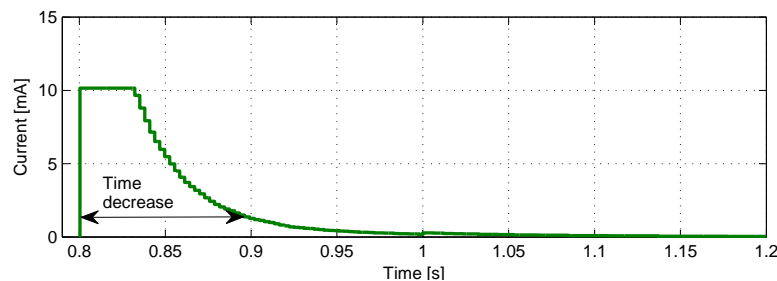
Figure 7.6: Current step part

Maximum ramp current   The current of the servo valve which is generated in response to a command to ramp it is also a ramp that reached a certain value remains stationary (figure 7.7); the value reached is the one that ensures the opening of the servovalve spool sufficient to move the cylinder with the same ratio of the command. The algorithm implemented extracts the maximum value reached by the ramp, which coincides with the value to which the current stops growing and stabilizes.
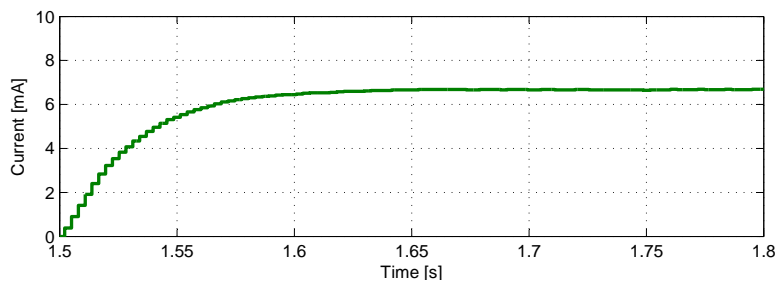
Figure 7.7: Current ramp part

7.2   Influence of operative conditions

The features extracted, being dependent on the response of the actuator, are influenced by the operating conditions mainly supply pressure, and oil temperature. The evaluation of the impact that the main operating conditions have on the performance of features is essential in order to understand if these can affect the correct operation of the PHM algorithms. A variation of the features caused by external parameters, can lead to an identification of a degradation that does not exist, and therefore a false alarm. Evaluate the influence of external parameters is also the first step to evaluate the need for corrective measures to eliminate or reduce the influence of various operating conditions on the extracted features.

Two subsequent analyzes were carried out: the first manage the influence of parameters involved in the hydraulic fluid, which supply pressure and oil temperature. The second one focused on electrical noise, disturbance of current and errors in the analog / digital converter, and on environmental disturbances such as wind.

7.2.1 Fluid parameters

As noted many times during this thesis, the supply pressure and the oil temperature affect in important way on the performance of electrohydraulic servoactuator, and consequently also on the value of features extracted. In the development of a prognostic system understand how these two parameters affect the condition indicator is essential to define what is the best strategy to make the features robust to the variation of the characteristics of the hydraulic fluid.

The study of the influence of the parameters was carried out using the mathematical model implemented, a series of simulations varying pressure and oil temperature were carried out; in order to separate the effects of various noises agents from the effects of the properties of the oil, the first have been disabled completely, also the load acting on the wing surface is placed null for all simulations. In these circumstances, the variations of the features are due uniquely to the different conditions of the oil.

In general, a reduction in the supply pressure, or a decrease of the oil temperature causes a worsening of the dynamic performance of the EHSA (figure 7.8). What happens is a deterioration of the features related to the position: a greater attenuation and phase shift of the sinusoidal response, a increase of the rime time and finally a rise of steady state error. The features of current instead are influenced by the fact that the controllers tend to compensate the deterioration of the dynamic performance, then: in the sinusoidal part current maximum and minimum increase in modulus, while the average remains approximately constant, time decrease grows as well as the maximum current of the ramp.

The value of the supply pressure and oil temperature can be considered known even though with some limitations: firs, both parameters are acquired after the pump of the hydraulic system and not close to the EHSA; second each parameter is acquired only once for each test. Both the temperature and the pressure may be, however, assumed to be constant throughout the test, as their dynamics is slow.

Given the possibility to know the two parameters, and their important influence on the values of the features, a mathematical model that links features with pressure and temperature has been implemented for each condition indicator. Mathematical models implemented can be generically described by the equation 7.6, dove T' e P' are conditions taken as reference, f is a function, and t and P are the pressure and the temperature acquired during the test. The idea is to exploit the mathematical models to bring the value of the features acquired during the test to those corresponding to a known operating condition, T equal to 0 $°C$ and 18 MPa of supply pressure.
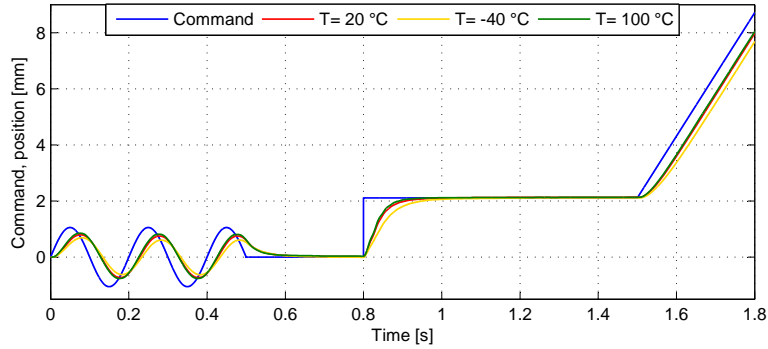
(a) Position
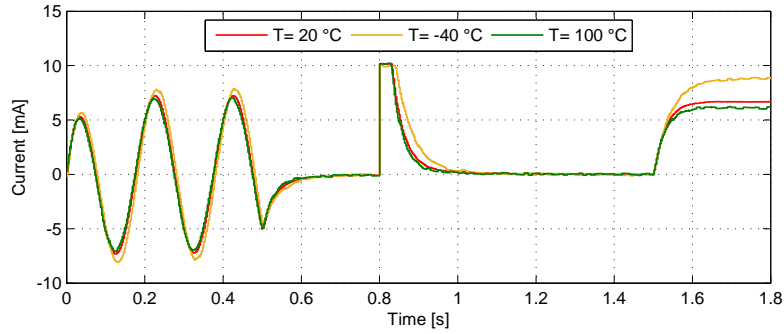
(b) EHSV current

Figure 7.8: Influence of temperature on EHSA behavior

$$Feature(T', P') = Feature(T, P) + f(Feature, T, P) \qquad (7.6)$$

In order to find the best mathematical models a modeling framework called Symbolic Regression was exploited. Symbolic Regression searches the space of mathematical expressions to find the model that best fits a given data-set, both in terms of accuracy and simplicity (Zelinka 2004) and no particular model is provided as a starting point to the algorithm. Instead, initial expressions are formed by randomly combining mathematical building blocks such as mathematical operators, analytic functions, constants, and state variables; usually, a subset of these primitives will be specified by the operator, but that is not a requirement of the technique. New equations are then formed by combining previous ones, using genetic programming (McKay, Willis, and Barton 1995 and Hoai et al. 2002). In linear regression, the dependent variable is a linear combination of the parameters, but need

not be linear in the independent variables.

The problem of the Symbolic Regression is the generation of models with a very high degree of complexity, which require a large computing power to be solved. In this case of studies, however, the thesis has been done trying to contain the computing power, therefore the model chosen is the one with lower degree, which provides an absolute error less than $1 \cdot 10^{-6}$. In this way, the model accuracy is sufficiently high and at the same time the computational load is minimal.

Following, for each features the influence of temperature in a range from -40°C to 100°C ,and for four different pressure value, 18 MPa 17 MPa 16 MPa and 15 MPa are show. Furthermore, for each condition indicator the mathematical model identified are described.

Gain   The gain is affected both by the supply pressure on both the temperature, as one can see in the graph the effect of temperature is predominant, at the same pressure there is a variation of about 45% between 100°C and -40°C; the pressure change results in a shift of the curves, which are maintained parallel (figure 7.9).
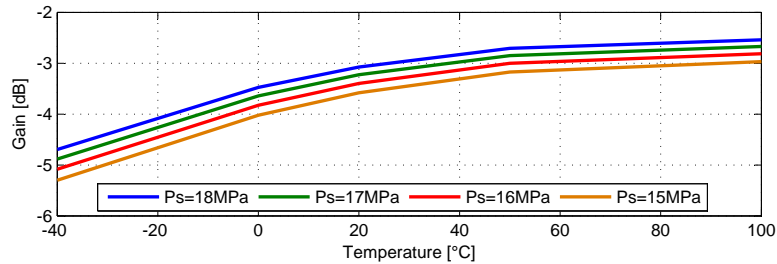
Figure 7.9: Influence of oil pressure and temperature on gain

The development of the mathematical model required the assessment of the sensitivity of each parameter on the equation 7.6, the analyzes have shown that the model is more sensitive to temperature than the pressure. The table 7.2 shows the results of the analysis, the sensitivity is defined he relative impact that a variable has on the target variable and was calculated from the equation 7.7, where z is the generic variable, in this case (T or P) and y is the fitting data, while σ is the standard deviation. The percentage of positive is the likelihood that increasing one variable will increase the target variable.

$$Sensitivity = \left\|\frac{\bar{\partial}y}{\partial z}\right\|\frac{\sigma(z)}{\sigma(y)} \tag{7.7}$$

Table 7.2: Influence on gain of operative conditions

Variable	Sensitivity	Percentage positive	Percentage negative
Temperature	0.838	0	100
Pressure	0.192	0	100

The mathematical model obtained is a nineteenth order, which can be written as shown in equation 7.8; where *a,b,c* and *d* are numerical coefficient, $Feature(T, P)$ is the feature obtained from the data acquired during the test, T and P are temperature and pressure of the hydraulic fluid during the test.

$$f(Feature, T, P) = Feature(T, P)(aP + bTP + c + dPT^3) \qquad (7.8)$$

Applying equation 7.6, and by replacing the $f(Feature, T, P)$ with the model of equation 7.8, the features which are no longer influenced by the operating parameters of the oil are obtained. Comparing the figures 7.9 and 7.10, is evident that the features no longer have a dependence on oil temperature and supply pressure, small oscillations remain, but are no longer significant.
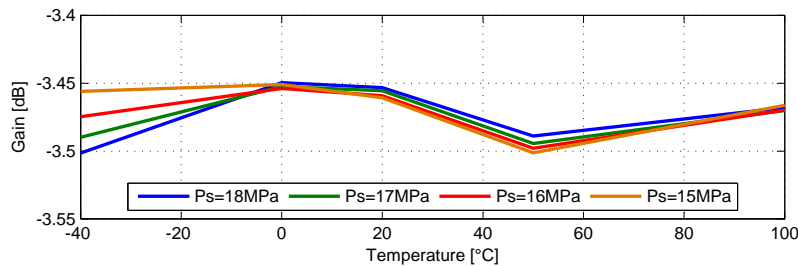
Figure 7.10: Feature gain correct

Phase   The phase is principally influenced by oil temperature, as shown by the diagram of figure 7.11, the information extracted from the graph are also confirmed from the analysis on the sensitivity of the phase to oil temperature and supply pressure, the analysis results are reported in table 7.3.

The mathematical model obtained, equation 7.9, is a twenty-third order; *a,b,c*, *d* and *e* are numerical coefficient, $Feature(T, P)$ is the feature obtained from the data acquired during the test, T and P are temperature and pressure of the hydraulic fluid during the test.

Figure 7.11: Influence of oil pressure and temperature on phase

Table 7.3: Influence on phase of operative conditions

Variable	Sensitivity	Percentage positive	Percentage negative
Temperature	0.858	0	100
Pressure	0.234	0	100

$$f(Feature, T, P) = Feature(T, P)(aP + bT + cTP^3 + d + ePT^2) \quad (7.9)$$

The phase feature corrected using the equation 7.6 and the model 7.9, are show in figure 7.12. The graph shows that the feature phase, after correction, remains almost constant for all possible value of supply pressure and oil temperature.
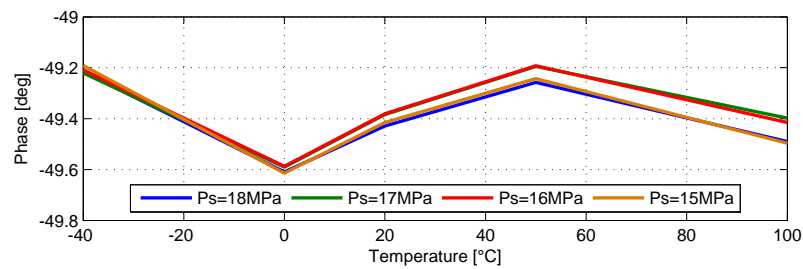
Figure 7.12: Feature phase correct

Rise time   The rise time is principally influenced by oil temperature, as shown by the diagram of figure 7.13, the indications extracted from the graph
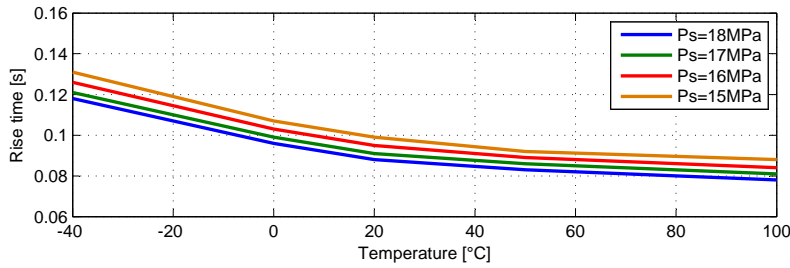
Figure 7.13: Influence of oil pressure and temperature on rise time

Table 7.4: Influence on rise time of operative conditions

Variable	Sensitivity	Percentage positive	Percentage negative
Temperature	0.825	100	0
Pressure	0.218	100	0

are validate from the analysis on the sensitivity of the rise time to oil temperature and supply pressure, the analysis results are reported in table 7.4.

The mathematical model obtained, equation 7.10, is a twenty-first order; a,b,c, d and e are numerical coefficient, $Feature(T,P)$ is the feature obtained from the data acquired during the test, T and P are temperature and pressure of the hydraulic fluid during the test.

$$f(Feature, T, P) = Feature(T, P)(aP + bT + cTP + d + eT^2) \qquad (7.10)$$

The rise time corrected using the equation 7.6 and the model 7.10, are show in figure 7.14. The rise time, after correction, remains almost constant for all possible value of supply pressure and oil temperature.
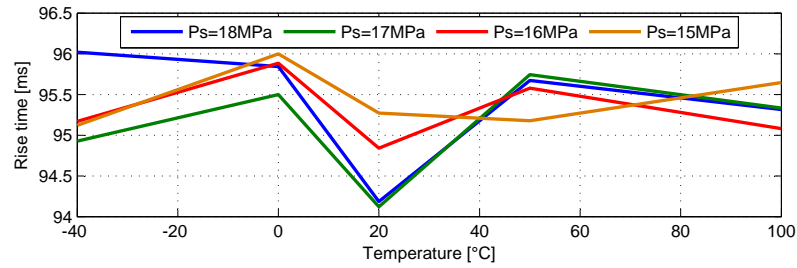
Figure 7.14: Feature rise time correct

Steady state error The steady state error is positive influenced by oil temperature and supply pressure, as shown by the diagram of figure 7.15. The indications extracted from the graph are validate from the analysis on the sensitivity of the phase to oil temperature and supply pressure, the analysis results are reported in table 7.5.
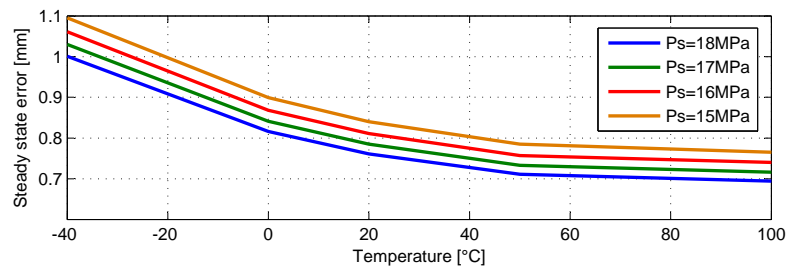
Figure 7.15: Influence of oil pressure and temperature on steady state error

Table 7.5: Influence on steady state error of operative conditions

Variable	Sensitivity	Percentage positive	Percentage negative
Temperature	0.819	100	0
Pressure	0.207	100	0

The mathematical model obtained, equation 7.11, is a twenty-first order; a,b,c,d and e are numerical coefficient, $Feature(T,P)$ is the feature obtained from the data acquired during the test, T and P are temperature and pressure of the hydraulic fluid during the test.

$$f(Feature, T, P) = Feature(T, P)(aP + bT + cTP + d + eT^2) \qquad (7.11)$$

The steady state error corrected using the equation 7.6 and the model 7.11, are show in figure 7.16. The steady state error, after correction, remains almost constant for all possible value of supply pressure and oil temperature.
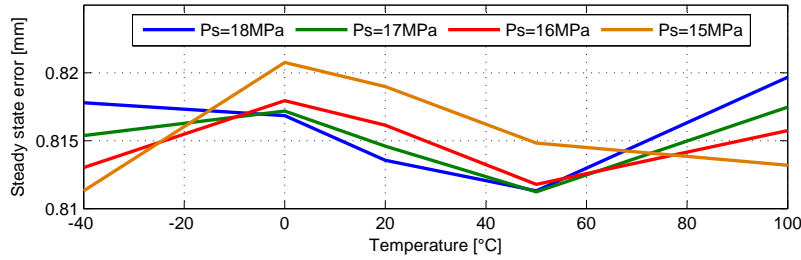
Figure 7.16: Feature steady state error correct

EHSV current max, min, mean The three current features extracted from the sinusoidal part are influenced by oil temperature and supply pressure in a different way, as shown by the diagram of figure 7.17. The analysis of sensitivity reveals that the maximum current is positively influenced by both parameters, in contrast to the minimum current that is negative affected. The average current is affected in a completely positive way from pressure, while the temperature acts both positively, in the majority of cases, either negatively (table 7.6).

Table 7.6: Influence on sinusoidal current of operative conditions

Features	Variable	Sensitivity	Percentage positive	Percentage negative
Current Max	Temperature	0.987	100	0
	Pressure	0.198	100	0
Current Min	Temperature	0.971	0	100
	Pressure	0.203	0	100
Current Mean	Temperature	1.082	93	7
	Pressure	0.242	100	0

The mathematical model obtained for minimum and maximum currents are very close, both are twenty-third order and include a natural exponential as show in equations 7.12 and 7.14; where the small letters from a to n are numerical coefficient, $Feature(T, P)$ is the feature obtained from the acquired

(a) Current max

(b) Current min

(c) Current mean
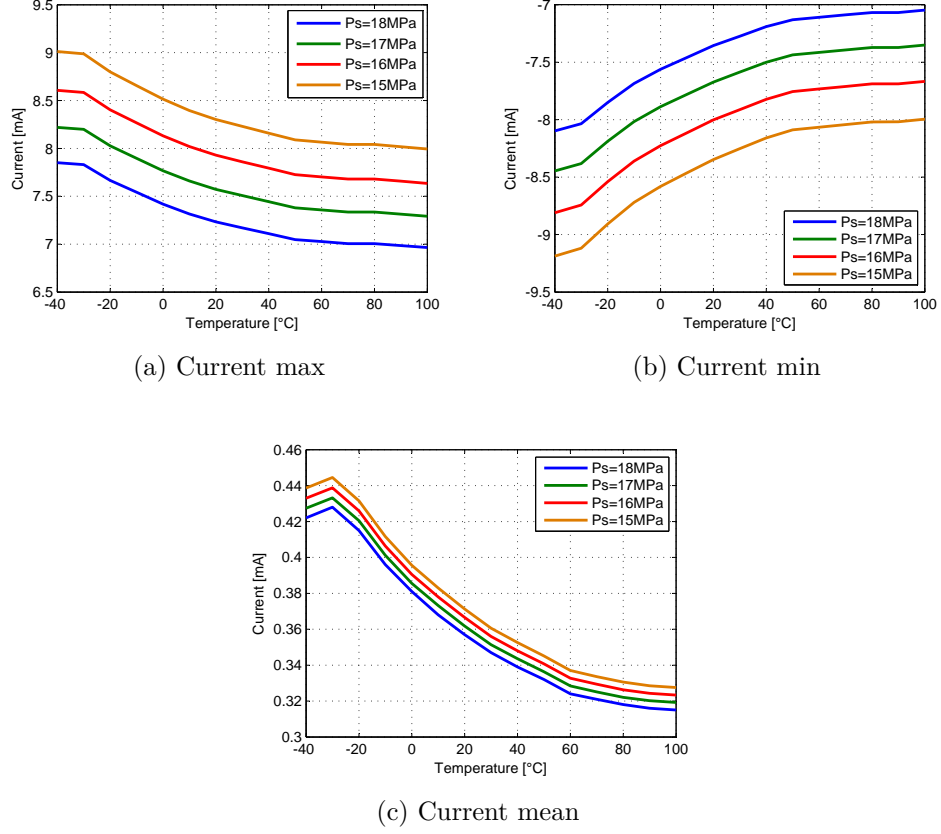
Figure 7.17: Influence of oil pressure and temperature on sinusoidal current

data, T and P are temperature and pressure of the hydraulic fluid during the test. Equation 7.14 is the model related to the mean EHSV current, it is the model with the maximum degree among those implemented, thirty-ninth: o,p,q, r and s are numerical coefficient, $Feature(T, P)$ is the feature obtained from the data, T and P are temperature and pressure of the hydraulic fluid.

$$f(Feature, T, P) = Feature(T, P)(aTP + be^{cT} + d + fPT^2) \qquad (7.12)$$

$$f(Feature, T, P) = Feature(T, P)(gTP + he^{lT} + m + nPT^2) \qquad (7.13)$$

$$f(Feature, T, P) = Feature(T, P)(oT + pPT^2 + qT^4 + rPT + sP^2T^3) \qquad (7.14)$$

The current extracted from the sinusoidal part corrected using the equation 7.6 and the three models from 7.12 to 7.14, are show in figure 7.18.

(a) Current max

(b) Current min

(c) Current mean
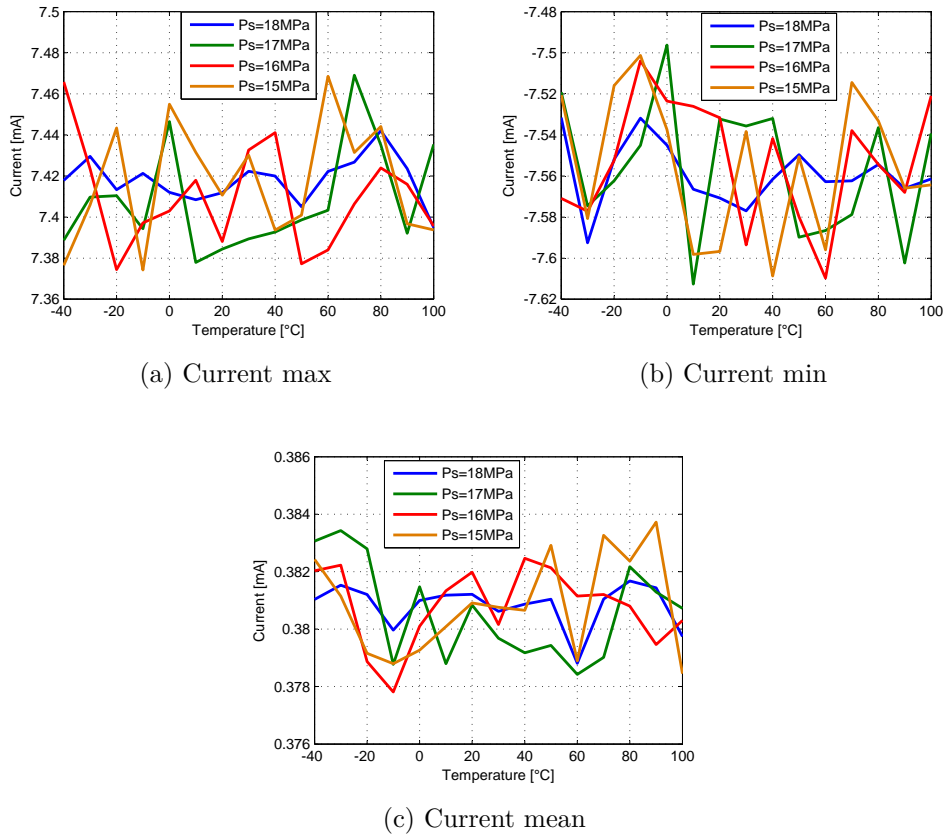
Figure 7.18: Feature sinusoidal current correct

Time decrease   The influence of oil temperature and supply pressure on time decrease is shown by the diagram of figure 7.19. The results of the sensitivity test are displayed in table 7.7.
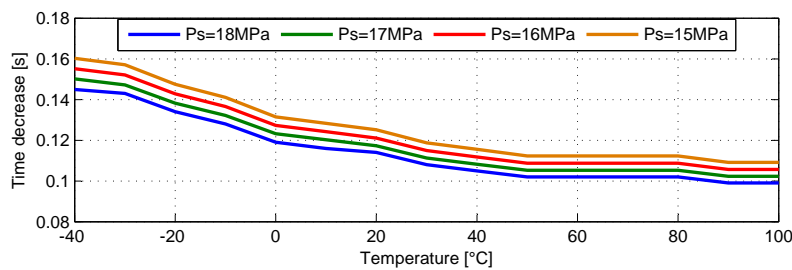
Figure 7.19: Influence of oil pressure and temperature on time decrease

Table 7.7: Influence on time decrease of operative conditions

Variable	Sensitivity	Percentage positive	Percentage negative
Temperature	0.819	100	0
Pressure	0.207	100	0

The mathematical model obtained, equation 7.15, is a twenty-ninth order; *a,b,c, d* and *e* are numerical coefficient, $Feature(T, P)$ is the feature obtained from the data acquired, T and P are temperature and pressure of the hydraulic fluid.

$$f(Feature, T, P) = Feature(T, P)(aT + bPT^3 + cT^2P^2 + d + eT^2) \quad (7.15)$$

The feature corrected using the equation 7.6 and the model 7.15, are show in figure 7.20. After correction, the feature remains almost constant for all possible value of supply pressure and oil temperature.
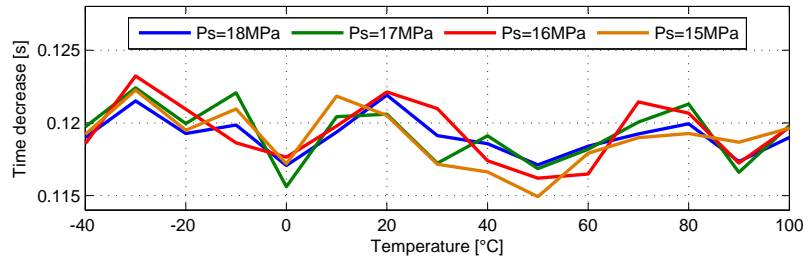
Figure 7.20: Feature time decrease correct

EHSV current max ramp The influence of oil temperature and supply pressure on maximum current ramp is shown by the diagram of figure 7.22. The results of the sensitivity test are displayed in table 7.8.

The mathematical model obtained, equation 7.16, is a twenty-seventh order; *a,b,c, d* and *e* are numerical coefficient, $Feature(T, P)$ is the feature obtained from the data acquired during the test, T and P are temperature and pressure of the hydraulic fluid.

$$f(Feature, T, P) = Feature(T, P)(aT + bPT^3 + cPT^2 + dPT) \quad (7.16)$$

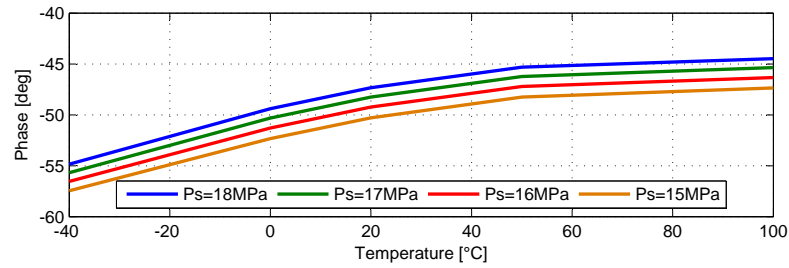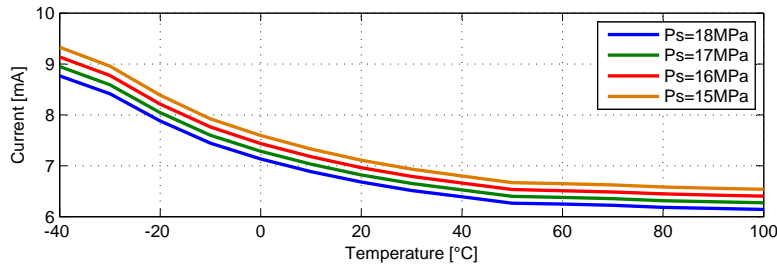Figure 7.21: Influence of oil pressure and temperature on current max ramp

Table 7.8: Influence on current max ramp of operative conditions

Variable	Sensitivity	Percentage positive	Percentage negative
Temperature	0.819	100	0
Pressure	0.207	100	0

The maximum current ramp corrected using the equation 7.6 and the model 7.16, are show in figure 7.22. After correction, the feature remains almost constant for all possible value of supply pressure and oil temperature.
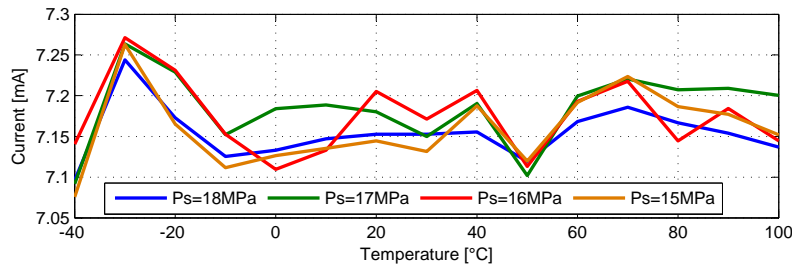
Figure 7.22: Feature current max ramp correct

7.2.2 Noise and environmental disturbances

The influence of the noises and the environmental conditions was made using of the mathematical model, a series of simulations were carried out by activating all the sources of noise and varying the speed of the wind from 4 m/s (gentle breeze, Beaufort number 3) to 17 m/s defined as moderate gale or Beaufort number 7 (Saucier 1989).

The simulations have shown that both noise and the aerodynamic force do not affect in a substantial manner the features, indicators extracted from the position are practically insensitive to the wind, as the graphs of figure 7.23 demonstrate, the features oscillate at around of the predicted values with a very small deviation. The same considerations can be apply at the current features, shown in figure 7.24.

Because of the limited influence of environmental conditions and noise, mathematical models to eliminate the influence of these factors have not been implemented, the variance of the indicators introduced by these disturbances will be taken into account with appropriate approaches based on tolerance bands

(a) Gain

(b) Phase

(c) Rise time

(d) Steady state error
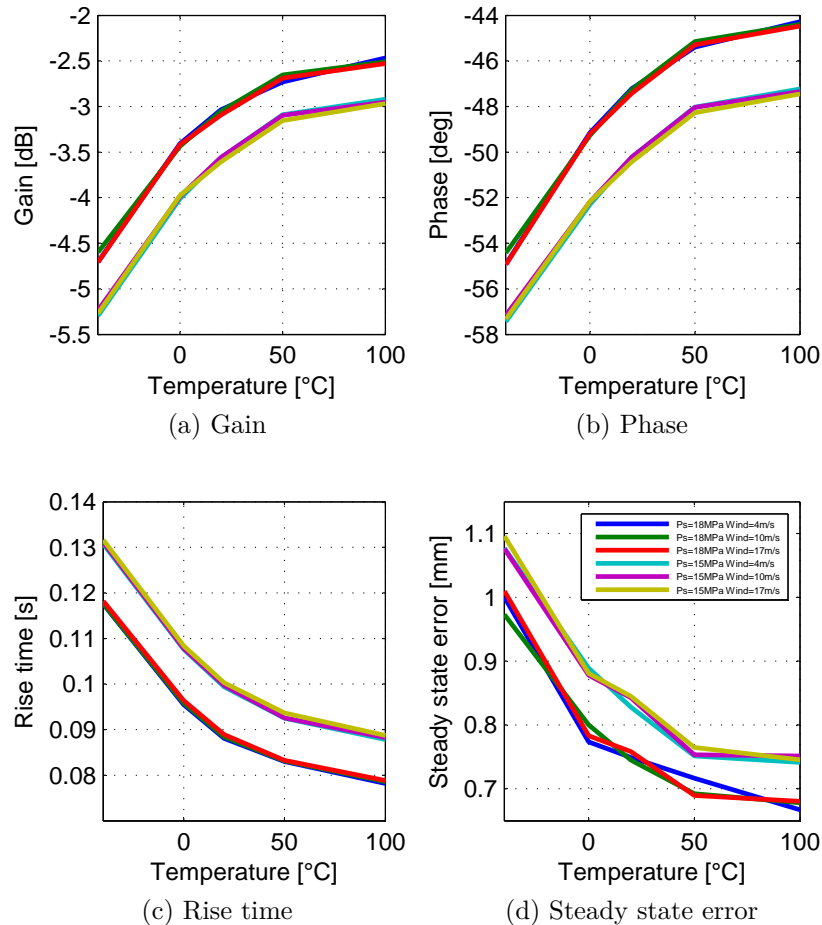
Figure 7.23: Influence of noise and wind speed on position features
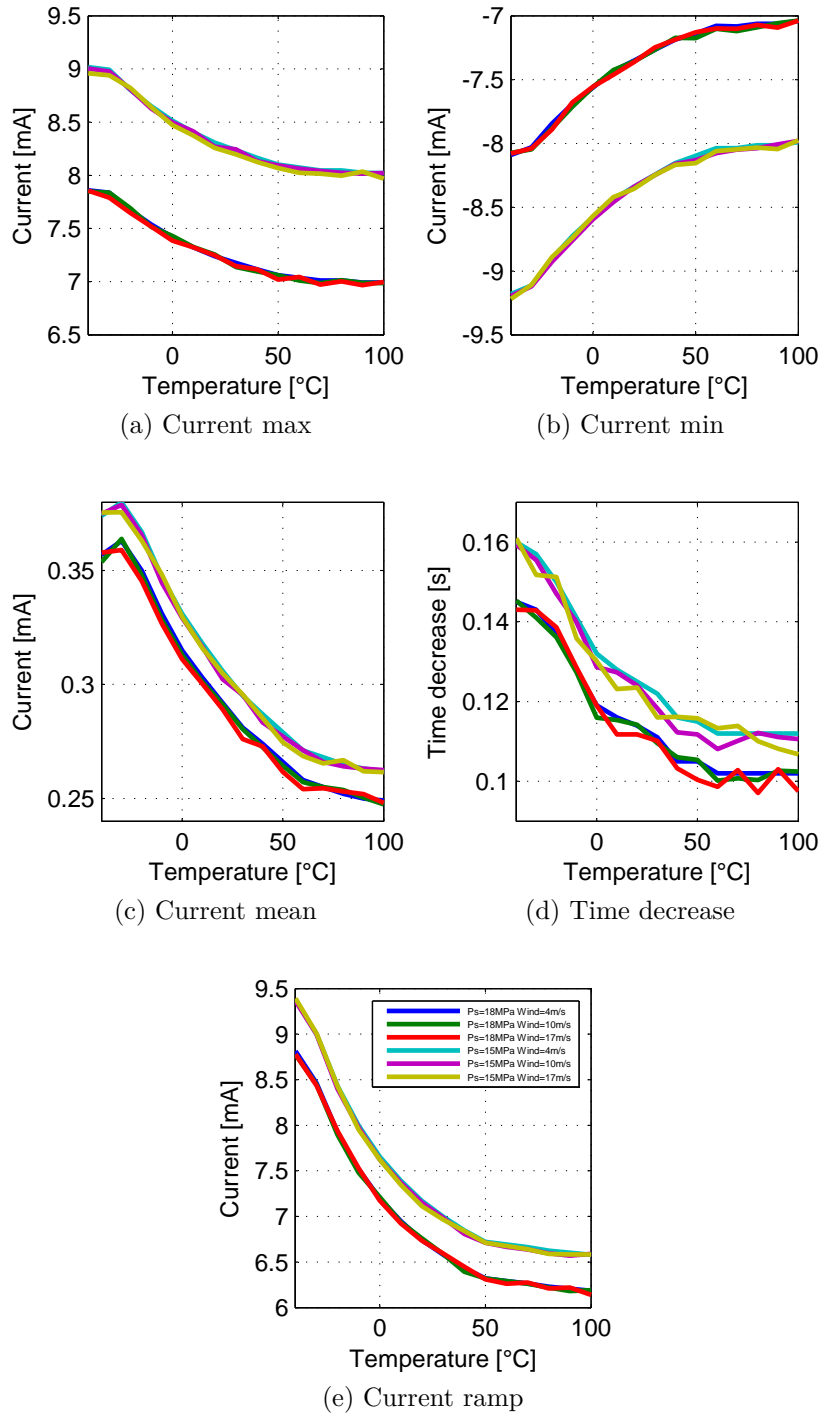
Figure 7.24: Influence of noise and wind speed on current features

7.3   Influence of manufacturing tolerances

The manufacturing tolerances affect the features as well as influence the behavior in general of the EHSA, their presence can make ineffective PHM algorithms, especially if this last have been calibrated on data from mathematical models, because in most cases these tolerances are not considered. With modern manufacturing techniques the influence of manufacturing tolerances are becoming less important in components such as the cylinder, but spools of electrohydraulic servovalves are designed with micrometric tolerances, so even small changes in the gap or in the shape of the spool can have an important influence on the behavior of the valve.

The manufacturing tolerances of the valve can be translated into a variation in flow gain and in the pressure gain. The flow gain is defined as the nominal relationship of control flow to input current; the pressure gain as the change of load pressure drop with input current and zero control flow. Moog in its catalog (Moog 2009) indicates as allowable tolerance on the flow gain $\pm 10\%$, while the gain variation in flow rate is a much more considerable equal to $\pm 95\%$.

The influence of these tolerances was investigated by a series of simulations carried out with the mathematical model in which the geometric dimensions of the radial gap and overlaps were varied to achieve variations of the two gains, the two gains have been made vary individually.

The results of the simulations, presented in the figures 7.25, show that a good approximation of the effect of manufacturing tolerances on the position of features is a shift of the curve than the nominal trend. The variation of the flow gain proved to be the most influential on the various features of position, except in the case of rise time where for temperatures greater than zero the variation of pressure gain in becomes the more influential. In general, save the temperature of hydraulic fluid, geometric tolerances are the parameters that most influence on the features of position.

Similar results were obtained for the features of EHSV current, also in this case the variation of the two gains entails the translation of the curves compared to the nominal value. The effect of the flow rate gain is not as more important than the pressure, actually the variation introduced by the manufacturing tolerances in both cases is comparable, as shown in figure 7.26. Special case for the features is the time of decrease, the flow gain has an effect on features greater than the pressure one at low temperatures, but the situation is reversed at temperatures exceeding the zero. The manufacturing tolerances can be considered the second cause of variation of the current features after the oil temperature, therefore find a way to deal with this

problem then becomes of prime importance to get a robust PHM algorithm.

Different strategies have been developed to address the problem in the two algorithms of automatic diagnostic implemented. In the algorithm that exploits the alarm bounds approach, the possible range of variation of tolerances has been taken into account in the definition of the alarm bound. These were made deep enough to contain within them the variations of the features related of production tolerances; this solution minimizes the possibility of false alarms, but at the same time requires a greater degradation, and consequently a greater variation of the health indicator, so that the degradation could be identified. Probability density function comparison approach addresses the problem with a self-adaptive algorithm, the PDF of features is calibrated on the component during the early stages of work, so as to contemplate autonomously geometric tolerances.

(a) Gain

(b) Phase

(c) Rise time

(d) Steady state error
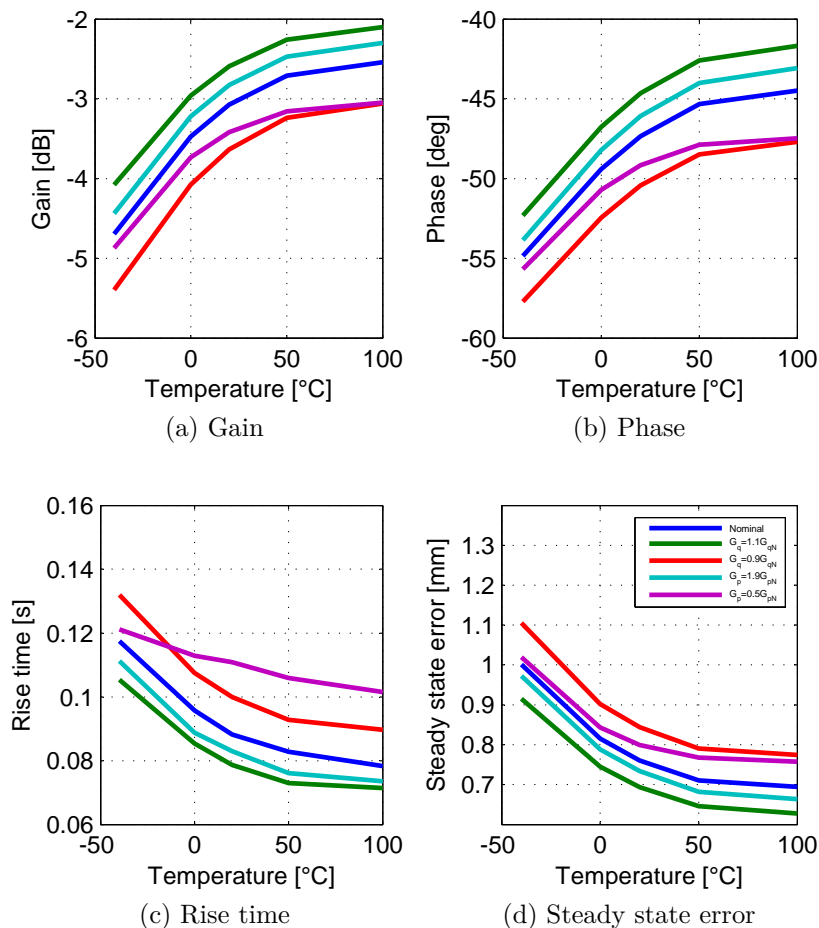
Figure 7.25: Influence of manufacturing tolerances on position features

(a) Current max

(b) Current min

(c) Current mean

(d) Time decrease

(e) Current ramp
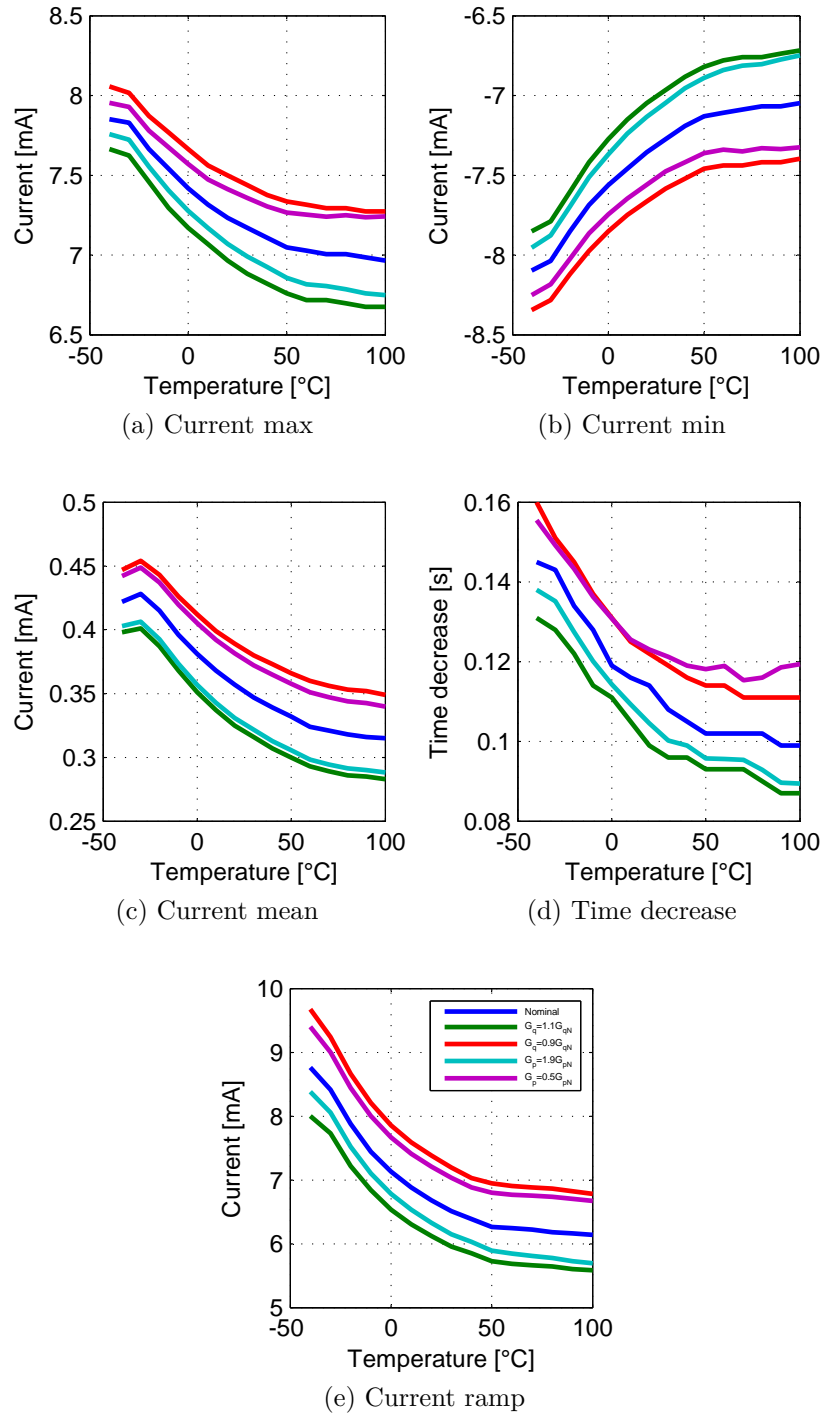
Figure 7.26: Influence of manufacturing tolerances on current features

7.4 Features evaluation

Evaluate features means defining as these are a good indicator of presence of different degradations, in order to do this operation as the features vary in the presence of a degradation must obligatorily be known. A series of different simulations have been implemented, by imposing the growth of a degradation at a time so as to define as a single degradation affects the trend of the features. Right now defined as degradations evolve over time is not important, in that the objective is to correlate to a level of degradation to the corresponding variation of the features, therefore be defined as that level of degradation is reached is not important.

For all the degradations, a ratio of linear growth function of flight hours was therefore hypothesized, the slope of the curve was set constant for all the degradations since even this does not affect the evaluation of the features. For each degradation were carried out three different campaigns simulations, by varying the operating scienario and consequently the oil temperature and the supply pressure; in total for each degradation were simulated fourteen hundred pre/post -flight tests.

The features are evaluated using the features suggested by G. Vachtsevanos et al. (2006) and H. Liu and Motoda (2012): distance measures, correlation coefficient and moving-window correlation coefficient. The distance measures are also known as separability, typically, they are derived from distances between the class-conditional density functions, in this in this project the distance is defined as the absolute variation in percentage between the average value of the features in the absence of degradation and the average value with a maximum degradation, obtained with the following equation.

$$Dist = \frac{|\mu_{Fnom} - \mu_{Fdeg}|}{|\mu_{Fnom}|} * 100 \qquad (7.17)$$

Where $Dist$ is distance measures in percentage, μ_{Fnom} is the mean of the selected feature in nominal condition and μ_{Fdeg} is the average of the selected feature in degradation condition.

A larger distance implies a greater possibility of identifying degradation without false alarms, because the small variations introduced by the noises become negligible, furthermore in the presence of a large variation also features that have a high dispersion can become very significant.

Correlation coefficient and moving correlation coefficient are designed to quantify how strongly two variables are associated or correlated with each other so that by knowing the value of one variable one can predict the value of the other; the aim is to define how strongly a feature is associated with a

degradation. The correlation coefficient between to degradation (D) and one feature (F) is obtained usion equation 7.18, where μ and σ are the mean and the standard deviation of the variable, respectively and N is the number of samples.

$$r_{D,F} = \frac{1}{N-1} \sum_{i=1}^{N} \left(\frac{(D_i - \mu_D)(F_i - \mu_F)}{\sigma_D \sigma_F} \right) \tag{7.18}$$

The equation shows that the correlation coefficient can be understood as an average of the correlation between the different samples- Such indication is normally considered enough to evaluate a feature; a refinement of information may be obtained by considering besides the normal correlation coefficient also the moving correlation coefficient.

The moving correlation coefficient allows to identify the evolution of the correlation between futures and degradation in function of growth of the fault. Such information is essential for understanding the quality of features, health indicators that have a high overall correlation may have a low linearity in the initial phase of growth where the relationship between features and degradation is more important; on the contrary might exist features that have a low overall correlation, but a great value of the coefficient in the initial stages. The moving correlation is calculated using the equation 7.18 on a moving window of twenty points with a overlap of nineteen.

In the following of this section, for each degradation, the results of the three metrics are introduced, the overall correlation coefficient and the distance are proposed both in the case with the influence of the temperature of the hydraulic fluid and in the version with the effect correct using the equations presented in subsection 7.2.1; whereas the moving correlation is shown only for the second case. In the following diagrams, the degradations and health indicators are normalizate in the range 0-1, so as to allow an easier representation of more features on the same graph, the figures show the features cleaned by disorders of pressure and temperature.

7.4.1   Reduction magnetomotive force

The reduction of the magnetomotive force of the torque motor involves important variations of the features of both position (figure 7.27a) and current (figure 7.27b). The features of position have a high correlation with the degradation, the phase practically linear, and the rest have a pattern of order higher than the first, the dispersion is minimal. Also the features of the current show an excellent correlation with the degradation and contained a dispersion, the only exception is the mean current that has a significant

dispersion of the values.

(a) Position features   (b) Current features
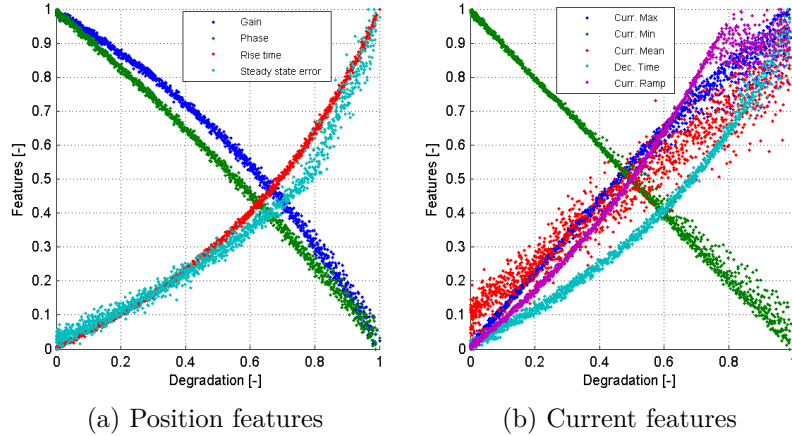
Figure 7.27: Influence of magnetomotive force reduction

The evaluation of the features using three metrics provides optimal results: as shown in the table 7.9 all the features have a higher correlation, higher than 0.96, before elimination of disturbances induced by the oil temperature; after the correction process, the correction of single features is always greater than 0.97 in absolute value, there is an improvement for all indicators. The distance is optimal for gain, rise time, steady state error and decrease time that have a variation greater than 100 %, while it is very small for the maximum and minimum current; the temperature correction does not affect the distance.

Table 7.9: Features evaluation for reduction magnetomotive force

| | Temperature influence | | No temperature influence | |
	Correlation	Distance [%]	Correlation	Distance [%]
Gain	-0.979	165.88	-0.989	165.52
Phase	-0.990	40.28	-0.998	40.37
Rise time	0.970	126.96	0.977	126.71
Steady state e.	0.950	126.47	0.958	126.30
Current max	0.992	17.88	0.996	17.84
Current min	-0.992	22.70	-0.998	22.65
Current mean	-0.976	51.71	-0.979	51.82
Time decrease	0.972	113.31	0.980	113.10
Ramp current	0.983	56.849	0.988	56.74

Although the overall correlation coefficient is high for all the features, the moving coefficient highlights how certain features have low correlations for certain values of degradation. The position features (figure 7.28a) have a stable correlation close to one or minus one, except the steady state error that is very disturbed and oscillates around 0.5. The features extracted from current (figure 7.28b) show disturbed trends, current minimum and maximum and current ramp forgiveness linearity with increasing degradation, but they are of good features because at the degradation start have a correlation next to unit. The mean current and the decrease time, instead, have a correlation coefficient too low and oscillating for all values of degradation.

(a) Position features   (b) Current features
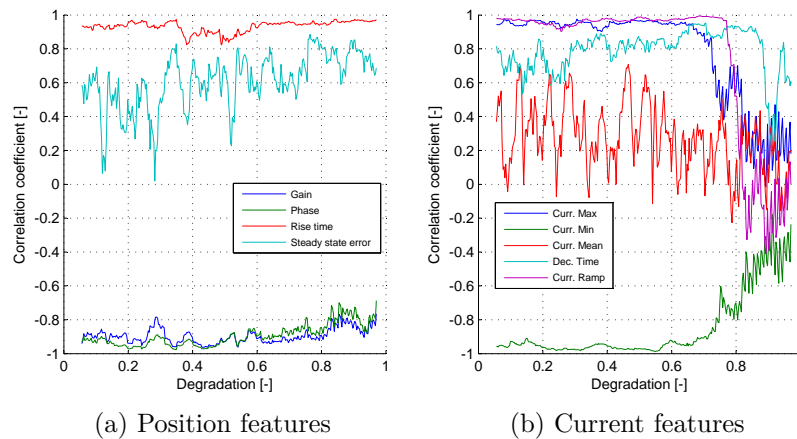
Figure 7.28: Moving correlation magnetomotive force reduction

7.4.2   Contamination of nozzles

The contamination of right and left nozzle have been study, the results are not equal because the stimuli selected is not symmetric, in general can be said that the occlusion of the two nozzles is better identified by the current features which appear to have higher correlations and less dispersion of the points.

The left nozzle clogging results in a increase almost linear of gain and phase, while a linear reduction of steady state error; rise time is not correlate with the degradation (figure 7.29a). The all features of the current show, however, an excellent behavior inversely linear, with a very low dispersion of the points (figure 7.29b).

The correlation analysis, show in table 7.10, has achieved excellent results for the features of the current, which are coefficients grater than 0.99, after

(a) Position features

(b) Current features
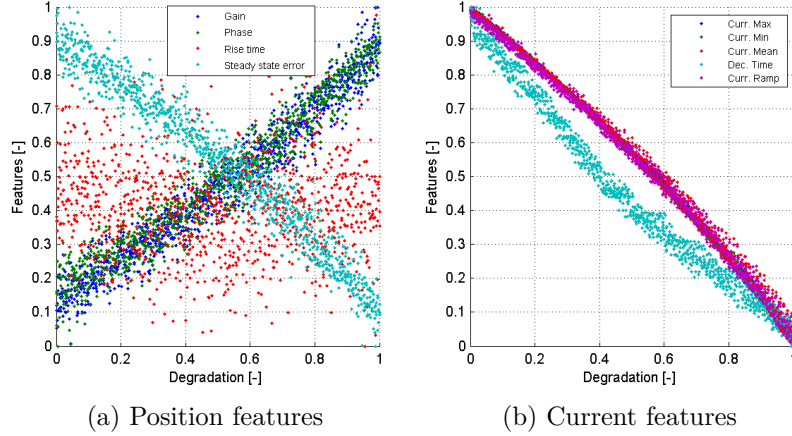
Figure 7.29: Influence of left nozzle occlusion

eliminating the influence of temperature. The features of position instead have low correlations when considering the influence of temperature, otherwise the values are around 0.96 for all, with the exception of the rise time, which is absolutely not influenced by the occlusion of the left nozzle.The great problem for correctly identifying the left nozzle clogging is the low evolution of features, which are all very small distances between nominal and degraded state.

Table 7.10: Features evaluation for left nozzle occlusion

| | Temperature influence | | No temperature influence | |
	Correlation	Distance [%]	Correlation	Distance [%]
Gain	0.593	16.15	0.974	16.57
Phase	0.227	2.99	0.966	3.12
Rise time	0.416	0.44	0.016	0.24
Steady state e.	-0.976	31.25	-0.976	31.43
Current max	-0.991	25.02	-0.998	25.09
Current min	-0.992	24.83	-0.998	24.69
Current mean	-0.998	258.88	-0.997	258.31
Time decrease	0.980	33.23	-0.993	33.43
Ramp current	0.964	27.55	-0.996	27.74

The moving correlation coefficients confirm the results obtained with the analysis of the overall correlations, the indicators extracted from the position are little correlated with the degradation (figure 7.30a), while those of

the current have correlation constant and almost unitary, except the time decrease (figure 7.30b).

(a) Position features

(b) Current features
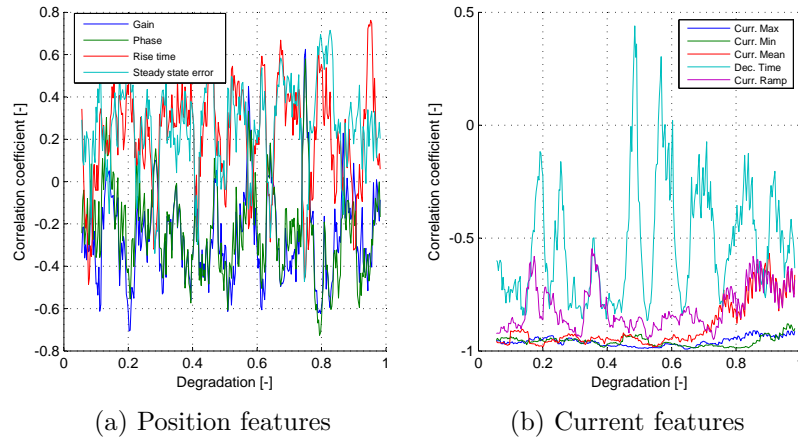
Figure 7.30: Moving correlation left nozzle occlusion

The clogging of right nozzle involves approximately symmetrical results in relation to what was seen previously. The left nozzle clogging results in a decrease almost linear of gain and phase, while in a linear increase of steady state error and rise (figure 7.31a). The all features of the current show an excellent linear behavior, but the time decrease saturates for values of degradation above the 0.5 (figure 7.31b).

(a) Position features
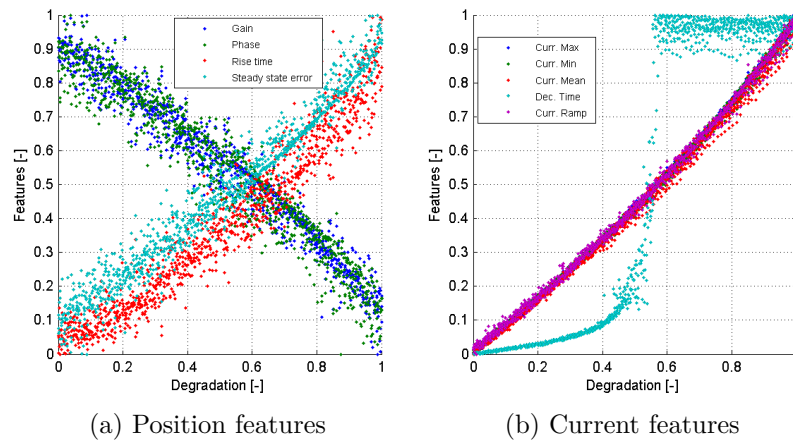
(b) Current features

Figure 7.31: Influence of right nozzle occlusion

The correlation analysis, show in table 7.11, has achieved excellent results

for the features of the current and for the position health indicators. The lowest correlation is shown from the decrease time which saturates, as seen in the previous charts. The great problem for correctly identifying the right nozzle clogging is the low evolution of features, which are all very small distances between nominal and degraded state.

Table 7.11: Features evaluation for right nozzle occlusion

| | Temperature influence | | No temperature influence | |
	Correlation	Distance [%]	Correlation	Distance [%]
Gain	-0.830	20.49	-0.980	20.29
Phase	-0.690	3.94	-0.969	3.89
Rise time	0.825	10.08	0.971	9.965
Steady state e.	0.961	36.66	0.982	36.53
Current max	0.993	28.89	0.997	28.85
Current min	0.990	28.03	0.997	28.06
Current mean	0.997	523.14	0.996	522.67
Time decrease	0.907	574.50	0.907	573.87
Ramp current	0.976	32.00	0.997	31.87

The moving correlation coefficients show that position indicators are little correlated with the degradation (figure 7.32a), while those of the current have correlation constant and almost unitary, except the time decrease (figure 7.32b).

(a) Position features (b) Current features
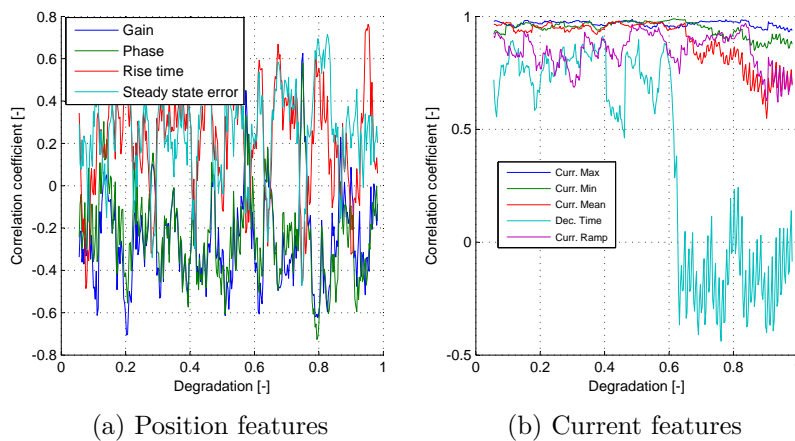
Figure 7.32: Moving correlation right nozzle occlusion

7.4.3 Variation of the stiffness of the feedback spring

The reduction of the of the stiffness of the feedback spring involves important variations of the features of both position (figure 7.33a) and current (figure 7.33b). The features of position have a high correlation with the degradation; also the features of current show an excellent correlation with the degradation and contained a dispersion.

(a) Position features (b) Current features
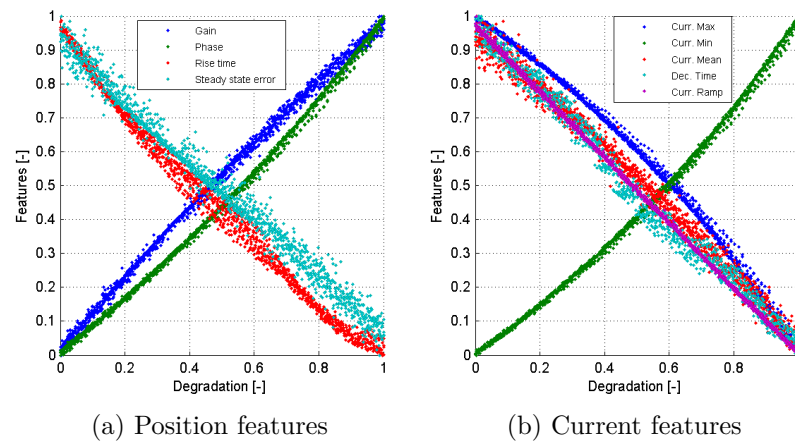
Figure 7.33: Influence of feedback spring yield

The correlation analysis, show in table 7.12, has achieved excellent results for the features of the current and for the position health indicators. The distances between the mean value of the features in nominal conditions and that are contained in the nominal conditions, but sufficient to permit easy identification.

Although the overall correlation coefficient is high for all the features, the moving coefficient highlights how certain features have low correlations for certain values of degradation. Phase (figure 7.34a) has stable correlation close to one, gain and rise time show a good correlation for small degradation, but diverge for high value of yield; the steady state error is very unstable. The features extracted from current (figure 7.34b) could be divided in two groups: current minimum and maximum and current ramp have a very good linearity. The mean current and the decrease time, instead, have a correlation coefficient too low and oscillating for all values of degradation.

Table 7.12: Features evaluation for feedback spring yield

	Temperature influence		No temperature influence	
	Correlation	Distance [%]	Correlation	Distance [%]
Gain	0.993	85.06	0.998	86.15
Phase	0.993	41.47	0.997	41.56
Rise time	-0.978	31.37	-0.994	31.55
Steady state e.	-0.988	52.71	-0.994	52.84
Current max	-0.988	32.38	-0.993	32.44
Current min	0.990	32.88	0.995	32.96
Current mean	-0.990	62.74	-0.995	62.84
Time decrease	-0.982	37.23	-0.995	37.42
Ramp current	0.994	47.04	0.988	47.16

(a) Position features   (b) Current features
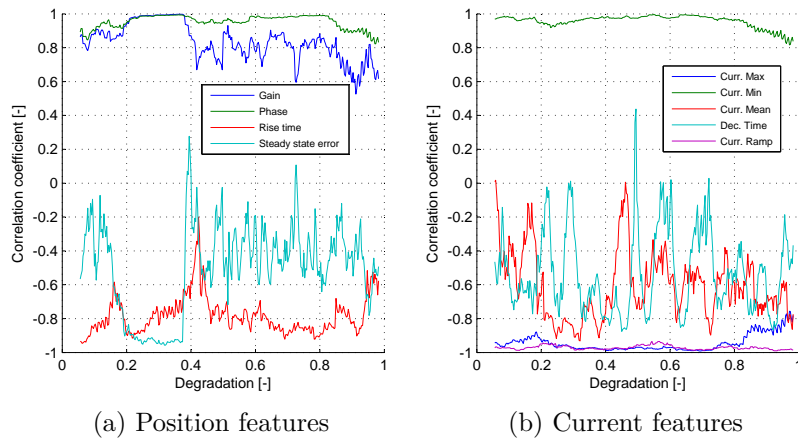
Figure 7.34: Moving correlation feedback spring yield

7.4.4   Increase of the backlash between spool and feedback spring

Increase of the backlash between spool and feedback spring can be well represented by gain and phase, as regards the position features, as shown in the figure (figure 7.35a), while the rise time has an oscillatory trend and steady state error has a too wide dispersion of the points. The features of current (figure 7.35b) show an excellent correlation with the degradation and contained a dispersion, except the average current that, despite having a good correlation, has very dispersed samples.

(a) Position features   (b) Current features
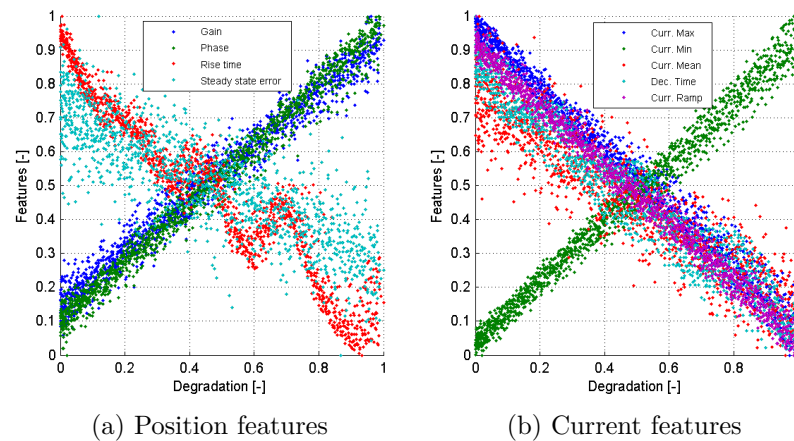
Figure 7.35: Influence of backlash between spool and spring

The increase of the backlash between the feedback spring and the spool has a little influence on health indicators, as evidenced by the distance between the mean value of the features between nominal and degraded conditions (table 7.13), this condition implies that the effect of oil temperature and the supply pressure is amplified compared to other degradations. In fact the overall correlation coefficients greatly improve if the features are cleaned effect introduced by the operating conditions,: the average increase of the coefficients is about 0.2, while for the other degradations, that are less influenced by the hydraulic fluid conditions, is generally an order of magnitude lower.

The analysis of the moving correlation provides results not too encouraging, all the features have a strongly oscillatory trend for both high and low levels of degradation. The position features (figure 7.36a) are the worst results, with the exception of the phase, all the other indicators present multiple

changes of correlation coefficients sign during the evolution of the degradation. Same problem occurs for current mean, current ramp and decrease time as shown in figure 7.36b; the correlations of minimum and maximum current, although have not sign reversal, are however very disturbed.

Table 7.13: Features evaluation for backlash between spool and spring

	Temperature influence		No temperature influence	
	Correlation	Distance [%]	Correlation	Distance [%]
Gain	0.800	22.12	0.986	22.29
Phase	0.795	7.52	0.992	7.58
Rise time	-0.751	11.61	-0.961	11.70
Steady state e.	-0.663	11.02	-0.836	11.11
Current max	-0.792	4.88	-0.992	4.92
Current min	0.764	4.94	0.993	4.98
Current mean	-0.838	18.12	-0.930	18.21
Time decrease	-0.854	14.05	-0.972	14.14
Ramp current	-0.755	9.61	-0.994	9.69

(a) Position features   (b) Current features
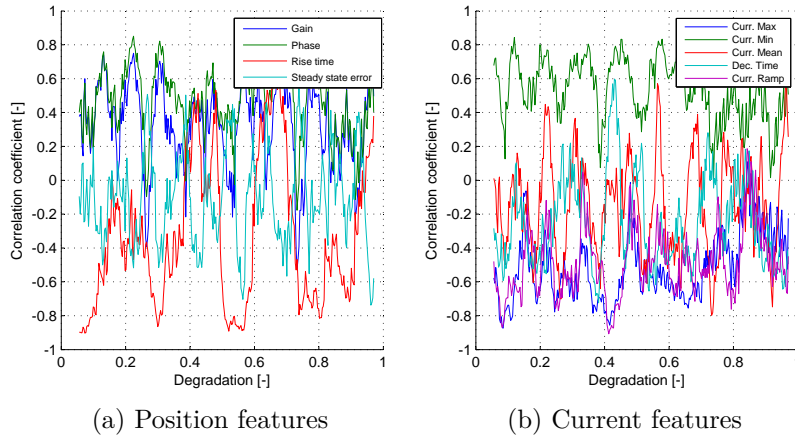
Figure 7.36: Moving correlation backlash between spool and spring

7.4.5 Variation of the friction force between spool and sleeve

The increase of the friction force is the most difficult degradation to identify due to its little influence on the behavior of the servovalve, since the pressure

force that is generated at the ends of the spool is about two orders of magnitude greater than the force of the nominal friction. As for the backlash, even for friction identifying health indicators trends is very complicated, because the little influence of the degradation is cover up by the effect of the operating conditions.

Gain and phase are the only position features that provides useful information, the steady state error has a too high dispersion of the points, to be used to identify the degradation, while the rise time seems immune to the variation of the friction force (figure 7.37a). Maximum current, minimum current and decrease time have a good behavior in the initial stage of degradation, while with the increase of the friction force the clouds of acquired points begin to expand, and consequently the correlation coefficients decreases; instead the average current and current ramp present a very poor behavior for all the degradation values (figure 7.37b).

(a) Position features   (b) Current features
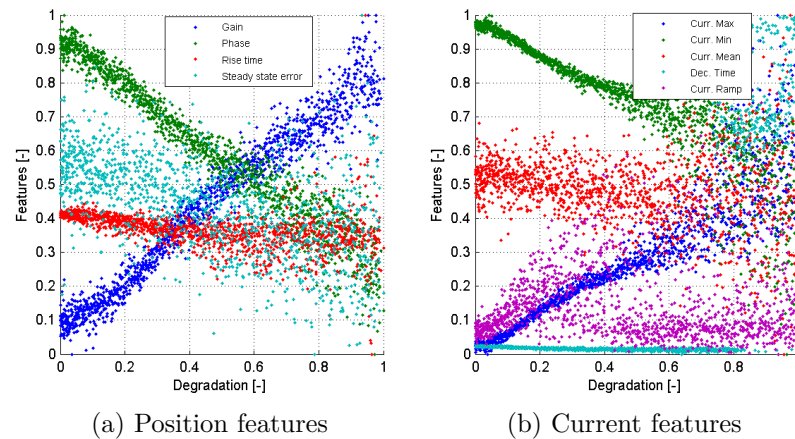
Figure 7.37: Influence of friction force

The increase of the friction force between the spool and servovalve sleeve has a little influence on health indicators, as evidenced by the distance between the mean value of the features between nominal and degraded conditions (table 7.14). The unique features that show a sufficiently high correlation coefficient are gain, phase, current minimum and current maximum, from these four, however, the only indicator of health that provide interesting indications is the gain, because the other three have too low a distance and hardly allows to identify the degradation.

The analysis of the moving correlation provides results not too encouraging, all the features have a strongly oscillatory trend for both high and

low levels of degradation. The position features (figure 7.38a) have a large variation of the correlation coefficients during the degradation evolution, not a single features can be considered efficient. Same problem occurs for all current health indicators as shown in figure 7.38b, between current indicators only maximum and minimum current can save, though with reserve, since have sufficiently high correlation values in the early phase of degradation.

Table 7.14: Features evaluation for friction force

| | Temperature influence | | No temperature influence | |
	Correlation	Distance [%]	Correlation	Distance [%]
Gain	0.871	25.58	0.981	25.78
Phase	-0.825	7.22	-0.975	7.14
Rise time	-0.235	3.92	-0.468	4.00
Steady state e.	-0.352	3.91	-0.547	4.03
Current max	0.889	8.38	0.929	8.33
Current min	-0.863	8.28	-0.909	8.25
Current mean	-0.101	4.34	-0.207	4.53
Time decrease	0.657	478.13	0.656	477.63
Ramp current	0.171	0.76	0.042	0.86

(a) Position features
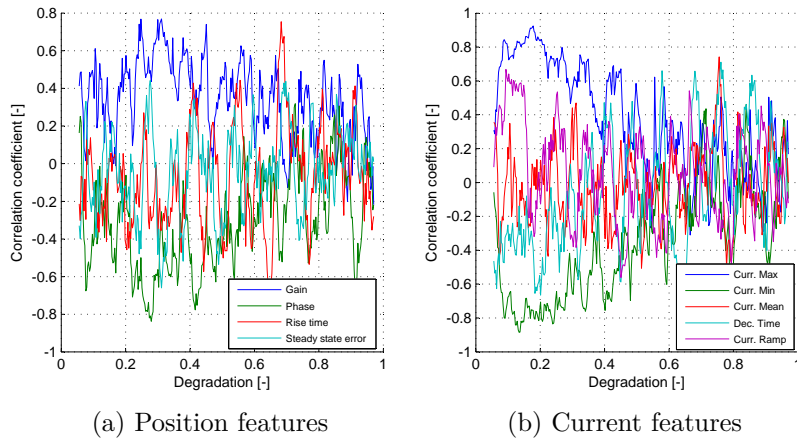
(b) Current features

Figure 7.38: Moving correlation friction force

7.4.6 Increase of the radial gap

The increase of the radial clearance and the features of position (figure 7.39a) and current (figure 7.39b) have a strongly correlated trends, all health indicators evolve in a linear manner, demonstrating to be optimal indexes to identify the degradation. The problem is the dispersion of acquisitions that, especially for the current features, may create difficulties in identifying the fault in the initial state, and also may result in the emergence of false alarms.

(a) Position features   (b) Current features
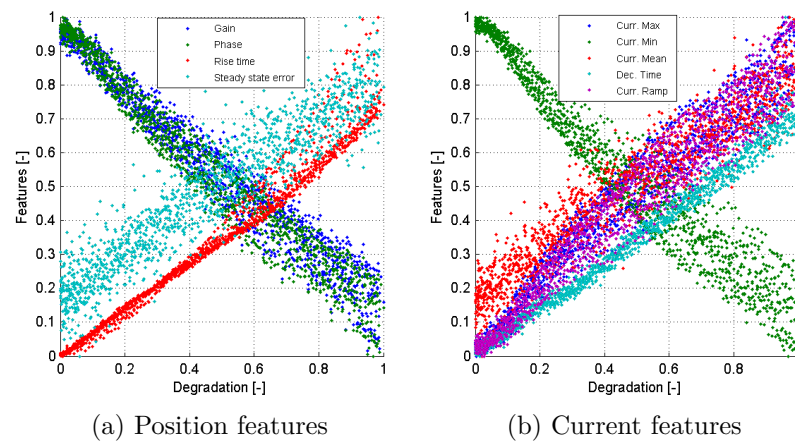
Figure 7.39: Influence of radial gap

The correlation analysis, show in table 7.15, has achieved excellent results for the features of the current and for the position health indicators. The distances between the mean value of the features in nominal conditions and that are contained in the nominal conditions, but sufficient to permit easy identification.

Although the overall correlation coefficient is high for all the features, the moving coefficient highlights how certain features have low correlations for certain values of degradation. All the position indicator (figure 7.40a) has stable high correlation for early degradation step, the steady state error is very unstable. The features extracted from current (figure 7.40b), except for current mean, have a good correlation for small increase of radial clearance; the mean current instead has a correlation coefficient too low and oscillating for all values of degradation.

Table 7.15: Features evaluation for radial gap

| | Temperature influence | | No temperature influence | |
	Correlation	Distance [%]	Correlation	Distance [%]
Gain	-0.964	41.89	-0.983	41.67
Phase	-0.968	12.82	-0.983	12.76
Rise time	0.959	59.98	0.987	59.71
Steady state e.	0.923	18.41	-0.941	18.33
Current max	0.970	7.57	0.979	7.53
Current min	-0.965	7.99	-0.977	7.95
Current mean	0.947	31.18	0.953	31.06
Time decrease	0.972	56.55	0.993	53.35
Ramp current	0.963	17.28	0.979	17.19

(a) Position features

(b) Current features
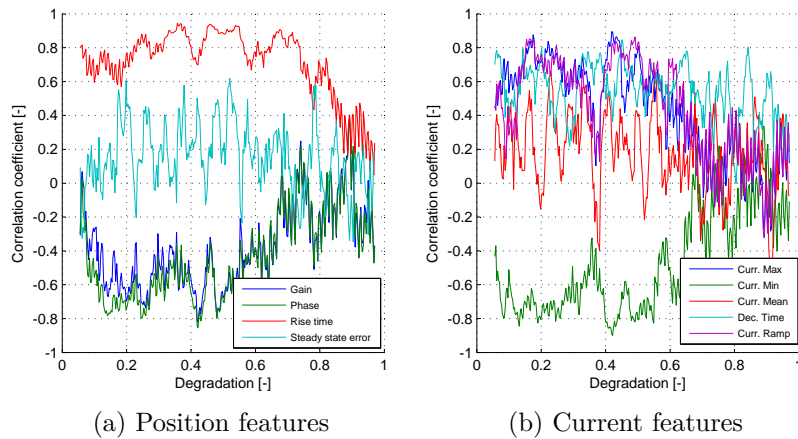
Figure 7.40: Moving correlation radial gap

7.4.7   Summary

The evaluation process of the features has confirmed that the health indicators selected provide a good representation of the status of the electrohydraulic servovalve, thus allowing an identification of the main deteriorations. Furthermore the stimulus specially created for the prognostic and health management algorithm allows to observe, in just 1.8 seconds, all the different operating conditions of the EHSA.

The metrics have shown how the operating conditions, oil temperature and the supply pressure, negatively affect the features, therefore a strategy that would eliminate such influence must be strictly planned and implemented. The equations presented in sub-section 7.2.1 have to demonstrate a valid solution, in the following chapters another approach will be presented, this second one has the advantage of requiring less computing resources.

The gain and phase are closely correlated, so the same information about the state of the system could be following only one of the two features. In the present work, however, both indexes are stored as, although the evolution is similar the amplitude of the variation is different. Follow the two indicators thus enables a quicker identification of faults, because the one that evolves faster will be the one that triggers the alarm.

The analysis showed that the effectiveness of a feature depends on the type of degradation that must be detected, but for any deterioration a set of features with optimum performances could be identified; only exception is the variation of the friction force between spool and sleeve, for which a good group of features can not be selected. Below for each deterioration the set of health indicators that have obtained better results in the metrics applied are presented.

- **Reduction magnetomotive force:** gain, phase, current minimum and decrease time, but also the others features provide a good indication

- **Contamination of nozzles left:** current maximum, current minimum and current mean, no useful information from rise time and phase

- **Contamination of nozzles right:** current maximum, current minimum and current mean, but also rise time and gain provide a good indication

- **Variation of the stiffness of the feedback spring:** gain, phase, steady state error and current mean. Also the others features provide a good indication

- **Backlash between spool and spring:** gain, rise time, current mean and time decrease

- **Friction force increase:** none particularly suitable features has been identified. Possible indicator are gain and phase

- **Radial gap increase:** gain, rise time, current mean, time decrease.

As can be seen from the list presented above, each degradation afflict different features. This property has been exploited in this thesis, to implement an algorithm, base on neural network, for classify the detected deterioration in order to provide additional support to maintenance operations.

8

Fault diagnosis

Fault diagnosis, in contrast to the less well-understood prognosis, has been the subject of numerous investigations over the past decades. Researchers in such diverse disciplines have been developing methodologies to detect fault (failure) or anomaly conditions, pinpoint or isolate which component/object in a system/process is faulty; the diversity of application domains is matched by the plurality of enabling technologies that have surfaced over the years in attempts to diagnose such detrimental events while meeting certain performance specifications.

The automatically identification of degradations is one of the focal points of a prognostic algorithm, good detection subroutine is the basis for a robust and reliable PHM algorithm, this part must be prove particularly sensitive to health status changes of the system observed, and at the same time insensitive to external disturbances; the goal is to identify degradations to their initial state and to avoid false alarms.

An algorithm that are not able to identify a degradation leads to a reduction of the safety of the airplane, since the occurrence of ruptures is favored; a detection routine which provides an alarm when there is no degradation due to an raise in maintenance costs resulting from unexpected , and unnecessary, machine stops and the increase in man-hours required to check the system and make a new Acceptance Test Procedure (ATP).

This chapter first presented the objectives of a degradation detection routine detection, introducing the metrics used in the scientific community to evaluate the efficiency of the algorithm. Then the three different approaches implemented are discussed and evaluated using the appropriate metrics.

8.1   Fault diagnosis requirements

Fault detection is typically defined as the ability to detect system degradation below required performance levels (incipient or impending failure) owing to physical property changes through detectable phenomena. Requirements are stated as the algorithm shall detect no less than a specific percentage of all failures specifically identified through Failure Modes and Effects Criticality Analysis (FMECA) analyses.

The PHM system shall demonstrate the capability to detect the failure, identified with the FMECA, in at least defined percent limit of cases, this limit, exactly like the ones that will be discussed below, are set based on customer requests and it is normally in the range 95% and 98%. The failure not detected are called false negative, they may present major risks to the health of the equipment under test; missed fault conditions may lead to a catastrophic failure resulting in loss of life or loss of the system.

Two other important metrics used to evaluate the detection algorithms are the confidence and the percentage of false alarm: the first is the confidence that expresses the level of certainty with which a degradation is detected, it is express as percentage and often is expressed as $100 - Type_{IIerror}$, where $Type_{IIerror}$ is defined as the accepted confidence error. The second metric is the number of false alarms, called also the number of false positive. False alarms is less safety critical than the false negative, but they could be accommodated with an unavoidable loss of confidence on the part of the system operator as to the effectiveness of the diagnostic tools. Normally the rate of false alarms accepted by the client is indicated as $Type_{Ierror}$ and is in the range 3% and 5%.

Fault-detection events may be evaluated through the decision matrix (H. Liu and Motoda 2012) based on a hypothesis-testing methodology and represents the possible fault-detection combinations that may occur (8.1).

From this matrix the probability of detection (POD) can be estimate as shown in equation 8.1.

$$POD = P(D_1/F_1) = \frac{a}{a + c} \tag{8.1}$$

The probability of a false alarm (POFA) considers the number of all fault-free cases that trigger a fault detection alarm (equation 8.2).

$$POFA = P(D_1/F_0) = \frac{b}{b + d} \tag{8.2}$$

A metric of accuracy is used to measure the effectiveness of the algorithm in correctly distinguishing between a fault-present and fault-free condition

(equation 8.3), the metric uses all available data for analysis.

$$Accuracy = P(D_1/F_1 \& D_0/F_0) = \frac{a+d}{a+b+c+d} \qquad (8.3)$$

Table 8.1: Decision matrix for detection evaluation

Outcome	Fault (F_1)	No fault (F_0)	Total
Detected (D_1)	a Number of detected faults	b Number of false alarms	$a+b$ Number of alarm
Not detected (D_0)	c Number of missed faults	d Number of correct rejections	$c+d$ Number of non-alarms
Total	$a+c$ Number of faults	$b+d$ Number of fault-free	$a+b+c+d$ Number of total cases

The previous metrics only evaluate the accuracy of the algorithm, but do not provide indications about the degradation level required from the PHM system to identify the fault, for this reason the technical literature (A. Saxena et al. 2008, Wheeler, Kurtoglu, and Poll 2009, Abhinav Saxena et al. 2009) recommended to add at the previous metrics the degradation level or the time-delay: the first is defined as the level of degradation necessary for the system to identify the fault, the second is defined as the time span between the initiation and the detection of a fault event. The time-delay or us metrics only evaluate the accuracy of the algorithm, but do not provide indications about the degradation level metrics are important not only as an early warning to the operator of an impending failure but also in terms of providing a sufficient time window that allows a prognostic algorithm to perform its intended task.

In the thesis level of degradation has been used as metrics because, not being known to the laws of propagation of degradation is impossible to compare the time because it depends mainly on how the degradations grow.

8.2 Fault diagnosis techniques

The technical literature presents several possible approaches to implementing detection degradations algorithm, but many of these are not suitable for use

in the project presented in this thesis; and in general all the data-based approaches were discarded, since large series of validated data are not present. The use of mathematical models approach has been considered one of the opportunities, but the implementation of an effective model to identify degradations would have required to set up a specific test bench and especially to find a large number of flying actuators that can be test in nominal and degraded conditions, reaching up to breakage of the same. The investment in terms of time and cost were not considered compatible with the PhD, and also find the flight components which could damage has been proved almost impossible; these facts have led to discard the idea to implement mathematical models to detect degradations.

The optimal approaches have proven to be the alarm bounds and the data-driven approaches, both allow to implement the algorithms can be calibrated easily, so that they can be easily adapted to the real components, also do not require set of historical data and knowledge of the degradations propagation models, this has allowed the development of solutions for the identification of the fault, starting only from a model validate in the absence of degradation.

The approach based on alarm bounds required the definition of the limits of variation of the different features under normal operating conditions, these normally are known in the design stage, and also may be further refined in the qualification test and with a smart use of data obtained from acceptance tests.

The data-driven approach proves to be the most flexible among those up to now used, as it not requires series of historical data and can easily be combined, as done in this project, with techniques based on self-learning. In the following of the chapter the two solutions based on data-driven implemented will be illustrated, in both cases an algorithm that allows the self learning, or the auto-calibration, has been implemented. The first solution operates exclusively using the data acquired during the operative life the aircraft, the second, which is an evolution of the first, takes advantage of the particle filter for estimating a distribution of probability of the features. The main disadvantage of using self-learning techniques is the inability to exploit the advantages offered by the PHM from the beginning, but a more or less long calibration period is necessary before being able to start the phase of the fault identification.

8.3   Alarm bounds approach

The approach based on alarm bands is one of the first which has been used in the field of PHM to identify degradations, but still today is particularly

appreciated because it is easy to implement, does not require high computing resources and generally proves robust to external disturbances.

The implemented algorithm, shown schematically in the figure 8.1, at the end of each test carried out in pre / post-flight makes a connection between the features extracted during the analysis of data and compares them with the threshold parameters; if one of the features is beyond the threshold of a first alarm will be activated, after three consecutive exits the system diagnoses the presence of a degradation and inform the maintainers. The decision to wait three consecutive alarms has been implemented in order to minimize false alarms due to possible unexpected fluctuations of the parameters.
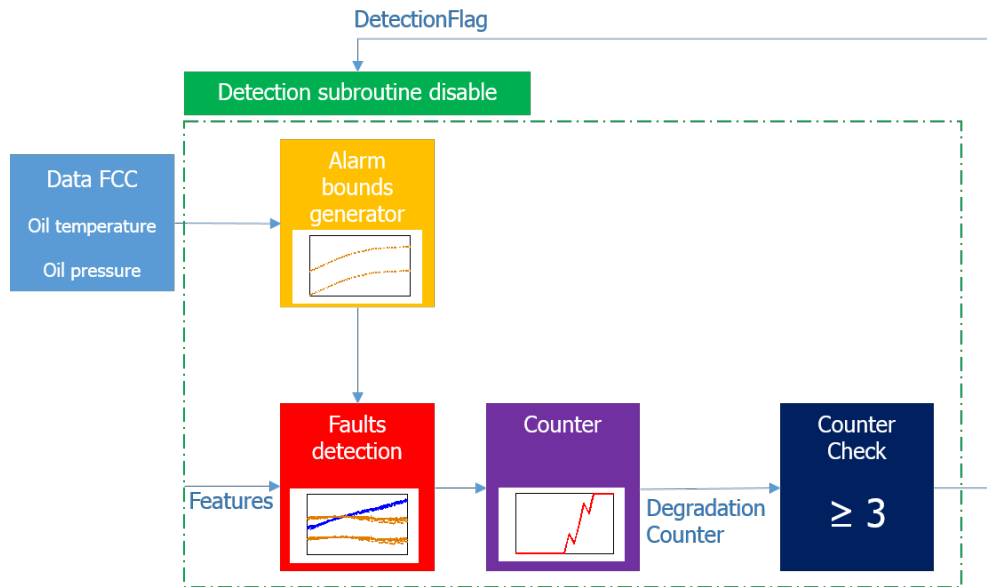
Figure 8.1: Alarm bound subroutine scheme

The main problem of this approach is the definition of the threshold parameters for each features, as seen in the chapter 7 the health indicators are strongly dependent on the operating conditions and by the manufacturing tolerances of the components. The bands must be constructed to be sensitive to the presence of any degradation, but very robust to different operating conditions.

The variables that significantly affect the features are: the oil temperature, the supply pressure and the constructive tolerances. The external disturbances, as shown above, have a very limited impact, and were not considered in the process of determining the level of alarm bands.

Compensate all three variables that affect the value of the features has proved impossible, therefore, the solution adopted contemplate mobile alarm

bands, that are generated from time to time as a function of temperature and oil pressure; in this configuration, the tolerance band must have a width such as to cover only geometric tolerances and the minimum noise introduced by external conditions.

Starting from the analysis of the influence of manufacturing tolerances, introduced in section 7.3, the maximum absolute difference between the nominal value of each features and that caused by the variation of flow rate and/or pressure gains has been identified, regardless of the temperature of the oil. The identified values, shown in the table 8.2, are the preliminary amplitude of the alarm bands and are assumed to be constant whatever are the temperature and oil pressure. In order to reduce the possible emergence of false alarms the width of the bands previously obtained has been multiplied by a safety factor (K_{ab}) set equal to 1.05; this value was chosen because it offers the best compromise between reducing earned alarms and identification speed of degradation. The process for obtaining the amplitude of the alarm bands can be synthesized with the equation 8.4 shown below, where A_{ab} is the amplitude of the alarm bound, F_{no} and F_{mt} are the values of the features in nominal conditions and with the application of the maximum obstructive tolerances, respectively. T and P are the pressure and the temperature of the oil, i represents the different features.

$$A_{ab_i} = K_{ab} \cdot max(|F_{no_i}(T, P) - F_{mt_i}(T, P)|) \qquad i = 1, ..., 9 \qquad (8.4)$$

Table 8.2: Amplitude of alarm bounds

Feature	Amplitude	Feature	Amplitude
Gain	0.840 dB	Current max	0.370 mA
Phase	3.860 deg	Current min	0.420 mA
Rise time	0.028 s	Current mean	0.043 mA
Steady state error	0.125 mm	Time decrease	0.017 s
		Current max ramp	1.09 mA

Alarm bands for different oil temperatures are shown in the graphs of figure 8.2 and figure 8.3, these limits have been obtained by setting an oil supply pressure of 18 MPa.

(a) Gain

(b) Phase

(c) Rise time

(d) Steady state error
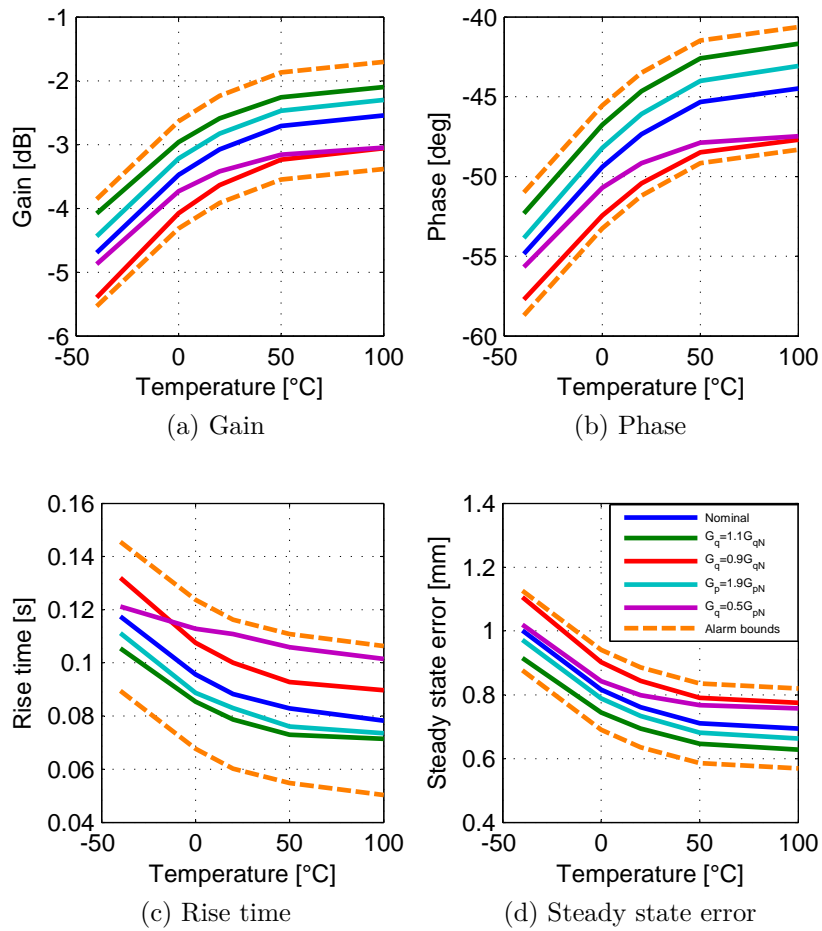
Figure 8.2: Alarm bounds on position features

(a) Current max

(b) Current min

(c) Current mean

(d) Time decrease

(e) Current ramp
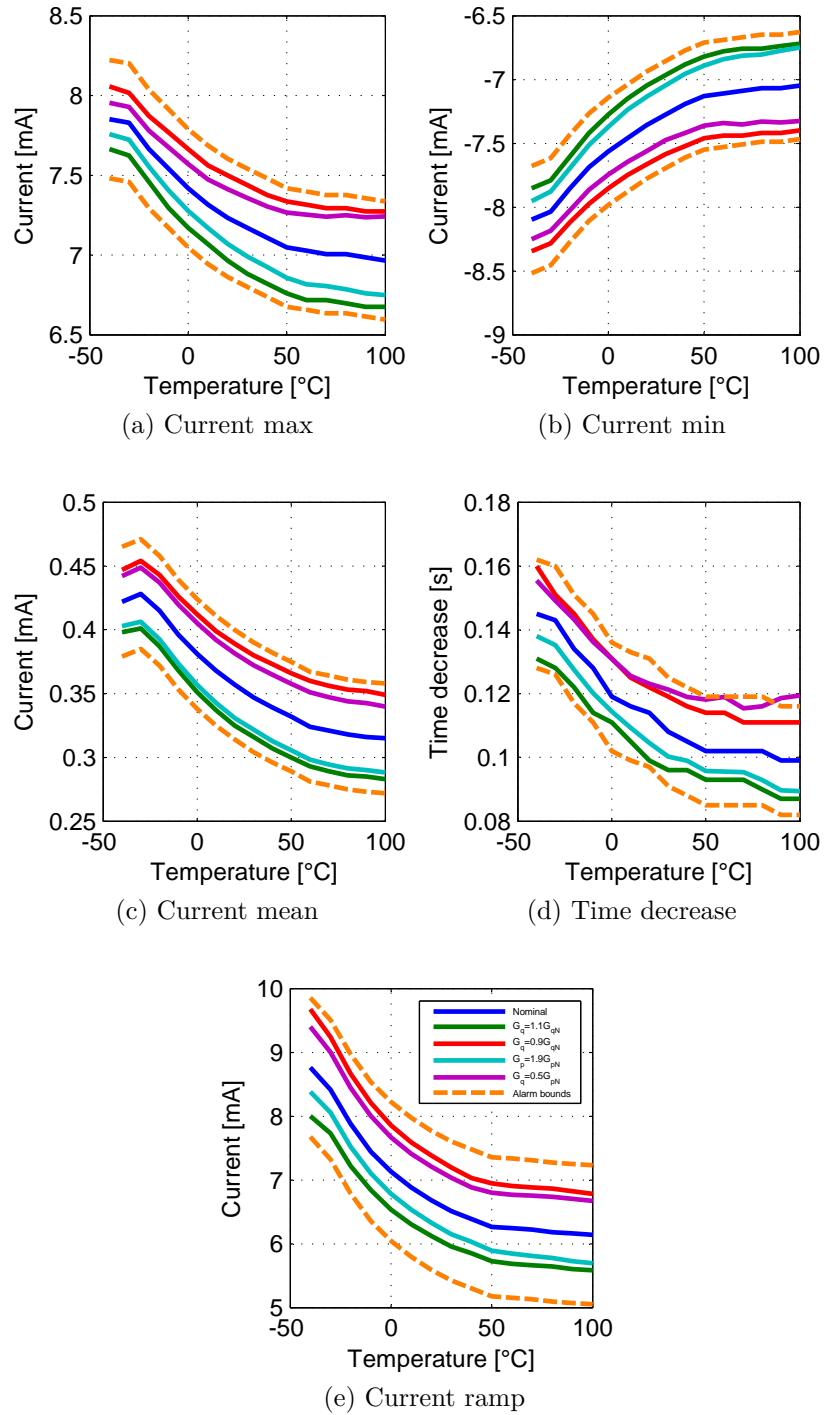
Figure 8.3: Alarm bounds on current features

The identified amplitude of the alarm bands remain constant whatever the operating conditions, while at the end of the test carried out in pre/post-flight starting from the oil temperature values and the algorithm registered supply pressure calculates the nominal value for each of the nine features. The nominal value of each of the features is obtained by polynomial equations of different orders extracted from the results provided by the simulations; the results were used to identify the best fitting a modeling framework called Symbolic Regression was exploited; the model chosen is the one with lower degree, which provides an absolute error less than $1 \cdot 10^{-6}$. In the table 8.3 indicates the best fitting equations identified for each features, where $\hat{F}_{no}$ is the approximate value of the feature, T and P are the pressure and the temperature of the oil, and the small letter form a to f are numerical coefficients.

Table 8.3: Fitting nominal features equations

Feature	Amplitude
Gain	$\hat{F}_{no} = aP + bTP + c + dPT^3$
Phase	$\hat{F}_{no} = aP + bT + cTP^3 + d + ePT^2$
Rise time	$\hat{F}_{no} = aP + bT + cTP + d + eT^2$
Steady state error	$\hat{F}_{no} = aP + bT + cTP + d + eT^2$
Current max	$\hat{F}_{no} = aTP + be^{cT} + d + fPT^2$
Current min	$\hat{F}_{no} = aTP + be^{cT} + d + fPT^2$
Current mean	$\hat{F}_{no} = aT + bPT^2 + cT^4 + dPT + eP^2T^3$
Time decrease	$\hat{F}_{no} = aT + bPT^3 + cT^2P^2 + d + eT^2$
Current max ramp	$\hat{F}_{no} = aT + bPT^3 + cPT^2 + dPT$

Calculated the nominal value function of pressure and oil temperature for each features, the PHM system identifies the alarm thresholds for that specific operating condition by the equations 8.5, where $LimU$ and $LimD$ are the up and the down limits, respectively; $\hat{F}_{no}$ is the approximate value of the feature A_{ab} is the amplitude of the alarm bound and , i represents the different features.

$$LimU_i = \hat{F}_{no_i} + A_{ab_i} \tag{8.5}$$
$$LimD_i = \hat{F}_{no_i} - A_{ab_i}$$

The features derived from an analysis of the data acquired during the tests are compared with the thresholds obtained with the equations presented

above, if all features are within the thresholds the EHSA has no degradations, otherwise called a counter is activated *"DegradationCounter"*, this counter is set to zero when the EHSA is installed in the airplane, and is saturated between 0 and 3. For each test, if all the features are within the thresholds, the previous value of the counter will be reduced by 0.5, while if at least one of the features out by the thresholds, the counter is incremented by 1, when the counter reaches the 3 prognostic system communicates to the maintainer and the user to have identified a degradation in servocommand and the *"Detection flag"* is enable. The flag disables subroutine detection of degradation and enables the estimation algorithm of the useful life and the one that allows to classify the type of degradation.The detection system based on the counter allows to minimize false alarms as it requires that at least one the features outside of alarm bands for three consecutive tests or fifty percent of negative tests in a given time window.

8.3.1 Results overview

The algorithm for detect degradations was verified through more than ninety different simulations, in which have been made to change the type of degradation and the number of degradation presents, also for each of the simulations pressure, oil temperature and conditions environmental have been set follow a random pattern. Moreover, as already it stated in the course of the document, Moreover, as already it stated in the course of the document, in the technical literature information about the evolution of degradations in a servovalve are not present, thus different possible evolution of profiles have been tested, they include growth of degradation as linear, square pr cube function of hours of flight, step evolution and random profiles.

The results of the tests carried out have shown that the algorithm implemented are independent from the type of degradation law of growth set, as the comparison between the values of the features and the respective bands of alarm occurs time step by time step. In other words the comparison between the value of the features extracted from the analysis of data obtained in the pre/post-flight test and alarm bands takes place at the end of each acquisition process,the process does not require any kind of storing of past features values, then the identification process considers only the values of the features in that moment and not the evolution of these over time.

In the following of this section some of the obtained results provided by the subroutine are presented as an example: the results of four tests are shown in detail: three in which the degradation evolves as function of time, two first (one single and one double degradation) and a third order, and a series data in which the degradation evolves following a step function.

Variation of the stiffness of the feedback spring (first order)

The reduction of the stiffness of the spring is described in this test as linear with the hours of flight by the equation 8.6, where *Deg* is the variation of the stiffness in percentage, FH is the actual flight hours, FH_0 is the time when the degradation occur and K_{stiff} is the linear coefficient.

$$Deg = K_{stiff} * (FH - FH_0) \tag{8.6}$$

The degradation begins to occur after 11.5 hours of flight, and increases linearly up to a value slightly less than 50%; in the figure 8.4 the trend of degradation is shown in blue and in red the instant of start.

Figure 8.4: Variation of stiffness

The algorithm implemented, at the end of each acquisition carried out in pre/post-flight, compares the features extracted with alarm bands obtained starting from oil temperature and pressure, until the *"DegradationCounter"* reaches the value three. In the case presented this counter reaches the maximum after 52 hours of flight, then the degradation is detected with a delay of 40.5 flight hours, equivalent to a spring yield equal to 10.25%.

The diagrams of figure 8.5 and figure 8.6 reporting the performance of features than the alarm band, the red vertical line represents the beginning of the degradation, while the green the time when the degradation is identified. All the features are influenced by the presence of the degradation, but the minimum and the maximum current are the two health indicators that undergo the greatest variation in fact, the alarm is due from these two features. Other two values that are particularly sensitive to the variation of the stiffness of the feedback spring are the phase and the steady state error, which, however, are slightly lagging behind the two current features.

In general the degradation could be not immediately observed after its beginning, since the influence of the stiffness variation is too small to affect

the behavior of the EHSA; for the first few tens of hours of flight subsequent to the onset of degradation of the servo valve has a behavior and the characteristics fully comparable to those nominal.

(a) Gain

(b) Phase

(c) Rise time

(d) Steady state error
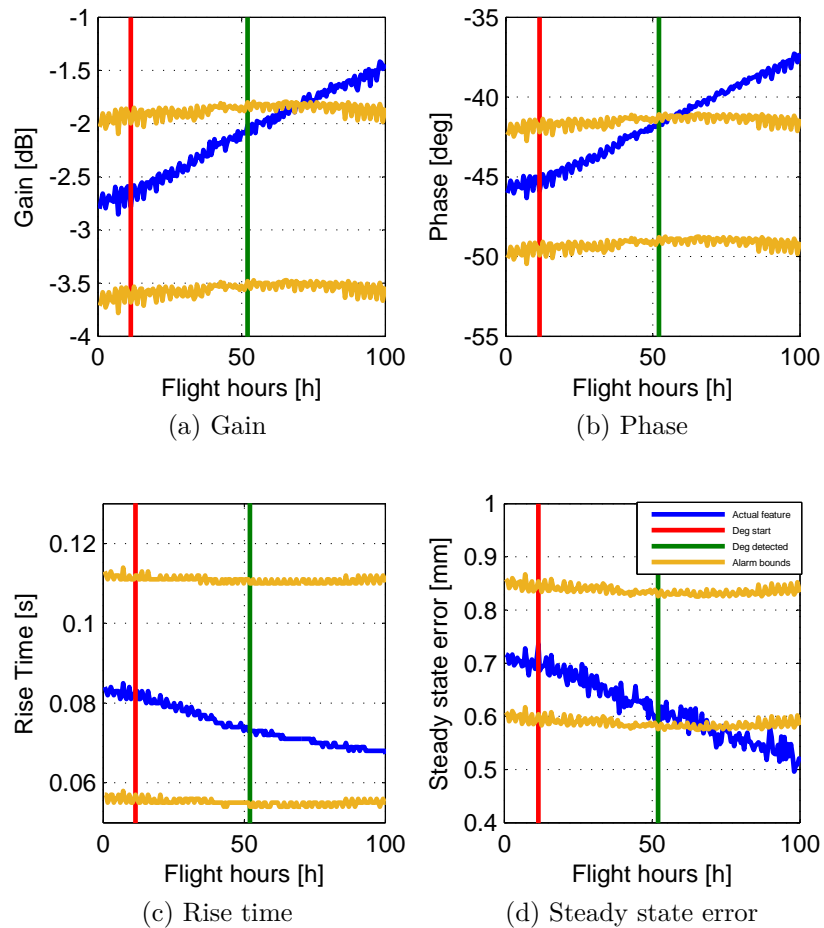
Figure 8.5: Position features yield

(a) Current max

(b) Current min

(c) Current mean

(d) Time decrease

(e) Current ramp
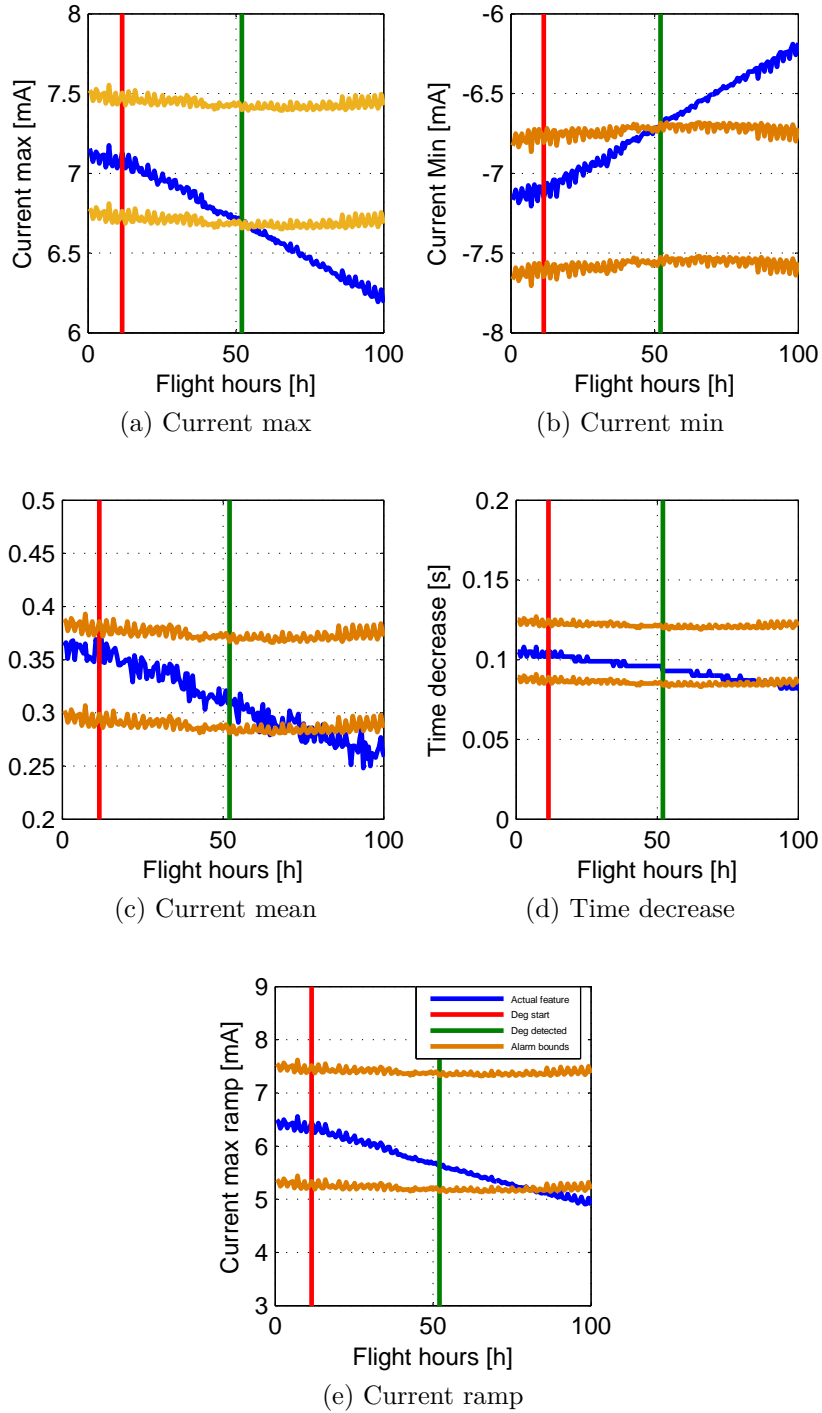
Figure 8.6: Current features yield

Reduction of magnetomotive force and radial gap increase (second order)

The following test is characterized by the presence of two degradations that develop at different times on the servovalve, the first is reduction of magnetomotive force described as first order function of the hours of flight, the second is the increase of the radial gap described as fisrt order function, both equation are presented above (eq. 8.7), where *Deg* is the variation of the stiffness in percentage, FH is the actual flight hours, FH_0 is the time when the degradation occur and K is the linear coefficient, the subscripts FMM and GR indicate the reduction of magnetomotive force and the increase of radial gap.

$$Deg_{FMM} = K_{FMM} * (FH - FH_{0FMM})$$
$$Deg_{RG} = K_{RG} * (FH - FH_{0RG}) \tag{8.7}$$

The fist degradation occurs after 11.5 hours of flight, and increases up to a value slightly less than 50%, the second after 136.5 flight hours; in the figure 8.7 the trend of degradation is shown in blue and green and in red and orange the instant of start.
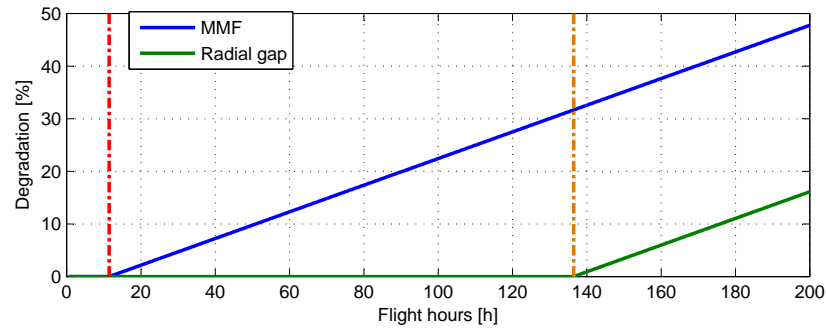
Figure 8.7: Variation of magnetomotive force and radial gap

The algorithm implemented, at the end of each acquisition carried out in pre/post-flight, compares the features extracted with alarm bands obtained starting from oil temperature and pressure, until the *"DegradationCounter"* reaches the value three. In the case presented this counter reaches the maximum after 93 hours of flight, then the degradation is detected with a delay of 44.3 flight hours, equivalent to magnetomotive force reduction equal to 6.37%.

The diagrams of figure 8.8 and figure 8.9 reporting the performance of features than the alarm band, the red vertical line represents the beginning of the magnetomotive force degradation, the lilac line the beginning of the radial gap variation while the green the time when the degradation is identified. All the features are influenced by the presence of the degradation, but the mean current is the health indicators that undergo the greatest variation in fact, the alarm is due from this feature. The other features are particularly no sensitive to the variation of the magnetomotive force of torque motor, at least in the initial phase.

In general the degradation could be not immediately observed after its beginning, since the influence of the magnetomotive force variation is too small to affect the behavior of the EHSA; for the a reduction under the 10% is very difficult notice the degradation effects.

(a) Gain

(b) Phase

(c) Rise time

(d) Steady state error
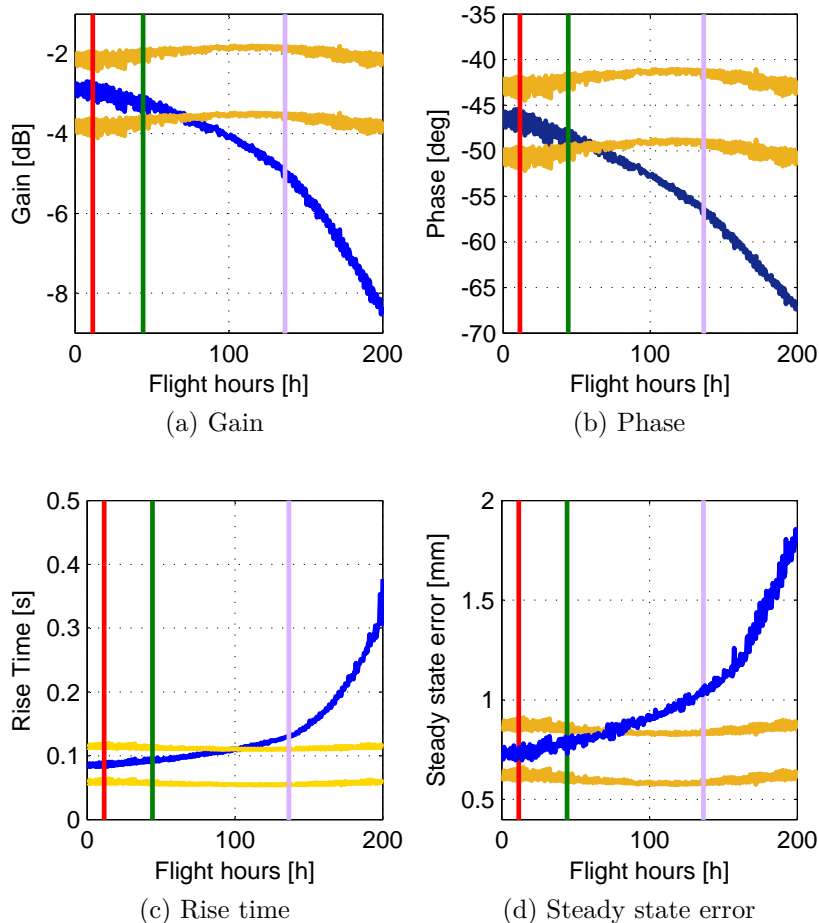
Figure 8.8: Position features double degradations

(a) Current max

(b) Current min

(c) Current mean

(d) Time decrease

(e) Current ramp
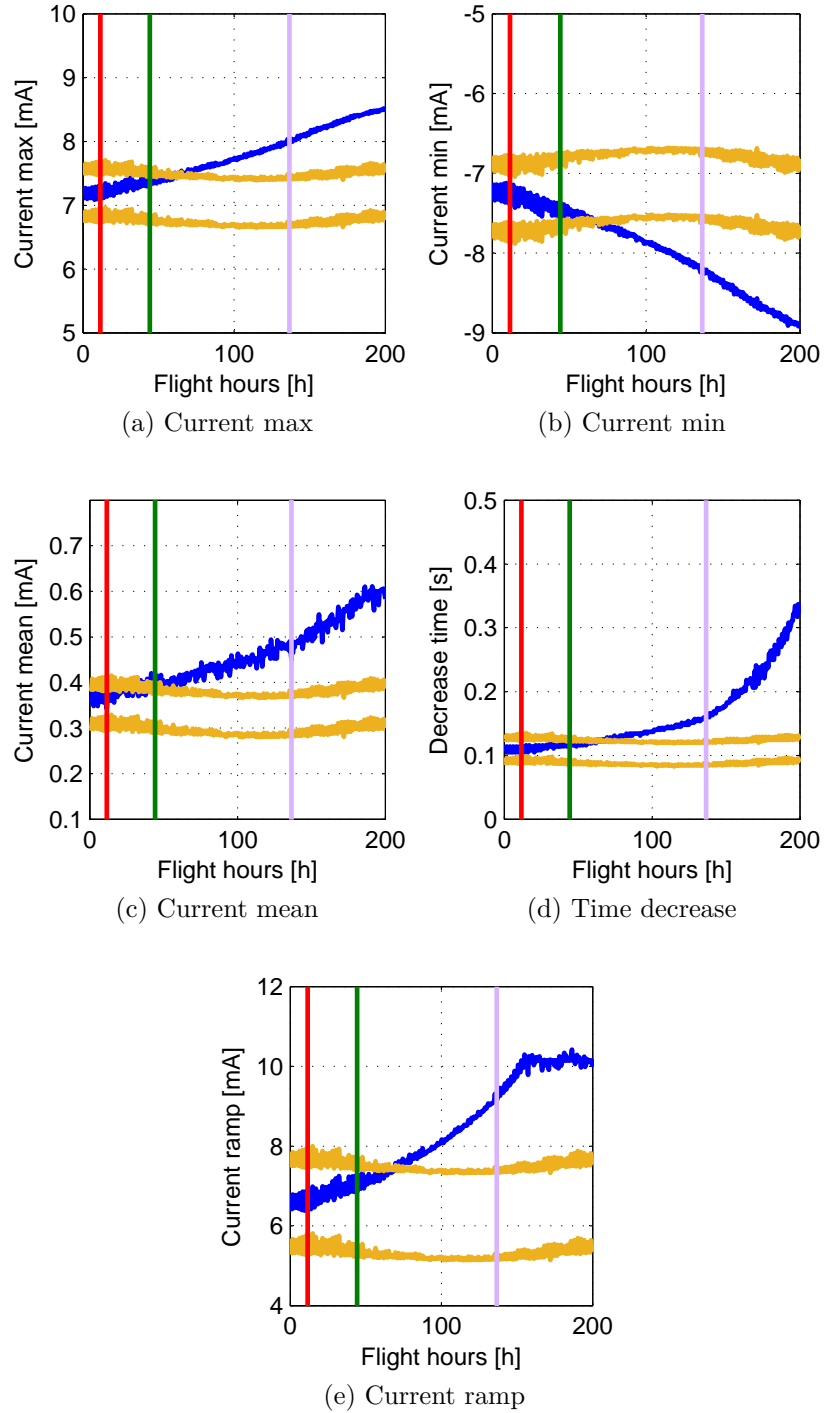
Figure 8.9: Current features double degradations

Reduction of magnetomotive force (third order)

The reduction of magnetomotive force is described in this test as third order function of the hours of flight by the equation 8.8, where Deg is the variation of the stiffness in percentage, FH is the actual flight hours, FH_0 is the time when the degradation occur and K_{FMM} is the linear coefficient.

$$Deg = K_{FMM} * (FH - FH_0)^3 \tag{8.8}$$

The degradation occurs after 13 hours of flight, and increases up to a value slightly less than 50%; in the figure 8.10 the trend of degradation is shown in blue and in red the instant of start.
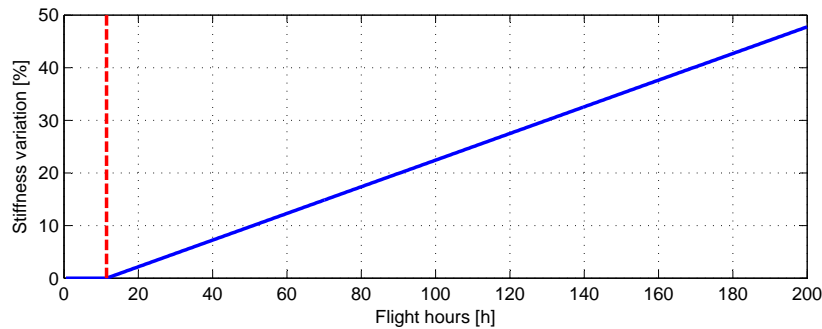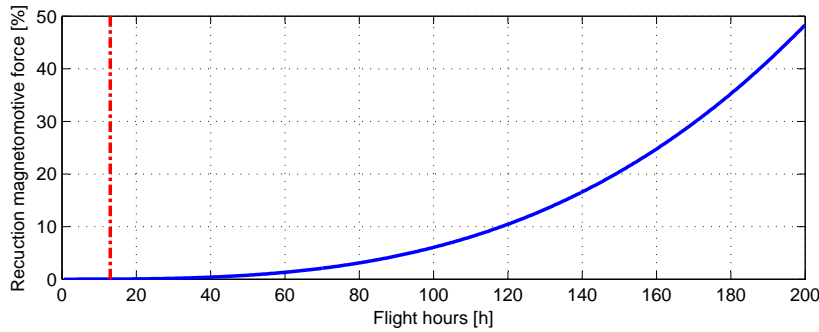

Figure 8.10: Variation of magnetomotive force

The algorithm implemented, at the end of each acquisition carried out in pre/post-flight, compares the features extracted with alarm bands obtained starting from oil temperature and pressure, until the *"DegradationCounter"* reaches the value three. In the case presented this counter reaches the maximum after 93 hours of flight, then the degradation is detected with a delay of 80 flight hours, equivalent to magnetomotive force reduction equal to 4.97%.

The diagrams of figure 8.11 and figure 8.12 reporting the performance of features than the alarm band, the red vertical line represents the beginning of the degradation, while the green the time when the degradation is identified. All the features are influenced by the presence of the degradation, but the mean current is the health indicators that undergo the greatest variation in fact, the alarm is due from this feature. The other features are particularly no sensitive to the variation of the magnetomotive force of torque motor, at least in the initial phase.

In general the degradation could be not immediately observed after its beginning, since the influence of the magnetomotive force variation is too

small to affect the behavior of the EHSA; for the a reduction under the 10%
is very difficult notice the degradation effects.

(a) Gain

(b) Phase

(c) Rise time

(d) Steady state error

Figure 8.11: Position features reduction of magnetomotive force

(a) Current max

(b) Current min

(c) Current mean

(d) Time decrease

(e) Current ramp
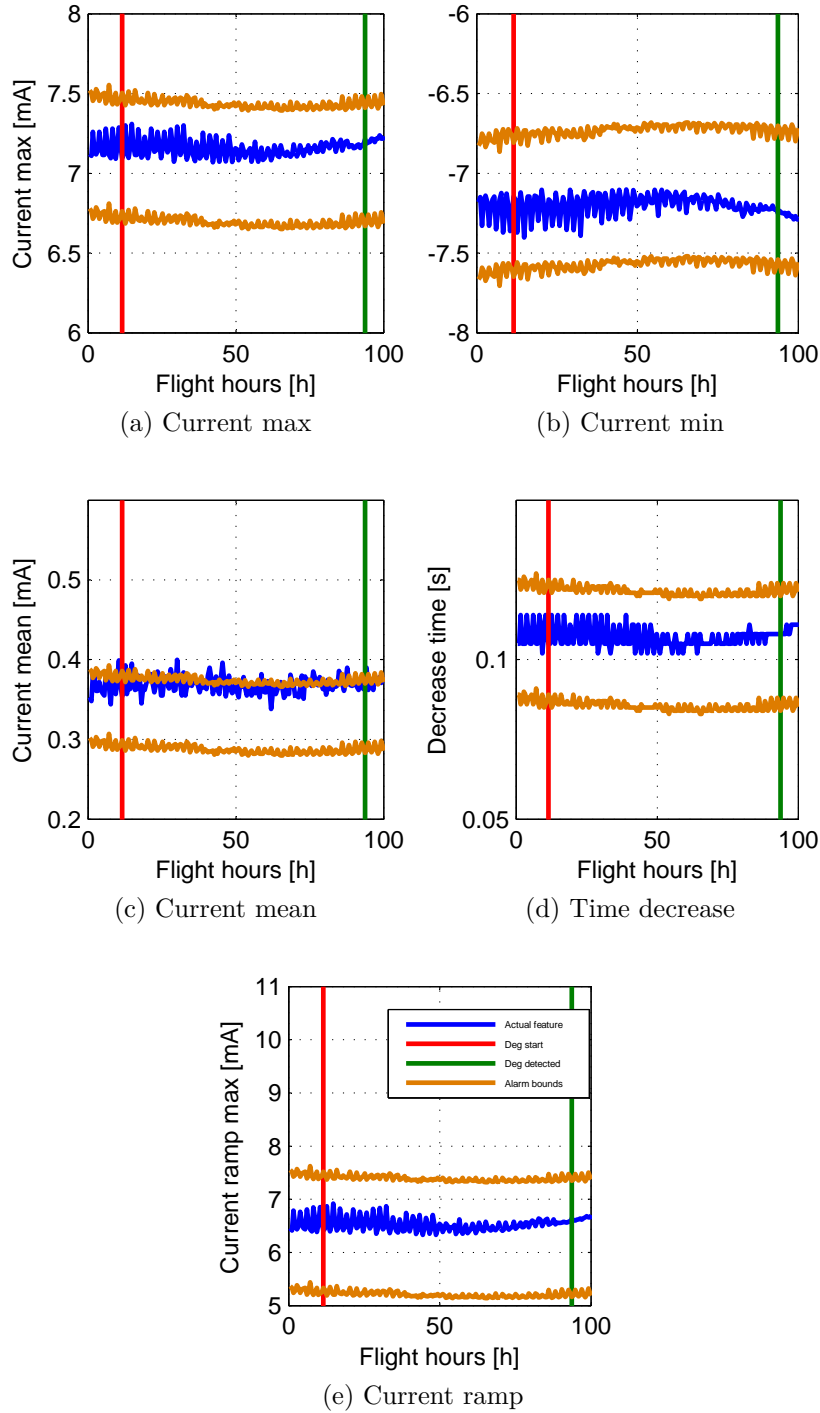
Figure 8.12: Current features reduction of magnetomotive force

Clogging of right nozzle (step)

The clogging of right nozzle is described in this test as third step function, where the amplitude of the steps and the presence of the same is decided randomly.

The degradation begins to occur after 25 hours of flight, and increases up to a value slightly less than 35%; in the figure 8.13 the trend of degradation is shown in blue and in red the instant of start.
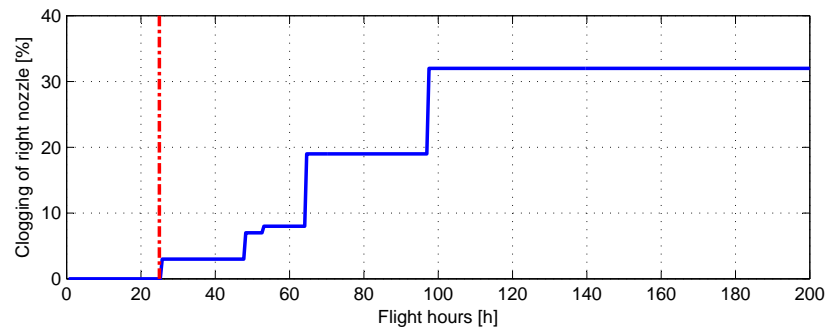
Figure 8.13: Variation of clogging of right nozzle

The algorithm implemented, at the end of each acquisition carried out in pre/post-flight, compares the features extracted with alarm bands obtained starting from oil temperature and pressure, until the *"DegradationCounter"* reaches the value three. In the case presented this counter reaches the maximum after 31 hours of flight, then the degradation is detected with a delay of 6 flight hours, equivalent to a clogging of right nozzle equal to 3%. The algorithm is actually able to identify the degradation soon as this occurs, since the amplitude of the first step is sufficient, however, the system based on the *"DegradationCounter"* obliges to wait for three consecutive alarms, so the degradation occurs after three flights, with the respective tests carried out in the pre / post flight.

The diagrams of figure 8.14 and figure 8.15 reporting the performance of features than the alarm band, the red vertical line represents the beginning of the degradation, while the green the time when the degradation is identified. All the features are influenced by the presence of the degradation, but the mean current is the health indicators that undergo the greatest variation in fact, the alarm is due from this feature. The other features are particularly no sensitive to the variation of the clogging of right nozzle, at least in the initial phase.

(a) Gain

(b) Phase

(c) Rise time

(d) Steady state error
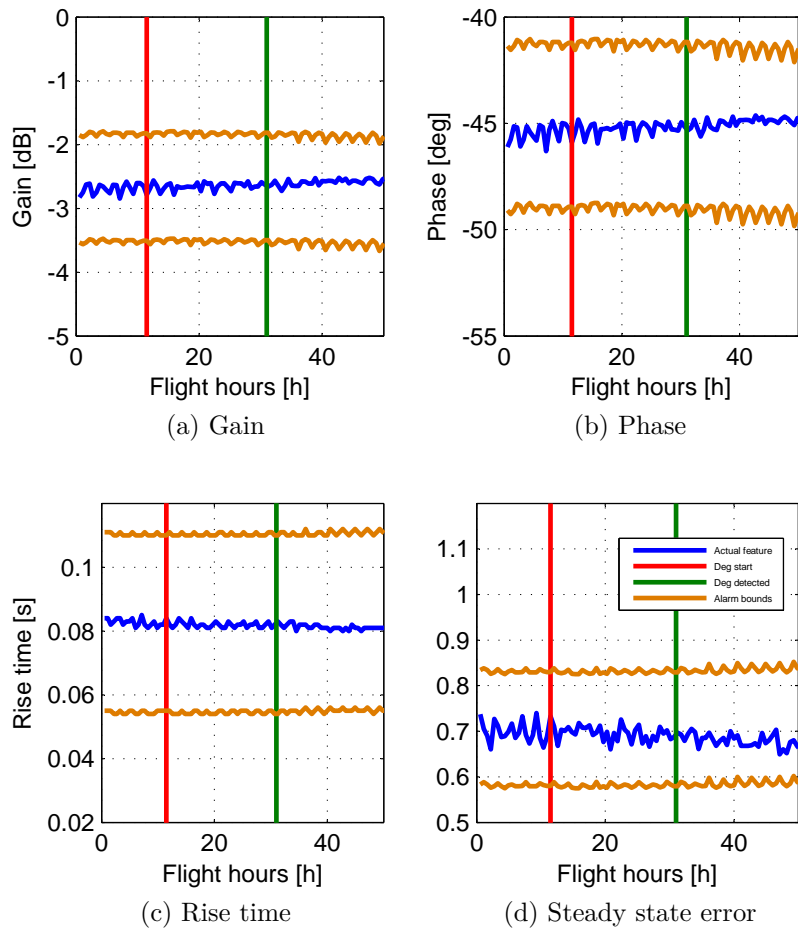
Figure 8.14: Position clogging of right nozzle

(a) Current max

(b) Current min

(c) Current mean

(d) Time decrease

(e) Current ramp
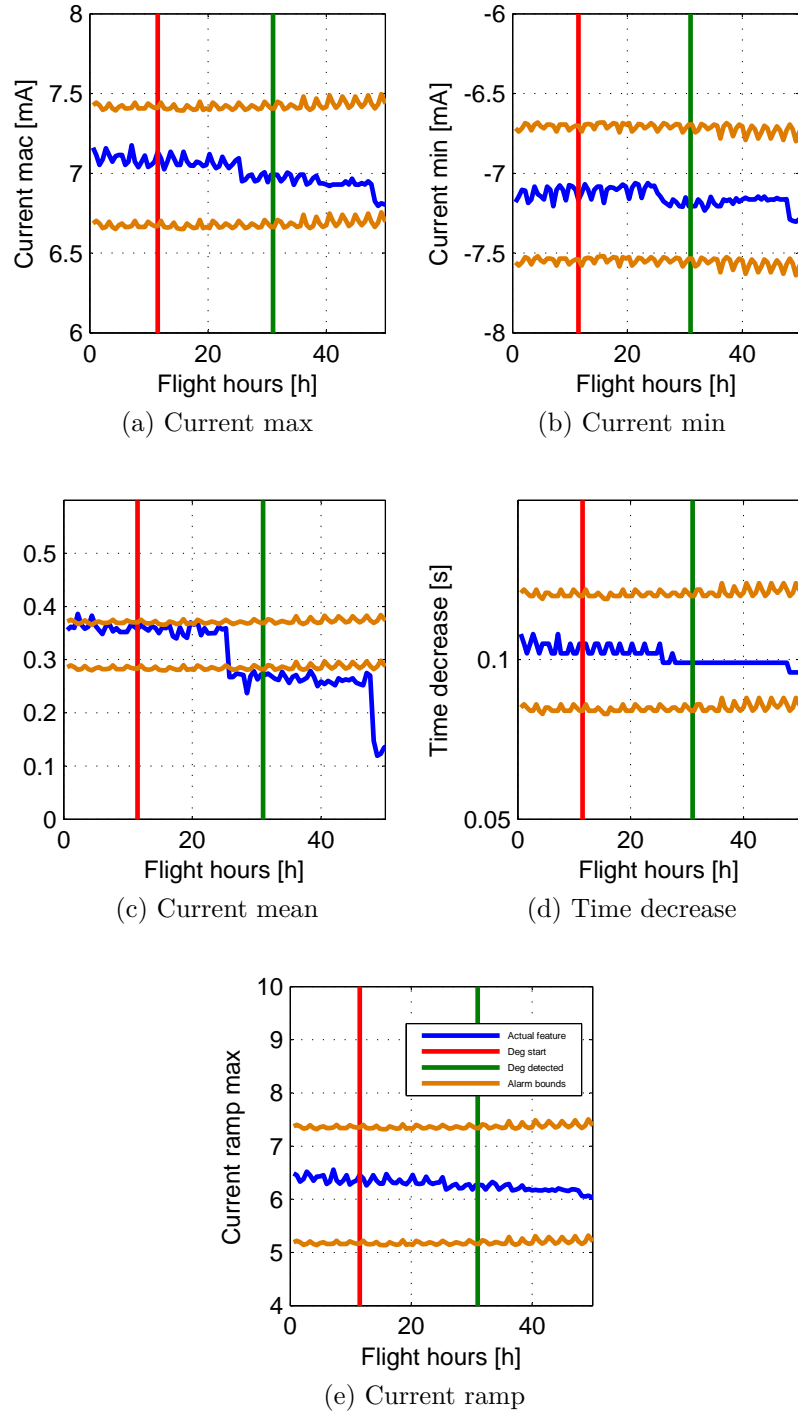
Figure 8.15: Current clogging of right nozzle

8.3.2 Summary

The approach based on alarm bands proves reliable and robust, the detection of failures is always whatever the degradation or degradations present; In addition operand with the current values, the detection of the degradation is not dependent on the fault propagation law.

The decision matrix for detection evaluation, reported in table 8.4, allows to fully appreciate the potential of the implemented algorithm. The subroutine correctly classified the situation in 89 cases: 85 degradation identified and 4 cases in which there was not degradation and warning was no given. The wrong classifications have been in total 4: a single false alarm, which is originated in a particular test, in which the servovalve is set with the worst manufacturing tolerances and in addition the environmental conditions were simulated particularly adverse. In 3 cases instead the algorithm was not able to recognize the presence of the degradation, which was in all cases an increase of the friction force between spool and the valve body, however, this weakness is not be attributed to the algorithm but decided about the features, which are not very sensitive to this type of fault.

Table 8.4: Decision matrix for detection evaluation for alarm bounds

Outcome	Fault (F_1)	No fault (F_0)	Total
Detected	a	b	$a + b$
(D_1)	85	1	86
Not detected	c	d	$c + d$
(D_0)	3	4	7
Total	$a + c$	$b + d$	$a + b + c + d$
	88	5	93

From the matrix the metrics for evaluate the algorithm have been extracted:

- **Probability of detection (POD):** 96.5%

- **Probability of a false alarm (POFA):** 20%

- **Accuracy:** 95.70%

The metrics show the goodness of the algorithm which has a higher accuracy level of 95%, as well as the probability of making a detection of the degradation. Only negative note is the probability of false alarms equal to

20%, however, this level is highly influenced by the low number of tests that have been carried out without degradation.

The degradation level required is relatively low for all the degradations, except for the increase of the friction force which when is identified requires an increase of the force in the order of twenty times the nominal value. Table 8.5 shows the average for each degradation level required to be identified, in the case of multiple degradations account was taken only of the predominant degradation.

Table 8.5: Degradation level required for alarm bounds

Degradation	Value
Reduction magnetomotive force	5.47%
Contamination of nozzles right	3.15%
Contamination of nozzles left	3.27%
Variation of the stiffness of the feedback spring	12.13%
Increase of the backlash	$12.57\mu m$
Increase of the radial gap	$7.99\ \mu m$
Variation of the friction force	$50.95 N$

8.4 Probability Density Function approach

The analysis of the variation of the features in time, using the probability density functions, is one approach that in recent periods are having the most success in technical literature (Hardman, Hess, and Sheaffer 1999, Hyers et al. 2006). The advantage of this approach is that it is very flexible and can also be easily coupled with techniques based on self learning,this allows to implement a non specific algorithm and subsequently through fitting and automatic optimization is possible specialize the algorithm on actual application.

The basis of this approach is the idea that the dispersion of the features in extracted different tests depending exclusively on the health of the system, consequently when the PDF move away from the reference value taken at nominal conditions the component observed is degraded. In reality, as highlighted in the chapter 7, the features are influenced in important way also by other parameters, for the precision pressure and oil temperature and the constructional tolerances.

However, the influence of the noises on the features value can be minimized by taking advantage of subroutines included in the algorithm of detec-

tion able to filter the features; in this case the actual values of the features are mainly depends on the health condition. Among the different possible ways to eliminate the influence of the operating conditions of the oil and of the manufacturing tolerances, the following were chosen:

- The supply pressure and the oil temperature are compensated by exploiting the set of polynomial equations presented in section 7.2.1. Starting from data on oil condition, acquired during each test, the influence of these two parameters could be eliminate in order to obtain the value of the features referred to normal condition.

- The manufacturing tolerances can not be eliminated by mathematical equations, as obtain numerical parameters easily traceable to these tolerances is not possible; therefore their compensation is implemented taking advantage of the natural inclination of PDF approach to self learning.

In the course of this discussion two different implemented to exploit the PDF approach are presented: the first builds the probability distribution curves of each features starting from the real data acquired in a floating window, while the second estimates the PDF from the last acquired value by exploiting the particle filter. The following are described in detail the two solutions implemented.

8.4.1 Detection with PDF from real-data

The first approach works implemented using only the features extracted from real data collected during each test. The detection of degradation is performed by comparing two probability density functions, one called *baseline* which is considered the reference PDF and remains constant throughout the operating life of the component, the second PDF, *actual* is instead updated at the end of each test, taking data from a moving window of 50 tests with overlap of 49.

The two probability density functions are not obtained directly from the analysis of the features, but the error percentage of the actual value and the nominal value of each features. The choice of the nominal value of each features does not affect the results of the algorithm, on condition to use the same both in the estimationof *baseline* and *actual* PDFs. In this way, the algorithm makes a comparison between two variable, features, to which was subtracted the same value, the nominal features.

The implemented algorithm, see scheme in figure 8.16 can be divided into three subroutines: the first composed of the blocks orange, brown and light

blue work at the end of each test until the detection subroutine is active. The second, composed only by the purple block, baseline PDF, operates only at the beginning of the useful life of the component and has the task of generating the reference PDF. The last generates the current PDF, blue block, and performs the comparison between the two curves, red block, in order to identify the degradation.
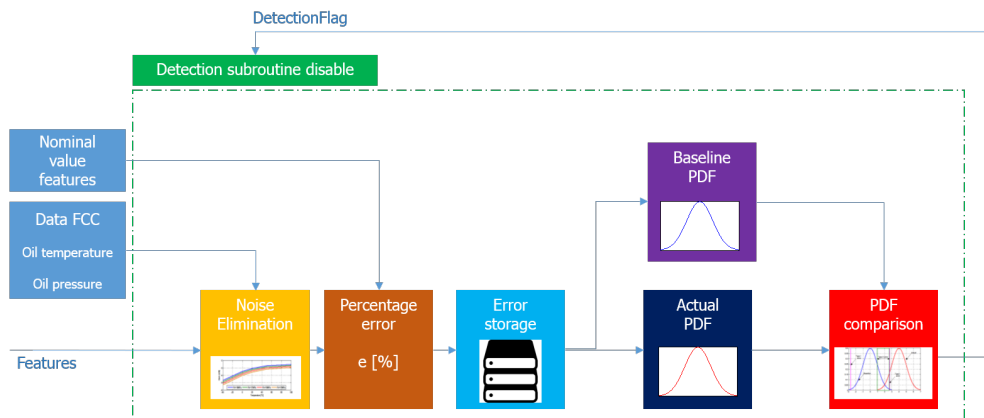
Figure 8.16: PDF with real data subroutine scheme

Following the operational life of the functionality of the algorithm component change, soon as the component the algorithm has only loaded is installed the nominal values of the features and the equations that allow to eliminate the influence of temperature and oil pressure; in these conditions the PHM function is not yet active. Subsequently, the algorithm requires a series of tests to calibrate its parameters, in this phase of tuning, following the flow chart, the features are cleared from the influence of the oil characteristics, then the percentage errors respect the nominal values are obtained.

The percentages for each error features are saved in a memory until fifty tests were not carried out; completed all tests, errors are used to define the relative PDFs called *Baselines*, these are recorded and maintained constant until the end of the useful life of the component or up to when they are not made of maintenance operations.

The definition of *baselines* using data obtained directly from the component allows you to eliminate the influence of manufacturing tolerances on features, because thanks to this feature of the self-learning, the design of operating limits are optimized directly for each component.

End the calibration phase, the PHM algorithm begins to function properly, at the end of each new test the errors percentage of every health indicator save on the memory are update: the oldest value is deleted and the new one

is integrated into the matrix. The update set of errors is use for estimate the new actual PDFs.

The comparison between *baseline* and *actual* PDFs takes place following the guidelines provided by the user and converted in the parameters:

- **False alarm rate:** defined as the probability of a false alarm. It is translate in type I error coefficient, set equal to 5%.

- **Confidence:** coincides with 100-Type II error and it expresses the level of confidence with which a degradation is detected. Type II error is set equal to 5%.

Type I error expresses the portion of the *baseline* which is discarded, in this case is only conserved part of the curve which represents 90% of probability. Type II error indicates the minimum overlap between the two PDFs in addition to which it is declared the presence of a degradation. Figure 8.17 shows how the identification is carried out.
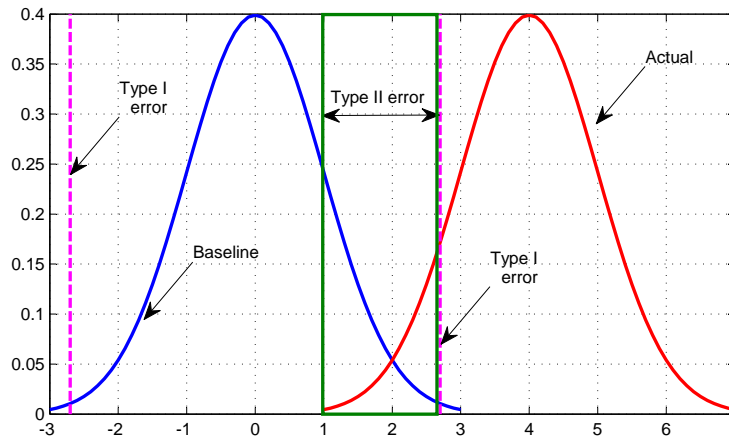
Figure 8.17: Detection with PDF from real-data

When the overlap of the *baseline* and the *actual*, for any of the features, is less than Type II error the detection algorithm recognizes the presence of a degradation and notifies the maintainer changing the value of *"Detection flag"* from 0 to 1, the Detection sub routine will be disable and the RUL sub routine will be enable.

8.4.2   Detection with PDF from particle filter

In the second PDF approach, the *actual* PDF are generated using the particle filter, while the *baseline* estimation uses only the features extracted from

real data collected during the tuning tests. The detection of degradation is performed by comparing two probability density functions; the *baseline* which is considered the reference PDF and remains constant throughout the operating life of the component, and the *actual* is instead updated at the end of each test.

The two probability density functions are not obtained directly from the analysis of the features, but the error percentage of the actual value and the nominal value of each features. The choice of the nominal value of each features does not affect the results of the algorithm, on condition to use the same both in the estimationof *baseline* and *actual* PDFs. In this way, the algorithm makes a comparison between two variable, features, to which was subtracted the same value, the nominal features.

The implemented algorithm, see scheme in figure 8.18 can be divided into three subroutines: the first composed of the blocks orange and brown runs at the end of each test until the detection subroutine is active. The second, composed light and purple block operates only at the beginning of the useful life of the component and has the task of generating the reference PDF. The last generates the current PDF, blue block, starting from the particle filter, yellow block, and at the end performs the comparison between the two curves, red block, in order to identify the degradation.
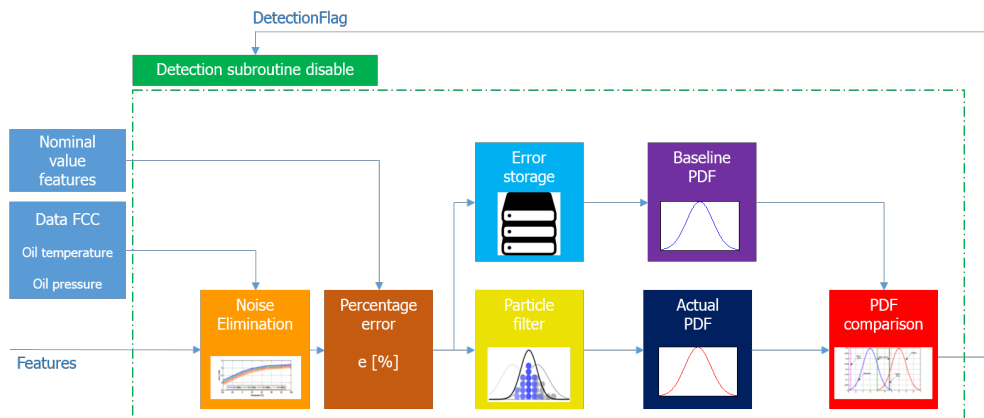
Figure 8.18: Alarm bound subroutine scheme

Following the operational life of the functionality of the algorithm component change, soon as the component the algorithm has only loaded is installed the nominal values of the features and the equations that allow to eliminate the influence of temperature and oil pressure; in these conditions the PHM function is not yet active. Subsequently, the algorithm requires a series of tests to calibrate its parameters, in this phase of tuning, following the flow

chart, the features are cleared from the influence of the oil characteristics, then the percentage errors respect the nominal values are obtained.

The percentages for each error features are saved in a memory until fifty tests were not carried out; completed all tests, errors are used to define the relative PDFs called *Baselines*, these are recorded and maintained constant until the end of the useful life of the component or up to when they are not made of maintenance operations.

The definition of *baselines* using data obtained directly from the component allows you to eliminate the influence of manufacturing tolerances on features, because thanks to this feature of the self-learning, the design of operating limits are optimized directly for each component.

End the calibration phase, the PHM algorithm begins to function properly, at the end of each test carried out in the pre/post flight phase the acquired data are analyzed in order to obtain the features, which are compared with the nominal values and calculate the percentage error. The PDFs in this approach are not extracted considering a sliding window of data but using the particle filter, which allows to estimate the distribution of each error starting from the last.

The particle filter used is a simplified version of the particulate filter, proposed by G. Vachtsevanos et al. 2006, which can be written generically as reported in 8.9, where $\mathbf{y}$ is a vector of a generic variable, and ω are non-Gaussian noises that characterize the process, t is the time index.

$$\mathbf{y}(t) = \mathbf{y}(t-1) + \Delta\mathbf{y} + \omega(t) \qquad (8.9)$$

In the specific case the equation 8.9 is adjusted as shown in equation 8.10; where $\mathbf{e}$ is the real percentage error obtained from the data acquired during the test, $\hat{\mathbf{e}}$ is the vector of estimate percentage error size $[nx1]$, $\mathbb{1}$ is the identity matrix size $[nx1]$ ω are non-Gaussian noises that characterize the process size $[nx1]$. n is the number of particle, t is the time index and i is the feature index equal 1 to 9. In order to obtain a good result n must be very large, in this algorithm was set equal to 5000, so the end of each iteration, the system provides nine error vectors, one for each features, each of 5000 elements.

$$\hat{\mathbf{e}}_i(t) = \hat{\mathbf{e}}_i(t-1) + (\mathbf{e}_i(t)\mathbb{1} - \hat{\mathbf{e}}_i(t-1)) + \omega(t) \qquad (8.10)$$

The transition between the calibration phase and the operational needs to define, for each features, the first vector of the estimate, in order to initialize the algorithm with the most possible close to reality values the $\hat{\mathbf{e}}_i(0)$ are extracted from the PDFs obtained in calibration. the variance and the aver-

age value of non-Gaussian noises are also extracted from the values obtained during the calibration phase.

The PDFs estimated through the particle filter are defined *actual*, and represent the punctual error between the nominal value and the acquired. The mean value of the *actual* curves depends on the servo valve, in so far as the temperature and oil pressure state of health are compensated by means of equations, while the manufacturing tolerances are influential as has been defined for the algorithm. Therefore in optimal conditions the two curves, *baseline* and *actual*, are virtually superposed, while the appearance of one or more degradations errors calculated at the end of each test run from those calculated during calibration.

The comparison between *baseline* and *actual* PDFs takes place following the guidelines provided by the user and converted in the parameters:

- **False alarm rate:** defined as the probability of a false alarm. It is translate in type I error coefficient, set equal to 5%.

- **Confidence:** coincides with 100-Type II error and it expresses the level of confidence with which a degradation is detected. Type II error is set equal to 5%.

Type I error expresses the portion of the *baseline* which is discarded, in this case is only conserved part of the curve which represents 90% of probability. Type II error indicates the minimum overlap between the two PDFs in addition to which it is declared the presence of a degradation.

When the overlap of the *baseline* and the *actual*, for any of the features, is less than Type II error the detection algorithm recognizes the presence of a degradation and notifies the maintainer changing the value of *"Detection flag"* from 0 to 1, the Detection sub routine will be disable and the RUL sub routine will be enable.

8.4.3   Result overview

Variation of the stiffness of the feedback spring (first order)

The reduction of the stiffness of the spring is described in this test as linear with the hours of flight by the equation 8.11, where Deg is the variation of the stiffness in percentage, FH is the actual flight hours, FH_0 is the time when the degradation occur and K_{stiff} is the linear coefficient.

$$Deg = K_{stiff} * (FH - FH_0) \tag{8.11}$$

The degradation begins to occur after 11.5 hours of flight, and increases linearly up to a value slightly less than 50%; in the figure 8.19 the trend of degradation is shown in blue and in red the instant of start.
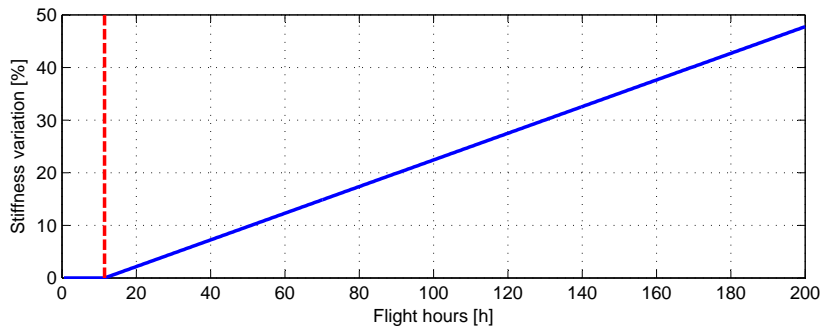
Figure 8.19: Variation of stiffness

Regardless approach used by the first step is the definition of the reference probability density curves, the *baselines*, these are generated, during the training process, starting from the acquired data in a window of 50 samples. The figures 8.20 and 8.21 show the *baseline* histograms, which are the PDFs of all nine features, , the red vertical line represents the 95% probability, which corresponds to 100 - false alarm rate.

(a) Gain

(b) Phase

(c) Rise time

(d) Steady state error
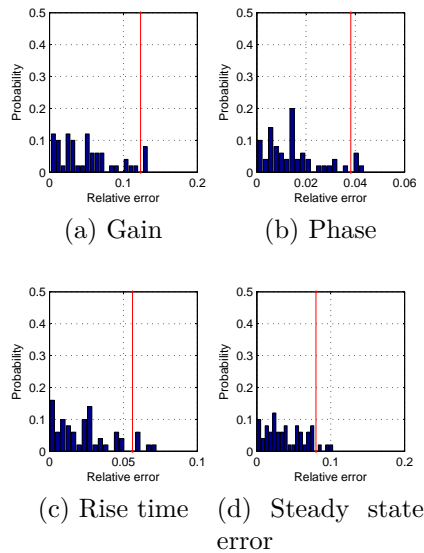
Figure 8.20: Position baseline PDF yield degradation

(a) Current max   (b) Current min

(c) Current mean (d) Time decrease

(e) Current ramp
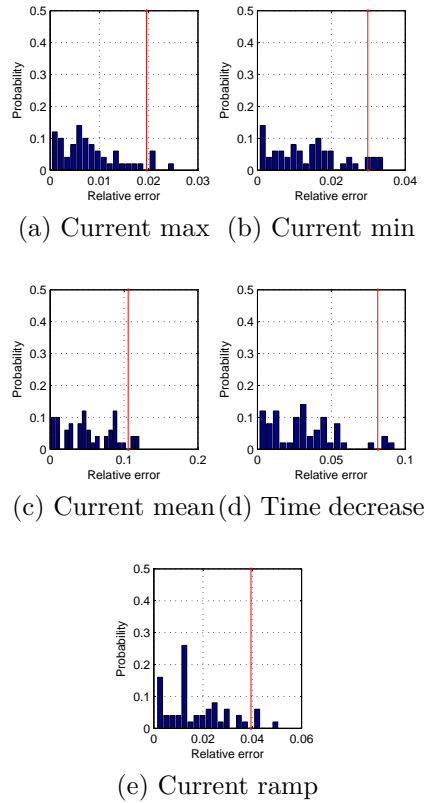
Figure 8.21: Current baseline PDF yield degradation

Detection with PDF from real-data   At the beginning of the acquisition campaign, after 8.5 hours the PDFs *actual* and *baseline* are practically superimposed since the degradation has not yet started; in the figure 8.22 are reported the PDFs relating to all the features, in blue the *baseline* and the *actual* in green, each graph shows the probability of the presence of a degradation for that specific feature, this value is calculated as 100 - the percentage of overlap between the two histograms.
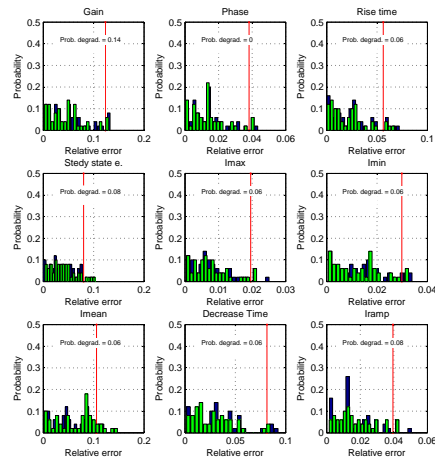
Figure 8.22: Actual and baseline PDFs comparison after 8.5 hours

When the degradation begins to grow its influence on PDFs is still limited, due to the filter effect caused by the floating window used to generate PDFs. In the figure it is shown 8.23 the actual histograms after 13 flight hours, which still show a good overlap with those of reference.
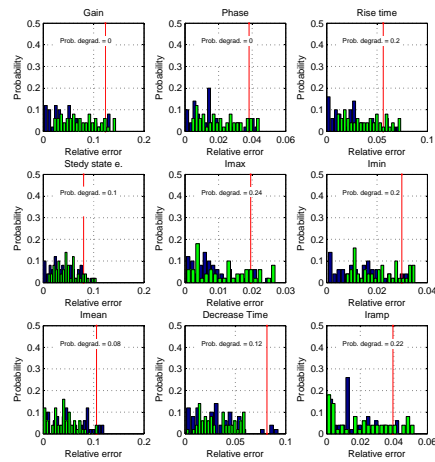
Figure 8.23: Actual and baseline PDFs comparison after 13 hours

The detection of degradation takes place after 34.5 hours of flight of flight with a degradation level equal to 7.32% , as is seen from the figure 8.24, the PDF related to current max and current ramp have a overlap less than the

required limit, which corresponds to a probability of the presence of a fault equal to 98% and 96%, respectively.

Figure 8.24: Actual and baseline PDFs comparison at detection time

Detection with PDF from particle filter The detection of degradation takes place after 28.57 hours of flight of flight with a degradation level equal to 5.45% , as is seen from the figure 8.25, the PDF related to current max, current min and current ramp have a overlap less than the required limit, which corresponds to a probability of the presence of a fault equal to 95% and 98% and 98%, respectively.

Figure 8.25: Actual and baseline PDFs comparison at detection time

Reduction of magnetomotive force and radial gap increase (second order)

The following test is characterized by the presence of two degradations that develop at different times on the servovalve, the first is reduction of magnetomotive force described as first order function of the hours of flight, the second is the increase of the radial gap described as fisrt order function, both equation are presented above (eq. 8.12), where Deg is the variation of the stiffness in percentage, FH is the actual flight hours, FH_0 is the time when the degradation occur and K is the linear coefficient, the subscripts FMM and GR indicate the reduction of magnetomotive force and the increase of radial gap.

$$Deg_{FMM} = K_{FMM} * (FH - FH_{0FMM})$$
$$Deg_{RG} = K_{RG} * (FH - FH_{0RG}) \tag{8.12}$$

The fist degradation occurs after 11.5 hours of flight, and increases up to a value slightly less than 50%, the second after 136.5 flight hours; in the figure 8.26 the trend of degradation is shown in blue and green and in red and orange the instant of start.

Detection with PDF from real-data The detection of degradation takes place after 27.9 hours of flight,of flight with a degradation level equal to 5.32% as is seen from the figure 8.27, the PDF related to current ramp and rise time
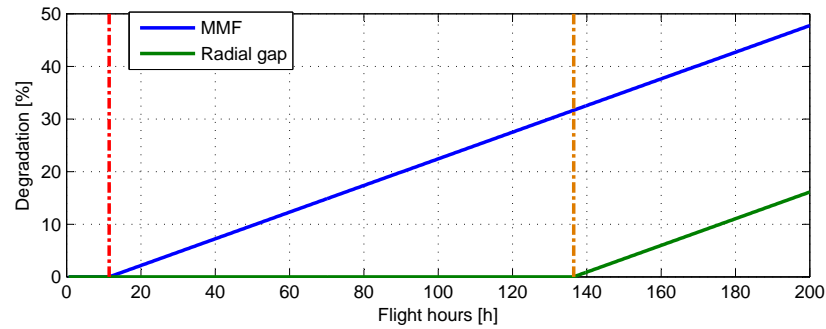
Figure 8.26: Variation of magnetomotive force and radial gap

have a overlap less than the required limit, which corresponds to a probability of the presence of a fault equal to 96%.
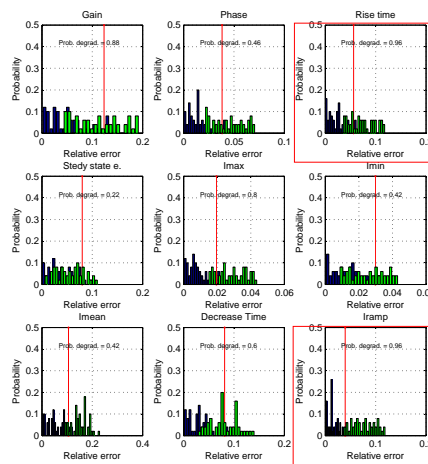
Figure 8.27: Actual and baseline PDFs comparison at detection time

Detection with PDF from particle filter   The detection of degradation takes place after 25.2 hours of flight,of flight with a degradation level equal to 3.98% as is seen from the figure 8.28, the PDF related to current max, current mean and current ramp have a overlap less than the required limit, which corresponds to a probability of the presence of a fault equal to 95%, 99% and 95%, respectively.
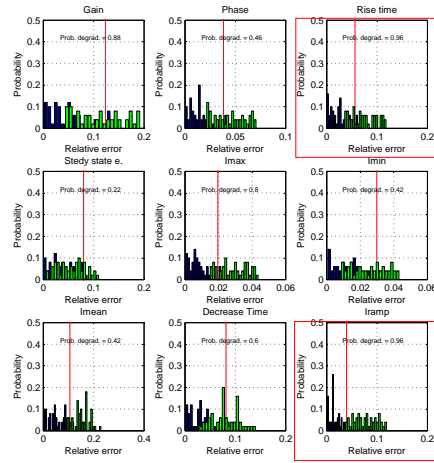
Figure 8.28: Actual and baseline PDFs comparison at detection time

Reduction of magnetomotive force (third order)

The reduction of magnetomotive force is described in this test as third order function of the hours of flight by the equation 8.13, where Deg is the variation of the stiffness in percentage, FH is the actual flight hours, FH_0 is the time when the degradation occur and K_{FMM} is the linear coefficient.

$$Deg = K_{FMM} * (FH - FH_0)^3 \qquad (8.13)$$

The degradation occurs after 13 hours of flight, and increases up to a value slightly less than 50%; in the figure 8.29 the trend of degradation is shown in blue and in red the instant of start.
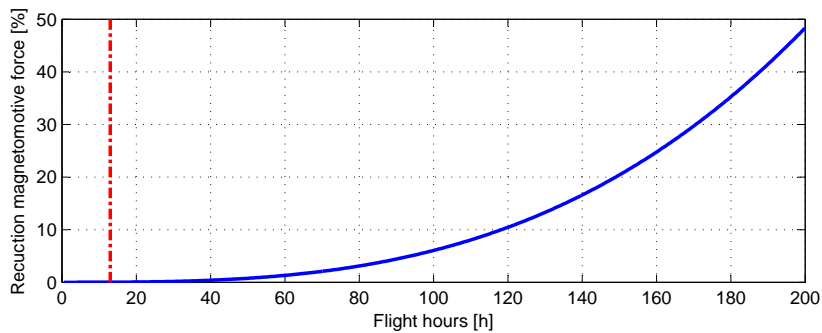

Figure 8.29: Variation of magnetomotive force

Detection with PDF from real-data The detection of degradation takes place after 72.2 hours of flight,of flight with a degradation level equal to 4.15% as is seen from the figure 8.30, the PDF related to rise time has a overlap less than the required limit, which corresponds to a probability of the presence of a fault equal to 95%.
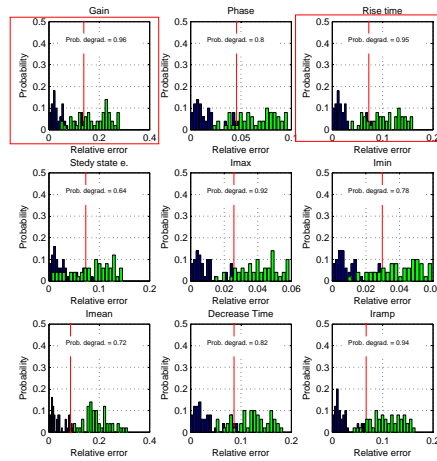
Figure 8.30: Actual and baseline PDFs comparison at detection time

Detection with PDF from particle filter The detection of degradation takes place after 68.3 hours of flight,of flight with a degradation level equal to 4.01% as is seen from the figure 8.31, the PDF related to rise time has a overlap less than the required limit, which corresponds to a probability of the presence of a fault equal to 97%.
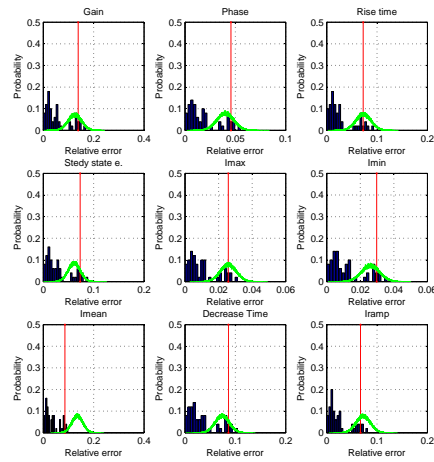
Figure 8.31: Actual and baseline PDFs comparison at detection time

Clogging of right nozzle (step)

The clogging of right nozzle is described in this test as third step function, where the amplitude of the steps and the presence of the same is decided randomly.

The degradation begins to occur after 25 hours of flight, and increases up to a value slightly less than 35%; in the figure 8.32 the trend of degradation is shown in blue and in red the instant of start.
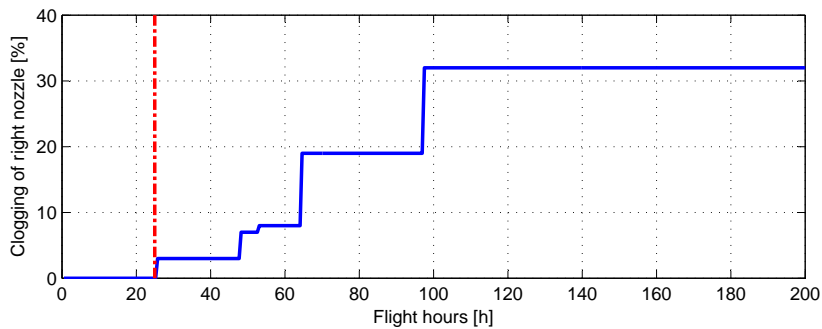
Figure 8.32: Variation of clogging of right nozzle

Detection with PDF from real-data The detection of degradation takes place after 39 hours of flight, the degradation is detected with a delay of 4 flight hours of flight,equivalent to a clogging of right nozzle equal to 3%.

From the figure 8.33, the PDF related to current mean has a overlap less than the required limit, which corresponds to a probability of the presence of a fault equal to 98%.
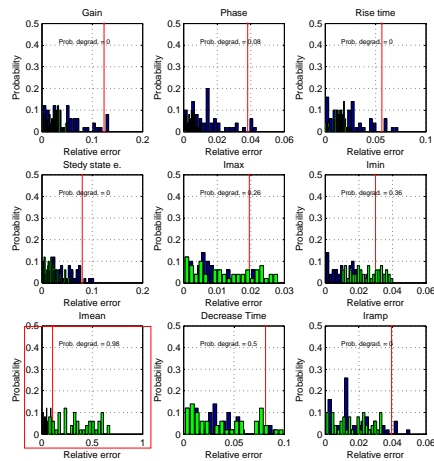
Figure 8.33: Actual and baseline PDFs comparison at detection time

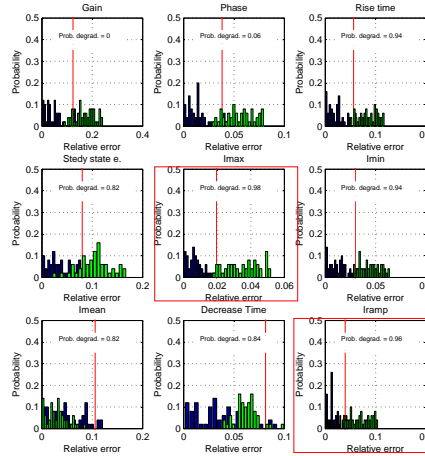**Detection with PDF from particle filter**   The detection of degradation takes place after 36 hours of flight, the degradation is detected with a single hours delay,thanks to the system for the estimation of the probability curves that introduces no filtering effect. equivalent to a clogging of right nozzle equal to 3%. From the figure 8.34, the PDF related to current mean has a overlap less than the required limit, which corresponds to a probability of the presence of a fault equal to 98%.
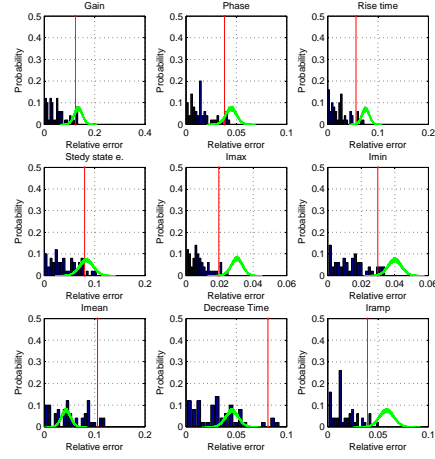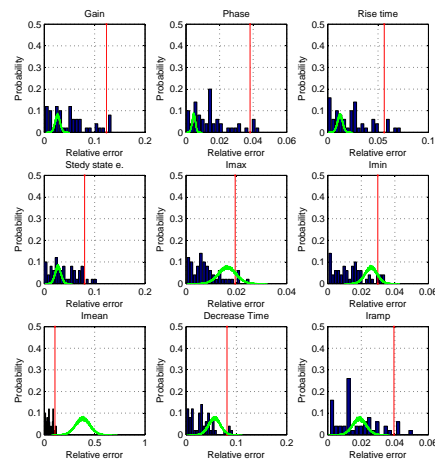
Figure 8.34: Actual and baseline PDFs comparison at detection time

8.4.4   Summary

The use of probability density function for identifying the presence of one or more degradations has shown several advantages, the most important of all is the possibility to calibrate the algorithm directly on board the aircraft, through simplified self learning techniques; this property greatly simplifies the implementation of the algorithm process and the choice of the servocommand operating limits.

The opportunity to adjust the parameters of code directly on the plane allows for the very performance algorithms without the need for large sets of historical data and / or extensive testing campaigns. Moreover calibrating the code of a specific component, strategies to eliminate or compensate for production tolerances are not required, because the system is able to tell whether an error of the features and their par value due to tolerances or to deterioration.

The main limitation of this approach is the period of non-operation of the PHM system during which the calibration is performed; during this time window the start of a degradation is not identified by the automatic detection system, with inevitable risks to the safety. However the calibration period is very short when compared to the normal life of a flight component, the ratio is in the order of 1 to 200. In addition all the flight components are subject to Acceptance Test Procedure (ATP) carried out in order to demonstrate that the new component is able to operate correctly and that does not present any kind of taste or degradation; then is possible assume that in the very

first stage of life of the component integrity is certified by the acceptance tests.

Both the adopted solutions have proven very quick to identify degradation, thus leaving a large interval to estimate the remaining useful life. The use of the particle filter allows to emphasize this feature, just as the onset of a minimum degradation to obtain an important displacement of the probability curves. This characteristic is closely related to the way in which the PDFs are generated, in the case of PDF obtained from real data a floating window with updates to a single sample is used, its use can be compared to a moving average, where the change of a single acquisition will not greatly affect the final value; therefore the beginning of a degradation several acquisitions must perform before that the *actual* start to diverge from the *baseline*. The estimate of the distribution by means instead particle filter is much faster, since at the end of each acquisition the average value of the PDF coincides with the last acquired value, thus a fast increase of the distancing between the two steepest PDF is obtained.

The decision matrix for detection evaluation, reported in table 8.6, shows as the PDF real-data approach, tested with the same 93 cases used to the approach based on alarm bands, generates a the same number of false alarm: 1 on 5 case without degradation. At the same time the algorithm was able to identified 87 degradation case in 88 possibility; also the increase of the friction in the spool are easy detected except for a single case.

Table 8.6: Decision matrix for detection evaluation for real-data PDF

Outcome	Fault (F_1)	No fault (F_0)	Total
Detected	a	b	$a + b$
(D_1)	87	1	88
Not detected	c	d	$c + d$
(D_0)	1	4	5
Total	$a + c$	$b + d$	$a + b + c + d$
	88	5	93

From the matrix the metrics for evaluate the algorithm have been extracted:

- **Probability of detection (POD):** 98.8%

- **Probability of a false alarm (POFA):** 20%

- **Accuracy:** 97.8%

The metrics show the goodness of the algorithm which has a higher accuracy level of 96%, as well as the probability of making a detection of the degradation. Only negative note is the probability of false alarms equal to 20%, however, this level is highly influenced by the low number of tests that have been carried out without degradation.

Similar results are obtained using the PDF estimate using the particle filter, the decision matrix for detection evaluation, reported in table 8.7, shows as approach generates a higher number of false alarms: 2 on 5 case without degradation, but the same number of correct detection: 87 degradation case in 88 possibility; also the increase of the friction in the spool are easy detected except for a single case.

Table 8.7: Decision matrix for detection evaluation for particle filter PDF

Outcome	Fault (F_1)	No fault (F_0)	Total
Detected	a	b	$a + b$
(D_1)	87	2	89
Not detected	c	d	$c + d$
(D_0)	1	3	4
Total	$a + c$	$b + d$	$a + b + c + d$
	88	5	93

From the matrix the metrics for evaluate the algorithm have been extracted:

- **Probability of detection (POD):** 98.8%

- **Probability of a false alarm (POFA):** 40%

- **Accuracy:** 96.7%

The metrics show the goodness of the algorithm which has a higher accuracy level of 96%, as well as the probability of making a detection of the degradation. Only negative note is the probability of false alarms equal to 40%, however, this level is highly influenced by the low number of tests that have been carried out without degradation, in addition obviously a higher identification rate results in a lower accuracy of the automatic diagnostic system:

The high sensitivity of the two approaches based on PDF allows detection of degradations to an almost embryonic stage, ensuring of the big advantages in terms of time available to estimate the remaining useful life and management of the operations necessary for the maintenance. Even a degradation

normally tricky to identify as the increase of the frictional force by means of this approach is detected as a result of a relatively low increase. The approach base on particle filter for the generation of the probability density function shows the slight advantages in terms of speed of identification, but which are not considered relevant. Table 8.8 and table 8.9 show the average for each degradation level required to be identified in case of real data and particle filter respectively, in the case of multiple degradations account was taken only of the predominant degradation.

Table 8.8: Degradation level required for real-data PDF

Degradation	Value
Reduction magnetomotive force	4.22%
Contamination of nozzles right	2.83%
Contamination of nozzles left	2.85%
Variation of the stiffness of the feedback spring	10.05%
Increase of the backlash	11.77μm
Increase of the radial gap	6.15 μm
Variation of the friction force	20.12 N

Table 8.9: Degradation level required for particle filter PDF

Degradation	Value
Reduction magnetomotive force	4.11%
Contamination of nozzles right	1.95%
Contamination of nozzles left	2.03%
Variation of the stiffness of the feedback spring	9.53%
Increase of the backlash	10.32μm
Increase of the radial gap	5.78 μm
Variation of the friction force	19.98N

8.5   Summary

The three approaches implemented for automatic detection of degradation have proved powerful and reliable, being able to identify the presence of one or more degradations in all the different operating conditions. In particular in order to properly handle the three algorithms developed, 93 simulations were performed by varying:

- Type of degradation

- Number of simultaneous degradations

- Degradation propagation law: linear, square or cubic function of time

- Oil temperature and pressure supply

- Environmental condition

In all cases the accuracy of the algorithms is higher than the 95%, 95.7% for the precision in the case of alarm bands, 97.8% for the PDF-based approach extracted from real data and 96.7% for the PDF combined with particle filter. Instead there are important differences as regards the probability of a false alarm (POFA) which stops at 20% for the first two techniques, whereas it reaches 40% for the last approach. Although as mentioned above this value is not totally significant home of the very low number of tests performed with no degradation, the numbers allow to have an idea of how the latter approach may prove you faster and more accurate in recognizing the degradation, but also more unstable and prone to providing false alarm.

The levels of degradation which allows a correct recognition of faults are small in all cases, but the approach based on alarm bands is decidedly inferior to the other two, which are equivalent. Low levels lead to faster detection that allow for ample time to estimate the remaining useful life and start the maintenance process.

The PDF-based approaches as well as guaranteeing better results, have the great potential to be self calibrating, thus reducing the number of experimental tests or historical data necessary for the optimization of the algorithms. The biggest advantage is connected to manufacturing tolerances, which can appreciably change the dynamic and static characteristics of the valve; taking advantage of the auto-calibration performed directly on each component, after it has been installed on the aircraft, the manufacturing tolerances are intrinsically compensated. The main disadvantage is represented by the time required for the calibration, during which the PHM system is not able to work, however, this problem is only minimally influential because the calibration time is significantly less than the operational life of a servo control and also all flight components are verified and validated by ATP tests.

In conclusion, the PDF-based system extracted from real data proved to be the best of the three, as it has significantly better performance than that enough of alarm bands, and proves to be more accurate and stable than the one that exploits the particle filter. the two PDF-based systems have very similar results in terms of degradation level required for the detection, but

the PDF obtained with real data have a probability of false alarm equal to half of the other. In the remainder of the research project it was therefore only used the algorithm that provides identification of the dead using the probability density function extracted from real data acquired during each test.

9

Fault classification

The classification of degradation is a process that is not part of the normal procedures required in a prognostic and health management system, because nowadays the maintenance mainly involves the replacement of degraded components and no longer the repair of the same. Despite the knowledge of how the component is degraded it can offer considerable advantages both to the maintenance level both for the design and development of new components.

In view of these considerations, a classification of degradation system was developed taking advantage, as each different degradation affects different features. The classification is obtained by combining neural networks and the principal component analysis, the first is used to classify the dominant degradation, while the second allows to identify and classify the presence of one or more additional degradations.

9.1 Classification technique

The analysis of how the features are influenced by degradations, presented in section 7.4, made possible to see how each fault causes in the health indicators of a unique combination system, analysis of the features becomes possible to identify the type of degradation in a certain way.

The results presented in the previous chapter (section 7.4) can be summarized in the figure 9.1, where the up arrow and the down arrow indicate that the features grow or decrease with the progress of the degradation, while

the horizontal double arrow indicates that the feature is not affected by the degradation.

Degradation	Features								
	Position						Current		
	Gain	Phase	Rise time	Steady state error	Max	Min	Mean	Decrease time	Ramp
Reduction magnetomotive force	↓	↓	↑	↑	↑	↓	↓	↑	↑
Contamination of right nozzles	↓	↓	↑	↑	↑	↑	↑	↑	↑
Increase of the radial gap	↓	↓	↑	↑	↑	↓	↓	↑	↑
Contamination of left nozzles	↑	↑	↔	↓	↓	↓	↓	↓	↓
Variation of the stiffness of the feedback spring	↑	↑	↓	↓	↓	↑	↑	↓	↓
Increase of the backlash between spool and feedback spring	↑	↑	↓	↓	↓	↑	↑	↓	↓
Increase of the friction	↑	↓	↔	↔	↑	↓	↔	↑	↑

Figure 9.1: Influence of degradations on features (summary)

In addition to the type of variation, increase or decrease, that degradation requires different features, another factor that allows to discriminate the agent fault is the ratio with which the health indicator vary.With this additional parameter is possible to discriminate those pairs of degradation that affect the same features as increase of the radial gap and Reduction magnetomotive force, increase of the backlash between spool and feedback spring and variation of the stiffness of the feedback spring.

The use of these technicians to classify the degradation is valid only if there is a fault dominant over all others, however if two or more degradations occur on the component simultaneously with the same intensity, recourse to PCA combined with neural networks becomes necessary. In this second case the algorithm involves first analysis of the data using a neural network that aimed to identify a degradation of the agents, then the features are analyzed with the analysis of the main components in order to reduce from nine to two variables. The new dummy variables, are analyzed with a further neural network to identify the successive faults.

The start of the classification procedure takes place only after the automatic diagnostics has detected the presence of a degradation, and does not stop until the end of the useful life remain, this allows to continuously monitor the status of the servo valve in order to identify any changes. The technical classifications are only valid until the impact degradations are modest, in proximity of the end of the useful life of the component the effect of different degradations on features tend to become similar because the servovalve behaves are completely degraded.

9.2 Classification of the first degradation

The classification of the first degradation, or the one most influential in case they are present in a number greater than one, is done through the use of a multilayer neural network. A neural network is typically defined by three types of parameters (Hagan et al. 1996):

- The interconnection pattern between the different layers of neurons

- The activation function that converts a neuron's weighted input to its output activation

- The learning process for updating the weights of the interconnections

The classical structure of neural networks provides a layer division, two levels are always present, the input and the output and according to need one or more intermediate levels, called hiden layers, can be added, as shown in figure 9.2.
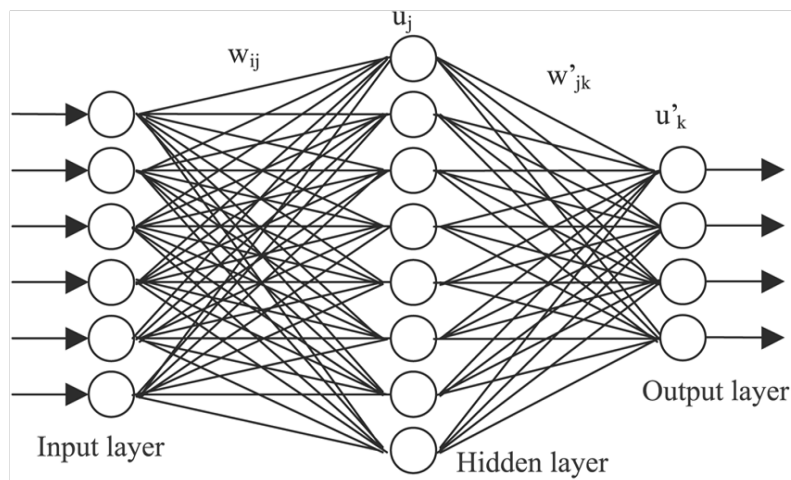
Figure 9.2: Neural Network example

Each neuron has a number of inputs and one output, and is connected with all neurons of the subsequent layer (figures 9.3);the connections have numeric weights that can be tuned based on experience, making neural nets adaptive to inputs and capable of learning. Mathematically, a neuron is defined as single function $f(\mathbf{x})$ that starting from the inputs generates a single output. The function implemented in the neuron can be as generic as possible, a widely used type of composition is the nonlinear weighted sum presented in equation 9.1, where φ, commonly referred to as the activation

function (Jeanette 1994), is some predefined function, such as the hyperbolic tangent, $\mathbf{x}$ is the vector of the input, ω is the input weight, and i is the index of the input.

$$f(\mathbf{x}) = \varphi(\sum_i \omega_i x_i) \tag{9.1}$$
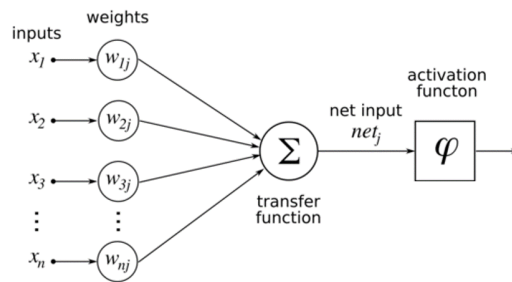
Figure 9.3: Neural Network neuron example

The implemented neural network for the classification of the first degradation is specially designed to make the data cluster (Anthony and Bartlett 2009), it has three layers: the input has nine neurons, one for each features, the output level has seven of them, as the number of possible degradation, while the hidden layer presents fourteen neurons, the hidden layer has been introduced in order to refine the classification process. Within individual neurons two different activation functions have been use, the neurons of the input and hidden layers using a trigger function, while those of the output layer a hyperbolic tangent. The scheme of the algoritm use for the classification of the first degradation is shown in figure 9.4.
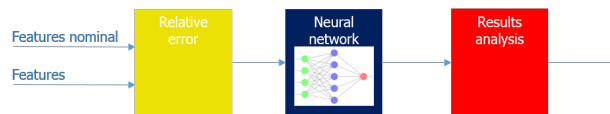
Figure 9.4: Classification algorithm scheme

The inputs of the neural network must be a real number include in the interval -1 to 1, therefore in order to make the features compatible with the algorithm request these are used to calculate the relative error respect the nominal value with the equation 9.2, where feN is the nominal value of the feature, fe in the actual value of the feature, i is the index of the features; the value obtained is saturated to the extreme values -1 and 1. Therefore an

error value equal to 1 indicates that the features had a variation of 100%, -1 a variation of 100%.

$$e_i = \frac{feN_i - fe_i}{feN_i} \qquad (9.2)$$

The input of the neural network then become errors related, while the output is a vector of seven elements between 0 and 1, the element of the vector that has a greater value indicates the present degradation. If there were two elements that have the same value the degradation can not be correctly classify, so the algorithm will provide an error message and the classification will be retried after the next test.

The training procedure of the neural network was performed using the large database of tests: eighty-eight different tests were carried out, including single or multiple degradation, each trial has an average of 250 vectors of features extracted from the data acquired in as many carried out in pre / post test flight. The vector of relative error relating to tests with degradations not yet active and those who have at least five errors saturated were excluded from the training process, the number of sets of data actually available is therefore of 12000, these were divided in random manner in the two groups : 5000 were used for the training procedure of the neural network, while the remaining were stored for subsequent checks. The 5000 data sets were further divided into:

- **Training:** 2500 sets of data

- **Validation:** 1500 sets of data

- **Testing:** 1000 sets of data

The training procedure is carried out take advantage from the Bayesian regularization backpropagation a function that updates the weight and bias values according to Levenberg-Marquardt optimization. It minimizes a combination of squared errors and weights, and then determines the correct combination so as to produce a network that generalizes well (Foresee and Hagan 1997). Bayesian regularization backpropagation uses the Jacobian for calculations, which assumes that performance is a mean or sum of squared errors. Therefore networks trained with this function must use either the mean squared error or the sum squared error performance function; in this project the sun squared error are used. Levenberg-Marquardt is one of the fastest algorithm, it was designed to approach second-order training speed without having to compute the Hessian matrix.

Concluded the process of training the neural network was tested using the renaming 7000 data sets are used for test the neural network with real case. The classification results obtained are very encouraging, the best results are obtained when the neural network are supplied with the values of relative errors extracts from tests in which there is only one degradation, the confusion matrix presented in figure 9.5 shows an average classification error of 1%. Some kind of degradations as friction increase and variation of the radial clearance have an error double respect the mean value, but as mentioned in previous chapters, the selected health indicators are not very sensitive to such faults and also they have a limited impact on the overall behavior of EHSA.

	Target Class						
Output class	**Reduction MMF**	**Yield Spring**	**Backlash**	**Nozzle left**	**Nozzle right**	**Radial gap**	**Friction**
Reduction MMF	776					14	4
Yield Spring	1	847	5				2
Backlash		3	653	2			
Nozzle left			2	588			
Nozzle right					586		
Radial gap	3				4	616	3
Friction							391
	99.5% 0.5%	99.7% 0.3%	99.0% 1.0%	99.6% 0.4%	99.4% 0.6%	97.9% 2.1%	97.8% 2.2%
Total				99.0% 1.0%			

Figure 9.5: Confusion matrix for single degradation

Worst results are obtained if instead of multiple degradations, the implemented system should be able to classify the most influential degradation, but this happens on average only 87% of cases, as show in figure 9.6. The greatest number of errors is mainly linked to the difficulty of the neural network to understand which degradation is more important, especially in the presence of faults that have a very similar impact on the behavior of the servosystem, also when two or more degradations act simultaneously on the EHSA individual effects introduced on the features from any faults are added together, thereby generating a superimposition of the effects. Therefore, the indications presented in the figure 9.1 are valid only if either one degradation has a much greater effect or the two degradations have similar effects on health indicators.

Friction increase and variation of the radial clearance are still the degradations more difficult to identify, the presence of other degradations further complicates the possibility of obtaining a correct result since their small in-

	Target Class						
Output class	**Reduction MMF**	**Yield Spring**	**Backlash**	**Nozzle left**	**Nozzle right**	**Radial gap**	**Friction**
Reduction MMF	392	4	5	1	4	53	11
Yield Spring	2	436	10		16	6	24
Backlash		5	270	19	6	7	
Nozzle left	4	2		437		3	
Nozzle right		3	7	7	446		
Radial gap	2		7	6	6	197	6
Friction				1	2	4	80
Total	98.0% 2.0%	97.0% 3.0%	90.0% 10.0%	91.0% 9.0%	93.0% 7.0%	73.0% 27.0%	67.0% 33.0%
				87.0% 13.0%			

Figure 9.6: Confusion matrix for predominated fault in multiple degradations

fluence on the features is easily covered by other faults, which, although still at the initial stage cause major changes to the servovalve behavior.

The high level of uncertainty when the algorithm has to classify the predominant degradation due to cascading problems to the next step, where further degradations present are classified. Clearly a mistake in the first classification generates an unfavorable starting position for the next algorithm, which will have to classify further degradations without knowing what is the predominant degradation. Unfortunately, the neural network can not make an inspection to see if the result is to consider true or not, because the true degradation is unknown during normal operation of the PHM, so the algorithm can not be interrupted in case of incorrect output, but will continue to work through the next step.

9.3 Classification of additional degradations

The idea at the base of the code used for the identification of further degradation is to observe how after the start of the first fault the features evolve over time. The algorithm, whose scheme is shown in the figure 9.7, made the analysis of the features by means of the Principal Component Analysis (PCA), followed by the transformation of the main components in Bartlett factors; these values become the input of a neural network, whose job is to classify new degradations as these are revealed.

The influence of degradation on features, and consequently on errors between features and nominal features can be observed in a timely manner even by observing the arrangement of the points in the vector space expressed by the vector of errors, the challenge of this technique is that the vector space
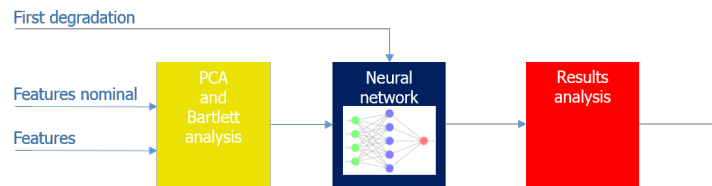
Figure 9.7: Classification of additional faults algorithm scheme

defined by the features has nine dimension, therefore its representation and understanding is difficult.

In order to reduce the size of the vector space it is possible to resort to the principal component analysis, is a statistical procedure that uses an orthogonal transformation to convert a set of observations of possibly correlated variables into a set of values of linearly uncorrelated variables called principal components. The number of principal components is equal or less respect the original set of variable (Jolliffe 2002). In the transformation between main variables features the physical meaning of each variable is lost in favor of a reduction of the variables needed to represent the system.

This transformation is defined in such a way that the first principal component has the largest possible variance and each succeeding component in turn has the highest variance possible under the constraint that it is orthogonal to the preceding components. Therefore, the use of the first two or three principal components is sufficient to express more than 95% of the variance expressed from the original data.

The analysis of data sets obtained in the case of single degradations allowed to identify the minimum number of principal components to obtain a variance higher than the 98%, in the table 9.1 are reported for each degradation variance expressed by the main components.

The data in the table above show that only two principal components are sufficient to obtain a representation of the variance of sufficiently accurate; this allows to reduce the vector space of dimension dimension 9 to 2, thus allowing a more immediate representation of the data.

Analyzing the new variables, the principal components, by applying the Bartlett's approach the factor, o score, are obtained. Bartlett factor scores are computed by multiplying the row vector of observed variables, by the inverse of the diagonal matrix of variances of the unique factor scores, and the factor pattern matrix of loadings (DiStefano, Zhu, and Mindrila 2009). Resulting values are then multiplied by the inverse of the matrix product of the matrices of factor loadings and the inverse of the diagonal matrix of variances of the unique factor scores (equation 9.3).

Table 9.1: Features extracted

P.C.	MMF	Yield spring	Back lasch	Nozzle left	Nozzle right	Radial gap	Friction
I	0.9986	0.9996	0.9989	0.8319	0.9242	0.9997	0.9707
II	0.0011	0.0004	0.0008	0.1676	0.0724	0.0002	0.0178
III	0.0003	0.0000	0.0002	0.0004	0.0032	0.0001	0.0062
IV	0.0000	0.0000	0.0001	0.0001	0.0002	0.0000	0.0020
V	0.0000	0.0000	0.0001	0.0000	0.0000	0.0000	0.0019
VI	0.0000	0.0000	0.0000	0.0000	0.0000	0.0000	0.0012
VII	0.0000	0.0000	0.0000	0.0000	0.0000	0.0000	0.0001
VIII	0.0000	0.0000	0.0000	0.0000	0.0000	0.0000	0.0000
IX	0.0000	0.0000	0.0000	0.0000	0.0000	0.0000	0.0000

$$\hat{\mathbf{F}}_{1xm} = \mathbf{Z}_{1xn}\mathbf{U}_{nxn}^{-2}\mathbf{A}_{nxm}(\mathbf{A}'_{mxn}\mathbf{U}_{nxn}^{-2}\mathbf{A}_{nxm})^{-1} \qquad (9.3)$$

Where $\hat{\mathbf{F}}$ is the row vector of m estimate factor score, $\mathbf{Z}$ is the vector of standardized observed variables, $\mathbf{A}$ is pattern matrices of loadings of n observed variables on m factors or components and $\mathbf{U}^{-2}$ is the inverse of a diagonal matrix of the variances of the n unique factor scores.

One advantage of Bartlett factor scores over the other two refined methods presented here is that this procedure produces unbiased estimates of the true factor scores (Hershberger 2005). This is because Bartlett scores are produced by using maximum likelihood estimates a statistical procedure which produces estimates that are the most likely to represent the factor scores.

An analysis of the factors Bartlett demonstrates how the position of these in the two dimensions vector space depends strictly on the type of degradations present on servovalve, furthermore the factors of the position is always the same purposes when a new degradation does not start. As an example, the figure 9.8 shows the case of the degradation of the magnetomotive force reduction, the data relating to the presence of a single degradation (in green) are collected in the same all around, while when a second degradation is revealed the factors move in the plane until it reaches a new configuration where they remain concentrated until the birth of a subsequent degradation.

The transition from one group to another does not happen instantaneously at the beginning of the new degradation, but it takes place in time. The paths made by the greasy described by Bartlett factors are well recognizable on the diagram of figure 9.8, there is a first phase in which the new points are mixed with those relating to the case of single degradation, then
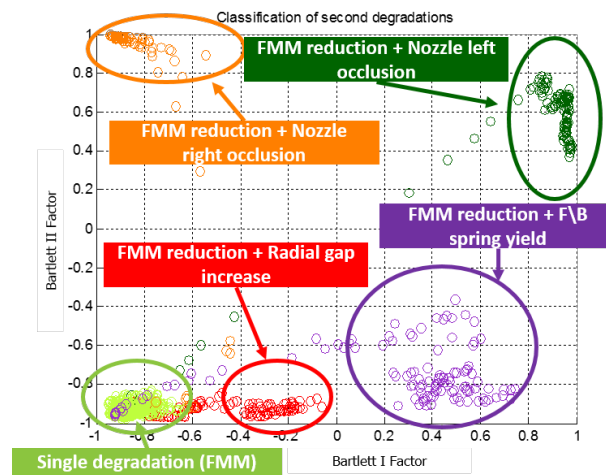
Figure 9.8: Bartlett factor clustering

a transition path, and finally the new cluster.

The identification process is done by a neural network with three layers, the first has nine neurons, the second fourteen and eight the output layer one for each type of possible degradation while the latter indicates that there are no additional degradations; in neurons two different activation functions have been use, the neurons of the input and hidden layers using a trigger function, while those of the output layer a hyperbolic tangent. The training procedure is carried out take advantage from the Bayesian regularization backpropagation.

The inputs of the neural network are the two Bartlett' factors and the output of the first degradation neural network and must be included in the range [-1 1], but in this case: the factors are by definition included in that range and the output of the previous neural network is comprised between 0 and 1.

The training procedure of the neural network was performed using the large database of tests: thirty different tests were carried out with multiple degradation, each trial has an average of 250 vectors of features extracted from the data acquired in as many carried out in pre / post test flight. The vector of relative error relating to tests with degradations not yet active and those who have at least five errors saturated were excluded from the training process, the number of sets of data actually available is therefore of 4500, these were divided in random manner in the two groups : 1500 were used for the training procedure of the neural network, while the remaining were stored for subsequent checks. The 1500 data sets were further divided into:

- **Training:** 700 sets of data

- **Validation:** 600 sets of data

- **Testing:** 200 sets of data

At the end of the training process of the neural network it was used to classify the remaining 3000 data sets, obtaining results not too encouraging at least for certain types of degradations, the mean accuracy is lower than 80%. The new degradations that have a minor influence on the servovalve are no correctly classified in the majority of cases, since their effect is negligible compared to earlier degradation: friction increase, increase of backlasch and variation of the radial clearance are classified correctly only in 72%, 60% and 40% of the cases, respectively.

Target Class

Output class	Reduction MMF	Yield Spring	Backlash	Nozzle left	Nozzle right	Radial gap	Friction
Reduction MMF	432		30		25	10	5
Yield Spring	6	436	35	20		20	2
Backlash			270		15		14
Nozzle left	5	6	15	418		15	10
Nozzle right	7	4	18		405	10	8
Radial gap			4	12	5	360	131
Friction							180
No degradation			10			35	100
	96.0%	97.0%	72.0%	93.0%	90.0%	60.0%	45.0%
	4.0%	3.0%	28.0%	7.0%	10.0%	40.0%	55.0%
Total			75.5%				
			21.5%				

Figure 9.9: Confusion matrix for additional degradations

The overall result of correct identifications is strongly negative influenced by the three degradations previously mentioned , in the case of the other four the results are really interesting, in fact they have a maximum classification error of 10%. Their strong influence on the behavior of the actuator allows to speed up and better the grouping process of Bartlett factors, the groups are better separated and the transition process tends to end up in a shorter time; these factors allow to have clusters more easily separable by the neural network, which is less likely to make errors of classification.

9.4 Summary

The classification degradations agents on the servo valve is not considered nor in the academic field nor in the industrial field a priority for a prognostic

system, in that the servovalve is generally classified as a closed component, therefore in phase of maintenance is not adjusted but is totally changed. In any case, the information that can be obtained from the classification can be very useful in the phase of new valve design, or to understand and correct any defects in the production servovalves.

The procedure followed in the course of the thesis not always proved effective, but certainly provides a solid base for further development, the idea of reducing the number of variables by analysis of main components and to transform the dummy variables thus obtained in Bartlett factors is definitely an effective choice, as well as the idea of using neural networks to perform the classification. The latter due to their characteristic of self-learning, and the ease of calibration, is excellent allies have proved, as it does not require large data set and expensive manual tuning processes.

What has been implemented should be revised and corrected after a thorough study of how different degradations work together, study that can only be conducted through experimental test benches or field trials, large series of data acquired during normal operation of the aircraft may certainly provide support in future developments.

In the case of single or degradation of a predominant degradation the implemented algorithm proves very robust and able to make the correct classification with high accuracy, especially for what concerns the most invasive faults. Also working on the data vector acquired from time to time, the operation of the neural network is not influenced by the propagation law of degradation.

Opposite goes for what concerns the second part of the algorithm, which is concerned with identifying the additional degradation, although this with the previous year is not affected by the trend in the degradation, it has an accuracy very low, especially when it has to classify little influence degradations as friction increase, increase of backlasch and variation of the radial clearance. In this case the implementation of a system that can amplify the effect of these degradations, or the use of new features, could effectively solve the problem, thus ensuring a complete and functional classification algorithm.

10

Residual useful life estimation

Estimation of the Residual Useful Life (RUL), or prognosis, is the ability to predict accurately and precisely the failing time of component or subsystem. It is the biggest challenge of the condition-based maintenance/prognostic health management (CBM/PHM) because it entails large-grain uncertainty. Long-term prediction of the fault evolution to the point that may result in a failure requires means to represent and manage the inherent uncertainty; uncertainty representation implies the ability to model various forms of uncertainty stemming from a variety of sources, whereas uncertainty management concerns itself with the methodologies and tools needed to continuously optimize the uncertainty bounds as more data become available.

Accurate and precise prognosis demands good probabilistic models of the fault growth and statistically sufficient samples of failure data to assist in training, validating, and fine-tuning prognostic algorithms. Prognosis performance metrics, robust algorithms, and test platforms that may provide needed data have been the target of CBM/PHM researchers in the recent past.

Unfortunately in the development of this project accurate models of degradations or large number of historical data were not available, so the strategy involves the use of a system able to calibrate itself automatically. This approach even allows to decouple the algorithm from the request of prior knowledge, calibration requires a relatively long period of during which the prediction of the RUL is not available. During the implementation of the algorithm is therefore necessary to find the correct compromise between length of time we calibration and accuracy of the estimate, the longer the

199

better training period is the accuracy that can be achieved, but at the same time to increase the window time of system inactivity.

This chapter is analyzed the procedure implemented to estimate the remaining useful life, highlighting the steps and the merits and defects of each. The results will then be evaluated by means of appropriate metrics.

10.1   RUL estimation technique

The estimate of the remaining useful life requires four consecutive steps (Figure 10.1): extraction of relative absolute error, models identification, prediction ane RUL estimation. Since these processes require a very high number of computational resources, the reduction of the number of observed features has been decided. This consideration may seem daring and risky, but the ultimate objective of all EHSAs is to make a correct positioning of a wing area respecting the dynamic and static requirements. Therefore the features most important and connected with the safety and the use of the aircraft are those of position and not those of the current; the latter are an excellent indicator of the health of the system state, because when a component is degraded, the controller in order to ensure the same performance generally increases the valve control current. In order to ensure the operability of the aircraft it is not important if the control current is higher than normal, but it is essential to know that the wing area is moving properly, therefore it was decided to focus only on position features.

In the first step the features obtained from the analysis of acquired data during testing are compared with the nominal value in order to obtain the relative absolute error. Subsequently these values are entered into a historical data set which stores the results of the last 60 tests.

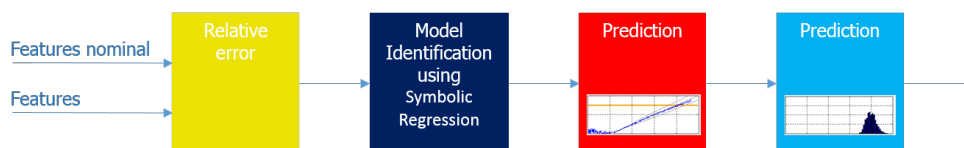Figure 10.1: Estimation RUL algorithm scheme

The stored values of the four features are then processed through symbolic regression thus obtaining four mathematical models, which must represent faithfully as the features of value evolves over time. Accurate models is the essential first step to ensure that the next prediction and so the estimate of the remaining useful life are sufficiently accurate.

The prediction of the evolution of the position of features is implemented by taking advantage of the particle filter, which is a particularly flexible instrument and able to work even in the presence of non-Gaussian noise. The first estimate of the remaining useful life is performed on average 10 tests carried out in the pre / post-flight, and because of the other computational cost is not updated after each new test, but after 5 events.

10.2 Degradation model fitting

The identification of mathematical models that better approximates the trend of the four features is one of the crucial points of the estimated useful life of stay, normally this operation is carried out or working with mathematical models validated by experimental evidence or historical data. In the project presented neither roads were passable, it was decided to use a system that obtains the models from the data that is captured during normal operations.

In order to obtain the best mathematical models a modeling framework called Symbolic Regression was exploited. Symbolic Regression searches the space of mathematical expressions to find the model that best fits a given data-set, both in terms of accuracy and simplicity (Zelinka 2004) and no particular model is provided as a starting point to the algorithm. Instead, initial expressions are formed by randomly combining mathematical building blocks such as mathematical operators, analytic functions, constants, and state variables; usually, a subset of these primitives will be specified by the operator, but that is not a requirement of the technique. New equations are then formed by combining previous ones, using genetic programming (McKay, Willis, and Barton 1995 and Hoai et al. 2002). In linear regression, the dependent variable is a linear combination of the parameters, but need not be linear in the independent variables.

The problem of the Symbolic Regression is the generation of models with a very high degree of complexity, which require a large computing power to be solved. In this case of studies, however, the thesis has been done trying to contain the computing power, therefore the model chosen is the one with lower degree, which provides an absolute error less than $1 \cdot 10^{-3}$. In this way, the model accuracy is sufficiently high and at the same time the computational load is minimal.

The data obtained from the acquisitions carried out during normal operations are particularly disturbed because the features are dependent on the operating characteristics of the oil and the acting loads. Although these disorders are compensated, carriers of absolute relative errors are filtered by

means of a mobile filter with a 5 sample window.

The theory and practice shows that in order to obtain a good model it is necessary to use a set of experimental values as wide as possible, in order to get more samples with which to compare the result. But this badly constraint is coupled with the need for speed required by the estimated useful life remain. The problem has been addressed by observing how the automatic diagnostic system implemented due to a delay between the time at which the degradation begins and the time at which this is detected. This delay is attributable in part to the same degradation, which affects the features very few until it is still little, especially the position indicator; other cause of the delay is the methodology implemented for obtaining the PDF, this uses a floating window with updates to a single sample, therefore, the PDF is not immediately affected by the growth of degradation.

This delay, however, allows to use the latest data of the floating window, those used for the latest PDF, to estimate the mathematical model of growth. Referring to figure 10.2, the interval between the start of degradation and the detection thereof are well evident, the last window of data used to obtain the PDF is the one between the first yellow line and the line which represents the instant of detection, this window is 50 samples. in order to increase the number of available data for the estimate of the growth model in this window ten additional samples were added, thus obtaining a series of 60 data.
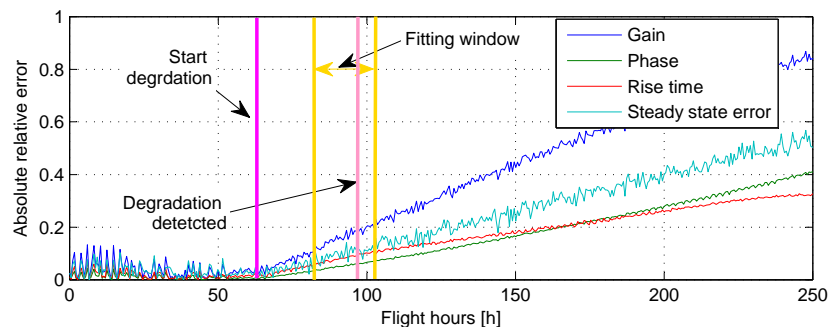
Figure 10.2: Model estimation data

Although a 60 samples window is still relatively small this allows you to make a first estimate of the useful life stay with a sufficiently high degree of accuracy, the prediction of the RUL in the continuation of the life of the aircraft will be successively updated with the new data acquired.

The extracted patterns, reported in the figure 10.3 , show that for a first approximation of a data window 60 is more than enough. The models identified approximates in a precise manner the trend of the four parameters, and

also maintaining a level of absolute error less than $1 \cdot 10^{-3}$ the mathematical models obtained have a low order and then carry out a kind of filtering on the signals, performing an interpolation that eliminates some fluctuations.

(a) Gain model

(b) Phase model

(c) Rise time model

(d) Stedy state error model
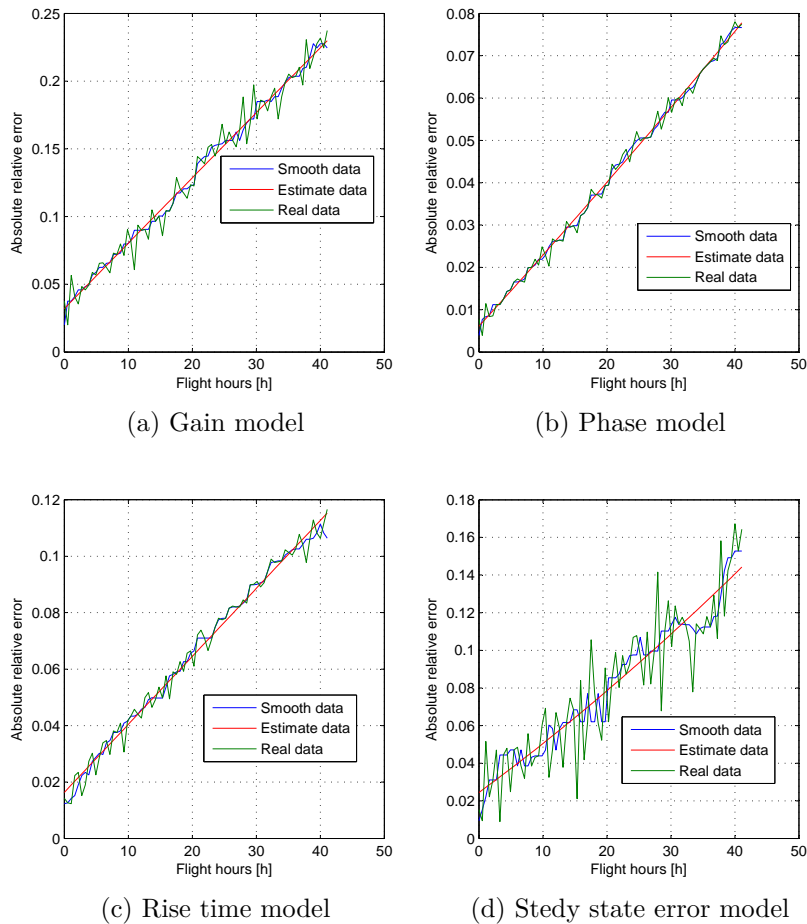
Figure 10.3: Model estimation results

10.3   RUL estimation

The process for estimating the remaining useful life is composed of two sub routine, the first deals to predict the trend of the absolute relative errors, while the second to estimate the RUL. In order to complete the task it is therefore necessary to implement an estimation algorithm and set the operating limits of the test component. For predicting the evolution of its absolute

error in this thesis it was adopted on particle filter, while the definition of the limits of use of EHSA was particularly complex.

The prediction of the remaining useful life is schematized effectively from graphic in figure 10.4, the start of prediction is indicated by the point "Initialize long-term prediction", from that point the algorithm must estimate the performance of the observed variable both the mean value and the uncertainty bands; the end of prediction occurs when both the average value that the extreme values of the overtaking prediction of the correct operation limit. The limit of operation can not be described in a timely manner since each dial can have slightly different break points, for this normally this value is described by a normal distribution curve. The remaining useful life is obtained by calculating the PDF of the points that surpass the breaking value for the whole duration of the prediction, then also the RUL is expressed medians probability curves in which the average value is the most probable instant of rupture.
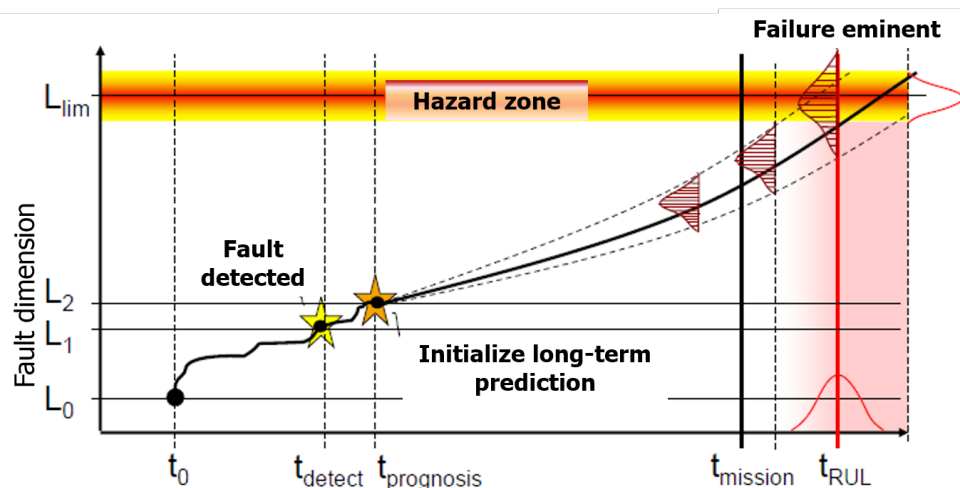
Figure 10.4: RUL scheme

In the literature there are no articles or studies that point to the actual usage limits of a degraded flight components, and operators or aircraft maintenance personnel who have been contacted have provided no information. Therefore, a flexible solution was implemented, which allows the operator of maintenance to fix, based on experience or on the technical specifications of the component, the maximum permissible relative error on the four position features: gain, phase, rise time and steady state error. In the tests that the limit of normal operation will be presented in this thesis it coincides with a variation of the four indicators of health of 35%, with a variance of 1%.

The particle filter implementation is a simplification of the original version, proposed by Ochard (2007): the full version of the particle filter is presented in equation 10.1, where where f_k and h_k are nonlinear mappings, $x_d(k)$ is a collection of Boolean states associated with the presence of a particular operational condition in the system (normal operation, fault type 1, 2, etc.), $x_c(k)$ is a set of continuous-valued states that describe the evolution of the system given certain operational conditions, $Er(k)$ is the relative error, $n(k)$ is zero-mean independent and identically distributed white noise, and $\omega(k)$ and $\upsilon(k)$ are non-Gaussian noises that characterize the process and feature noise PDF, respectively.

$$\begin{cases} x_d(k+1) = x_d(k) + n(k) \\ x_c(k+1) = f_k[x_d(k), x_c(k), \omega(k)] \\ Er(k) = h_k[x_d(k), x_c(k), \upsilon(k)] \end{cases} \qquad (10.1)$$

The first two equations of the system are not useful for estimating the useful life remain, since the prediction is made only in the presence of a previously identified degradation, therefore x_d has a constant value that does not vary in time. The evolution of its absolute error is evaluated directly by identifying the mathematical model and does not depend from the set of continuous-valued states that describe the evolution of the system x_c.

The equation system 10.1 can therefore be simplified and expressed as shown in equation 10.2; the relative error evolution will only function of the value to the previous year and the not-Gaussian noise.

$$Er(k) = h_k[Er(k-1), \upsilon(k)] \qquad (10.2)$$

In order to implement the particle filter algorithm for estimating the RUL, the equation was discretized in time, the new formulation of the particle filter is shown equation 10.3.

$$Er(k) = Er(k-1) + \Delta h_k(t) + \upsilon(t) \qquad (10.3)$$

Defined the formulation of the particle filter to be implemented, the next step was the identification of the number of particle-to-use, the initial condition and the noise variance is not Gaussian.

The number of particles is positively correlated with the accuracy of the prediction and inversely related to the solution time of algorithm. Doing some empirical evidence has been seen as 100000 particle represent a compromise between computational speed and accuracy, over that value required resources in terms of processor and RAM are too high to be able to provide an implementation of the algorithm in the field of aeronautics.

The initial condition, $Er(0)$, coincides with the last value detected during the tests carried out in the pre / post-flight. The particle filter requires as an initial condition not a single value, but a distribution with a number of elements equal to the number of particle used. Therefore, the algorithm to generate a normal distribution in which the last acquired value becomes the average value, while the variance is obtained as the standard deviation between the actual values used for the identification of the model and those obtained from the model, with the following equation, where n is the number of element in the sample.

$$s = \left(\frac{1}{n-1} \sum_{i=1}^{2} (Er_i - \hat{E}r_i)^2 \right)^{\frac{1}{2}} \tag{10.4}$$

The characteristics of the noise is not Gaussian have been chosen in order to better simulate the actual variability of the data that are estimated, the noise has been modeled with a random distribution of mean value zero and variance equal to the maximum variance introduced by the measurement chain and acquisition on the aircraft.

The algorithm follows the evolution of four different absolute relative errors, the definition of a strategy to define a single value to be supplied to the maintainer was then implemented. The most logical solution is to set a maximum limit of use of the RUL value for the features that first reaches the limit. In other words, the component is considered to be still usable until all location features still comply with the imposed parameters.

10.4   Results overview

This section presented an excerpt of the results obtained by calculating the remaining useful life of eighty-eight tests conducted. The cases illustrated are two: one relative to the yield of the spring and the last in which are present two simultaneous degradations, the reduction of the magnetomotive force and the increase of the friction force.

For each case study shown, the first prediction, that carried out at the end of detection as it is considered the most important and the most difficult to obtain with a high degree of accuracy.

Variation of the stiffness of the feedback spring   The estimate of the useful life remaining for the test in question is a little tough because the relative phase error, rise time and steady state eror have a particularly broad time interval, thus the estimate is more likely to be inaccurate.

The figure diagrams 10.5, in blu the real data an in gray the predicted data, shows how the features longer subject to the yield strength of the spring is the gain, the error which grows much more rapidly than others. The most important prediction is therefore that of the gain that defines the RUL, the graph relating to this magnitude shows how the prediction is very accurate, real data and those predicted are overlapped. Although the predictions made on rise time and steady state error are not accurate, the result of the algorithm is very accurate because it coincides with the gain result.

(a) Gain

(b) Phase

(c) Rise time

(d) Stedy state error
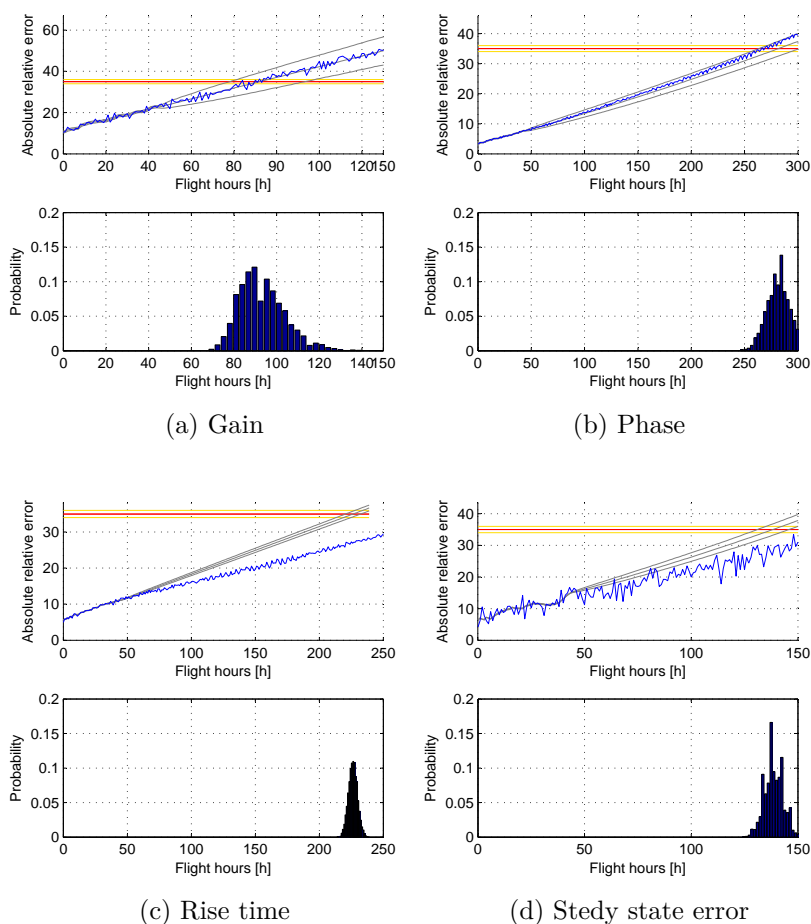
Figure 10.5: RUL estimation for spring yield

Magnetomotive force and friction   In the presence of two simultaneous degradation the estimation algorithm are able to make an accurate estimate,

as in the case of single degradation, because mathematical models of growth of the errors are estimated directly from the scanned data, then the presence of multiple faults do not influence the efficiency of the algorithm.

The results demonstrate that the first indicator of health that reaches an unacceptable level is the gain, then the RUL will depend on the time taken by such features to reach the limit. Gain, phase and rise time are of sufficiently accurate, although not excellent, while the estimate of the steady-state error is inaccurate. The total estimate of the remaining useful life, however, is accurate because it depends on gain.

(a) Gain

(b) Phase

(c) Rise time

(d) Stedy state error
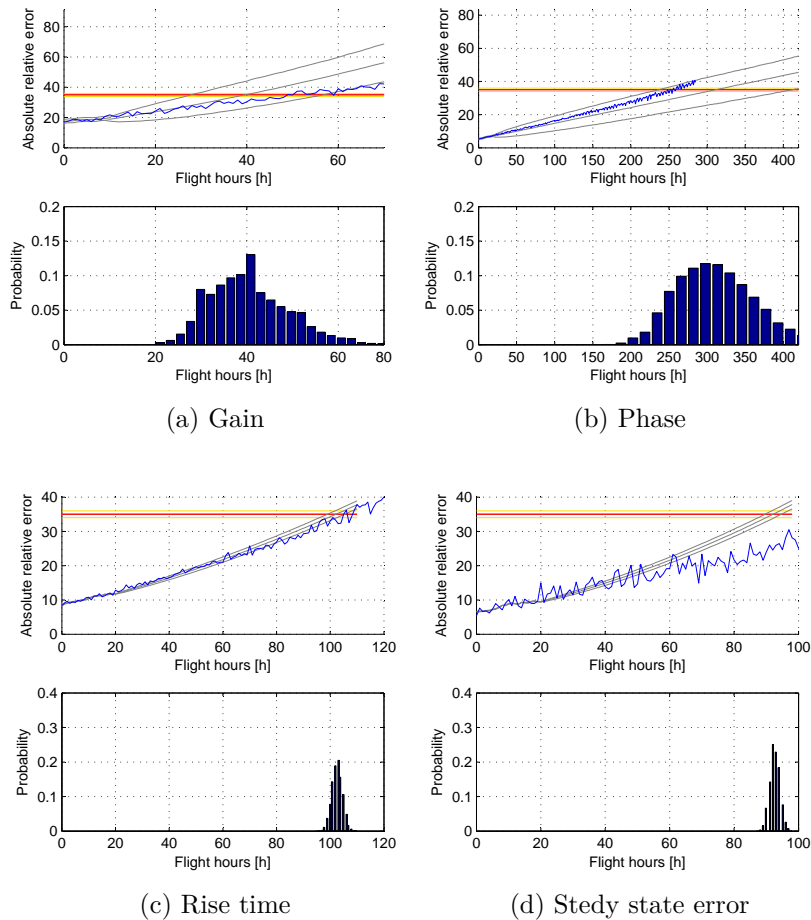
Figure 10.6: RUL estimation for clogging of nozzle left

10.5   Evaluation

The results obtained from the estimation algorithms of the remaining useful life were assessed by the metrics proposed by A. Saxena et al. (2008), presented in the section 1.4.1. The evaluation of the accuracy using the metrics has been performed exclusively on the error connected to the features that first reaches the limit that separates the normal operation from the not acceptable condition. This choice is supported by the fact that the feature that first reaches the operating limit is the one that defines the renaming useful life; therefore the prediction of other features has no impact on the output of the algorithm in question.

Relative accuracy (RA)   Defined as the relative accuracy between actual and estimate end of life time instant, perfect score is obtained for RA = 1. It is calculated using the equation 10.5, where t_λ is defined as $t_\lambda = t_P + \lambda(t_{EOL} - t_P)$, λ is in the rage 0 to 1.

$$RA(t_\lambda) = 1 - \frac{r_*(t_\lambda) - r'(t_\lambda)}{r_*(t_\lambda)} \tag{10.5}$$

The relative accuracy depends on the test considered, in tests in which the time interval between the detection of degradation and the end of its useful life is short, about 50 flight hours, accuracy is very high, between 90 and 98%, as show in figure 10.7a, while in the tests that have a long estimate window, 100 hours of flight, the accuracy of the first estimate falls to 85% in same case, but improving with arrives new data, coming to 98% (10.7b).

(a) Short prediction   (b) Long prediction
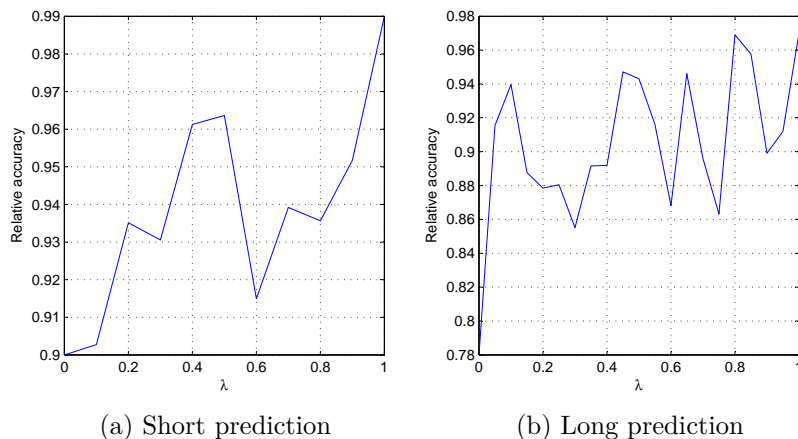
Figure 10.7: Relative accuracy example

In order to obtain a good representation of the relative accuracy in all the tests, the figure 10.8 show the distribution of RA values for three values of λ: $\lambda = 0$ coinciding with the first estimate, $\lambda = 0.5$ and $\lambda = 0.9$.

(a) $\lambda = 0$

(b) $\lambda = 0.5$

(c) $\lambda = 0.9$
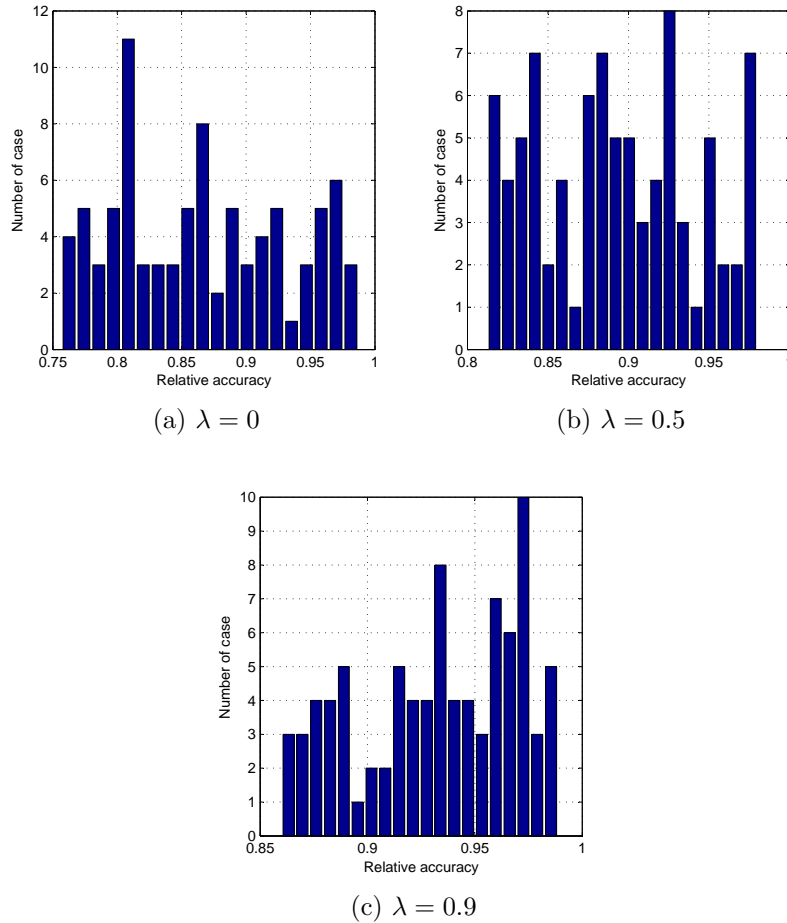
Figure 10.8: Relative accuracy

Cumulative Relative Accuracy (CRA)   The cumulative relative accuracy is the normalized sum of the relative prediction accuracy, it provides a more complete idea respect the relative accuracy, since no only evaluate in a specific time instant but offers a overall valuation of the algorithm.

$$RA(t_\lambda) = \frac{1}{t_{EOL} - tP - 1} \sum k = 1^2 RA(k) \qquad (10.6)$$

The cumulative relative accuracy is closely related with the relative accu-

racy, therefore the value of this metric is highly dependent on the amplitude of the prediction window, the best way to represent all of the results is histogram figure 10.9, which shows that CRA for all different test combination is between 0.86% and 0.96%, the CRA mean is equal to 0.912%. The overall value is encouraging, because it means that the average accuracy of the remaining useful life estimation is higher than by 85% for all test.
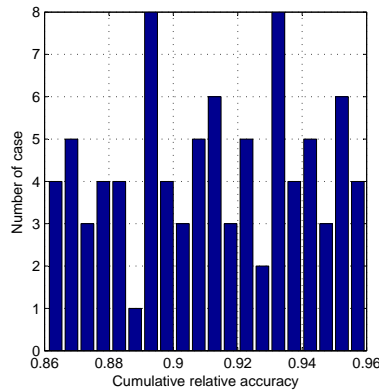
Figure 10.9: Cumulative relative accuracy

α-λ **performance**   Allows to verify that the prediction to a generic time instant λ has an accuracy better than α, where α is a percentage indication of the desired accuracy. The results of equation 10.7 are two bounds that represent the minimum accuracy required, if the prediction is inside of the bounds the accuracy is achieved. t_λ is defined as $t_\lambda = t_P + \lambda(t_{EOL} - t_P)$, λ is in the rage 0 to 1.

In this project α is set equal to 20%. Figure 10.10 show the distribution of prediction values for three cases: $\lambda = 0$ coinciding with the first estimate, $\lambda = 0.5$ and $\lambda = 0.9$, the metric is met when the histogram values stay in range [-0.2 0.2].

$$(1 - \alpha)r_*(t_\lambda) \leq r'(t_\lambda) \leq (1 + \alpha)r_*(t_\lambda) \tag{10.7}$$

(a) $\lambda = 0$

(b) $\lambda = 0.5$

(c) $\lambda = 0.9$
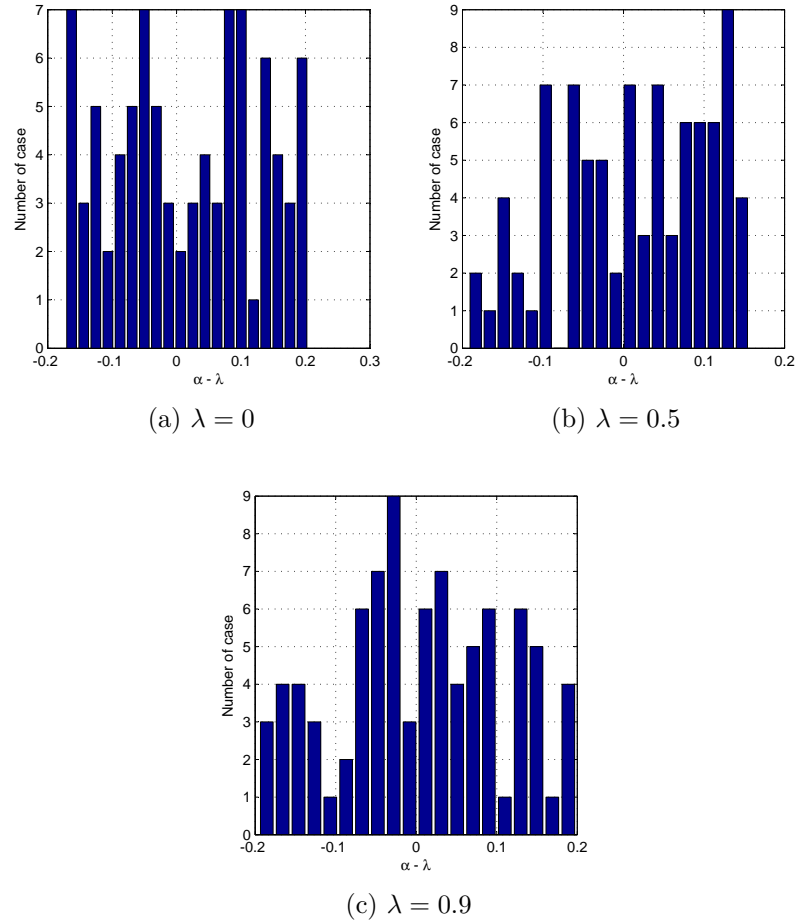
Figure 10.10: Relative accuracy

In all cases simulated the metric is met, although especially with the approaching end of life auks predictions are close to the limit imposed; this is due to the inevitable narrowing in terms of absolute error of the acceptance bandwidth .

Prognostic horizon $(H(i))$ Defined as the difference between the current time index i and the end of prediction (EOP) utilizing data accumulated up to the index i, provided the prediction meets desired specification. Wider prognostic horizon ensures more time between the prediction and the need for maintenance, thus facilitating logistics operations and the schedule of maintenance.

This metric has a merely indicative, since the time required depends on

the evolution speed of the degradation and from the influence that the faults has on features. In this project different degradations have been tested , single or combined, and different degradation laws was implemented, so it is not possible to obtain specific information from the prognostic horizon. The metric does provide an idea of the time that remains to agonize for maintenance operations necessary to restore the aircraft.

In the figure 10.11 the prognostic horizons of all tests are shown the lesser time between detective and end of the RUL is 35 hours of flight, while the greater is about 110 hours of flight, the mean value is 92.26 flight hours.
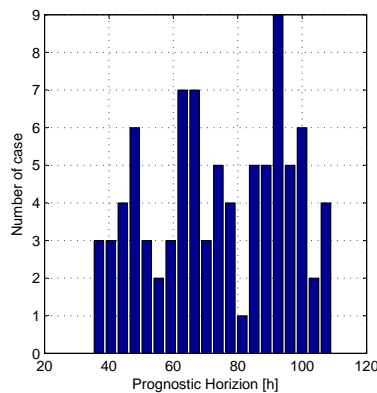
Figure 10.11: Prognostic Horizon

10.6 Summary

The algorithm for the estimation of the useful life remain implemented it proves reliable and accurate, able to predict the RUL in all different cases tested, albeit in the presence of long time windows the algorithm accuracy is greatly reduced.

The main advantage of the solution adopted is that of not requiring any type of prior knowledge, and to be automatically adaptable to different EHSAs and various configurations of the aircraft. But these advantages mean less overall accuracy of the prediction.

The extraction of mathematical growth models from real data involves a small number of samples available to carry out the fitting, or better the right balance between accuracy of the model and number of tests needed to perform the prediction is to be found.

An excessive number of samples entails a high number of tests which must be carried out from the time when the degradation is detected the

instant at which the prediction is made, with the risk of reducing excessively the prognostic horizon, or worse to make the prediction of RUL when the component is already too degraded. At the same time a too low number of samples is synonymous with an inaccurate mathematical model and then a wrong estimate.

The idea of using the latest data used to create the PDF during the automatic diagnostics to complement the data available for the fitting of the model is certainly interesting, it allows to reduce the time between detection and prediction without sacrificing the accuracy of the mathematical model, and it also allows to take advantage from one of the limitation of the chosen approach for automatic diagnostics.

Access to a test bench or data from airlines allow to optimize the model, setting the real operating limits and trying to identify a priori the growth patterns of degradation, thereby limiting the need of actual data, acquired during the operative life.

11

Conclusion

The research project developed during the PhD aims to demonstrate the possibility to implement a prognostic and health management system for fly-by-wire primary flight control electrohydraulic servoactuators both for new platforms and for legacy airplanes. The PHM is a relatively young field of research that has experienced a wide spread in different areas of engineering, though without ever being developed for this type of servocommand. In literature there are some jobs that offer solutions for the aeronautics field, but are primarily focused on power transmission and electromechanical drives.

Now-days , however, almost all the circulating airplane using EHSAs for primary flight control surface, and also for the platforms in developing the designers seem to prefer this actuation systems than electromechanical solutions. Considering the useful life of aircraft and the propensity of the designers for the water supply, is obvious as an effective PHM system for EHSAs could provide a large benefit to aircraft operations.

This chapter summarized the work done, highlighting the strengths and flaws. Then outlines the guidelines for a future project development.

11.1   Summary

The presented thesis does not have aim of developing a running PHM system, but want to investigate the possibility of implementing a solution that use the transducers and the information already present in the aircraft in order to recognize the presence of a degradation and estimate the remaining useful life. The project is focused on the servovalve, one of the main components

that make up a EHSA, which it is generally considered one of the most delicate components and subject to degradation.

The first step of the research project was the study of EHSA and servo-valve, in order to identify the possible causes of degradation, choosing the most probable and / or those which carry a higher risk for the aircraft.

In order to compensate the impossibility of obtain real flight component to carry out test in nominal and degraded conditions, a mathematical high fidelity model has been implemented. The model has all the main non-linearity that characterize a EHSA, also offering the possibility to simulate degraded operative conditions. In order to make the simulations as realistic as possible the model has the possibility of setting environmental conditions and the oil characteristics, temperature and pressure. The model was validated on normal conditions, with the support of Lufthansa Technik.

Taking advantage of the mathematical model, the influence of the various degradations on the behavior of EHSA was studied, this allows to identified nine indicators of health system, which allow the detection of degradation present in the valve. The indicators are extracted from the data that are purchases during a specific test that is carried out in pre / post-flight, four come from the ram position and five from the command current.

The influence of environmental conditions, temperature and oil pressure and of the constructional tolerances on indicators has been studied, and where possible techniques to eliminate it have been implemented . The features, or indicators, were evaluated by means of appropriate metrics that have been shown, highlighting how the nine selected parameters are influenced by all the degradations.

Taking advantage of the indicators was implemented three automatic diagnostic systems, able to detect the presence of degradation in the observed system. The first based on alarm bands is easy to implement and very accurate, but requires high prior knowledge, or of tests campaigns, in order to define the width of the bands. The second and the third approach is based on comparison of the probability density functions, one of the two estimate the PDF by the use of the particle filter, while the other working exclusively with the data acquired. Both PDF-based systems have the great advantage of being self adaptive, since the calibration of parameters are carried out by a campaign of acquisition that is just make when the system is installed on board the aircraft.

Although the particle filter allows to have a fast detection, estimation of PDF involves a high number of false alarms, it was decided to time, especially in light of the results of metrics to use in the thesis project the diagnostic system based on PDF obtained from real data.

The particle filter is the tool of choice for the prediction of reaming useful

life, as it is demonstrated accurate, robust and flexible. In the absence of historical data or models of growth of validated degradations, also for predicting a self-calibrating system it was chosen. The results of the metrics confirm that the direction taken is valid and effective even if it has a poor accuracy when the prediction window is particularly large.

The project demonstrated that the technologies to implement a PHM system for fly-by-wire primary flight control electrohydraulic servoactuators is available, and also good results can be obtained using only the information and transducers already on board the aircraft.

11.2   Future developments

The work must surely be deepened before knowing an actual use in the field of aeronautical, research should evolve along two different paths: the first aimed at creating a better understanding of the degradation mechanisms, notions unknown to today throughout the technical literature. The development of test benches in which to test new and degraded components, also developing endurance activities are therefore needed, as well as the creation of relationships with manufacturers and component users. Moreover, the results obtained from the experimental tests provide a great added value for the mathematical model to winged fidelity, it would also be validate in degraded conditions.

The second branch of research is more aimed at the development of algorithms, trying to optimize the individual parts, also in view of a possible use on board aircraft. The definition of standards to be followed, the choice of computers and code implementation are essential steps to get to complete development.

An analysis of the data extracted from new features benches could be obtained, perhaps taking advantage of data fusion techniques. Moreover, the importance of some degradation may be reassessed in the light of their actual impact

The combination of the two branches could provide the decisive to the development of prognostic system, and maybe the prognostic would place the aircraft in a short time.

A | Random pattern generator

Matlab and Matlab Simulink generates deterministic distributed random numbers, this means that the series of random numbers are repeatable setting the same starting seed. The seed resets to the specified value each time a simulation starts, consequently every time a new simulation starts, with the default settings, the sequence of random number generated from the model is always the same as show in diagram , the three results are completely superimposed.

Figure A.1: Random series using default settings
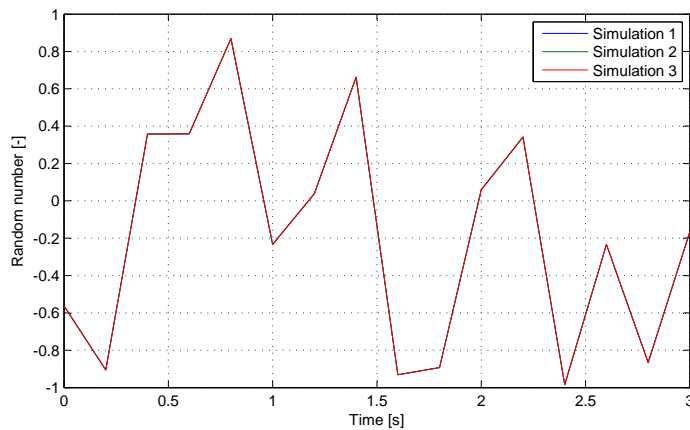
The *Random Number* block in Simulink use the algorithm called *mcg16807* for generate the sequence; it is 32 bit multiplicative congruential generator, as described in Park and Miller 1988, with a period, defined as the maximum number of number after which the sequence starts over, of $2^{31} - 2$. The algorithm used by default for *mcg16807* streams is the polar algorithm

219

(Devroye 1986) and start the generation from the seed, which it can not be varied during the simulation.

Identical series of random numbers involve that noise and disturbance in the model became identical for each simulation, this condition leads to problems in the moment in which PHM algorithms are implemented. Inasmuch , especially if the PHM systems are based on self-adaptive algorithms, the system is able to easily identify, by analyzing data from different simulations, the random series which generates the noise. Identified the source, which is always repeated in identical way, the algorithm is able to eliminate it and become therefore immune to the noise and disturbance. Obviously in a real operative condition the noise does not follow a pattern always the same; therefore, the results obtained from the model would be hugely better than those who archived in real applications.

The problem was solved by generated the seeds of the *Random Number* blocks during the model initialization function with the equation:

$$seed_N = mod(N \prod(clock), 2^{31}) \tag{A.1}$$

Where N indicates the number of *Random Number* block, *clock* returns a six-element date vector containing the current date and time in decimal form, *mod* returns the remainder after division. The introduction of the function *clock* allows to have a semi-deterministic random number generator, because it introduces in generation algorithm a truly random variable which coincides with the time instant in which the simulation starts; this moment can not be determined in advance as it depends on several external conditions including the human willpower.
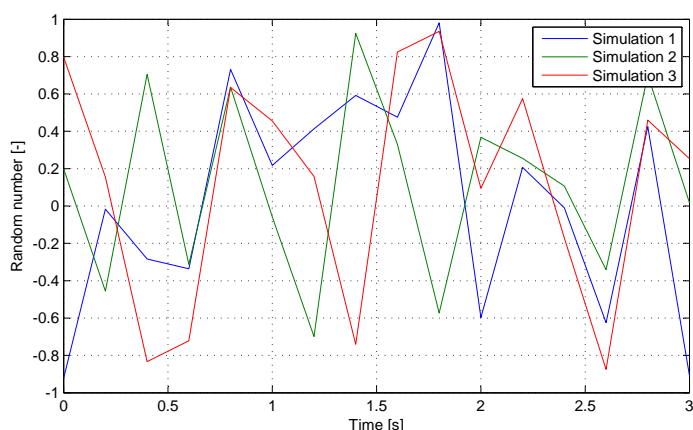

Figure A.2: Random series using seed generator

The diagram shows, as after applying the changes presented above, that three simulations started in three successive time instants provide a complete different random paths.

Bibliography

Airbus S.A.S. (2013). *Historical Orders and Deliveries 1974-2013*.

An, L. and N. Sepehri (2003). "Hydraulic actuator circuit fault detection using extended kalman filter". In: *Proceeding of the American Control Conference*, pp. 4261–4266.

Angadi, SV et al. (2009a). "Reliability and life study of hydraulic solenoid valve. Part 1: A multi-physics finite element model". In: *Engineering Failure Analysis* 16.3, pp. 874–887.

— (2009b). "Reliability and life study of hydraulic solenoid valve. Part 2: Experimental study". In: *Engineering Failure Analysis* 16.3, pp. 944–963.

Anthony, Martin and Peter L Bartlett (2009). *Neural network learning: Theoretical foundations*. cambridge university press.

Arulampalam, M. Sanjeev et al. (2002). "A tutorial on particle filters for online nonlinear/non-Gaussian Bayesian tracking". In: *IEEE Transactions on Signal Processing* 50.2, pp. 174–188.

ATA (1968). *Maintenance Evaluation and Program Development (MSG-1)*. Air Transport Association of America.

— (1970). *Airline/Manufacturer Maintenance Program Planning Document (MSG-2)*. Air Transport Association of America.

— (2001). *The Airline Handbook*. Air Transport Association of America.

Balaban, Edward et al. (2009). "A diagnostic approach for electro-mechanical actuators in aerospace systems". In: *IEEE Aerospace conference*.

Barabady, Javad (2007). "Production Assurance: Concept, Implementation and Implementation". Ph.D. Thesis. Lulea University of Technology.

Battino, Rubin, Timothy R. Rettich, and Toshihiro Tominaga (1983). "The solubity of Oxigen and Ozone in Liquids". In: *Journal of Physical and Chemical Reference Data* 12.2, pp. 163–178.

Boeing Company (2010). *B777 Aircraft Maintenance Manual*.

— (2015). *Historical Deliveries*.

Bollinger, John (2001). *Bollinger on Bollinger bands*. Mc Graw Hill.

Borello, Lorenzo et al. (2009). "A Prognostic Model for Electrohydraulic Servovalves". In: *Annual Conference of the Prognostics and Health Management Society.*

Brian, Armstrong and Carlos Canudas De Wit (1995). "Friction Modeling and Compensation". In: *The Control Handbook.* CRC Press. Chap. 77.1, pp. 1369–1381.

Brown, D. et al. (2009). "Particle filter based anomaly detection for aircraft actuator systems". In: *Aerospace conference.* IEEE.

Byington, Carl S., Matthew. Watson, and Doug. Edwards (2004). "Data-driven neural network methodology to remaining life predictions for aircraft actuator components". In: *Proceedings of IEEE Aerospace Conference.* Vol. 6, pp. 3581–3589.

Carney, John G, Pádraig Cunningham, and Umesh Bhagwan (1999). "Confidence and prediction intervals for neural network ensembles". In: *Neural Networks, 1999. IJCNN'99. International Joint Conference on.* Vol. 2, pp. 1215–1218.

Chryssolouris, George, Moshin Lee, and Alvin Ramsey (1996). "Confidence interval prediction for neural network models". In: *IEEE Transactions on Neural Networks* 7.1, pp. 229–232.

De Oliveira Bizarria, Cintia and Takashi Yoneyama (2009). "Prognostics and Health Monitoring for an electro-hydraulic flight control actuator". In: *IEEE Aerospace conference.*

Del Moral, Pierre (1996). "Non-linear filtering: interacting particle resolution". In: *Markov processes and related fields* 2.4, pp. 555–581.

Devroye, Luc (1986). "Sample-based non-uniform random variate generation". In: *Proceedings of the 18th conference on Winter simulation.* ACM, pp. 260–265.

DiStefano, Christine, Min Zhu, and Diana Mindrila (2009). "Understanding and using factor scores: Considerations for the applied researcher". In: *Practical Assessment, Research & Evaluation* 14.20, pp. 1–11.

Eckert, D., D. Hinz, et al. (1987). "Thermal ageing and coercivity of sintered $(Nd, Dy)_{15}(Fe, Co, Mo, Al)_{77}B_8$ magnets". In: *physica status solidi (a)* 101.2, pp. 563–566.

Eckert, D., K.H. Muller, et al. (1993). "Ageing effects in sintered $(Nd, Dy)_{15}$ $(Fe, Co, Mo, Al)_{77}B_8$ permanent magnets". In: *Magnetics, IEEE Transactions on* 29.6, pp. 2755–2757.

Engel, Stephen J. et al. (2000). "Prognostics, the real issues involved with predicting life remaining". In: *Aerospace Conference Proceedings, 2000 IEEE.* Vol. 6. IEEE, pp. 457–469.

FED-STD-1037C (1997). *Federal Standard 1037C - Telecommunications: Glossary of Telecommunication Terms.* Ed. by General Services Administration.

Ferrel, Barry L. (1999). "JSF prognostics and health management". In: *Proceedings of IEEE Aerospace Conference.* Vol. 2.

Ferri, Carlo Antonio (2014). "Fly-By-Wire Primary Flight Control Actuators: Modelling, Validation, Health Monitoring". Supervisors: Prof. Jacazio G., Prof. Sorli M., Dipl. Eng. Ritter O. Master degree. Politecnico di Torino.

Foresee, F Dan and Martin T Hagan (1997). "Gauss-Newton approximation to Bayesian learning". In: *Neural Networks, 1997., International Conference on.* Vol. 3. IEEE, pp. 1930–1935.

Fredlund, DG (1976). "Density and compressibility characteristics of air-water mixtures". In: *Canadian Geotechnical Journal.*

Gillen, KT, R Bernstein, and MH Wilson (2005). "Predicting and confirming the lifetime of o-rings". In: *Polymer degradation and stability* 87.2, pp. 257–270.

Guyon, I. et al. (2006). *Feature Extraction, Foundations and Applications.* Springer.

Hadden, George D et al. (1999a). "Shipboard machinery diagnostics and prognostics/condition based maintenance: a progress report". In: *Maintenance and Reliability Conference, MARCON*, pp. 73.01–73.16.

— (1999b). "Shipboard machinery diagnostics and prognostics/condition based maintenance: a progress report, failure analysis: a foundation for diagnostics and prognostics development". In: *Proceedings of the 53rd Meeting of the Society for Machine Failure Prevention Technology.*

Hagan, Martin T et al. (1996). *Neural network design.* Vol. 20. PWS publishing company Boston.

Hansen, Charles M. (2007). *Hansen Solubility Parameters: A User's Handbook.* CRC Press.

Hardman, William, Andrew Hess, and Jonathan Sheaffer (1999). "SH-60 helicopter integrated diagnostic system (HIDS) program-diagnostic and prognostic development experience". In: *Aerospace Conference, 1999. Proceedings. 1999 IEEE.* Vol. 2. IEEE, pp. 473–491.

Haykin, Simon (2011). *Neural networks and learning machines.* Vol. 3. Pearson Education.

Hershberger, Scott L (2005). "Factor score estimation". In: *Encyclopedia of statistics in behavioral science.*

Hess, Andrew (2001). "The joint strike fighter (JSF) prognostics and health management". In: *NDIA Conference.*

Hoai, Nguyen Xuan et al. (2002). "Solving the symbolic regression problem with tree-adjunct grammar guided genetic programming: The compara-

tive results". In: *Proceedings of the Congress on Evolutionary Computation.* Vol. 2, pp. 1326–1331.

Hwang, JT Gene and A Adam Ding (1997). "Prediction intervals for artificial neural networks". In: *Journal of the American Statistical Association* 92.438, pp. 748–757.

Hyers, RW et al. (2006). "Condition monitoring and prognosis of utility scale wind turbines". In: *Energy Materials* 1.3, pp. 187–203.

Isermann, Rolf (1984). "Process fault detection based on modeling and estimation methods: a survey". In: *Automatica* 20.4, pp. 387–404.

Jacazio, Giovannni (2008). "The evolution of fly-by-wire flight control systems". In: *IASTED conference on Modelling, Identification, and Control. Guest speaker presentation.*

Jardim-Goncalves, Ricardo et al. (1996). "Application of stochastic modelling to support predictive maintenance for industrial environments". In: *IEEE International Conference on Systems, Man, and Cybernetics.* Vol. 1, pp. 117–122.

Jeanette, Lawrence (1994). *Introduction to Neural Networks.*

Jolliffe, Ian (2002). *Principal component analysis.* Wiley Online Library.

Konrad, H. and R. Isermann (1996). "Diagnosis of different faults in milling using drive signals and process models". In: *Proceedings of the 13th World Congress, International Federation of Automatic Control, Vol. B., Manufacturing*, pp. 91–96.

Levine, William S (1996). *The control handbook.* CRC press.

Lewis, F. W., S. Jagannathan, and A. Yesildirak (1998). *Neural network control of robot manipulators and non-linear systems.* CRC Press.

Lewis, Frank L. (1986). *Optimal estimation: with an introduction to stochastic control theory.* Wiley New York et al.

— (1992). *Applied optimal control and estimation.* Prentice Hall PTR.

Lippmann, Richard P. (1987). "An introduction to computing with neural network". In: *ASSP Magazine, IEEE* 4.2, pp. 4–22.

Liu, Huan and Hiroshi Motoda (2012). *Feature selection for knowledge discovery and data mining.* Springer Science & Business Media.

Liu, T. I., J. H. Singonahalli, and N. R. Iyer (1996). "Detection of roller bearing defects using expert system and fuzzy logic". In: *Mechanical Systems and Signal Processing* 10.5, pp. 595–614.

Ljung, Lennart (1987). "System Identification: Theory for the user". In: *PTR Prentice Hall Information and System Sciences Series* 198.

Makridakis, Spyros, Steven C. Wheelwright, and Rob J. Hyndman (2008). *Forecasting methods and applications.* John Wiley & Sons.

Martini, Leonard J. (1984). "Reciprocating Seals - Pistons and Cylinders". In: *Practical Seal Design.* New York: CRC Press. Chap. 5, pp. 108–131.

MathWorks Inc (2013). *Matlab Reference Guide.*

McKay, Ben, Mark J Willis, and Geoffrey W Barton (1995). "Using a tree structured genetic algorithm to perform symbolic regression". In: *First International Conference on Genetic Algorithms in Engineering Systems: Innovations and Applications*, pp. 487–492.

Mechefske, C. K. (1998). "Objective machinery fault diagnosis using fuzzy logic". In: *Mechanical systems and signal processing* 12.6, pp. 855–862.

Merritt, Herbert E (1967). *Hydraulic control systems.* John Wiley & Sons.

MIL-F-8785C (1991). *U.S. Military Specification MIL-F-8785C: Flying Qualities of Piloted Aircraft.* U.S. Department of Defense.

MIL-HDBK-1797 (1997). *U.S. Military Handbook MIL-HDBK-1797: Flying Qualities of Piloted Aircraft.* Ed. by U.S. Department of Defense.

Moog (2009). *Moog type 30 nozzle-flapper flow control servovalves.*

Mylaraswamy, Dinkar and Venkat Venkatasubramanian (1997). "A hybrid framework for large scale process fault diagnosis". In: *Computers & chemical engineering* 21, S935–S940.

Narasimhan, Sriram et al. (2010). "Combining model-based and feature-driven diagnosis approaches–a case study on electromechanical actuators". In: *21st International Workshop on Principles of Diagnosis.*

Nowlan, Stanley F. and Howard F. Heap (1978). *Reliability-Centered Maintenance.*

Oliva, JA, Christoph Weihrauch, and Torsten Bertram (2011). "A Model-Based Approach for Predicting the Remaining Driving Range in Electric Vehicles". In: *phmsociety*, pp. 1–11.

Orchard, Marcos E. and George J. Vachtsevanos (2007). "A particle filtering-based framework for real-time fault diagnosis and failure prognosis in a turbine engine". In: *Mediterranean Conference on Control & Automation.* IEEE.

— (2009). "A particle-filtering approach for on-line fault diagnosis and failure prognosis". In: *Transactions of the Institute of Measurement and Control.*

Orchard, Marcos, Biqing Wu, and George Vachtsevanos (2005). "A particle filtering framework for failure prognosis". In: *World tribology congress III.* American Society of Mechanical Engineers, pp. 883–884.

Park, Stephen K. and Keith W. Miller (1988). "Random number generators: good ones are hard to find". In: *Communications of the ACM* 31.10, pp. 1192–1201.

Pratt, Roger (2000). *Flight control systems: practical issues in design and implementation.* Iet.

Ramos Filho, José Roberto Branco and Victor Juliano De Negri (2013). "Model-Based Fault Detection for Hydraulic Servoproportional Valves".

In: *The 13th Scandinavian International Conference on Fluid Power, SICFP2013,*

Ribeiro, Ananda S. et al. (2015). "Variable Selection and Indices Proposal for the Determination of an Aeronautic Valve Degradation". In: *Annual conference of the Prognostics and Health Management Society.* Ed. by PHM Society.

Rosenberg, Bruce J. (1989). "The Navy IDSS program: adaptive diagnostics and feedback analysis-precursors to a fault prognostics capability". In: *Proceedings of the IEEE National Aerospace and Electronics Conference, NAECON 1989*, pp. 1334–1338.

SAE International Group (2012). "Aerospace information report AIR4253 Rev. B". In:

Saucier, Walter J (1989). *Principles of meteorological analysis.* Courier Corporation.

Saxena, Abhinav et al. (2009). "On applying the prognostic performance metrics". In:

Saxena, A. et al. (2008). "Metrics for evaluating performance of prognostic techniques". In:

Sharda, Ramesh (1994). "Neural networks for the MS/OR analyst: An application bibliography". In: *Interfaces* 24.2, pp. 116–130.

Sinha, Sunil K. and Mahesh D. Pandey (2002). "Probabilistic neural network for reliability assessment of oil and gas pipelines". In: *Computer-Aided Civil and Infrastructure Engineering* 17.5, pp. 320–329.

Skormin, Victor A., Joseph Apone, and Jhon J. Dunphy (1994). "On-line diagnostics of a self-contained flight actuator". In: *IEEE Transactions onAerospace and Electronic Systems* 30.1, pp. 186–196.

Skydrol Overview (2014). *Skydrol Overview - Specifically formulated to meet the changing needs of the aviation industry.* Eastman Aviation Solutions.

Studer, Léonard and Francesco Masulli (1996). "On the structure of a neuro-fuzzy system to forecast chaotic time series". In: *International Symposium on Neuro-Fuzzy Systems*, pp. 103–110.

Taylor, John William Ransom (1996). *The lore of flight.* Barnes & Noble Books.

Underground, Weather (2012). The Weather Channel, LLC. URL: `http://www.wunderground.com/history/`.

Ungar, Lyle H, Richard D De Veaux, and Evelyn Rosengarten (1996). "Estimating prediction intervals for artificial neural networks". In: *Proc. of the 9th Yale Workshop on Adaptive and Learning Systems.*

Urata, E. (2007a). "On the torque generated in a servo valve torque motor using permanent magnets". In: *Proceedings of the Institution of Mechani-*

cal Engineers, Part C: Journal of Mechanical Engineering Science 221.5, pp. 519–525.

— (2007b). "Influence of unequal air-gap thickness in servo valve torque motors". In: *Proceedings of the Institution of Mechanical Engineers, Part C: Journal of Mechanical Engineering Science* 221.11, pp. 1287–1297.

Urata, E. and K. Suzuki (2011). "Stiffness of the elastic system in a servo-valve torque motor". In: *Proceedings of the Institution of Mechanical Engineers, Part C: Journal of Mechanical Engineering Science* 225.8, pp. 1963–1972.

Vachtsevanos, George et al. (2006). *Intelligent fault diagnosis and prognosis for engineering systems.* John Wiley & Sons.

Werbos, Paul J (1988). "Generalization of backpropagation with application to a recurrent gas market model". In: *Neural Networks* 1.4, pp. 339–356.

Wheeler, Kevin R, Tolga Kurtoglu, and Scott D Poll (2009). "A survey of health management user objectives related to diagnostic and prognostic metrics". In: *ASME 2009 International Design Engineering Technical Conferences and Computers and Information in Engineering Conference.* American Society of Mechanical Engineers, pp. 1287–1298.

Willsky, Alan S. (1976). "A survey of design methods for failure detection in dynamic systems". In: *Automatica* 12.6, pp. 601–611.

Zelinka, I (2004). *Symbolic regression-an overview.*